THE
PHYSICAL REVIEW
A Journal of Experimental and Theoretical Physics Established by E. L. Nichols in 1893
VOL. 58, NO. 6 SEPTEMBER 15, 1940 SECOND SERIES

Radioactivity Produced by Proton Bombardment of Bromine and Iodine

E. C. CREUTZ, L. A. DELSASSO, R. B. SUTTON, M. G. WHITE AND W. H. BARKAS*
Palmer Physical Laboratory, Princeton, New Jersey
(Received June 26, 1940)

Bromine bombarded with 5–6-Mev protons emits electrons with half-lives 13 ± 2 seconds and 55 ± 2 seconds. A β-spectrograph shows these to be conversion electrons from at least two gamma-rays of energies 127 and 187 kev. Physical and chemical tests indicate the activity is from a krypton isotope. The long period $Kr^{79,81}$ reported by Snell is found to have a half-life of 34.5 ± 1 hours and a positron upper limit of about 0.4 Mev. Iodine targets similarly emit electrons with a half-life of 75 ± 1 seconds, shown to be conversion electrons from at least two gamma-rays of energies 125 and 175 kev, coming from a xenon isotope. Radiation consisting of electrons, x-rays, and probably gamma-rays, decaying with a half-life of 34 ± 2 days is also found. Secondary electrons produced in the target material or in Pb absorbers by x-rays from the source account for about $\frac{2}{3}$ of the total activity measured by the electroscope.

BROMINE

LEAD bromide, when bombarded with protons of 5–6 Mev energy was found to emit electrons in two radioactive periods of half-lives 13 ± 2 seconds and 55 ± 2 seconds (Fig. 1). The same activities were found in potassium bromide. Since no short periods were found in potassium or lead, these activities must be due to some process taking place in the bromine.

To test whether the element responsible was Br ($z=35$) or Kr ($z=36$), the potassium bromide target was dissolved and boiled to dryness, which procedure caused the activity to disappear. A proof that bromine is not volatile under similar conditions was given by bombarding potassium bromide with slow neutrons, forming $Br^{80,82}$, and then boiling the target to dryness. Since the activity remained in this case, we believe the 55-second period to be due to a krypton isotope. Because of its shortness, no definite information could be obtained on the 13-second period, although the indication was that it also is volatile.

A further check for the source of the activity was made with the apparatus shown in Fig. 2. Lead bromide was coated on the nickel foil, and bombarded in vacuum. Solid carbon dioxide and alcohol slush was then put into the small trap, and liquid air in the larger one, while krypton gas flowed into the apparatus. The foil was then heated to vaporize the lead bromide and release any occluded gas. Free bromine should be frozen out by the carbon dioxide, and some of the krypton by the liquid air. The activity on the liquid-air trap was then measured and found to be of about 55-seconds half-life. As a check experiment the carbon dioxide trap was left empty and the CO_2-alcohol mixture put in the liquid-air trap. A bombardment and heating of a new lead bromide target then caused less activity

* Member, the Institute for Advanced Study, Princeton, New Jersey.

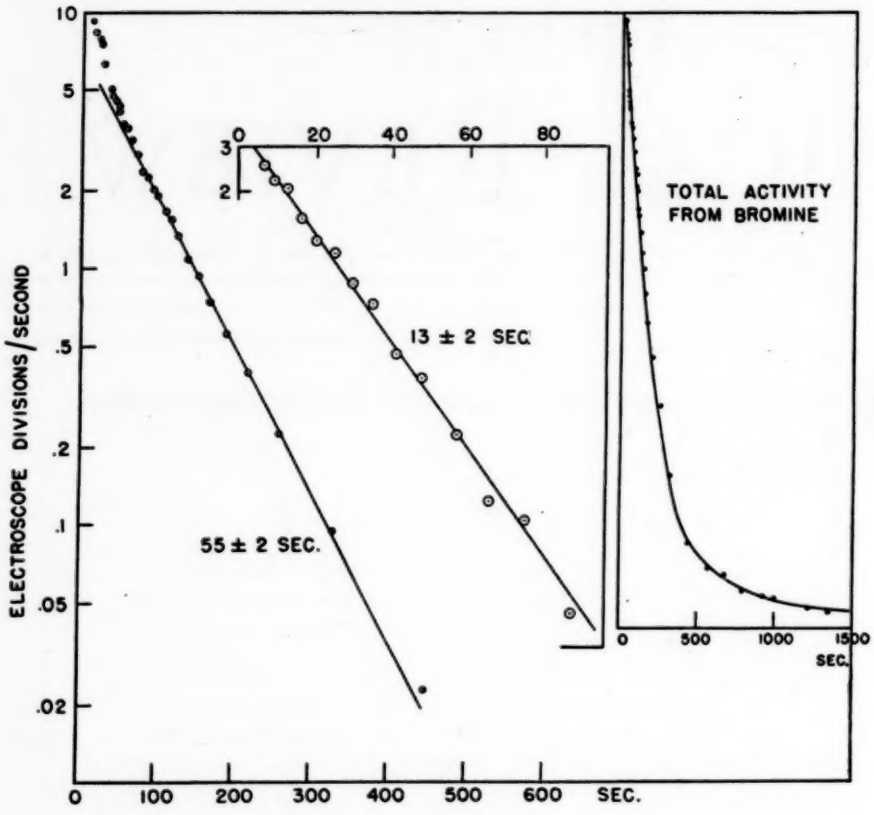

FIG. 1. Short periods from bromine bombarded by protons.

to appear on the liquid-air trap than in the previous experiment, with little or no 55-second period measurable.

These experiments make it seem probable that the electrons are from krypton. The stable isotopes of bromine and krypton are shown in Fig. 3. Krypton could be produced in the following ways:

(1) $Br^{79,81}(p, n)Kr^{79,81}$
(2) $Br^{79,81}(p, \gamma)Kr^{80,82}$.

Because the occurrence of negative electrons suggested an internally converted gamma-ray, a β-ray spectrograph was fitted with a vacuum lock for introducing targets repeatedly until sufficient effect was built up on the photographic film. This lock is described in a note soon to appear in *Review of Scientific Instruments*. One thousand and one bombardments were made to obtain the spectrum. Bombardment time was about one minute, while fifteen seconds elapsed between removing the target from the hydrogen-filled bombarding chamber of the cyclotron and placing it in the spectrograph. Since the intensities of the two periods were about the same immediately after bombardment, the longer should emit approximately four times as many electrons as the shorter. About one-half of the short period electrons were lost while the target was being placed in the spectrograph, while only one-half of the long period electrons were used during the one-minute exposure in the spectrograph. Therefore the lines due to the 55-second period should be about four times as strong as

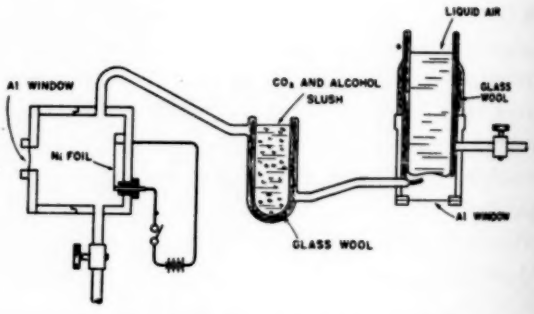

FIG. 2. Apparatus used to freeze out the radioactive krypton.

those due to the 13-second period. For this reason the stronger two lines may be tentatively assigned to the long period, and the weaker lines to the 13-second period. In Fig. 3, which reproduces the spectrogram, three lines are visible. The very weak fourth line can be seen but poorly on the original. The spectrograph was calibrated with the active deposit of thorium, and on various trials the magnetic field (furnished by an electromagnet and storage batteries) could be reproduced to within $\frac{1}{2}$ percent.

The energies of the electron lines are 0.113, 0.125, 0.173, and 0.185 Mev, respectively. The separation of the K and L_{III} x-ray absorption edges in bromine is 0.0116 Mev, and that in krypton is 0.0124 Mev, while the separation of the two lower energy electron lines is observed to be 0.012, and of the higher two, 0.012 Mev. Because the uncertainty in measuring the lines is about 1 percent, this cannot be considered definite evidence that the lines are from krypton, but if so, the energies of the gamma-rays are:

γ (strong) $= 0.125 + 0.002$ (= Kr L_{III} absorption edge)
$= 0.127$
$= 0.113 + 0.014$ (= Kr K absorption edge)
$= 0.127$ Mev.

γ (weak) $= 0.185 + 0.002 = 0.187$
$= 0.173 + 0.014 = 0.187$ Mev.

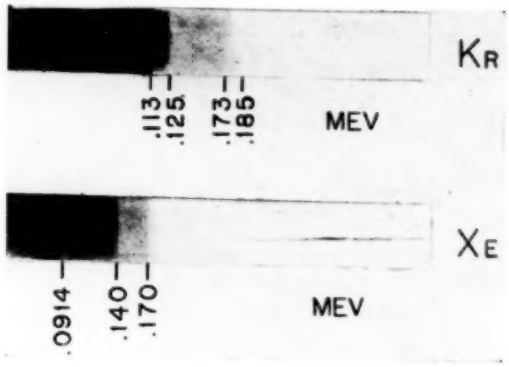

FIG. 3. Upper photograph: conversion electrons from krypton. Lower photograph: conversion electrons from xenon.

The uncertainty in these values is about 1.5 percent. If the gamma-rays are from bromine, their energies will be lowered by 1 percent, since the K and L electron binding is smaller than in krypton.

Another check on the element was made by studying the x-rays accompanying the 55-second period. No absorbers are available to distinguish Br characteristic x-rays from those of Kr by use of the K-absorption edges, so it was necessary to use the L edges of Au and Pt. A thin layer of lead bromide was melted onto 0.2-mil platinum, and bombarded for two minutes. The 13-second period was allowed to decay for 45 seconds, after which 3 to 4 electroscope readings were

TABLE I. *Stable isotopes.*

Bromine and krypton

Z \ A	78	79	80	81	82	83	84	85	86				
$_{35}$Br		50.6		49.4									
$_{36}$Kr	0.35		2.01		11.53	11.53	57.10		17.47				

Iodine and xenon

Z \ A	124	125	126	127	128	129	130	131	132	133	134	135	136
$_{53}$I				100									
$_{54}$Xe	0.094		0.088		1.90	26.23	4.07	21.17	26.96		10.54		8.95

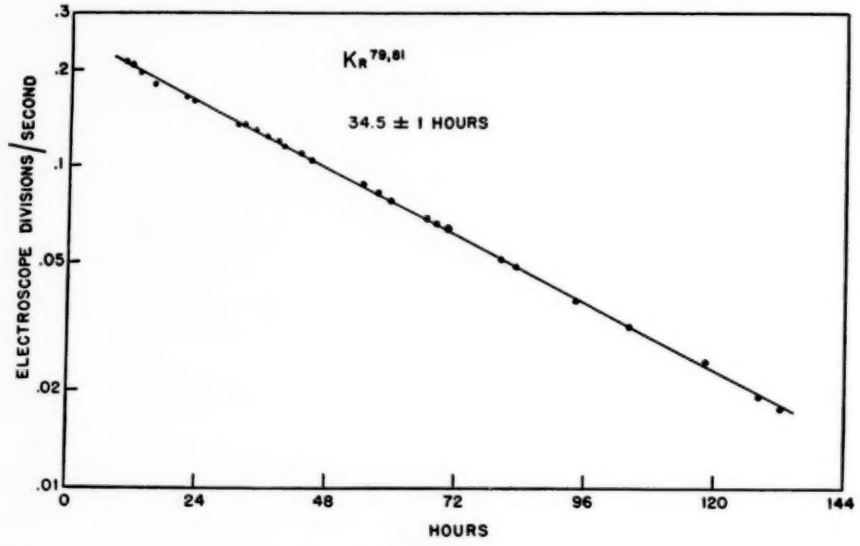

FIG. 4. Positron decay of $Kr^{79, 81}$.

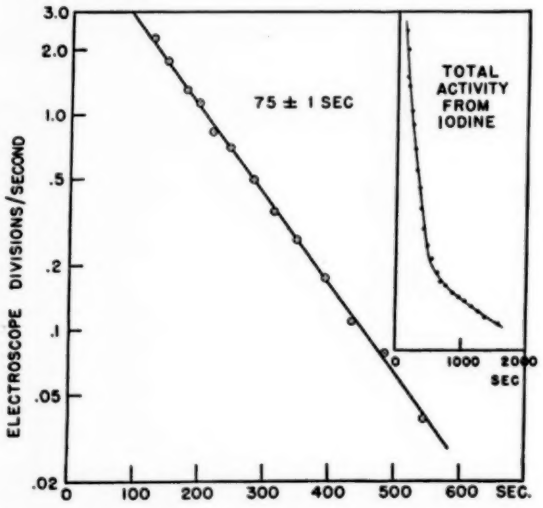

FIG. 5. Short period from iodine bombarded by protons.

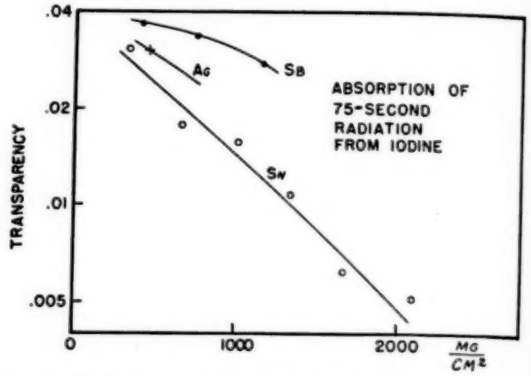

FIG. 6. Absorption of 75-second radiation from $I^{127}+H^1$, showing the x-rays are characteristic of xenon. Total activity was about 1 division/second. Absorption coefficients interpolated from data given in Compton and Allison, *X-Rays in Theory and Experiment*, are as follows: For iodine characteristic K radiation: in Sn, $\mu/\rho=9$; Ag, 62; Sb, 15. For xenon K radiation: in Sn, 45; Ag, 40; Sb, 10.

made with the absorber in place. The absorber was then removed, and 6 to 8 readings taken. The data suggest that the x-rays are from krypton.

$Kr^{79, 81}$ postulated in reaction (1) above is not stable. It has been produced by Snell[1] by deuteron bombardment with a half-life of the order of magnitude of 18 hours. We have bombarded lead bromide and also sodium bromide with protons for about 30 hours and obtained a half-life of 34.5±1 hours which magnetic analysis shows to consist of positrons. See Fig. 4. Examination of these positrons in a cloud chamber reveals an upper energy limit of 0.4 Mev. Scattering in the gas is rather bad at this energy, however, so the uncertainty in this value is about 0.1 Mev.

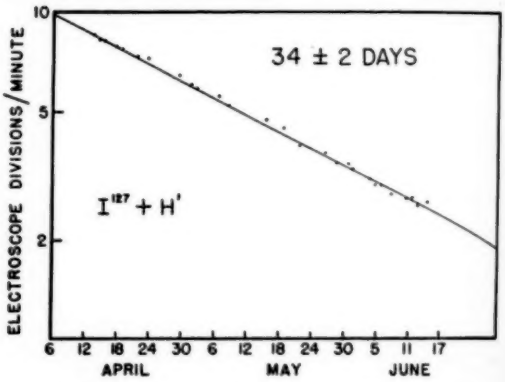

FIG. 7. Long period decay of $I^{127}+H^1$.

[1] A. H. Snell, Phys. Rev. **52**, 1007 (1937).

Iodine

The procedure with iodine closely parallels that with bromine. The stable isotopes, and those of xenon, are shown in Table I. When lead iodide, potassium iodide, and lead on which iodine had been melted and recrystallized were bombarded with protons, an activity of 75 ± 1 seconds was observed (Fig. 5). This activity was volatile, while I^{128} formed by slow neutron capture was not volatile under similar conditions.

Two β-ray spectrograms were made of the electrons, one using 801 lead iodide targets, and one using 1301 potassium iodide targets. Figure 3 shows that obtained from lead iodide which differs in no important respect from the other. Three lines are visible, at 0.0914, 0.140, and 0.170 Mev, respectively. The $K-L_{III}$ separation in xenon is 0.029 Mev, while that in iodine is 0.0278 Mev. Here, as in the case of bromine, the error is too great to assign definitely the observed separation $(0.170-0.140=0.030)$ of the upper two lines to either element. The lowest energy line appears to be single, although one several times weaker could be lost in the background. If this is assumed to be a K line from xenon, the gamma-ray energy is:

$$0.0915+0.034 \text{ (Xe } K\text{-absorption edge)} = 0.125 \text{ Mev.}$$

The higher energy gamma-ray is, similarly,

$$0.140+0.034=0.174$$

or $0.170+0.005$ (Xe L_{III}-absorption edge) $=0.175$ Mev.

The uncertainty in these values is about 1.5 percent. A chemical investigation showed that the amount of bromine in the lead iodide, or iodine in the lead bromide, if any at all, was much too small to account for the coincidence in energy of the two gamma-rays (Br, 127 kev and I, 125 kev).

An attempt was made to freeze out the active material with liquid air, but the results were less positive than in the case of bromine, which is perhaps not surprising, as the vapor pressure of xenon at liquid-air temperature is about 13 centimeters, and only a small amount was used as a carrier. However, the volatility of this

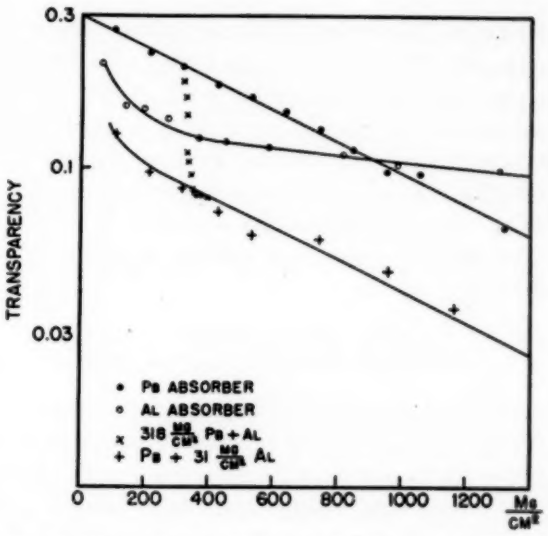

FIG. 9. Absorption of 34-day period from $I^{127}+H^1$. The filled-in circles show the absorption by lead alone; the open circles, by aluminum alone. The points marked x were obtained by putting various thicknesses of aluminum between 318 mg/cm² of lead and the electroscope. The points marked + show the activity observed through lead absorbers, but with 31 mg/cm² of aluminum absorbing the secondary electrons produced in the lead.

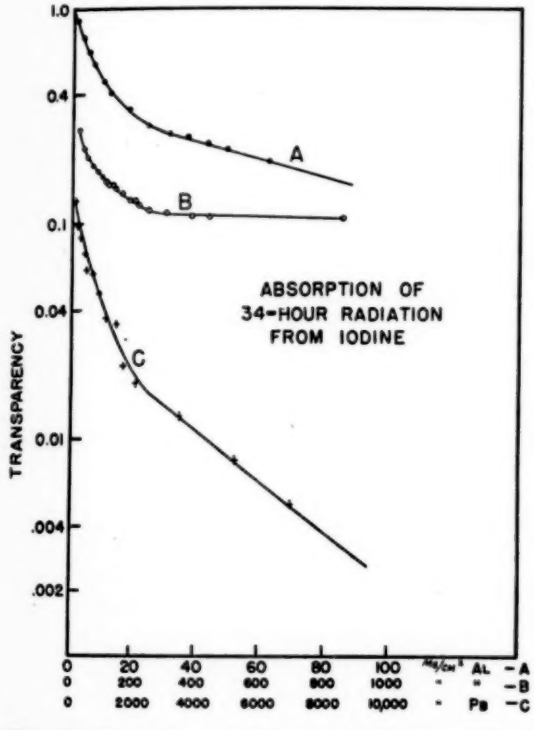

FIG. 8. Absorption of 34-day period from $I^{127}+H^1$. Curves A and B show absorption in aluminum. Curve C was made with lead absorbers but with 31 mg/cm² of aluminum between the absorber and the electroscope to remove the soft secondary radiation produced in the lead. Total activity was about 2 divisions/minute.

activity makes it seem that a xenon isotope is responsible. Furthermore, the x-rays accompanying the internal conversion were shown to be characteristic of xenon. See Fig. 6. A more complete study of the absorption in silver showed the ionization due to the x-rays was about equal to that of the unconverted gamma-rays.

The possible ways of producing xenon are the following:

$$(3)\quad I^{127}(p, n)Xe^{127}$$
$$(4)\quad I^{127}(p, \gamma)Xe^{128}.$$

Xe^{128} is stable, and the gamma-rays may arise from an excited state in it. Xe^{127} is not found in nature, nor has it been reported as a radioactive isotope. We have bombarded lead iodide and also sodium iodide for about 30 hours and obtained an activity of 34 ± 2 days half-life (see Fig. 7), consisting of electrons, x-rays and probably some gamma-rays. The range of the electrons is about 350 mg/cm² of aluminum. By means of a counter kindly supplied by Mr. J. G. Fox, they were found to be negative. A softer (negative) group also appears in the complete absorption curve (Fig. 8), with range about 35 mg/cm² of aluminum. These, however, are undoubtedly secondaries produced by the harder radiation in the material of the source and the absorber, since the same group is found by absorbing in aluminum the radiation that comes through various thicknesses of lead. The greater number of these secondaries produced in lead than in aluminum makes the total radiation received through a given mass of lead greater than that through the same mass of aluminum, until the total absorber thickness is about 0.9 gram/cm². This effect is shown in Fig. 9.

A study of the x-radiation with critical absorbers in an attempt to ascertain whether the x-ray is from iodine or xenon gave an inconclusive result. From the absorption coefficient in Pb, its energy is found to be about 40–45 kev.

Although the number of nuclei with the 75-second half-life made in a given bombardment is of the same order of magnitude as the number decaying with the 34-day period, no genetic relationship between the two processes has as yet been established.

SEPTEMBER 15, 1940 PHYSICAL REVIEW VOLUME 58

Internal Conversion of Gamma-Radiation in the *L* Shell

M. H. Hebb
Department of Physics, Duke University, Durham, North Carolina,

AND

Eldred Nelson,
Department of Physics, University of California, Berkeley, California

(Received May 31, 1940)

The nonrelativistic calculations of the internal conversion of electric multipole radiation which have been made for the *K* shell are extended to the *L* shell. Numerical values of the conversion coefficient for both the *K* and *L* shells are given and curves showing the ratio of the *K* conversion to the *L* conversion for different energies and atomic number are presented. This latter ratio is quite sensitive to the multipole order and varies between ~0.1 and 10 in the range in which the calculations are valid. A simple relativistic formula for the conversion of magnetic multipole radiation is given. In Section 5 we summarize selection rules and give applications of the formulas to experiments.

1. Introduction

THE increasing number of cases in the lighter elements in which the internal conversion of gamma-radiation has been observed makes a study of this phenomenon more important. Calculations of the ratio of the number of conversion electrons to the number of gamma-quanta N_e/N_γ

have already been carried through for electric and magnetic multipole radiation for electrons of the K shell.[1] In this paper we shall extend these calculations with the same restrictions on their validity to electrons of the L shell. This has seemed worth while because experimentally it is much easier to obtain the ratio of the conversion in the K shell to that in the L shell N_K/N_L than to measure either N_K/N_q or N_L/N_q separately. Consequently, with calculations of both N_K/N_q and N_L/N_q available, an easier and more accurate comparison of experiment and theory can be made. In order to facilitate this comparison we have made fairly extensive numerical calculations of both quantities N_K/N_q and N_L/N_q and of the ratio N_K/N_L.

First we present the calculations for conversion of electric multipole radiation; in Section 4 we consider the conversion of magnetic multipole radiation.

2. Conversion of Electric Multipole Radiation in the L Shell

In many of the artificially radioactive gamma-emitters nonrelativistic calculations of the conversion of electric multipole radiation are appropriate; namely, where the energy of the gamma-ray is small so that for the ejected electron $v \ll c$ and where Z is less than ~ 50. We present such calculations following rather closely the method of Dancoff and Morrison. Therefore we shall give only the most important steps and the results, referring to their paper for details.

We are concerned with the ratio N_e/N_q where N_e is the number of electrons per second ejected from a given state or shell by the gamma-radiation from the nucleus and N_q is the number of gamma-quanta per second which escape from the atom. In the nonrelativistic approximation in which the wave-length of the gamma-ray is large compared with atomic dimensions, we have[2]

$$\frac{N_e}{N_q} = 2\pi\alpha \frac{l}{l+1}\left[\frac{(2l)!}{2^l l!}\right]^2 W^{-2l-1}\left|\int dv \psi_f^* \psi_0 Y_l^m r^{-l-1}\right|^2 \tag{1}$$

for a single electron initially in the state ψ_0. For simplicity in writing we use the natural system of units in which the units of mass, action and velocity are, respectively, m, $\hbar$ and c. Thus in Eq. (1), W is the energy of the gamma-ray in units mc^2 and $2\pi/W$ is the wave-length of the gamma-ray in units of the Compton wave-length. Equation (1) holds for an electric 2^l-pole, l being the change of angular momentum of the nucleus in the gamma-transition. We use α to represent the fine-structure constant $\sim 1/137$, Y_l^m for the normalized surface harmonic and ψ_f for the final electronic state in the continuum, normalized to unit flux at infinity. We have

$$\psi_f^* = Y_{l'}^{-m'} \frac{|\Gamma(l'+1+in)|}{(2l'+1)!} 2p^{\frac{1}{2}} e^{\pi n/2} (2pr)^{l'} e^{-ipr} F(l'+1+in; 2l'+2; 2ipr),$$

where p is the momentum of the ejected electron (in units mc) and $n = \gamma/p = \alpha Z/p$.

For the L shell we have the $2s$-function

$$\psi_0 = (\gamma^3/8\pi)^{\frac{1}{2}}(1-\gamma r/2)e^{-\gamma r/2}$$

and the three $2p$-functions

$$\psi_0 = (\gamma^5/24)^{\frac{1}{2}} r e^{-\gamma r/2} Y_1^{0,\pm 1}.$$

The angular integrations in Eq. (1) require $l' = l$, $m' = m$ if ψ_0 is the $2s$-function and $l' = l \pm 1$, $m' = m$, $m \pm 1$ for the $2p$-functions. The radial integrations can be performed in series and we find for two

[1] M. H. Hebb and G. E. Uhlenbeck, Physica **7**, 605 (1938); S. M. Dancoff and P. Morrison, Phys. Rev. **55**, 122 (1939).

[2] Equation (1) can be obtained most easily by taking for the perturbation acting on the electron the potential of a static multipole $V = \text{const.}\ r^{-l-1} Y_l^m$ multiplied by e^{-iWt}. It is also in agreement with the method of Dancoff and Morrison as can be shown by transforming the potentials from their primed gauge for which div $\mathbf{A}' = \varphi' = 0$ to the conventional gauge. In the conventional gauge the only important potential in the nonrelativistic approximation is the scalar potential φ.

$2s$-electrons

$$\frac{N_e}{N_q}=2\alpha\gamma^2\frac{l}{l+1}\frac{|\Gamma(l+1+in)|^2}{(2l+1)^2(l!)^2}e^{\pi n}(p/W)^{2l+1}\left|\frac{1}{\rho^2}F_2{}^l-\frac{\gamma}{\rho^3}F_3{}^l\right|^2, \tag{2}$$

where $\rho=(\gamma/2)+ip$ and $F_q{}^l=F(q, l+1+in; 2l+2; 4/(2-in))$.

Similarly for the six $2p$-electrons, we find two terms. The first of these for which $l'=l-1$ is

$$\frac{N_e}{N_q}=\frac{\alpha\gamma^3}{2}\frac{l^2|\Gamma(l+in)|^2}{(l+1)(2l+1)(l-1)!^2}n^2e^{\pi n}(p/W)^{2l+1}\left|\frac{1}{\rho^2}F_2{}^{l-1}\right|^2 \tag{3}$$

and the second where $l'=l+1$ is

$$\frac{N_e}{N_q}=18\alpha\frac{\gamma^5 l|\Gamma(l+2+in)|^2}{(2l+3)^2(2l+1)^2(l+1)!^2}e^{\pi n}(p/W)^{2l+1}p^2|\rho^{-4}F_4{}^{l+1}|^2. \tag{4}$$

The sum of the expressions (2), (3) and (4) then gives the quantity N_L/N_q for the eight electrons of the complete L shell.

To evaluate the hypergeometric functions we apply the Gauss relations between contiguous hypergeometric functions[3] and the formula for the analytic continuation of the hypergeometric series.[4] Then

$$\gamma^{2l+2}\frac{N_L}{N_q}=128\pi\alpha\frac{l}{l+1}\left[\frac{(2l)!}{2^l l!}\right]^2 n^{2l+6}\{[l^2+n^2][(l-1)^2+n^2]\cdots[1+n^2][1-e^{-2\pi n}]\}^{-1}$$
$$\cdot(4+n^2)^{-3}\left\{A_l{}^2+\frac{9(l+1)}{4(2l+1)}\frac{n^2A_l{}^{+2}}{[(l+1)^2+n^2]}+\frac{16ln^2}{2l+1}\frac{[l^2+n^2]}{(4+n^2)^2}A_l{}^{-2}\right\}, \tag{5}$$

TABLE I. *Values of* $\log_{10}[\gamma^{2l+2}(N_e/N_q)]$ *for electric* 2^l*-pole radiation.* W*=energy of gamma-ray in units* mc^2, $\gamma=Z/137$.

	K Shell					L Shell				
W/γ^2	$l=1$	$l=2$	$l=3$	$l=4$	$l=5$	$l=1$	$l=2$	$l=3$	$l=4$	$l=5$
0.125						$\bar{1}.67$	2.11	3.83	4.95	5.71
0.25						$\bar{2}.80$	0.69	1.98	3.02	3.89
0.5	$\bar{2}.73$	$\bar{2}.67$	$\bar{2}.20$	$\bar{3}.47$	$\bar{4}.58$	$\bar{3}.94$	$\bar{1}.07$	0.14	0.96	1.65
	$\bar{2}.25$	$\bar{2}.33$	$\bar{2}.27$	$\bar{2}.17$	$\bar{2}.06$	$\bar{3}.42$	$\bar{2}.22$	$\bar{1}.06$	$\bar{1}.72$	0.28
1.0	$\bar{3}.90$	$\bar{3}.97$	$\bar{3}.93$	$\bar{3}.86$	$\bar{3}.79$	$\bar{3}.05$	$\bar{3}.62$	$\bar{2}.30$	$\bar{2}.84$	$\bar{1}.29$
	$\bar{3}.62$	$\bar{3}.65$	$\bar{3}.59$	$\bar{3}.50$	$\bar{3}.41$	$\bar{4}.76$	$\bar{3}.18$	$\bar{3}.72$	$\bar{2}.16$	$\bar{2}.52$
1.5	$\bar{3}.39$	$\bar{3}.38$	$\bar{3}.28$	$\bar{3}.16$	$\bar{3}.04$	$\bar{4}.52$	$\bar{4}.82$	$\bar{3}.25$	$\bar{3}.60$	$\bar{3}.89$
	$\bar{3}.19$	$\bar{3}.14$	$\bar{3}.01$	$\bar{4}.85$	$\bar{4}.70$	$\bar{4}.32$	$\bar{4}.52$	$\bar{4}.85$	$\bar{3}.13$	$\bar{3}.35$
2.0	$\bar{3}.02$	$\bar{4}.93$	$\bar{4}.76$	$\bar{4}.57$	$\bar{4}.38$	$\bar{4}.14$	$\bar{4}.27$	$\bar{4}.51$	$\bar{4}.72$	$\bar{4}.88$
	$\bar{4}.87$	$\bar{4}.75$	$\bar{4}.54$	$\bar{4}.32$	$\bar{4}.09$	$\bar{5}.98$	$\bar{4}.05$	$\bar{4}.21$	$\bar{4}.37$	$\bar{4}.47$
2.5	$\bar{4}.73$	$\bar{4}.57$	$\bar{4}.34$	$\bar{4}.09$	$\bar{5}.83$	$\bar{5}.84$	$\bar{5}.85$	$\bar{5}.95$	$\bar{4}.05$	$\bar{4}.11$
	$\bar{4}.60$	$\bar{4}.42$	$\bar{4}.15$	$\bar{5}.87$	$\bar{5}.58$	$\bar{5}.71$	$\bar{5}.67$	$\bar{5}.71$	$\bar{5}.76$	$\bar{5}.78$
3.0	$\bar{4}.49$	$\bar{4}.27$	$\bar{5}.98$	$\bar{5}.67$	$\bar{5}.36$	$\bar{5}.60$	$\bar{5}.51$	$\bar{5}.50$	$\bar{5}.50$	$\bar{5}.47$
	$\bar{4}.38$	$\bar{4}.14$	$\bar{5}.82$	$\bar{5}.48$	$\bar{5}.14$	$\bar{5}.49$	$\bar{5}.36$	$\bar{5}.30$	$\bar{5}.26$	$\bar{5}.20$
3.5	$\bar{4}.28$	$\bar{4}.02$	$\bar{5}.67$	$\bar{5}.31$	$\bar{6}.95$	$\bar{5}.39$	$\bar{5}.23$	$\bar{5}.12$	$\bar{5}.04$	$\bar{6}.94$
4.0	$\bar{4}.10$	$\bar{5}.79$	$\bar{5}.40$	$\bar{6}.99$	$\bar{6}.58$	$\bar{5}.21$	$\bar{6}.98$	$\bar{6}.80$	$\bar{6}.64$	$\bar{6}.48$
4.5	$\bar{5}.94$	$\bar{5}.59$	$\bar{5}.16$	$\bar{6}.71$	$\bar{6}.26$	$\bar{5}.05$	$\bar{6}.77$	$\bar{6}.52$	$\bar{6}.30$	$\bar{6}.08$
5.0	$\bar{5}.80$	$\bar{5}.41$	$\bar{6}.94$	$\bar{6}.45$	7.96	$\bar{6}.90$	$\bar{6}.58$	$\bar{6}.27$	7.99	7.71
5.5	$\bar{5}.67$	$\bar{5}.24$	$\bar{6}.74$	$\bar{6}.22$	7.69	$\bar{6}.77$	$\bar{6}.40$	$\bar{6}.04$	7.71	7.39
6.0	$\bar{5}.55$	$\bar{5}.09$	$\bar{6}.56$	$\bar{6}.00$	7.44	$\bar{6}.65$	$\bar{6}.24$	7.84	7.46	7.09
6.5	$\bar{5}.44$	$\bar{6}.95$	$\bar{6}.39$	7.80	7.21	$\bar{6}.54$	$\bar{6}.10$	7.65	7.23	8.82
7.0	$\bar{5}.34$	$\bar{6}.82$	$\bar{6}.23$	7.62	7.00	$\bar{6}.44$	7.96	7.48	7.02	8.57
7.5	$\bar{5}.24$	$\bar{6}.70$	$\bar{6}.08$	7.44	8.80	$\bar{6}.34$	7.84	7.32	8.82	8.34
8.0	$\bar{5}.16$	$\bar{6}.59$	7.94	7.28	8.61	$\bar{6}.25$	7.72	7.17	8.64	8.12
8.5	$\bar{5}.07$	$\bar{6}.48$	7.81	7.13	8.43	$\bar{6}.17$	7.61	7.03	8.47	9.92
9.0	$\bar{6}.99$	$\bar{6}.38$	7.69	8.98	8.27	$\bar{6}.09$	7.51	8.90	8.31	9.73
9.5	$\bar{6}.92$	$\bar{6}.28$	7.57	8.84	8.11	$\bar{6}.01$	7.41	8.77	8.15	9.55
10.0	$\bar{6}.84$	$\bar{6}.19$	7.46	8.71	9.96	7.94	7.31	8.65	8.01	9.38

[3] Gauss, *Werke* 3, 130.
[4] Whittaker and Watson, *Modern Analysis*(Cambridge, 4th ed.), Sec. 14.51.

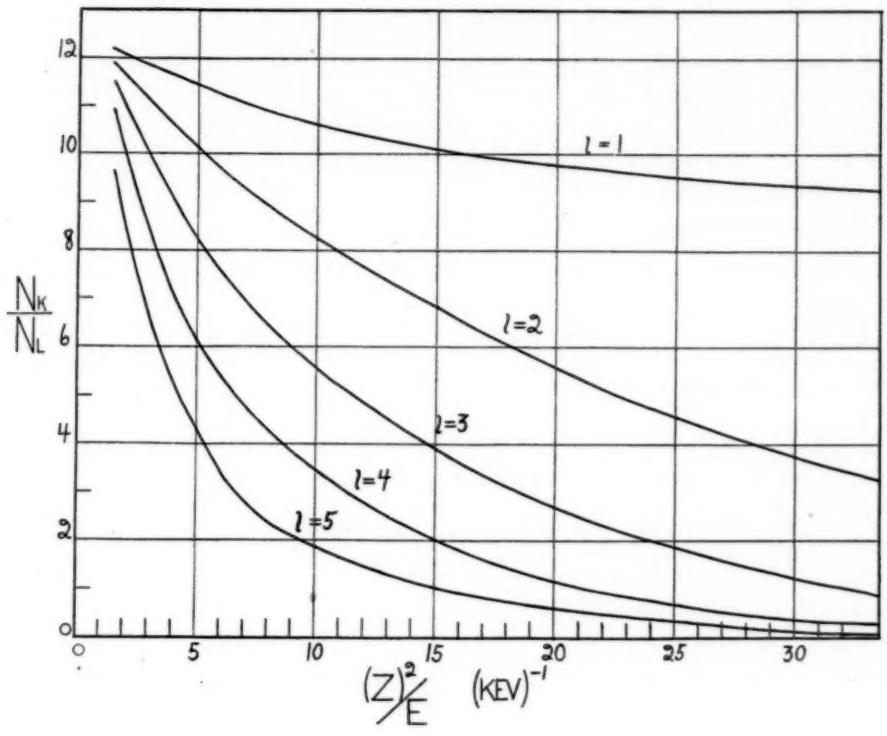

FIG. 1. Curves for N_K/N_L as a function of Z^2/E.

where

$$A_l=2(l+1)[4+(l+3)n^2](4+n^2)^{-1}e^{-2n\tan^{-1}(2/n)}-B_l,$$

$$A_l^+=\tfrac{1}{3}[4(3l^2+9l+4)+n^2(2l^3+15l^2+31l+16)](4+n^2)^{-1}e^{-2n\tan^{-1}(2/n)}-B_l^+,$$

$$A_l^-=(l+1)e^{-2n\tan^{-1}(2/n)}+B_l^-.$$

The B's are conveniently specified by giving the recurrence formulas which they satisfy.

$$(l+1)[4+n^2(l+3)]B_{l+1}=(l+2)[4+n^2(l+4)]B_l+\frac{l2^{4l+1}}{(2l+1)!}\frac{[l^2+n^2]\cdots[1+n^2][4-n^2(l-2)]}{(4+n^2)^l},$$

$$[4(3l^2+9l+4)+n^2(2l^3+15l^2+31l+16)^2]B_{l+1}^+=[4(3l^2+15l+16)+n^2(2l^3+21l^2+67l+64)]B_l^+$$
$$+\frac{l4^{2l+2}}{(2l+1)!}\frac{[(l+1)^2+n^2]\cdots[1+n^2]}{(4+n^2)^l},$$

$$(l+1)B_{l+1}^-=(l+2)B_l^--\frac{(l-2)}{(2l-1)!}2^{4l-3}\frac{[(l-1)^2+n^2]\cdots[1+n^2]}{(4+n^2)^{l-1}}.$$

The first few values are

$$B_1=0, \qquad B_1^+=0, \qquad B_1^-=0,$$

$$B_2=\tfrac{2}{3}, \qquad B_2^+=\tfrac{2}{3}, \qquad B_2^-=1,$$

$$B_3=16(6+n^2)/15(4+n^2), \qquad B_3^+=2(68+13n^2)/15(4+n^2), \qquad B_3^-=\tfrac{4}{3}.$$

3. Numerical Results

In Table I are shown the results of the calculations. The values for the K shell given in the left half of the table were calculated from the formulas previously obtained by Hebb and Uhlenbeck and by Dancoff and Morrison. The right half of the table refers to the L shell and was computed with the aid of Eq. (5). We have tabulated the quantity $\log_{10}[\gamma^{2l+2}(N_e/N_q)]$ since this depends on W and Z only in the combination W/γ^2. The energy of the gamma-ray is related to the momentum of the electron and the parameter n by

$$W=\tfrac{1}{2}(p^2+\gamma^2), \quad W/\gamma^2=(1+n^2)/2n^2$$

for the K shell and by

$$W=\tfrac{1}{2}(p^2+\gamma^2/4), \quad W/\gamma^2=(4+n^2)/8n^2$$

for the L shell. If E represents the energy of the gamma-ray in kev, then $W=E/511$ and $W/\gamma^2=36.7E/Z^2$.

The influence of screening is easily taken into account in Eq. (5) and the table. One has simply to replace Z by $Z_{\text{eff}}=Z-\sigma$ where σ is a screening constant. According to Slater[5] one should take $\sigma=0.30$ for the K shell and $\sigma=4.15$ for the L shell. With neglect of screening it is possible to express N_K/N_L in terms of one parameter W/γ^2 or n, but when screening is taken into account this is no longer true, and N_K/N_L depends essentially on both W/γ^2 and Z. However, the dependence on Z is not strong, and it is still feasible to construct approximate curves giving N_K/N_L directly. These are shown in Fig. 1 plotted against Z^2/E. They are strictly correct only for $Z=35$; for higher Z the curves should be lowered somewhat and for smaller Z raised compared to the positions shown. With $25<Z<50$ the departures are ~ 10 to 20 percent.

4. Conversion of Magnetic Multipole Radiation in the L Shell

Since the conversion of magnetic multipole radiation by s electrons depends essentially on the electron spin,[1] its calculation must be relativistic. In the lighter elements for gamma-ray energies not too near the threshold, the binding of the electron will not play an important part and a good estimate of the magnetic conversion may be obtained by using the Born approximation in evaluating the matrix elements. We have calculated a simple relativistic formula giving the conversion of magnetic multipole radiation in the L shell similar to that obtained by Dancoff and Morrison for the K shell.

The number of electrons ejected per second from the L shell into a solid angle $d\Omega$ is

$$N_e d\Omega=\frac{2\pi e^2}{\hbar}d\Omega|H|^2,$$

where

$$|H|^2=\sum_{\lambda=0}^{\lambda=1}\sum_{\mu=-\lambda}^{\mu=+\lambda}\sum_{\text{spin}}\left|\int dv\psi_f^*(\boldsymbol{\alpha}\cdot\mathbf{A}')\psi_\lambda^\mu\right|^2.$$

$\boldsymbol{\alpha}$ is the vector whose components are the first three Dirac velocity matrices, $\mathbf{A}'$ is the vector potential of a magnetic multipole in the gauge div $\mathbf{A}'=0$, and ψ_f is normalized to unit energy. The sums are taken over the spin and orbital states of the L shell. To evaluate the matrix elements we use the Born approximation, neglecting the influence of the Coulomb field and taking a plane wave for the space-dependent part of ψ_f. Doing the sums and integrals and dividing by the rate of radiation, we have for eight electrons in the L shell:

$$\frac{N_e}{N_q}=\frac{Z^3\alpha^4}{4W}\left(\frac{W+2}{W}\right)^{l+1}\left\{1+\frac{(Z\alpha)^2}{4}\left(\frac{W+2}{W}\right)\left[\frac{l+1}{2l+1}+\frac{l(2l+1)}{4}\left(\frac{2l-1}{2l+1}-\frac{W}{W+2}\right)^2\right]\right\}. \tag{6}$$

[5] J. C. Slater, Phys. Rev. **36**, 57 (1930).

The first term in Eq. (6) comes from the $2s$ electrons and is just one-eighth of the conversion for the $1s$ electrons of the K shell. As pointed out by Dancoff and Morrison, conversion of magnetic radiation by s electrons is essentially relativistic. On the other hand, this is not so for p electrons for which nonrelativistic calculations give a finite conversion. The second term in Eq. (6) is the contribution from the $2p$ electrons. The ratio of the magnetic K conversion to the magnetic L conversion is readily obtained, since the formula for the K shell[1]

$$\frac{2Z^3\alpha^4}{W}\left(\frac{W+2}{W}\right)^{l+1}$$

is contained as a factor in Eq. (6). Like the corresponding ratio for electric multipole radiation, it is sensitive to the multipole order, but for a given case it is definitely larger than that for the electric multipoles.

5. Application to Experiments

A gamma-ray of energy W is emitted in a nuclear transition between states of total angular momentum J and J' and energy difference W. From two constants of the motion, the parity and the total angular momentum of the system nucleus+gamma-ray, we obtain the selection rules.[1] The gamma-ray will be predominantly multipole radiation of the lower order l in the range $|J-J'|\leq l \leq |J+J'|$ permitted by the parity and not reduced by special arguments of symmetry. If it is permitted by the parity, we need consider only electric multipole radiation of order $l=|J-J'|$; if it is not permitted by the parity, the gamma-ray will, in general, be a mixture of magnetic 2^l-pole and electric 2^{l+1}-pole radiation. It would seem that the occurrence of these two cases should be equally probable.

The type of radiation involved may be classified by fitting the experimentally determined values of the total internal conversion coefficient, the K to L conversion ratio, and the lifetime, each of which is sensitive to l. Since the dependence on l of the K to L ratio for electric and magnetic multipoles is different, it provides a method of distinguishing between them. A mixture of the two will appear in a larger K to L ratio than is consistent with the lifetime for electric multipole radiation.

In two cases sufficient information is available to assign the conversion to electric multipole radiation. In Zn^{67} the observed total internal conversion coefficient of ~ 0.5 to 1.0,[6] the K to L ratio of 8,[7] and the short lifetime are in good agreement with the calculated values for electric quadrupole radiation. The 6.4-hour Cd activity has a K to L ratio of one. This could be fitted to electric multipole radiation for $l=4$ if the conversion electrons came from a short-lived product of the disintegration. Experiments have shown that the gamma-ray and the conversion electrons actually come from a 40-sec. isomer of Ag.[8] The 170-kev internally converted gamma-ray of the 1.2-day Te has a K to L ratio of 2.[6] This can be interpreted consistently if the gamma-ray is $\frac{1}{3}$ magnetic multipole radiation, $l=4$, and $\frac{2}{3}$ electric multipole radiation, $l=5$.

From the preceding applications it is clear that the ratio of the K conversion to the L conversion N_K/N_L will be useful in determining the multipole order of gamma-rays of energy $\ll mc^2$. For gamma-rays of energy $\gtrsim mc^2$ the K to L ratio for both electric and magnetic multipoles approaches the same limit ~ 10 for all multipole orders.

The authors wish to thank Professor J. R. Oppenheimer, Professor G. E. Uhlenbeck, and Dr. P. Morrison for their interest and suggestions.

[6] The authors are indebted to Dr. A. C. Helmholz for this information.
[7] G. E. Valley and R. L. McCreary, Phys. Rev. **56**, 863 (1939).
[8] L. W. Alvarez, A. C. Helmholz and E. Nelson, Phys. Rev. **57**, 660 (1940).

Theoretical Maxima and Minima in the Anomalous Scattering of Alpha-Particles

PAUL SELIGMANN
Ryerson Physical Laboratory, University of Chicago, Chicago, Illinois
(Received June 8, 1940)

The work of Wenzel on the determination of theoretical maxima for the anomalous scattering of α-particles by light nuclei under the assumptions of the two-body problem has been generalized to the case of an finite number of l values and extended to include minima. The results have a more general validity if the scattering nucleus has zero spin. Possible applications to analyses of experimental data are discussed. Treatment of the existing data for α-particles scattered by carbon and oxygen indicates that l values at least as large as two are effective in producing the anomalies in both cases. This conclusion is verified for carbon by a phase-shift analysis.

I. INTRODUCTION

EXPERIMENTS on the anomalous scattering of alpha-particles by light elements heavier than He[4] have been performed by Rutherford and Chadwick,[1] Riezler,[2] Brubaker,[3] and Devons.[4] Although no complete phase-shift analyses have been made, the data of Riezler have been studied by Wenzel,[5] who calculated maximum values for the anomaly in the scattering due to a single value of the orbital angular momentum of the incident particle.

In the present paper, the work of Wenzel is extended to include the derivation of expressions for maximum anomalies in the scattering due to combinations of two or more values of the orbital angular momentum of the incident particle as well as expressions for the minimum anomalies under the same conditions. The expressions are then applied to the computation of maxima and minima for the cases of carbon and oxygen. Comparisons with the experimental data are carried through. It is found that values of l at least as large as two are needed to account for the observed results. This is verified in the case of carbon by an actual phase-shift analysis on the Riezler data.

II. THEORETICAL MAXIMA AND MINIMA

The analysis to follow is based on the assumption that the scattering anomaly R for alpha-particles (ratio of the scattering cross section to that for a pure Coulomb field) can be written in the form:[6]

$$R=\left|1+\frac{i\sin^2\frac{1}{2}\theta}{\eta}\exp\left[i\eta\log\sin^2\tfrac{1}{2}\theta\right]\sum_l(2l+1)\exp\left[2i(\sigma_l-\sigma_0)\right](\exp\left[2iK_l\right]-1)P_l(\cos\theta)\right|^2, \quad (1)$$

where θ is the angle of scattering in the center of gravity system, $\eta=2Ze^2/hv$ with v the velocity of the incident α-particles, $\sigma_l=\arg\Gamma(l+1+i\eta)$, and the P_l are zonal harmonics. The K_l are here treated as arbitrary parameters characteristic of the nuclear interaction, dependent on the energy but independent of the scattering angle. As is usual in empirical phase-shift analyses, the sum in the expression will be taken to consist of only a few terms.

The above form for R is the familiar one which can be deduced rigorously when the interaction is treated as a two-body problem with the forces derivable from a potential dependent only on the separation of the α-particle from the nucleus and behaving at infinity like a Coulomb field. The K_l are then the usual phase shifts over Coulomb for the radial wave functions at infinity. However, there is reason to believe that an expression of the form (1) has more general validity, with, of course, a modified interpretation of the K_l. Thus, according to Bethe,[6] the following assumptions are at least necessary and possibly sufficient for its validity:

[1] E. Rutherford and J. Chadwick, Phil. Mag. **50**, 889 (1925).
[2] W. Riezler, Proc. Roy. Soc. **134**, 154 (1931); Ann. d. Physik **23**, 198 (1935).
[3] G. Brubaker, Phys. Rev. **54**, 1011 (1938).
[4] S. Devons, Proc. Roy. Soc. **172**, 127 (1939).
[5] P. Wenzel, Zeits. f. Physik **90**, 754 (1934).
[6] H. A. Bethe, Rev. Mod. Phys. **9**, 69 (1937), §73.

(a) There is no competing reaction, i.e., there is no other reaction such as disintegration of the nucleus which can occur with a probability comparable with that to be described.

(b) Orbital angular momentum is conserved. This condition is most easily satisfied in cases where the scattering nucleus has zero spin, but might be satisfied in other cases as well if the probability of transformation of orbital angular momentum of the α-particle into spin angular momentum of the nucleus is negligible.

In order to bring out the dependence on the K_l, Eq. (1) may be rewritten in the form

$$R=|1-\sum_l S_l \exp[i\alpha_l]+\sum_l S_l \exp[i(\alpha_l+2K_l)]|^2=|A\exp[i\delta]+\sum_l S_l \exp[i(\alpha_l+2K_l)]|^2,$$

where

$$S_l=\frac{(2l+1)\sin^2\tfrac{1}{2}\theta}{\eta}|P_l(\cos\theta)|, \tag{2a}$$

$$\alpha_l=\eta\log\sin^2\tfrac{1}{2}\theta+2(\sigma_l-\sigma_0) \tag{2b}$$

$$+\pi/2 \text{ when } P_l(\cos\theta)>0$$

$$+3\pi/2 \text{ when } P_l(\cos\theta)<0$$

and

$$Ae^{i\delta}=1-\sum_l S_l \exp[i\alpha_l] \tag{3}$$

with A and δ real.

An equivalent and more convenient form for R is

$$R=|A+\sum_l S_l \exp[i(\alpha_l+2K_l-\delta)]|^2. \tag{4}$$

The maxima of R as a function of any finite number of K_l at a fixed value of θ are now readily investigated, since Eq. (4) expresses R as the square of the length of the sum of a number of vectors in the complex plane, and the maximum will be attained when these vectors are all colinear. The desired condition for a maximum is therefore simply that

$$\alpha_l+2K_l-\delta=0 \tag{5}$$

for each value of l involved in the analysis.

Since, for the analysis of experimental data, the K_l are considered arbitrary parameters, a set of K_l values can always be found which will satisfy the set of conditions represented by (5). The maximum of (4) is then

$$R^{\max}=|A+\sum_l S_l|^2=A^2+2A\sum_l S_l+\sum_l S_l^2+2\sum_{l'>l}\sum S_l S_{l'}. \tag{6}$$

The quantity A, evaluated from (3) is

$$A=(1+\sum_l S_l^2-2\sum_l S_l\cos\alpha_l+2\sum_{l'>l}\sum S_l S_{l'}\cos(\alpha_l-\alpha_{l'}))^{\frac{1}{2}}. \tag{7}$$

By the substitution of (7) into (6), and further reduction, one obtains

$$R^{\max}=1+D+2(\sum_l S_l)(1+D-(\sum_l S_l)^2)^{\frac{1}{2}}, \tag{8a}$$

where

$$D=2\sum_l S_l^2-2\sum_l S_l\cos\alpha_l+4\sum_{l'>l}\sum S_l S_{l'}\cos^2\tfrac{1}{2}(\alpha_l-\alpha_{l'}). \tag{8b}$$

Equations (8) then represent the maximum possible scattering for any case for which Eq. (1) is valid.

The minimum scattering may be calculated in an analogous fashion. Examination of Eq. (4) shows that the minimum will be zero unless one of the vectors is greater than the sum of all the others.

When a minimum other than zero is possible it is convenient to consider two cases separately:

Case i. $A > \sum_l S_l$. Then

$$R^{\min} = |A - \sum_l S_l|^2 \tag{9a}$$

and substitution of A from (7) yields

$$R^{\min} = 1 + D - 2(\sum_l S_l)(1 + D - (\sum_l S_l)^2)^{\frac{1}{2}}. \tag{10}$$

Case ii. $S_l > A + \sum_{l' \neq l} S_{l'}$. Then

$$R^{\min} = |S_l - A - \sum_{l' \neq l} S_{l'}|^2. \tag{9b}$$

In this case it is found more convenient to compute the minima from the magnitudes of the vectors concerned rather than to substitute (7) into (9b).

A procedure analogous to the above may be readily carried out for symmetric cases of scattering such as the scattering of α-particles by helium. The expression corresponding to (1) is[7]

$$R = \frac{\left| \frac{e^{-i\eta \log \sin^2 \theta}}{\sin^2 \theta} + \frac{e^{-i\eta \log \cos^2 \theta}}{\cos^2 \theta} + \frac{2i}{\eta} \sum_{l \text{ even}} (2l+1)(e^{2iK_l} - 1) e^{2i(\sigma_l - \sigma_0)} P_l(\cos 2\theta) \right|^2}{\frac{1}{\sin^4 \theta} + \frac{1}{\cos^4 \theta} + \frac{\eta \cos(\eta \log \tan^2 \theta)}{\sin^2 \theta \cos^2 \theta}},$$

which may be reduced to

$$R = \frac{|1 + \tan^2 \theta e^{i\eta \log \tan^2 \theta} - \sum_{l \text{ even}} T_l e^{i\beta_l} + \sum_{l \text{ even}} T_l e^{i(\beta_l + 2K_l)}|^2}{1 + \tan^4 \theta + \tan^2 \theta \cdot \eta \cos(\eta \log \tan^2 \theta)},$$

where

$$T_l = \frac{2(2l+1)\sin^2 \theta}{\eta} |P_l(\cos 2\theta)|,$$

$$\beta_l = \eta \log \sin^2 \theta + 2(\sigma_l - \sigma_0) \quad \begin{matrix} +\pi/2 \text{ when } P_l(\cos 2\theta) > 0 \\ +3\pi/2 \text{ when } P_l(\cos 2\theta) < 0. \end{matrix}$$

The derivation of an expression for the maximum may be carried through as before. The final result is

$$R^{\max} = \frac{1 + D_s - \tan^2 \theta + 2 \tan^2 \theta \sum_{l \text{ even}} T_l + 2(\sum_{l \text{ even}} T_l)[1 + D_s - (\sum_{l \text{ even}} T_l - \tan^2 \theta)^2]^{\frac{1}{2}}}{1 + \tan^4 \theta + \tan^2 \theta \cdot \eta \cos(\eta \log \tan^2 \theta)}$$

where

$$D_s = 2 \tan^2 \theta \cos(\eta \log \tan^2 \theta) + 2 \tan^4 \theta + 2 \sum_{l \text{ even}} T_l^2 - 2 \sum_{l \text{ even}} T_l \cos \beta_l$$
$$+ \sum_{l' > l \text{ even}} \sum T_l T_{l'} \cos^2 \tfrac{1}{2}(\beta_l - \beta_{l'}) - 2 \tan^2 \theta \sum_{l \text{ even}} T_l \cos^2 \tfrac{1}{2}(\eta \log \tan^2 \theta - \beta_l).$$

In the case of the minimum, it is necessary to find the quantity

$$A_s = [1 + D_s - (\sum_{l \text{ even}} T_l - \tan^2 \theta)^2]^{\frac{1}{2}}$$

and compare it as before with the values of T_l.

[7] H. A. Bethe, reference 6, §74.

Expressions for maxima and minima may be applied to experimental data in various ways, the most obvious of which is the comparison of theoretical maxima with those experimental data which give the variation of the scattering with energy at constant angle. This was the type of application made by Wenzel. The procedure consists in making assumptions about the l values effective in a specific case and then comparing the maxima or minima calculated on this basis with the experimental data. If the comparison shows that the experimental curve crosses the theoretical extremum curve, then the particular set of l values chosen is ruled out. As will be shown below, if it so happens that the experimental energy variation curve is tangent to a maximum or minimum curve, then the point of tangency will determine uniquely a set of phase shifts. The validity of such a set can be tested if the experimental angular distribution curve for that particular energy is known, since a theoretical angular distribution curve can be calculated from the phase shifts and then compared with the data. Such cases of tangency, although looked for, were not found in the applications to be discussed below.

It is also of interest to examine the behavior of the extremum curves as a function of angle. For the case of a single phase shift and a given constant energy, the maximum curve plotted as a function of angle will be an envelope of all possible angular distribution curves for varying values of the single K_l. From (5), the value of the phase shift is given by

$$K_l=\tfrac{1}{2}(\delta-\alpha_l). \tag{11}$$

For the maximum R, the quantity δ as determined from (3) is

$$\tan\delta=\frac{S_l\sin\alpha_l}{S_l\cos\alpha_l-1}. \tag{12}$$

When (12) is substituted into (11), one obtains

$$\tan 2K_l=\frac{\sin\alpha_l}{S_l-\cos\alpha_l}. \tag{13}$$

This expression establishes a correspondence between the K_l values and the points on the maximum curve. For every value of θ there can be calculated a value of α_l and also one of S_l and hence of K_l, since the K_l is usually restricted to the range 0 to π or $-\pi/2$ to $+\pi/2$. The same conclusions are readily seen to hold for minimum curves, the slight modification of (5) for this case resulting in corresponding changes in (13) and (14).

These properties may be of use in simplifying phase-shift analyses of experimental data. If an experimental angular distribution curve crosses an extremum curve, the corresponding set of K_l values is automatically excluded. Furthermore, for a single phase shift, if an angular distribution curve is tangent to an extremum curve a value of the phase shift is uniquely determined by Eq. (15) and its ability to account for the observations can be tested by calculation of the theoretical angular distribution curve. Similarly, the case of two phase shifts can be handled by the determination of any points of tangency between the observed curve and any member of the one-parameter family of extremum curves corresponding to the two values of l under consideration.

III. Applications

The cases treated will be those most nearly satisfying the conditions under which Eq. (1) is presumably valid. Of the light elements heavier than He^4, only carbon and oxygen satisfy the conditions of zero spin and nondisintegrability by alpha-particles.

A. Oxygen

The best available data seem to be those of Brubaker[3] and Devons.[4] These consist of energy-dependence curves at six angles. The required maxima and minima for all combinations of l values less than four were calculated and are shown in Fig. 1. Examination of these curves shows that there is no set of l values which will yield consistent maximum and minimum curves for the data, because of the rise above all the theoretical maxima in the experimental curves of Brubaker for higher energies at the largest angles considered. It is difficult to account for this phenomenon. A plausible explanation can be given, however, without assuming values of l greater than three, or that Eq. (1) is not valid. The theoretical curves may vary rapidly with

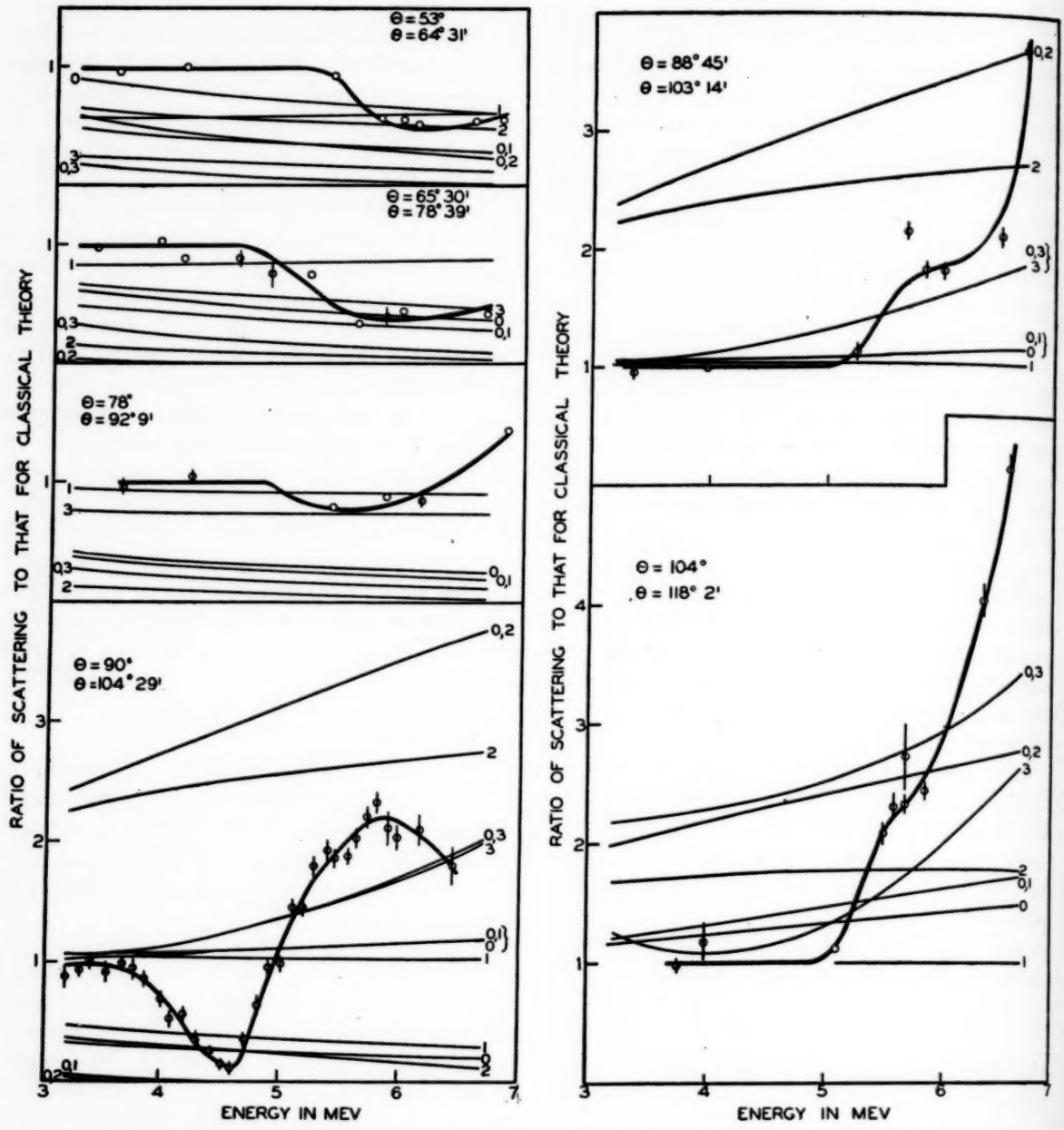

FIG. 1. Scattering of α-particles by oxygen. The heavy curves are the experimental values; the lighter ones are the theoretical maxima and minima, the numerals at the side indicating the l values for which they were computed. Θ denotes the scattering angle in the laboratory system of coordinates; θ, the corresponding angle in the center of gravity system. The experimental curve at Θ=90° is that of Devons; the rest are those of Brubaker. The minimum curves for l=0,2 at Θ=78° and l=0,3 at Θ=90° have not been plotted because they lie too close to zero to be observable on the vertical scale used.

angle[8] and the angular spread in Brubaker's apparatus was large. It is quite possible that a rapid rise in the scattering just above the angles in question would make the type of average value experimentally obtained much higher than the actual scattering at the mean angle given in the data. This conclusion is supported by the Devons data where better angular conditions existed. No such rise occurs, despite the fact that the mean angle given is very close

[8] G. Beck in *Handbuch für Radiologie*, Vol. 6 (1), Chapter IV, §25 (1933).

to one of the Brubaker curves being discussed.

Another marked difference between the two sets of experimental curves is the fact that what appears in Brubaker's work as an irregularity, appears as a maximum in the Devons data. It is quite possible that this "singularity" at 6 Mev, which was ascribed by Brubaker to a resonance level, is in reality a maximum which has been covered up by the much larger scattering at slightly higher energies and angles within the angular range of the detecting apparatus. Under this assumption, the Brubaker and Devons data become consistent in showing that the scattering at this energy is due to a d resonance, for there is no combination of the values 0, 1, and 3 for l, which will give maximum values higher than the experimental and minimum values lower than the experimental for all angles at this energy.

B. Carbon

The data available in this case are those of Riezler[2] and Devons.[4] They consist of energy dependence curves at two angles and one angular distribution curve. The maxima and minima for the energy variation are shown in Fig. 2. It will be observed that the curves differ from those of Wenzel,[5] the discrepancy being due on the one hand to the fact that Wenzel's curves were calculated for 180°, and on the other to an error in Wenzel's expression.[9] It is seen, in a manner similar to that for oxygen, that the resonance in the Riezler data is consistent with an l value of two rather than of one as postulated by Wenzel.

This conclusion was verified by a phase-shift analysis based on Riezler's angular distribution curve, which is at an energy slightly higher than the resonance maximum. It was found that K_0 and K_1 together could not account for the data and that K_2 at least had to be used. The procedure adopted was as follows:

Three points on the angular distribution curve determine, in principle, the three phases K_0, K_1, K_2 as the point of intersection in (K_0, K_1, K_2) space of the three surfaces

$$f_1(K_0, K_1, K_2) = R_1,$$
$$f_2(K_0, K_1, K_2) = R_2,$$
$$f_3(K_0, K_1, K_2) = R_3,$$

where f_1, f_2, and f_3 are the functional forms which Eq. (1) takes for the values θ_1, θ_2, and θ_3 corresponding to the experimental values R_1, R_2, and R_3. In the determination of the intersection of these three surfaces analytic methods were excluded because the complexity of the functional forms eliminated the possibility of an explicit solution; graphical and numerical methods were therefore resorted to. Tables were first constructed for values of f_1 and f_2 as functions of

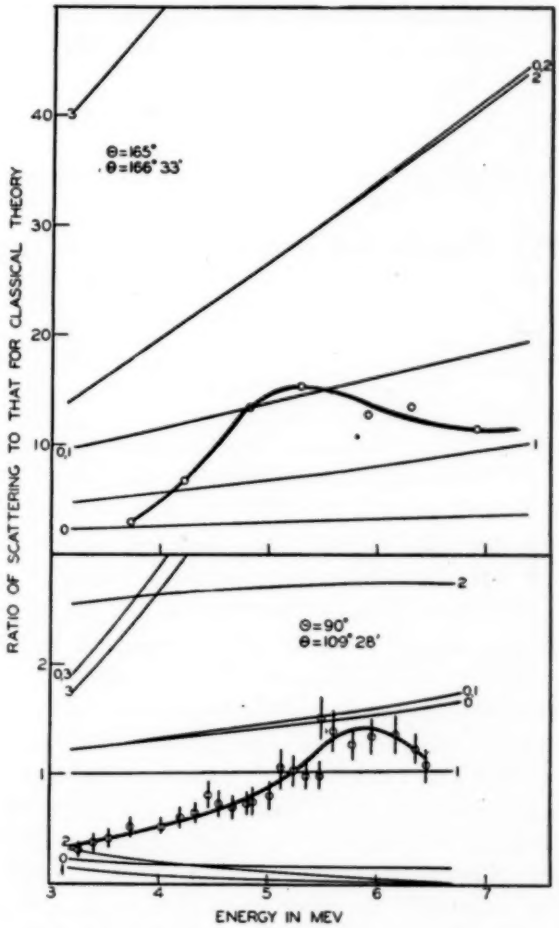

FIG. 2. Scattering of α-particles by carbon. The notation is the same as in Fig. 1. The upper experimental curve is that of Riezler; the lower, that of Devons. On the lower plot, only a few minimum curves have been shown; the rest lie in the same region and very close to those given. On the upper plot, the maximum curves not shown all lie above the range of the graph.

[9] A comparison of the first two terms of Wenzel's expression (12) with the corresponding terms derived from (1) of this paper shows that the relationship between the parameters used is $K_l = \gamma_l - \sigma_l + \frac{1}{2}\pi$. A comparison of the third term of Wenzel's expression with the corresponding term derived from (1) shows that, in Wenzel's expression, $2(\sigma_0 - \sigma_l)$ in the argument of the sine should be replaced by $2\sigma_0 - \sigma_l$.

K_0, K_1, and K_2 at intervals of $\pi/12$ for the parameters in the range 0 to π. For each $K_0=n\pi/12$, $(n=1, 2, \cdots, 12)$, the curves $f_1(n\pi/12, K_1, K_2)=R_1$, $f_2(n\pi/12, K_1, K_2)=R_2$ were then constructed and intersections of curves for the same K_0 were determined by Newton's method. The points of intersection determine the curve in (K_0, K_1, K_2) space on which the intersection of the three surfaces must lie, if, indeed, such an intersection exists at all. This point is determined as that point for which $f_3=R_3$, and was found, again, by Newton's method. The values used were: $\theta_1=142°\ 26'$, $R_1=1.10$; $\theta_2=166°\ 33'$, $R_2=11.5$; $\theta_3=152°\ 23'$, $R_3=3.62$. From these values, the procedure described yielded a set of values $K_0=105°$, $K_1=150°$, and $K_2=94°$. The curve calculated from these values gives approximate agreement with the Riezler data.

As far as the Devons data are concerned, it will be seen that the low values for the scattering at low energies are consistent with any values of the orbital angular momentum with l less than or equal to three, and data at other angles are needed in order to settle the nature of this phenomenon. The experimental maximum at a higher energy has about the same property, but if the theoretical curve found above is prolonged to $\theta=109°\ 28'$ (corresponding to 90° in the laboratory system), a very large discrepancy occurs. The question of whether this discrepancy is due to experimental error or to weaknesses in the theory can only be settled by the publication of more accurate data.

In conclusion, the writer wishes to express his thanks to Professor F. C. Hoyt and Professor Carl Eckart for suggestions in this work.

SEPTEMBER 15, 1940 PHYSICAL REVIEW VOLUME 58

The Distribution in Angle of Alpha-Particles from Lithium Bombarded with Protons

VICTOR J. YOUNG, A. ELLETT AND G. J. PLAIN
State University of Iowa, Iowa City, Iowa

(Received June 28, 1940)

The distribution in angle of alpha-particles from Li^7+H^1 is found to be of the form $1+A\cos^2\theta$. The variation of A with bombarding energy is characterized by a rapid increase in the range 250 to 325 kev presumably indicating resonance to a broad excited level of Be^8.

THE distribution in angle of α-particles from the $Li^7+H^1\rightarrow 2He^4$ reaction has been studied by Kirchner,[1] by Giarratana and Brennecke[2] and by Neuert,[3] all of whom report the distribution to be spherically symmetric. However, the data reported by these observers have in every case been taken at bombarding energies of 270 kev or less, and with relatively large statistical errors. We find that even at 100 kev there is a definite but small departure from spherical symmetry, while at energies of 350 kev the intensity in directions near that of the bombarding beam exceeds that in a direction at 90° to the beam by a factor of the order of 2. This is not surprising as it appears from other considerations that the reaction proceeds by p capture.[4]

APPARATUS

The apparatus is shown in Fig. 1. A lithium target formed by evaporation from the furnace upon one of the surfaces of the hexagonal target support is bombarded by a beam of magnetically resolved protons or H_2^+ ions defined by the apertures. The two upper apertures are $\frac{1}{8}''$ circular holes, while the lowest is reduced to $3/64''$ in the plane of the paper. The target surface being tipped at an angle of 22.5° to the beam results in an approximately rectangular target spot about 3×3 mm. The sensitive volume

[1] F. Kirchner, Physik. Zeits. **34**, 785 (1933).
[2] J. Giarratana and C. G. Brennecke, Phys. Rev. **49**, 35 (1936).
[3] H. Neuert, Ann. d. Physik **36**, 437 (1939).
[4] M. Ostrofsky, G. Breit and D. P. Johnson, Phys. Rev. **49**, 22 (1936).

in front of any one of the eight collector plates can see this target spot through a $\frac{1}{8}''$ clear aperture made vacuum tight with 0.0015" aluminum foil. The hole over which the foil is supported is $\frac{1}{4}''$ in diameter so that particles emerging through the $\frac{1}{8}''$ defining apertures do not strike the foil in the more steeply sloping region near its edge.

For counting, two independent linear amplifiers with associated scales-of-eight[5] and mechanical counters were used. The data obtained are the number of particles observed within a given time interval at any chosen window and the number observed in the same interval at the three forward windows. These three were connected in parallel to the input grid of one amplifier and the chosen window to the other, unless the latter was one of the forward three, in which case only two were in parallel and the total count on the three was obtained by adding the scores of the two counters. In any case the final result is the ratio of the number of particles counted at a given window to the number at the three forward windows. The latter number constitutes a measure of the number of disintegrations occurring in the interval in question. The use of such a monitoring arrangement eliminates obvious errors associated with measurement of bombarding current and the assumption of a yield proportional to the current.

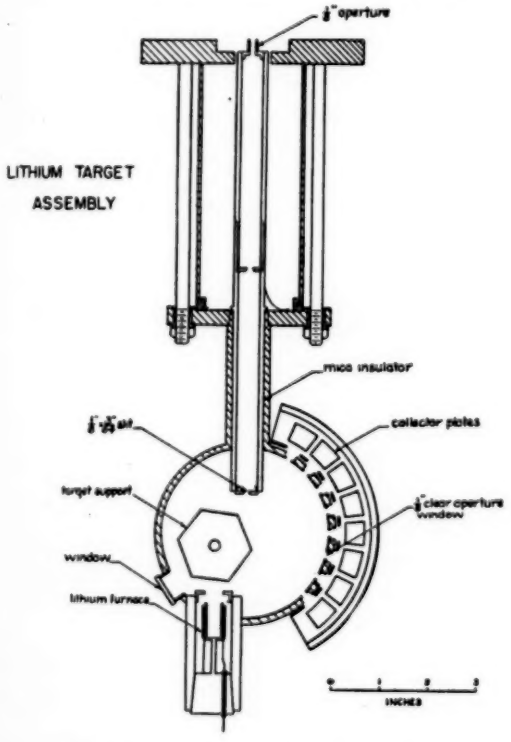

FIG. 1. Cross section of target chamber and defining apertures.

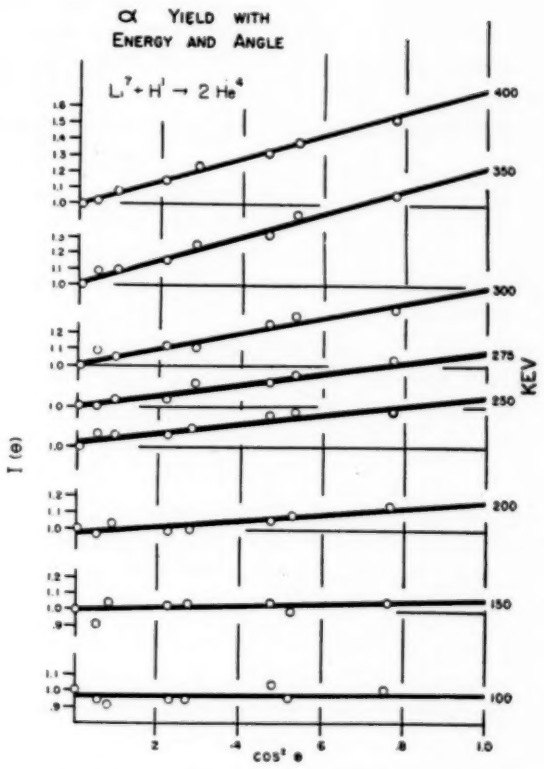

FIG. 2. Distribution in angle of alpha-particles from $Li^7+H^1 \rightarrow 2He^4$ for 8 bombarding energies from 100 to 400 kev. Relative numbers of alpha-particles per unit solid angle *vs.* square of cosine of angle between direction of emission and direction of bombarding beam in center of mass coordinate system.

Bombarding energies are taken from a magnet current *vs.* bombarding energy curve for which the 330-kev fluorine γ-ray resonance served as a fixed point, other points being interpolated by the usual procedure of bringing various m/e spots onto the target. This curve was checked using a resistance voltmeter. (450 10-megohm IRC resistors.)

Thickness of targets was estimated at from 2 to 40 kev stopping power, the thicker targets being used at low energies in order to secure increased yield. The estimate of target thickness was made by determining the yield from the

[5] H. Lifschutz and J. L. Lawson, Rev. Sci. Inst. 9, 83 (1938).

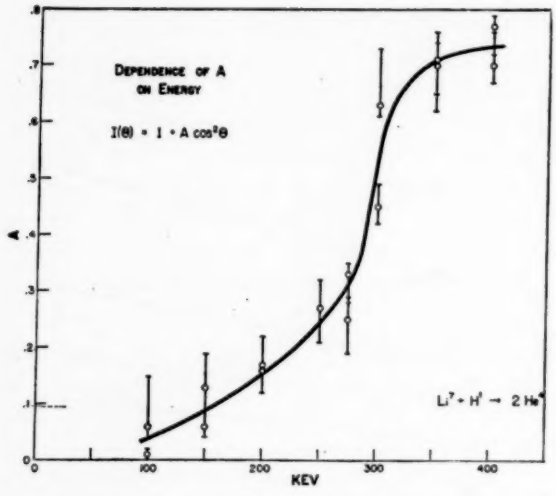

FIG. 3. The variation with bombarding energy of A in the expression $1+A\cos^2\theta$ which is found to represent the distribution in angle of the alpha-particles from $Li^7+H^1\rightarrow 2He^4$.

target in question at a particular bombarding energy, then the yield from a thick target both at this and at a somewhat lower energy so chosen that the decrease in thick target yield was approximately equal to the yield of the thin target. This gives only a rough value of target thickness, but probably good enough for the present purpose which is merely to make sure that the use of even thinner targets would not give sensibly different data. Targets were replaced after bombardment for less than half the time which experience showed to produce appreciable "fatigue."

RESULTS

The relative yields at various angles, transformed to the center of mass coordinate system, normalized to unity at 90°, and plotted against $\cos^2\theta$ are shown in Fig. 2 for several bombarding energies. The number of particles counted at any window is 3000 or more for the window in question and 10,000 or more on the monitor. Straight lines, $1+A\cos^2\theta$, have been drawn through these points by inspection and the values of A so determined are plotted against bombarding energy in Fig. 3. Vertical bars are estimated limits of error arrived at by drawing through the observed points of Fig. 2 straight lines of greatest and least admissible slope, admissibility being determined merely by the best judgment of the authors.

DISCUSSION

The appearance of Fig. 3 obviously suggests resonance to a rather broad excited state of Be^8.

SEPTEMBER 15, 1940 PHYSICAL REVIEW VOLUME 58

The Distribution in Angle of the Long Range Alpha-Particles from Fluorine Bombarded with Protons

W. B. McLEAN, A. ELLETT AND JAMES A. JACOBS
State University of Iowa, Iowa City, Iowa

(Received June 28, 1940)

The distribution in angle of the long alpha-particles from the reaction $F^{19}+H^1\rightarrow O^{16}+He^4$ has been determined at bombarding energies of 330, 375 and 435 kev. This distribution shows a very strong fore and aft asymmetry which varies only slightly with the bombarding voltage. The distribution is well represented by the expression $1+0.66\cos\theta+0.25\cos^3\theta+0.41\cos^5\theta$.

THE present paper is concerned with the distribution in angle of the long range alpha-particles from fluorine bombarded with protons. The apparatus shown in Fig. 1 differs essentially from that described in the previous[1] paper only in the form of target support and in the dimensions of the defining apertures, which are as given in Fig. 1. Targets were prepared by electrolysis of hydrofluoric acid onto tantalum. Care was used to avoid boron contamination arising from the solution of Pyrex glass in the

[1] Young, Ellett and Plain, Phys. Rev. this issue.

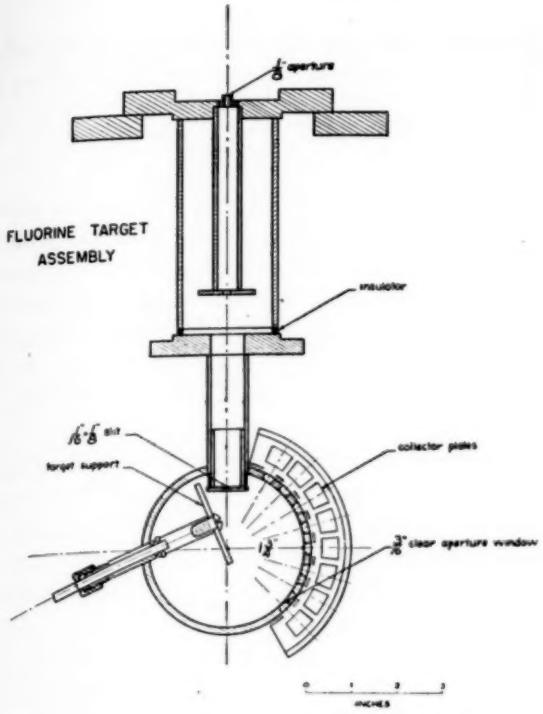

FIG. 1. Cross-sectional view of the target chamber and defining apertures. The chamber is connected to the accelerating tube by means of the greased joint shown at the top of the figure. The target spot is approximately a rectangle 3 mm wide by 4 mm long.

hydrofluoric acid, as the boron reaction has at low energies a much larger yield than the fluorine reaction. Observations were made at 330, 375 and 435 kev by the method outlined in the preceding paper, and the results are presented in Fig. 2.

RESULTS

The distribution shows a very large fore and aft asymmetry, with a strong preference for the forward direction. It appears to change very slightly with bombarding energy. It is true that the points taken at 330 kev and 435 kev do not coincide exactly, but their differences are hardly significant, as the number of counts was only about 500 on a particular point, giving a statistical probable error of 3 percent. These curves were taken with a relatively thin target (apparent width of the gamma-ray resonance was about 40 kev) and since the distribution appeared to change but little with energy we decided that the use of a somewhat thicker target would be legitimate and would permit the reduction of the statistical error. Data secured with a thicker target and larger number of counts (between 2000 and 3000 per point) at a bombarding energy of

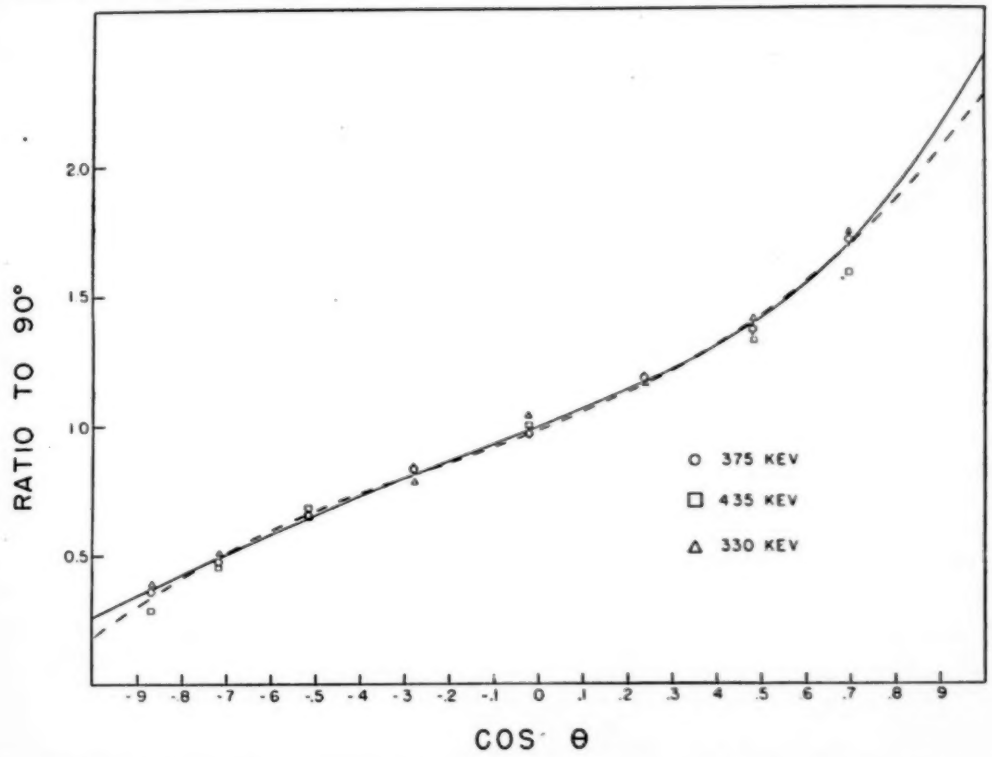

FIG. 2. The distribution in angle in the center of mass system of coordinates of the long range alpha-particles from the reaction $F^{19}+H^1 \rightarrow O^{16}+He^4$. The triangles are for a bombarding energy of 330 kev, the circles for 375 kev, and the squares for 435 kev. The broken line represents the expression $0.985+0.656\cos\theta+0.25\cos^2\theta+0.40\cos^3\theta$ and the solid line the expression $1+0.65\cos\theta+0.11\cos^2\theta+0.44\cos^3\theta+0.24\cos^4\theta$.

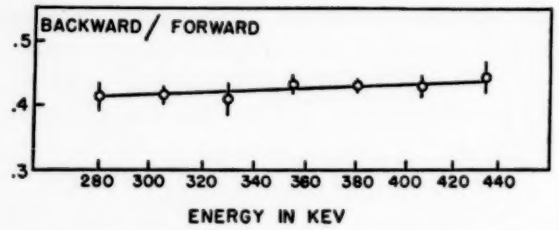

FIG. 3. The ratio of the yield of alpha-particles at three backward windows (105°, 120°, and 135°) to three forward windows (45°, 60°, and 75°) as a function of energy. This curve is plotted in the laboratory system of coordinates.

375 kev have been fitted with an empirical equation by the method of least squares. The best curve of the fourth degree is found to be:

$$1+0.650\cos\theta+0.11\cos^2\theta +0.44\cos^3\theta+0.24\cos^4\theta$$

and is shown in Fig. 2 by the solid curve. The best third degree curve is found to be:

$$0.985+0.656\cos\theta+0.25\cos^2\theta+0.40\cos^3\theta$$

and is shown by the broken curve in Fig. 2. It is clear that the inclusion of the fourth-degree term leads to no significant improvement in fit.

We have not been able to make similar observations at lower energies because of the low yield. However, we determined the ratio of the number of alpha-particles backward to forward (windows at 45°, 60°, and 75° were connected to one amplifier and those at 105°, 120°, and 135° to the other) down to 280 kev. This ratio, plotted as a function of bombarding energy, is shown in Fig. 3.

DISCUSSION

In view of the rather unexpected nature of this distribution we were careful to check possible sources of error in the experimental arrangement. The foils were measured by means of a standard polonium source and a shallow ionization chamber and found to have a stopping power of 2.3 centimeters air equivalent. The outer edges of the collector plates were at a distance of 1.5 centimeters from the foils so that all particles of range greater than 3.8 centimeters should traverse the full depth of the ion chamber. The pulses as seen on the screen of an oscilloscope were of uniform height, indicating that all of the alpha-particles were traversing the full depth of the sensitive volume of the ionization chamber. As a further check the alpha-particles from $B^{11}+H^1$ were observed using the same target chamber and foils. Since these particles, which have a range about one centimeter less than that of the fluorine alpha-particles, were counted at all windows it was certain that none of the fluorine alpha-particles was being lost. The distribution of the alpha-particles from Li^7+H^1 at bombarding voltages below 100 kev was also observed with this apparatus and found to be very nearly spherically symmetric in agreement with the results of the preceding paper.

On the Angular Distribution in the Reaction F^{19} (p, α)

E. GERJUOY
Department of Physics, University of California, Berkeley, California

The angular distribution of the long range α-particles shows marked lack of spherical symmetry, with asymmetry in the forward and backward directions. The distribution is constant with bombarding energy in the range 330 to 435 kev and contains large $\cos\theta$ and $\cos^2\theta$ terms with somewhat smaller and less certain amounts of the third and fourth powers. It is shown that the energy dependence implies broad levels and constant penetrabilities; the latter is found to agree with calculation. The experimental distributions can most simply be accounted for by the assumption that the chief contributions are from three levels of total angular momentum $J=0,1,2$. This leads to the experimental curves without arbitrary assumptions as to the values of the line breadths or detailed assumptions about the nuclear coupling scheme. Powers of $\cos\theta$ higher than the fourth in the angular distribution are not to be expected.

THE data obtained by Ellett and his coworkers on the angular distribution of the long range α-particles from the proton bombardment of F^{19} show a marked lack of spherical symmetry with asymmetry in the forward and backward directions. A distribution containing at least the first and second powers of $\cos\theta$ is required to fit the data at all well, and somewhat smaller and less certain amounts of $\cos^3\theta$ and $\cos^4\theta$ also seem to be present. More explicitly, the observed angular distribution is well represented by a fourth-degree equation of the form:

$$I(\theta)=1+0.65\cos\theta+0.11\cos^2\theta+0.44\cos^3\theta+0.24\cos^4\theta \quad (1)$$

or probably equally well by:

$$I(\theta)=1+0.66\cos\theta+0.25\cos^2\theta+0.41\cos^3\theta. \quad (2)$$

These curves are calculated to fit the data for the bombarding energy of 375 kev but they fit the distributions for bombarding energies of 330 and 435 kev almost as well, and in fact the quadratic equation:

$$I(\theta)=1+0.81\cos\theta+0.13\cos^2\theta \quad (3)$$

fits the data for the three bombarding energies to within less than ten percent.

On first sight these curves, drawn for the coordinate system in which the center of mass is at rest, present some surprising features, namely the pronounced asymmetry in the forward and backward directions, the large coefficients of the $\cos\theta$ and higher terms, and the marked constancy with bombarding energy. It is the purpose of this paper to show that none of these features is inconsistent with our present theory of nuclear reactions, and that it is possible to fit the experimental curves by making reasonable assumptions about the unknown quantities such as line breadths which occur in the theory.*

For any initial state of the system, the angular distribution of the final α-particle wave function, in the coordinate system in which the center of mass is at rest is:

$$\left|\sum_{l,m} A_{li}^{m} Y_l^m(\theta,\phi)\right|^2, \quad (4)$$

where the Y_l^m are the spherical harmonics and the A_{li}^m are complex coefficients which are determined by the initial state i and by the selection rules conserving the parity, total angular momentum J, and total magnetic quantum number m, as well as by the probabilities of capture and emission of the respective particles. The total angular momentum of F^{19} in its ground state is $\frac{1}{2}$. The resultant angular distribution, obtained by summing (4) over the statistically independent initial states i, may then be found by summing over the possible different orientations of the spin S_p of the incoming proton and the total angular momentum I of the F^{19} nucleus. We shall adopt the procedure of summing (4) over the four independent eigenfunctions of the operator $T=I+S_p$, the sum of the spin of the proton and the total angular momentum of the nucleus, indexing these states

* To calculate these unknown quantities explicitly, a detailed knowledge of the coupling scheme in the nucleus would be required. We shall fit these quantities to the experimental curves, and our calculation will then be carried through without any assumptions about the coupling.

by i. Furthermore, taking the parity of the ground state of F^{19} as even, because T is at most 1, and the final spin is 0, the disintegration into an α-particle of orbital angular momentum $L=l$ can only arise from the capture of a proton of equal L to form a compound state of Ne^{20*} of $J=l$.

It is, in principle, possible for any number of levels of $J=l$ of Ne^{20*} to contribute to A_{li}^{m} in (4) and it is clear that a complicated picture of the reaction of this sort could readily lead to the distributions (1), (2) or (3). We shall assume simply that the process is one of resonance with two, or at most three, broad overlapping levels of the compound nucleus Ne^{20*} of total angular momentum $J=0, 1, 2$, and therefore write:

$$A_{li}^{m}=\frac{\alpha_{li}^{m}(\Gamma_{plmi}\Gamma_{alm})^{\frac{1}{2}}e^{\omega_{lmi}}}{E-E_{rl}+\frac{1}{2}i\Gamma_{l}}. \tag{5}$$

In (5) α_{li}^{m} is the amount of $\psi(T_i llm)$ in the initial wave function, where $\psi(TLJm)$ is an eigenfunction of J expressed in terms of the initial eigenfunctions of T and L. Γ_l and E_{rl} are the total width and resonance energy of the level $J=l$ of the compound nucleus, Γ_{plmi} and Γ_{alm} the decay constants from this state to ψ_{li}^{m} and the final Y_l^m, respectively. The ω_{lmi} are determinate, though unknown phases, and finally we may write Γ_{plmi} as $P_{pl}\gamma_{plmi}$ the product of P_{pl}, the penetrability of the barrier for the state whose wave function is ψ_{li}^{m} and the "partial width without barrier," γ_{plmi}, which may also be regarded as the probability of forming the particular compound state once the particle has penetrated the nucleus.‡ It follows from (4) and (5) that the constancy of the distribution with energy will be highly unlikely unless the penetrabilities for the various l's are constant with energy. This necessary condition is satisfied as seen from Table I which summarizes the calculated penetrabilities for the three different energies and for two different values of the radius of F^{19}.

TABLE I. *Calculated penetrabilities of* F^{19}.

E	$R\times10^{13}$	$P_{p1=1}/P_{p1=0}$	$P_{p1=2}/P_{p1=0}$
330 kev	4.00	0.106	0.002
375	4.00	0.110	0.003
435	4.00	0.112	0.003
330	3.52	0.092	0.002
375	3.52	0.094	0.002
435	3.52	0.096	0.002

In addition, in order to explain particularly the constancy of the interference terms in (1), (2) and (3) with energy, it is necessary that the phases of the A_{li}^{m} remain essentially constant in the energy range considered, or at most vary so that the phase differences remain constant. It is this requirement which makes necessary the assumption that the levels are broad. We wish to stress that this requirement and the absence of marked resonance structure in the yield curve for this reaction at these energies, means that the assumption of resonance with three levels implies nothing more than that these levels contribute larger terms to the cross section than other levels. The assumption is by no means necessary and is justified only by the fact that it leads to the observed distribution without arbitrary assumptions about the values of the line breadths. In addition, in order to simplify the calculation, we shall assume at once that the level widths Γ_l in (5) are approximately equal.

We now note the following: The Clebsch-Gordan series gives $\alpha_{li}^{0}=0$ for i corresponding to the initial state $T=1$, $m=0$. This, coupled with the selection rules, will mean that we obtain interference between P and D waves in the final distribution for incident states $T=1$, $m=1$ and -1, and interference between all three S, P, D waves for the $T=0$ state. Or, alternatively, that there is interference between P and D when the z components of the angular momenta of the incident proton and F^{19} nucleus are parallel, and interference between the three waves when the z components are antiparallel. Moreover, we can now drop the i subscript in (5) and index the terms by their m values, $m=0$ corresponding to an initial $T=0$ state and the other m values to initial $T=1$ states. The Γ_{alm} are independent of m while the γ_{plm} and ω_{lm}

‡ The α_{li}^{m} are calculated with the aid of the Clebsch-Gordan series and depend on the order in which the eigenfunctions of the three operators I, S_p and L are combined. We have here chosen to combine first I and S_p but a different initial pair would lead to somewhat different numerical coefficients in (6) below and consequently require a different relation (7) to fit the observed distribution. The physical results are, of course, the same and this is simply a consequence of the fact that the different orders of combining the operators correspond to a different choice of the set of independent states of the initial system.

depend only on whether the initial state was of $T=1$ or 0. With our assumptions the denominator of (5) is approximately the same for all three levels and may be canceled from (4). The Γ_{alm} will form the largest part of Γ_l and our assumption of approximate equality for the Γ_l's implies approximate equality for the Γ_{alm}'s as well, and these may also be canceled. Now insert in (5) the calculated values of the α_l^m and the penetrabilities for $E=330$ kev, $R=4\times10^{-13}$, put $\omega_{00}=0$, and equate the $m=-1$ to the $m=1$ terms. If we substitute and sum over m in (4), the resultant angular distribution is:

$$\begin{aligned}I(\theta)=&\gamma_{00}+0.477\gamma_{11}+0.0125\gamma_{20}\\&-0.225(\gamma_{00}\gamma_{20})^{\frac{1}{2}}\cos\omega_{20}\\&+\cos\theta[1.956(\gamma_{00}\gamma_{10})^{\frac{1}{2}}\cos\omega_{10}\\&-0.220(\gamma_{10}\gamma_{20})^{\frac{1}{2}}\cos(\omega_{20}-\omega_{10})\\&+0.381(\gamma_{11}\gamma_{21})^{\frac{1}{2}}\cos(\omega_{21}-\omega_{11})]\\&+\cos^2\theta[0.954\gamma_{10}-0.477\gamma_{11}+0.075\gamma_{21}\\&-0.075\gamma_{20}+0.675(\gamma_{00}\gamma_{20})^{\frac{1}{2}}\cos\omega_{20}]\\&+\cos^3\theta[0.660(\gamma_{10}\gamma_{20})^{\frac{1}{2}}\cos(\omega_{20}-\omega_{10})\\&-0.381(\gamma_{11}\gamma_{21})^{\frac{1}{2}}\cos(\omega_{21}-\omega_{11})]\\&+\cos^4\theta[0.1125\gamma_{20}-0.075\gamma_{21}].\end{aligned}\quad(6)$$

All unnecessary subscripts have been omitted.

To fit the simple quadratic distribution (3) we need only assume the existence of two overlapping levels of total angular momentum $J=0$ and 1. Dropping the terms in γ_{20} and γ_{21} in (6) we find that with

$$\gamma_{11}=\gamma_{10}=\gamma_{00}/3,\quad(7)$$

the resultant angular distribution will be

$$I(\theta)=1+0.97\cos\omega_{10}\cos\theta+0.13\cos^2\theta.$$

The relation (7) is satisfactory because it is not improbable and is what might be expected from a nucleus in which Russell-Saunders coupling is not valid and the states of equal J are well mixed. Clearly (6) can be made to fit the observed distribution if we assume other sets of overlapping levels. These, however, will in general require rather more arbitrary assumptions about the values of the γ_{lm}'s. In particular, the assumption of S and D resonance will lead to a distribution with a negligible $\cos\theta$ term, and the assumption of P and D resonance requires juggling of the phases in order to make the $\cos\theta$ term larger than the $\cos^3\theta$ term. In addition, with either of these assumptions, as well as for the assumption of the overlapping of all three levels, or S, P, D resonance, the $\cos^4\theta$ term cannot be fitted without always assuming the γ_{2m}'s rather larger than the other γ_{lm}'s.

Because of the numerous assumptions involved, it is not possible to say any more than that the results of this paper suggest the following conclusions: The possibility of fitting the curve so well with the distribution (3) and of deriving this distribution without making arbitrary assumptions as to the values of the level widths seems to indicate that the observed distribution arises chiefly from a resonance, in the sense indicated, with two broad overlapping levels of $J=0$ and 1. The difficulties encountered in attempting to fit the $\cos^4\theta$ term might indicate that this term and the $\cos^3\theta$ term are actually somewhat smaller than observed, but it is quite possible that these terms arise from variation in the level widths among these three levels or even in a more complicated way from the contributions of other more distant levels. It should be noted that the possibility of large P scattering arises from the fairly large value of the penetrability, combined with the normalization factors of the spherical harmonics and the weights corresponding to the more numerous possible orientations of the particles of higher orbital angular momentum in the incident beam. These factors are not quite sufficient to compensate for the decrease of penetrability for the D wave, and the increasingly rapid rise of the potential barrier for waves of higher L make it unnecessary to consider these waves of higher L and similarly they should not appear noticeably in the angular distribution.

I wish to express my thanks to Professor J. R. Oppenheimer and Dr. L. I. Schiff for suggesting this problem and for much encouragement and helpful discussion. I should also like to thank Dr. Ellett for sending me his data in advance of publication.

The Interpretation of Resonances in Nuclear Reactions

G. BREIT
University of Wisconsin, Madison Wisconsin
(Received July 15, 1940)

The theory of resonances in the one-body problem model is systematized. Energy shifts in the apparent position of levels are found. The apparent position of levels in scattering and in γ-ray emission is expected to be the same to within $\sim\Gamma^2/E$ in the usual notation if the only repulsive barrier is the centrifugal one. In the absence of strong repulsive barriers there may be additional shifts of the order Γ. Interference between levels is shown to occur for the scattering cross section in the numerator and the denominator of a fraction in accordance with Eqs. (3.3), (3.6). The artificiality of usual formulas with interference for cross sections is discussed in this connection. The construction of Green's function for two-dimensional separable problems is described. The construction works also for some many-dimensional problems. The reduction of the number of essential dimensions is outlined by a reformulation of the problem in one less dimension. Applications are made to the solution of scattering problems which represent schematically idealized nuclear problems. The single particle potential barriers enter the solutions through the regular and irregular solutions f, g of the radial equation. It is seen from the solutions that the yield may depend on the f and g for various excited states of the residual nucleus. A simplification occurs if the interaction is highly repulsive and is localized in the two-dimensional space of the distances of the particles from the center. In this case the regular functions f for the incident and final state enter linearly in the wave function as in Eq. (15.5). If the interaction region is made large and if the incident state happens to be especially important in the expansion of Green's function then the factor g of the incident wave occurs in the formula for the cross section as in Eq. (16.4). A resonance model is worked out by assuming the interaction to be highly attractive within a circle and repulsive in a ring surrounding the circle in the two-dimensional diagram. The damping constants in the resultant formula contain f^2 as in Eq. (18.8). Here also the single dependence on f^2 is a consequence of having localized the interaction to a narrowly defined radius for the incident particle. In the general case each damping constant involves the g of different states. The examples show that quantitative applications with simplified forms of damping constants and with interference types of dispersion formulas have only a limited validity.

INTRODUCTION

MANY nuclear reactions show excitation curves with pronounced peaks which suggest that there is a resonance of the nuclear system to certain energies. The older discussions of such resonances have been concerned mainly with "one-body" models in which the actual system was schematically represented as a system consisting of the incident particle moving in the field of the bombarded nucleus. The large number of resonances discovered in the bombardment of nuclei by slow neutrons as well as other reactions have shown the inapplicability of the "one-body" picture in the majority of cases and it has become clear that many nuclear particles are usually involved in a resonance state.

The general physical aspects of the problem are clear and well known.[1-5] The bombarded nucleus together with the incident particle can form a state which has an appreciable stability and a relatively long mean life. The width of the state is connected with the mean life by the indeterminacy relation so that a long life corresponds to a sharp level. The compound state is formed with a maximum intensity when the incident particle has a suitable energy and with smaller intensity when the energy of the bombarding particle is varied through the resonance width. The compound state disintegrates in several energetically possible ways producing either scattered incident particles or disintegration fragments.

This picture is good enough for a qualitative understanding of some reactions. It is not entirely satisfactory for quantitative applications. The compound state used in the above description is not defined by the description itself and it is understood in different ways by different physicists. Some think of it in strict analogy to pre-wave-mechanical pictures as being like an excited state of the electronic system of an atom which can emit photons of several different

[1] N. Bohr, Nature **137**, 344 (1936).
[2] G. Breit and E. Wigner, Phys. Rev. **49**, 519 (1936). Referred to as BW.
[3] H. A. Bethe and G. Placzek, Phys. Rev. **51**, 450 (1937).
[4] F. Kalckar, J. R. Oppenheimer and R. Serber, Phys. Rev. **52**, 273 (1937).
[5] H. A. Bethe, Rev. Mod. Phys. **9**, 71 (1937).

wave-lengths by making optical transitions. This picture is correct except for its pre-wave-mechanical features. Without wave mechanics one can describe qualitatively the decay of the atomic level by introducing Einstein's emission probabilities and saying that the atomic system jumps to one or another of the lower levels with the simultaneous emission of a photon. So far the picture is correct. It is then said that the level width is increased because it is not a real stationary level and that the emitted lines will be fuzzy. For a justification of the latter view an appeal is made to the indeterminacy principle. At this point there is a bad mix-up, the word "level" being used in two different ways. In the first part of the picture it was used in the sense of an atomic level, the atomic system being pictured as an idealized mechanical unit with its interaction with radiation neglected. This kind of "level" is a clear concept as long as it lies in the discrete part of the spectrum, as it is supposed to lie. It is not diffuse but absolutely sharp. When, toward the end of the explanation, one speaks of the "level" as diffuse, it is the level of the compound system consisting of atom+radiation field that one is thinking about. This kind of level is not well defined in the above explanation.

The actual situation in the optical case has been cleared up by Weisskopf and Wigner.[6] They showed by a perturbation calculation that if an atom is put into an excited state j, so that it is definitely in that excited state at the time $t=0$, then at later times there is (a) an exponentially decaying probability of the atom being in the excited state j, (b) a growing probability of lower atomic states i, k, l and of photons with corresponding energies. The energies of the photons emitted in the ji jump are approximately equal to the energy difference $E_j-E_i=E_{ji}$ between the upper and lower atomic states. The band of photons emitted in such a jump is found to have an intensity distribution of the resonance type

$$\frac{\text{const.}}{(E-E_{ji})^2+(\Gamma_i+\Gamma_k+\Gamma_l)^2} \qquad (1)$$

with a peak at the emission center E_{ji}. The half-width of the line $2(\Gamma_i+\Gamma_k+\Gamma_l)$ was shown by them to be the sum of half-widths due to separate emissions ji, jk, jl with emission probabilities $4\pi\Gamma_i/h$, $4\pi\Gamma_k/h$, $4\pi\Gamma_l/h$. They have also explained that for the compound system atom +radiation the energy of the initial state (no photons, atom in state j) is not sharp but has a width connected with

$$\Gamma=\Gamma_i+\Gamma_k+\Gamma_l \qquad (1')$$

by the indeterminacy relation. In their theory the "compound state" is the state of the system

atom+radiation field

in which there are no photons and the atom is in the state j. This compound state does not have a definite energy. The energies of the compound system out of which the state is composed have a probability distribution of the form (1).

In the optical problem the optical transition probabilities are small and it is natural as well as useful to define the compound state in the above manner in most cases. But even here this definition is not the most natural under all circumstances. If a group of atomic levels E_1, E_2, etc. have energy differences $|E_{12}|$, $|E_{13}|$, etc. smaller than the energy widths Γ_1, Γ_2, etc. the compound state obtained by exciting the atom to a single level, say E_2, and having no photons at $t=0$ does not correspond to a simple physical condition. The photons emitted from E_2 are reabsorbed so that the atom is partly in E_2 and partly also in other states E_1, $E_3\cdots$. It is here also possible to define[7] the compound state in a sensible manner, at least approximately. This corresponds to an initial state of the atom with a wave function which is a proper linear combination of the wave functions ψ_1, ψ_2, ψ_3 corresponding to E_1, E_2, $E_3\cdots$. If, at $t=0$ the atom is put into such a state, represented by $c_1\psi_1+c_2\psi_2+\cdots$, and if initially there are no photons, then at later times the probability of the atomic state $c_1\psi_1+c_2\psi_2+\cdots$ decreases exponentially and photons appear within a band having a width connected with the mean life of the atomic state by the indeterminacy relation. It is to be noted that the atomic states E_1, E_2, $\cdots$ have

[6] V. Weisskopf and E. Wigner, Zeits. f. Physik **63**, 54 (1930); P. A. M. Dirac, Zeits. f. Physik **44**, 594 (1927); V. Weisskopf, Ann. d. Physik **9**, 23 (1931).

[7] G. Breit, Rev. Mod. Phys. **5**, 91, 117 (1933); G. Breit and I. S. Lowen, Phys. Rev. **46**, 590 (1934).

different energies. One could, if one liked, speak of ψ_2 as the compound state. This would not be an especially useful procedure for physical applications, however, because (a) this compound state would not decay exponentially; (b) the scattering of light is expressed more simply in terms of the states $c_1\psi_1+c_2\psi_2+\cdots$.

It is seen that even in the optical case the definition of the compound state requires caution. The natural and useful definition is that of using linear combinations of atomic states which give an exponentially decaying probability of atomic excitation. This definition is slightly more complicated than that for the problem of Weisskopf and Wigner. It is definite as long as the interaction of the atom with the radiation is sufficiently weak. If the interaction were strong the exponential decay of the atomic excitation would not be obtained and the compound state could not be defined in the above manner.

Nuclear resonances differ from the optical problem in the following respects: (a) There are cases of nuclear resonances in which the peaks of excitation curves overlap. The coupling through emission which has just been discussed can be expected, therefore, to be of more frequent occurrence. (b) In the optical problem the direct change of one type of photon into another is of secondary importance. With Dirac's electron equation it even disappears altogether. The scattering of photons in this formulation can be explained entirely by a succession of emissions and absorptions affecting the wave function. In the general nuclear problem such a simplification cannot be made. Direct transitions between states in the continuum are possible. (c) The effect of a nuclear resonance is of interest also outside the main resonance peak. For slow neutrons this effect gives the $1/v$ law. There is evidence for it also in the γ-rays emitted by Li^7 under proton bombardment below the 440-kev resonance. (d) The interaction of the atom with radiation is always small. The level of the compound system responsible for the resonance is a state in which there are no photons present. The interactions between nuclear particles are not sufficiently small to make the analogous simplification possible.

It is desirable to be able to use experimental yield-energy curves and to draw from them conclusions regarding properties of the nuclear system. Data on widths of nuclear levels due to neutron emission should be comparable with similar data for widths due to proton emission. The comparison can be made only if proper allowance is made for the effect of the Coulomb barrier. A quantitative understanding of the problem is necessary for this purpose. Similarly it is desirable to know whether peaks in yield-energy curves indicate the position of levels of the compound nucleus with any precision and just what relation these energy levels have to ordinary nuclear levels. For example, the compound state $(C^{12})^*$ formed as $B^{11}+H^1$ shows resonances in gamma-emission at proton energies that correspond to a mass difference between $(C^{12})^*-B^{12}$ which would be expected if $(C^{12})^*$ as well as B^{12} were stable and if the binding energy of $(C^{12})^*$ differed from the binding energy of B^{12} only on account of the Coulomb energy. A question of direct physical interest is whether the hypothesis of a symmetric Hamiltonian for nuclear particles makes one expect a coincidence of this sort and to what accuracy. Another type of question arises in observations of the same level under different circumstances. The position of the level is not expected to be exactly the same and some calculations regarding the magnitude of the energy shift are made in the present paper.

For the discussion of such questions it is difficult to use too general and formal treatments such as have been attempted by Bethe and Placzek[3] and by Kapur and Peierls.[8] The point of view of these authors is that one must represent the collision cross section of a reaction as the square of the absolute value of a sum of dispersion-like terms. Even if this were accomplished the result would not necessarily be useful for the above types of questions because it is impossible to compute all the terms in such formulas starting with expressions for nuclear

[8] P. L. Kapur and R. Peierls, Proc. Roy. Soc. **166**, 277 (1938). For the one-body problem at low energies this theory gives levels which correspond to $d\mathfrak{F}/dr=0$ at the nuclear radius. There are no perceptible resonances at such energies in the deuteron problem. This is due to the fact that the KP levels depend on the total energy and the caution, which must be used in attributing to their levels ordinary resonance properties, may be emphasized. These KP levels show pronounced resonance to change of depth of the potential well but not to change of total energy.

forces. It is practically hopeless to analyze data in terms of resonance levels having variable positions depending on the energy of incident particles, as well as on the assumed nuclear radius, as becomes necessary in the formulas of Kapur and Peierls.

The unsatisfactory state of the theory of nuclear resonance makes it desirable to consider some typical examples. Only partial answers to some of the above questions will be arrived at below.

One-Body Problem

(A) Method of complex eigenvalues

For the one-body problem a single and reasonably sharp level in the continuum has simple properties. The absolute value of the wave function, normalized to unit amplitude outside the nucleus, becomes a maximum inside the nucleus for the resonance energy. An incident plane wave of particles asymptotic to $\exp(i\rho\cos\theta)$ and scattered by a central field is represented by

$$\psi=\sum i^L(2L+1)P_L(\cos\theta)\mathfrak{F}_L(\rho)/\rho. \quad (1'')$$

The functions $\mathfrak{F}_L(\rho)$ are normalized to unit amplitude at $\rho=\infty$ and, therefore, a sharp maximum of $\mathfrak{F}_L$ inside the nucleus corresponds also to a maximum of ψ. The asymptotic form of $\mathfrak{F}_L$ is

$$\mathfrak{F}_L\sim e^{iK_L}\sin(\rho-L\pi/2+K_L).$$

For a given L a resonance can be expected in the neighborhood of a complex eigenvalue of the energy. The possibility of using complex eigenvalues of the energy has been first introduced into quantum theory by Gamow.[9] A connection with resonances has been described by Breit and Yost.[10] The latter connection has recently been pointed out again by Siegert.[11] A discussion of the one-body resonances making no use of complex eigenvalues has been given by Wigner and Breit.[2] Kapur and Peierls[8] have given a discussion of one-body resonances also using complex eigenvalues but along different lines.

By the method of complex eigenvalues one considers the asymptotic form of the solution of

$$d^2\Psi_E/dr^2+(2\mu/\hbar^2)(E-V)\Psi_E=0, \quad (2)$$

which is

$$\Psi_E\sim Ae^{ikr}+Be^{ikr}, \quad k=(2\mu E)^{\frac{1}{2}}/\hbar. \quad (2.1)$$

The normalization of Ψ_E is such that

$$(d\Psi_E/dr)_{r=0}=C$$

is kept constant for all energies E. If

$$(d\Psi_E/dr)_{r=0}=0$$

then one uses for C the first nonvanishing derivative of Ψ_E. The function $A(E)$ is supposed to have a root $E_0-i\Gamma_0$ so that

$$A(E_0-i\Gamma_0)=0. \quad (2.2)$$

For small values of $E-E_0+i\Gamma_0$ one has

$$\begin{aligned} A(E)&=(E-E_0+i\Gamma_0)(dA/dE)_{A=0},\\ B(E)&=(E-E_0-i\Gamma_0)(dA/dE)^*_{A=0}. \end{aligned} \quad (2.3)$$

It is assumed that for real E, $A^*=B$. The connection with Gamow's picture of an exponentially decaying state is obtained by forming a wave packet out of the solutions of (2) with real values of the energy. One has then as in Eqs. (20) of BY the following wave packet

$$\frac{\Gamma_0}{\pi}\int_{-\infty}^{+\infty}\Psi_E\frac{\exp(-iEt/\hbar)}{(E-E_0)^2+\Gamma_0^2}dE=\Psi. \quad (2.4)$$

This wave packet outside the nucleus i.e., in the region where (2.1) applies is given by

$$(t>0);\ \Psi=\begin{cases}=2A^*(E_0)\exp\left\{\dfrac{i}{\hbar}(-E_0t+\mu v_0r)-\dfrac{\Gamma_0}{\hbar}(t-r/v_0)\right\} & (t>r/v_0)\\ =0 \quad (t<r/v_0),\end{cases} \quad (2.5)$$

$$(t<0);\ \Psi=\begin{cases}=2A(E_0)\exp\left\{-\dfrac{i}{\hbar}(E_0t+\mu v_0r)+\dfrac{\Gamma_0}{\hbar}\left(t+\dfrac{r}{v_0}\right)\right\} & (t+r/v_0<0)\\ =0 \quad (t+r/v_0>0).\end{cases} \quad (2.6)$$

[9] G. Gamow, Zeits. f. Physik **51**, 204 (1928); H. Casimir, Physica **1**, 193 (1934).
[10] G. Breit and F. L. Yost, Phys. Rev. **48**, 203 (1935). Referred to as BY; G. Breit, Phys. Rev. **40**, 127 (1932).
[11] A. J. F. Siegert, Phys. Rev. **56**, 750 (1939).

Here v_0 is the classical value of the velocity of the particle outside the nucleus and is obtained from

$$E_0=\tfrac{1}{2}\mu v_0^2.$$

According to Eq. (2.5) the wave packet flows out of the nucleus for $t>0$ as a diverging wave. The place at which Ψ becomes zero moves with the constant velocity v_0. For a fixed r the amplitude of Ψ decreases exponentially at the rate $\exp(-\Gamma_0 t/\hbar)$. The sharp break in Ψ at $r=v_0t$ is not strictly correct. It is brought in by the approximation in the calculation of BY in the neglect of terms in $(E-E_0)^2$ in the expansion of k in powers of $E-E_0$. For $t<0$ one obtains only incoming waves as indicated by $-i\mu v_0 r/\hbar$ in Eq. (2.6) and for a fixed r the function increases exponentially with t up to $t=rv_0$. After this time $\Psi=0$ at this r. The wave packet (2.4) represents particles flowing out of the nucleus for $t>0$ and flowing into it for $t<0$.

The mean life of the nucleus is τ given by

$$1/\tau=2\Gamma_0/\hbar=4\pi\Gamma_0/h, \quad (\Gamma_0 \text{ in energy units}) \quad (2.7)$$

$$1/\tau=4\pi\Gamma_0. \quad (\Gamma_0 \text{ in frequency units}) \quad (2.8)$$

In energy units Γ_0 is the coefficient of $-i$ in the complex eigenvalue. This is convenient and this quantity will not be denoted here by $\gamma/2$ as is often done. The value of Γ_0 can be computed in some cases by finding the root of Eq. (2.2). This is not necessary, however, because one has [Eq. (21″) of BY]

$$1/\tau=v_0\Big/\int_0^r|\mathfrak{F}_{E_0}(\rho)|^2dr, \quad (3)$$

where $\mathfrak{F}_{E_0}$ is the real solution of Eq. (2) for $E=E_0$ normalized to have unit amplitude at ∞. The integral in Eq. (3) is taken through the nucleus and through a part of the barrier outside the nucleus along the rapidly decreasing portion of $\mathfrak{F}$. The qualitative meaning of Eq. (3) is clear when it is noted that the numerator is the velocity of the escaping particle while the denominator is the probability of the escaping particle being inside the nucleus. The correctness of the numerical factor 1 in the formula is not immediately obvious since the real function

$$\mathfrak{F}_{E_0}(\rho)$$

represents a standing wave and corresponds to a density (per unit thickness of a spherical shell) of $\frac{1}{2}$ rather than 1. The correctness of the factor 1 is shown in BY. It may also be seen from the fact that inside the nucleus there is little difference between $\mathfrak{F}_{E_0}(\rho)$ and the solution of Eq. (2) for $E=E_0-i\Gamma_0$ normalized so as to make

$$2|A(E_0)|=1 \quad (3.1)$$

in Eq. (2.5). If we assume for the moment that this is the case, the coefficient $2A^*(E_0)$ which multiplies the exp { } in Eq. (2.5) has absolute value one. The rate at which particles flow out for this wave packet is v_0 and Eq. (3) follows. The fact that $\int_0^r|\mathfrak{F}|^2dr$ is practically the same for the normalization (3.1) of the complex eigenvalue solution as for $E=E_0$ and $(|\mathfrak{F}|^2)_{\text{av}}=\frac{1}{2}$ follows from the assumed sharpness of resonance. This in fact makes $\int_0^r|\mathfrak{F}|^2dr$ dependent practically only on C and not on E as long as E is not changed by amounts greater in absolute value than Γ_0; and the real function $\mathfrak{F}_{E_0}(\rho)$ normalized so as to be a sine function of unit amplitude at $\rho=\infty$ satisfies Eq. (3.1) so that $\Psi_{E_0}=\mathfrak{F}_{E_0}$ makes the coefficient of the exp in (2.5) have absolute value 1 in agreement with Eq. (3).

The correctness of the coefficient $2A^*(E_0)$ in (2.5) can be seen without integration if one observes that this coefficient must be $B(E_0-i\Gamma_0)$ and that

$$B(E_0-i\Gamma_0)=A^*(E_0-i\Gamma_0+2i\Gamma_0)=2A^*(E_0).$$

Equation (3) is definite only if the upper limit can be defined without ambiguity. For cases where this cannot be done a more precise formulation has been given by BW. This makes no use of the complex eigenvalue point of view and allows a better definition of the upper limit. It follows from Eqs. (2.3) that for the wave (1″) the probability of finding the particle inside the nucleus is proportional to

$$1/[(E-E_0)^2+\Gamma_0^2]. \quad (3.2)$$

In fact outside the nucleus the normalization of Eq. (3.1) holds. Hence according to (2.3), $|C|^2$ is proportional to (3.2) and $|\mathfrak{F}|^2$ inside the nucleus is, therefore, also proportional to (3.2). A nuclear reaction which is proportional to the probability of finding the incident particle inside

the nucleus is also proportional to this expression and is thus represented by a resonance formula.

According to Eqs. (2.3) the phase of $\mathfrak{F}$ changes by $\sim\pi$ as E changes from $E_0-n\Gamma_0$ to $E_0+n\Gamma_0$ for n appreciably >1. One goes through a resonance for scattering in the vicinity of E_0. The explicit connection with the direct calculation of phase shifts is seen through Eqs. (9), (9'), (10'), (13), (17) of BY. The discussion of BY and of BW at this point is perhaps too brief and the discussion of Siegert brings in a distinction (mentioned in reference 13) between resonance and potential scattering which is rather artificial and does not correspond to the usual one. It may be permissible, therefore, to consider the connections again and to extend them so as to include the combined effect of several complex eigenvalues for the energy. It may be possible to represent the function $A(E)$ defined by Eq. (2.1) as

$$\frac{1}{A(E)}=\frac{1}{\alpha(E)}+\sum_{n=1}^{N}\frac{1}{A'(E_n-i\Gamma_n)}\left(\frac{1}{E-E_n+i\Gamma_n}+\frac{1}{E_n-i\Gamma_n}\right) \tag{3.3}$$

and to have $1/\alpha(E)$ a sufficiently smooth function of the energy to make its more detailed consideration unnecessary.[12] The chance of finding the particle in the nucleus, according to Eqs. (1'') and (2.1) is proportional to

$$|1/A(E)|^2$$

and shows, therefore, the interference of N terms of the resonance type. For special functions $A(E)$ it is possible to have $\alpha(E)=$ const. and $N=\infty$. The analytic character of $A(E)$ is not always easy to ascertain and it appears preferable, therefore, not to assume that $\alpha(E)$ is a constant. The representation of $1/A(E)$ by the sum on the right amounts then to splitting $1/A(E)$ into a smoothly varying part $1/\alpha(E)$ and a part represented by $\sum$ which is designed to take out the bumps of $1/A(E)$. The partial scattering cross section corresponding to angular momentum L is

$$\sigma_L=(2L+1)(\lambda^2/\pi)\sin^2 K_L. \tag{3.4}$$

The phase shift K_L is obtained from (2.1) which yields

$$\exp\{i(K_L-L\pi/2)\}=iB/|B|=iA^*/|A|$$

so that

$$\sin K_L=\frac{i^L}{2|A|}[A^*+(-)^L A] \tag{3.5}$$

and

$$\sigma_L=\frac{(2L+1)\lambda^2}{4\pi}\left[2+(-)^L\frac{A^*}{A}+(-)^L\frac{A}{A^*}\right]=\frac{(2L+1)\lambda^2}{4\pi}\frac{|1/A+(-)^L/A^*|^2}{|1/A|^2}. \tag{3.6}$$

Equation (3.6) shows that the partial scattering cross section σ_L is a fraction in which both the numerator and denominator are sums of the type of Eq. (3.3). This form of the scattering cross section is different from the formulas frequently given in which σ_L is represented as the square of the absolute value of a sum of terms of the type

$$\left|\sum\frac{a_n}{E-E_n'+i\Gamma_n'}\right|^2. \tag{3.7}$$

Even if the form (3.6) should be reducible to (3.7) there is no reason to expect $E_n-i\Gamma_n$ to be equal to $E_n'-i\Gamma_n'$. The representation of partial cross section by "dispersion theoretic formulas" is seen to be somewhat arbitrary in the case of interfering levels. The interference is seen to take place in two sums occurring in the numerator and the denominator of a fraction separately as in Eq. (3.6) rather than in a single sum such as is written in the form (3.7).

[12] Professor G. Y. Rainich has called the author's attention to the fact that for entire functions α may be set = const. and the summation is then an infinite series.

In the vicinity of a single sharp resonance level one may write

$$\frac{1}{A(E)}=\frac{1}{\beta(E)}+\frac{1/A'(E_n-i\Gamma_n)}{E-E_n+i\Gamma_n} \tag{3.8}$$

and consider $1/\beta(E)$ a smooth function of E. Since the whole scattering is due to the potential V no reasonable distinction between $1/\beta(E)$ and $1/A(E)-1/\beta(E)$ as referring to "potential" and "resonance" scattering can be made in this problem.[13] Both terms are in this case due to potential scattering. For large $\beta(E)$ one has

$$\sigma_L \backsimeq (2L+1)\frac{\Lambda^2}{\pi}\frac{[b_n\Gamma_n-a_n(E-E_n)]^2}{(a_n^2+b_n^2)[(E-E_n)^2+\Gamma_n^2]}, \quad (L \text{ even}) \tag{3.9}$$

where

$$1/A'(E_n-i\Gamma_n)=a_n-ib_n$$

and a similar formula for odd L. Thus even neglecting $1/\beta(E)$ in (3.8) one obtains a shift of the maximum of σ_L with respect to the maximum of

$$1/[(E-E_n)^2+\Gamma_n^2].$$

If we neglect the variation of Λ with E the maximum of σ_L is at an energy

$$E=E_n-a_n\Gamma_n/b_n$$

and is displaced with respect to $E=E_n$ by an amount of the order Γ_n. There is thus no exact agreement between the maximum of the scattering cross section and the maximum of the probability of the bombarding particle being in the nucleus. The two maxima are displaced relatively to each other by an amount of the order of magnitude of the width of the level. A displacement of the same order of magnitude can be expected between the maximum of the γ-ray yield curve and the maximum of the scattering cross section. Additional shifts are produced by $1/\beta(E)$ which has been neglected in Eq. (3.9). In the case of Coulomb scattering there are additional shifts which are due to the interference of the Coulomb wave with resonance scattering. These have not been considered above.

(B) The method of regular and irregular functions

The method of complex eigenvalues has some advantages in introducing from the beginning the quantities $E_n-i\Gamma_n$ which appear also in the final formulas. It is not a convenient method, however, for the computation of special problems. The values $E_n-i\Gamma_n$ are troublesome to find and an analysis of the series in Eq. (3.3) by Cauchy's theorem is complicated. The possibility of a continuous distribution of poles in $1/A(E)$ may also enter. For physical applications one needs $1/A(E)$ only for real E. For this reason the method of complex eigenvalues has been partially related to the straightforward use of wave functions for real E by BY to the extent of Eq. (3) of the present paper and by BW in a more thorough manner. The frequency shifts, discussed at the end of the preceding section have not been covered in these papers and will now be considered.

The value of $\mathfrak{F}_L$ outside the potential well ($r>a$) is obtained from the requirement of the continuity of $\mathfrak{F}_L$ and its derivative. This requirement gives

$$\frac{1}{\mathfrak{F}_L}=\frac{1}{F_L}(1-F_LG_L\delta-iF_L^2\delta)=\frac{\mathfrak{F}_L'}{\mathfrak{F}_L}(G_L+iF_L)-(G_L'+iF_L')$$
$$=\frac{1}{G_L}\left[G_L^2\left(\frac{\mathfrak{F}_L'}{\mathfrak{F}_L}-\frac{G_L'}{G_L}\right)+iF_LG_L\left(\frac{\mathfrak{F}_L'}{\mathfrak{F}_L}-\frac{F_L'}{F_L}\right)\right]; \quad (r>a) \tag{4}$$

$$\delta=F_L'/F_L-\mathfrak{F}_L'/\mathfrak{F}_L, \quad F_L'=dF_L/d\rho, \quad G_L'=dG_L/d\rho.$$

[13] Such a distinction is made in the one-body problem by Siegert, reference 11.

The second of the three forms for $1/\mathfrak{F}_L$ follows from the invariance of $\mathfrak{F}_L'(G_L+iF_L)-\mathfrak{F}_L(G_L'+iF_L')=1$ as is seen for large ρ. The functions $F_L(\rho)$, $G_L(\rho)$ are the regular and irregular solutions of the wave equation

$$\frac{d^2F_L}{d\rho^2}-\frac{L(L+1)}{r^2}F_L+\frac{2\mu}{\hbar^2}EF_L=0; \quad k^2=2\mu E/\hbar^2$$

defined by their asymptotic forms $\sin(\rho-L\pi/2)$, $\cos(\rho-L\pi/2)$. The only potential barrier considered for these functions is that due to the term $-L(L+1)/r^2$ in the wave equation. The nuclear potential is supposed to be zero for $r>a$. The maximum of $\mathfrak{F}_L$ for a high potential barrier corresponds approximately to

$$1-F_LG_L\delta=0, \quad G_L'/G_L=\mathfrak{F}_L'/\mathfrak{F}_L. \tag{4.1}$$

The first and second forms of the above equation are equivalent on account of

$$F_L'G_L-F_LG_L'=1 \tag{4.2}$$

and both give for the resonance of $\sigma_{\text{scatt}}/\Lambda^2$

$$\mathfrak{F}_L=iG_L. \tag{4.3}$$

This relation means that at resonance the wave function outside the nucleus is a multiple of the irregular function G_L. For the resonance conditions given by Eqs. (4.1), (4.3) one has

$$\tan K_L=\infty, \quad \sin^2 K_L=1. \tag{4.4}$$

These conditions correspond exactly to maxima of

$$\sigma_L/\Lambda^2 \ (=\text{maximum}) \tag{4.5}$$

and for sharp resonance give also maxima of the scattering cross section. Equations (4.1), (4.3) have been used by BY and BW both in the above sense and as an approximate way of finding the resonance energy of the maximum of $|\mathfrak{F}_L|^2$ inside the nucleus. For future reference there is given below also the formula for K_L

$$\tan K_L=\frac{\mathfrak{F}_LF_L'-\mathfrak{F}_L'F_L}{\mathfrak{F}_L'G_L-\mathfrak{F}_LG_L'}=\frac{F_L^2\delta}{1-F_LG_L\delta}. \tag{4.6}$$

The value of $\mathfrak{F}_L'/\mathfrak{F}_L$ at $r=a$ is determined by the wave equation and the boundary condition at $r=0$. Equations (4.6) and (4) may be used, therefore, for the calculation of $\tan K_L$ and $\mathfrak{F}_L$. The invariance of $\mathfrak{F}_LF_L'-\mathfrak{F}_L'F_L$, $\mathfrak{F}_L'G_L-\mathfrak{F}_LG_L'$ (Wronskians) for changes in ρ together with Eq. (4.2) shows the correctness of the second form of Eq. (4) and the first form of Eq. (4.6) practically without calculation. One has from the asymptotic form for

$$\mathfrak{F}_L=[F_L\cos K_L+G_L\sin K_L]\exp(iK_L), \quad (r>a) \tag{4.7}$$

which can also be verified by means of Eqs. (4.6) and (4).

For high barriers (i.e., high values of $L(L+1)/r^2$) one has

$$G_L(ka)\gg F_L(ka). \tag{5}$$

Equation (4.7) shows then that the maximum of $|\mathfrak{F}_L(ka)|^2$ should fall approximately at $\cos K_L=0$, $\sin K_L=1$. From Eq. (4) one obtains the condition for a maximum or minimum of $|\mathfrak{F}_L|^2$

$$\frac{\partial|\mathfrak{F}_L|^{-2}}{2\partial E}=(F_LG_L\delta-1)\left[\frac{\delta\partial G_L}{F_L\partial E}+\frac{\partial F_L}{F_L^3\partial E}+\frac{G_L\partial\delta}{F_L\partial E}\right]+\delta F_L\frac{\partial(\delta F_L)}{\partial E}. \tag{5.1}$$

Resonance to scattering maximum of σ_{sc}/Λ^2 occurs for $F_LG_L\delta=1$. At the energy for which this

happens one has

$$\frac{\partial|\mathfrak{F}_L|^{-2}}{\partial E}=\frac{\partial(F_L^2\delta^2)}{\partial E}\neq 0 \tag{5.2}$$

and the maximum of the wave function inside the nucleus is not reached at the same energy as the maximum of σ_{sc}/Λ^2. An estimate of the difference in energy for the two maxima will now be made. From the second of the three forms for $1/\mathfrak{F}_L$ given in Eq. (4) one obtains

$$\frac{1}{|\mathfrak{F}_L|^2}=\left[G_L\left(\frac{\mathfrak{F}_L'}{\mathfrak{F}_L}-\frac{G_L'}{G_L}\right)\right]^2+\left[F_L\left(\frac{\mathfrak{F}_L'}{\mathfrak{F}_L}-\frac{F_L'}{F_L}\right)\right]^2. \tag{5.3}$$

One has the relations

$$\frac{\partial}{\partial E}\left(\frac{\partial F_L}{F_L\partial r}\right)=-\frac{k^2}{EF_L^2}\int_0^a F_L^2dr,\quad \frac{\partial}{\partial E}\left(\frac{\partial\mathfrak{F}_L}{\mathfrak{F}_L\partial r}\right)=-\frac{k^2}{E\mathfrak{F}_L^2}\int_0^a\mathfrak{F}_L^2dr \tag{5.4}$$

and the resonance width is determined by

$$\frac{E}{\Delta E}=k\int_0^a|\mathfrak{F}_L|^2dr+\left[\frac{G_L^2E\partial}{k\partial E}\frac{\partial G_L}{G_L\partial r}\right]_{r=a} \tag{5.5}$$

with ΔE determined so that at a distance ΔE from the resonance energy $|\mathfrak{F}_L|^2$ has one-half its maximum value. In the derivation of Eq. (5.5) it has been assumed that the resonance is so sharp that the maximum of $|\mathfrak{F}_L|^2$ occurs at the same energy as the maximum of σ_{sc}/Λ^2. It was found by means of Eqs. (5.4) and

$$-\Delta E\frac{\partial}{\partial E}\left[G_L^2\left(\frac{\mathfrak{F}_L'}{\mathfrak{F}_L}-\frac{G_L'}{G_L}\right)\right]=1, \tag{5.5'}$$

which is suggested for sharp resonance by the last of the three expressions for $\mathfrak{F}_L$ in Eq. (4). At $E=E_0\pm\Delta E$ the scattering cross section is also approximately $\frac{1}{2}$ of its maximum value as is seen from the fact that (5.5′) makes $\tan K_L=1$. For large $|G_L/F_L|$ the scattering cross section and $|\mathfrak{F}_L(ka)|$ are nearly proportional to each other. This is seen from Eq. (4.7) which gives

$$|\mathfrak{F}_L|^2=[1+(F_L/G_L)\cot K_L]^2G_L^2\sin^2K_L. \tag{5.6}$$

The condition which must be satisfied for the proportionality of the scattering cross section in units Λ^2 and the probability of finding the particle in the nucleus is

$$|\mathfrak{F}_L|^2/\sin^2K_L=G_L^2[1+(F_L/G_L)\cot K_L]^2\leqq\text{const.} \tag{5.7}$$

Close to the resonance peak one may neglect $(F_L/G_L)\cot K_L$. The ratio is then G_L^2 which varies with the energy. For high barriers G_L^2 is likely to decrease with the energy. The scattering cross section is relatively higher, therefore, on the higher energy side of the peak around its main part. There is thus no exact correspondence between the maximum chance of the bombarding particle penetrating the nucleus and the scattering cross section and the correspondence becomes poor when

$$|\tan K_L|\sim|F_L/G_L|$$

on account of the first factor in Eq. (5.6). By means of Eqs. (5.4) one obtains

$$\frac{\partial}{\partial E}\left[G_L\left(\frac{\mathfrak{F}_L'}{\mathfrak{F}_L}-\frac{G_L'}{G_L}\right)\right]=-\frac{kG_L}{E_0\mathfrak{F}_L^2}\int\mathfrak{F}_L^2dr-\frac{G_L\partial}{k\partial E}\frac{\partial G_L}{G_L\partial r},$$

$$\frac{\partial}{\partial E}\left[F_L\left(\frac{\mathfrak{F}_L'}{\mathfrak{F}_L}-\frac{F_L'}{F_L}\right)\right]=-\frac{kF_L}{E_0\mathfrak{F}_L^2}\int\mathfrak{F}_L^2dr-\frac{F_L\partial}{k\partial E}\frac{\partial G_L}{G_L\partial r}-\frac{\partial(1/G_L)}{\partial E},$$

$$F_L\left(\frac{\mathfrak{F}_L'}{\mathfrak{F}_L}-\frac{F_L'}{F_L}\right)=-\frac{1}{G_L},\quad (E=E_0).$$

In these formulas E_0 is the energy for which the scattering resonance condition (4.1) is satisfied. The derivatives $\partial/\partial E$ are supposed to be evaluated for $E=E_0$. The same convention will be followed in the following approximate calculations of the energy shift. In the vicinity of $E=E_0$ one has according to Eq. (5.3)

$$\frac{1}{|\mathfrak{F}_L|_E^2}=(E-E_0)^2\left\{\frac{\partial}{\partial E}\left[G_L\left(\frac{\mathfrak{F}_L'}{\mathfrak{F}_L}-\frac{G_L'}{G_L}\right)\right]\right\}^2+\frac{1}{G_L^2}-2\frac{E-E_0}{G_L}\frac{\partial}{\partial E}\left[F_L\left(\frac{\mathfrak{F}_L'}{\mathfrak{F}_L}-\frac{F_L'}{F_L}\right)\right].$$

The second derivative of $[F_L(\mathfrak{F}_L'/\mathfrak{F}_L-F_L'/F_L)]^2$ is neglected. Minimizing the above expression, one obtains the condition

$$E-E_0=-\frac{E_0F_L}{G_L^3}\frac{\dfrac{1}{\mathfrak{F}_L^2}\displaystyle\int\mathfrak{F}_L^2d\rho+\frac{E_0\partial}{k\partial E}\frac{\partial G_L}{G_L\partial r}+\frac{E_0\partial(1/G_L)}{F_L\partial E}}{\left[\dfrac{1}{\mathfrak{F}_L^2}\displaystyle\int\mathfrak{F}_L^2d\rho+\frac{E_0\partial}{k\partial E}\frac{\partial G_L}{G_L\partial r}\right]^2}. \tag{5.8}$$

Similarly the corresponding approximate condition for the minimum of $|G_L/\mathfrak{F}_L|^2$ is

$$E'-E_0=\frac{-F_LE_0}{G_L^3\left[\dfrac{1}{\mathfrak{F}_L^2}\displaystyle\int\mathfrak{F}_L^2d\rho+\frac{E_0\partial}{k\partial E}\frac{\partial G_L}{G_L\partial r}\right]}=-\frac{F_L}{G_L}\Delta E. \tag{5.9}$$

Here ΔE is introduced by means of Eq. (5.5). For high barriers $|F_L/G_L|\ll 1$ and $|E'-E_0|\ll\Delta E$. The *shift* of the peak in such a case is *small in comparison with the resonance width* and the barrier penetration factors enter in the same power in $(E'-E_0)/\Delta E$ as in $\Delta E/E$. According to Eq. (5.8) $E-E_0$ is of the same order of magnitude as $E'-E_0$. The term $(E_0/F_L)\partial(1/G_L)/\partial E$ contains the penetration factors in the same power (zero) as the other two terms in the numerator of Eq. (5.8) and there is no special general distinction between them. It is thus seen that the energy shifts indicated by Eq. (3.9) are the less important the smaller $|F_L/G_L|$.

This conclusion can also be seen from Eq. (5.6). For $E=E_0+\Delta E$ the value of G_L^2 is

$$\sim(G_L^2)_{E_0}+2G_L(\partial G_L/\partial E)E\Big/\int G_L^2d\rho\sim G_L^2+2/\rho.$$

The latter estimate is very rough. The point is that the addition to G_L^2 is of zero degree in G_L^2. The fractional change of the factor G_L^2 at $E=E_0\pm\Delta E$ is roughly $1/G_L^2$ and becomes negligible for high barriers.

The essential point of the approximation to resonance by the method of complex eigenvalues and the method of regular and irregular functions is the same. Resonance occurs nearly at the energy for which $|1/\mathfrak{F}_L|^2$ has a minimum. At the minimum this quantity can be approximated by a parabola and in this approximation formulas of the resonance type are obtained for cross sections.

One-body problem with strong repulsion

If the nucleus is surrounded by a strong repulsive field acting in addition to the centrifugal barrier[14] then it is more natural to modify the above procedure and to introduce wave functions in the repulsive field. The repulsive field has to be continued to $r=0$ and there is some arbitrariness involved in this step. The procedure is illustrated in Fig. 1. The heavy line is the potential energy curve. The light line is the continuation of the

[14] The repulsive field considered here is not the Coulomb field. The calculations are easily modified to include this case also. The notation used here is convenient for applications to many dimensional problems.

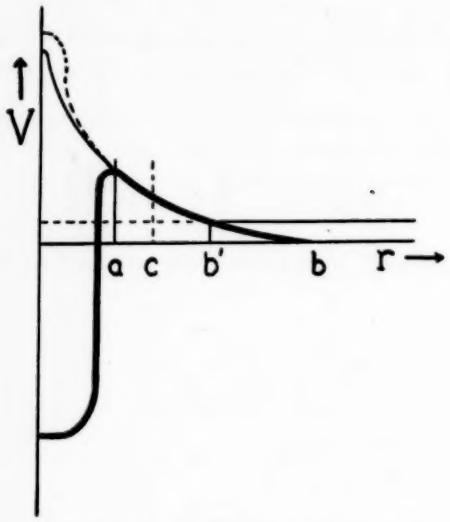

FIG. 1. Potential well and potential barrier. Heavy line represents the actual potential. The light and dotted lines represent auxiliary repulsive potentials. The height of the straight horizontal line is the energy.

repulsive potential to $r=0$. At $r=a$ the two curves part. The region from $r=a$ to $r=b$ is the potential energy barrier and the region $a<r<b'$ is the region of negative kinetic energy. The auxiliary repulsive potential could be drawn in also as the dotted curve and in an infinite number of other ways.

In the auxiliary repulsive potential one obtains a regular solution f_L for r times the radial function. For $r>b$ this function is a linear combination of corresponding functions without any potential. One has

$$f_L=F_L\cos\delta_L+G_L\sin\delta_L,$$
$$g_L=-F_L\sin\delta_L+G_L\cos\delta_L. \quad (6)$$

Here δ_L is the phase shift of f_L with respect to F_L and the function g_L is defined so as to be asymptotically the cos of the same argument of which f_L is the sine. For $r<b$ the function g_L is defined by the radial equation and continuity of the function and its derivative at $r=b$.

From Eq. (6) one obtains

$$f_L'g_L-f_Lg_L'=F_L'G_L-F_LG_L'=1. \quad (6.1)$$

The phase shift of $\mathfrak{F}_L$ with respect to f_L will be denoted by κ_L and one has

$$K_L=\kappa_L+\delta_L. \quad (6.2)$$

For $r>b$ one has according to Eq. (4.7) and Eq. (6)

$$\mathfrak{F}_L=(f_L\cos\kappa_L+g_L\sin\kappa_L)\exp\{i(\kappa_L+\delta_L)\}. \quad (6.3)$$

But from $r=a$ to $r=b$ the actual potential and the auxiliary repulsive potential are the same. Therefore Eq. (6.3) holds also for all $r>a$ and can be applied at $r=a$ where the attractive region begins.

The usefulness of this model is seen in cases in which the region $r<a$ can be pictured as an approximation to the interior of the nucleus, somewhat as in the case of the Coulomb barrier. In such a case one is interested in $|\mathfrak{F}_L|^2$ in this region and one can obtain an idea of these by studying $|\mathfrak{F}_L|^2$ at $r=a$ because in $0<r<a$ the shape of $\mathfrak{F}_L$ does not depend critically on the energy. At $r=a$ one has, on the other hand, $|g_L/f_L|\gg1$ for high barriers and one obtains, therefore, higher reaction yields for approximately those energies for which $\sin\kappa_L=\pm1$. The scattering cross section depends, on the other hand, on $\sin^2K_L$ and one has thus an energy shift between the peaks of the scattering cross section curve and the curve for $|\mathfrak{F}_L|^2$ which is due to δ_L. This shift is of the order of magnitude of the width of the resonance curve multiplied by δ_L/π because the half-value width of the resonance curve corresponds to a change in K_L by $\pi/2$.

It is natural to expect a shift between the energy of maximum penetration and the energy of maximum scattering. Suppose, for instance, that the maximum of $|\mathfrak{F}_L(kc)|^2$ occurs at the same energy (Fig. 1) as the maximum of $\sin^2K_L$. The maximum of $|\mathfrak{F}_L(ka)|^2$ will not occur at the same energy because the barrier between c and a affects the wave function. The ratio $|\mathfrak{F}_L(ka)/\mathfrak{F}_L(kc)|^2$ varies by large amounts in the vicinity of resonance, provided a and c are sufficiently far apart and an energy shift results.

Since the repulsive potential can be continued to the left of a in an infinite number of ways the method of the auxiliary repulsive potential is not unique. Even though the functions f_L, g_L are natural ones to use they are only auxiliary quantities, while $\mathfrak{F}_L$ is the actual wave function.

FIG. 2. Illustrating the cusp at the intersection of $-w$ and v.

One has

$$\tan \kappa_L=\frac{\mathfrak{F}_L f_L'-\mathfrak{F}_L' f_L}{\mathfrak{F}_L' g_L-\mathfrak{F}_L g_L'}=\frac{f_L^2\delta'}{1-f_L g_L\delta'}\left(\delta'=\frac{f_L'}{f_L}-\frac{\mathfrak{F}_L'}{\mathfrak{F}_L}\right), \tag{6.41}$$

$$\frac{1}{|\mathfrak{F}_L|^2}=\left[g_L\left(\frac{\mathfrak{F}_L'}{\mathfrak{F}_L}-\frac{g_L'}{g_L}\right)\right]^2+\left[f_L\left(\frac{\mathfrak{F}_L'}{\mathfrak{F}_L}-\frac{f_L'}{f_L}\right)\right]^2 \tag{6.42}$$

analogously to Eqs. (4.6), (5.3). For the width of resonance $(\Delta E)'$ as measured by $|\mathfrak{F}_L(ka)|^2$ one has

$$\frac{E}{(\Delta E)'}=k\int_0^a |\mathfrak{F}_L|^2 dr+\left[\frac{g_L^2 E\partial}{k\partial E}\frac{\partial g_L}{g_L\partial r}\right]_{r=a}\approx\int_0^b |\mathfrak{F}_L|^2 d\rho;\quad [\text{Maximum of } |\mathfrak{F}_L(ka)|^2]. \tag{6.43}$$

This formula is analogous to Eq. (5.5). The function $\mathfrak{F}_L$ and the other functions occurring in it are evaluated for the energy which gives maximum $|\mathfrak{F}_L|^2$ inside the repulsive barrier, however, and this energy is not the same as the energy for which $\sin^2 K_L$ is a maximum. Equation (6.43) should not be applied, therefore, to an estimate of the width of the scattering resonance in the general case.

A superficial comparison of Eq. (6.43) with Eq. (5.5) appears to indicate that $(\Delta E)'=\Delta E$ because the right-hand sides do not depend on the choice of the upper limit and Eq. (6.43) could equally well be written

$$\frac{E}{(\Delta E)'}=k\int_0^b |\mathfrak{F}_L|^2 dr+\left[\frac{g_L^2 E\partial}{k\partial E}\frac{\partial g_L}{g_L\partial r}\right]_{r=b}. \tag{6.43'}$$

The integral in this formula has the same form as in the corresponding modification of (5.5) *viz.*

$$\frac{E}{\Delta E}=k\int_0^b |\mathfrak{F}_L|^2 dr+\left[\frac{G_L^2 E\partial}{k\partial E}\frac{\partial G_L}{G_L\partial r}\right]_{r=b}, \tag{5.5'}$$

suggesting that $\Delta E=(\Delta E)'$. This is not the case because the energy which must be used in Eq. (6.43′) is for resonance at a while in Eq. (5.5′) the energy is for resonance at b.

Two-Dimensional Problems

Green's function for separable two-dimensional differential equations

Consider the differential equation

$$\mathfrak{L}\psi(x, y)=\left[\frac{\partial^2}{\partial x^2}+\frac{\partial^2}{\partial y^2}+\kappa^2-U(x)-V(y)\right]\psi(x, y)=0 \tag{7}$$

in the domain

$$\begin{aligned} -a<x<a,\\ -\infty<y<+\infty \end{aligned} \tag{7.1}$$

with boundary conditions

$$\psi(a, y)=\psi(-a, y)=0. \tag{7.2}$$

It will be required also that for $y=\pm\infty$ and fixed x the wave function should either vanish exponentially or else be asymptotic to a sum of a finite number of *sine* functions of multiples of y with a number of fixed but arbitrary phase constants. In order that the latter boundary condition be a possible one, it will be supposed that $V(y)$ approaches a constant value faster than $1/y$. This constant value can be made $=0$ without loss of generality by changing κ^2 so as to absorb the difference and this change will be supposed to be made.

The differential equation

$$[d^2/dx^2+\lambda_n-U(x)]u_n(x)=0 \tag{7.3}$$

with the boundary conditions (7.2) defines in $-a<x<a$ an orthonormal set with eigenvalues λ_n. The function $U(x)$ will be supposed to have either no singularities or if it has singularities these will be supposed to be sufficiently innocent so as to allow the existence of the set $\lambda_1<\lambda_2<\lambda_3\cdots$ with a minimum $\lambda_1\neq-\infty$. A particular solution of Eq. (7) is obtained by letting

$$\psi(x, y)=u_n(x)\,Y_k(y) \tag{7.4}$$

with

$$\kappa^2=k^2+\lambda_n \tag{7.5}$$

and with

$$[d^2/dy^2+k^2-V(y)]Y_k(y)=0. \tag{7.6}$$

The dependence of k on n is not explicitly indicated here so as not to complicate the notation. There are two linearly independent solutions of Eq. (7.6). These will be

$$v_k(y),\quad w_k(y),$$

respectively. The solution $v_k(y)$ will be chosen so as to be acceptable at $y=+\infty$ and $w_k(y)$ so as to be acceptable at $y=-\infty$. Thus if at $y=\pm\infty$ the solutions of Eq. (7.6) are of the exponential type, $v_k(y)$ will be taken as the exponentially decreasing branch and similarly $w_k(y)$ will be arranged to be exponentially increasing with increasing y. This condition is schematically indicated in Fig. 2. If, on the other hand, $k^2>0$ then one may use any pair of linearly independent solutions of (7.6) for v and w. These solutions will be restricted later so as to give either diverging or standing waves. In all cases the functions $v_k(y)$, $w_k(y)$ will be normalized so as to have

$$\begin{aligned} v_k'(y)w_k(y)-v_k(y)w_k'(y)&=1,\\ v_k'(y)&=dv_k(y)/dy. \end{aligned} \tag{7.7}$$

If Eq. (7.7) holds for one y then it holds also for all y as a consequence of Eq. (7.6) according to the theorem regarding the invariance of the Wronskian. A kernel will now be defined as follows

$$\begin{aligned} K(x, y; \xi, \eta)&=\sum v_k(y)w_k(\eta)u_n(x)u_n(\xi)\quad (y>\eta),\\ K(x, y; \xi, \eta)&=\sum v_k(\eta)w_k(y)u_n(x)u_n(\xi)\quad (y<\eta), \end{aligned} \tag{8}$$

where it is understood that k varies with n in accordance with Eq. (7.6). It will now be shown that

$$\mathfrak{L}\int\int K(x, y; \xi, \eta)\rho(\xi, \eta)d\xi d\eta=\rho(x, y). \tag{8.1}$$

This equation will be first verified for the special form

$$\rho(\xi, \eta)=u_n(\xi)f(\eta). \tag{8.2}$$

One has

$$\mathfrak{L}\int\int K(x, y; \xi, \eta)u_n(\xi)f(\eta)d\xi d\eta=\mathfrak{L}u_n(x)\int_{-\infty}^{+\infty}Y_k(y, \eta)f(\eta)d\eta=u_n(x)M\int_{-\infty}^{+\infty}Y_k(y, \eta)f(\eta)d\eta,$$

where

$$M=d^2/dy^2+\kappa^2-\lambda_n-V(y) \tag{8.3}$$

and

$$\begin{aligned} Y_k(y, \eta)&=v_k(y)w_k(\eta)\quad (y>\eta),\\ Y_k(y, \eta)&=v_k(\eta)w_k(y)\quad (y<\eta). \end{aligned} \tag{8.4}$$

It remains to show that

$$M\int_{-\infty}^{+\infty}Y_k(y, \eta)f(\eta)d\eta=f(y). \tag{8.5}$$

This is the case according to the construction of Green's function for one-dimensional problems as explained in Courant-Hilbert.[15] The special case in which $v_k(y), w_k(y)$ are the same is excluded for the present. The verification of Eq. (8.5) is indicated next for the sake of completeness.

$$\frac{d^2}{dy^2}\int_{-\infty}^{+\infty} Y_k(y,\eta)f(\eta)d\eta=\frac{d^2}{dy^2}\int_{-\infty}^{y} v_k(y)w_k(\eta)f(\eta)d\eta+\frac{d^2}{dy^2}\int_{y}^{\infty} v_k(\eta)w_k(y)f(\eta)d\eta$$

$$=\frac{d}{dy}\int_{-\infty}^{y} v_k'(y)w_k(\eta)f(\eta)d\eta+\frac{d}{dy}\int_{y}^{\infty} v_k(\eta)w_k'(y)f(\eta)d\eta=[v_k'(y)w_k(y)-v_k(y)w_k'(y)]f(y)$$

$$+\int_{-\infty}^{y} v_k''(y)w_k(\eta)f(\eta)d\eta+\int_{y}^{\infty} v_k(\eta)w_k''(y)f(\eta)d\eta.$$

Substituting this into Eq. (8.5), taking into account (7.7) and $Mv_k(y)=Mw_k(y)=0$ one verifies Eq. (8.5). In order that the calculation in Eq. (8.6) be valid it is necessary that the integrals occurring in it converge. In applications $\rho(x, y)$ will vanish except in a finite range of values of y so that no difficulty will be met in this connection. Having verified Eq. (8.1) for the special form (8.2) one sees also that Eq. (8.1) holds for

$$\rho(x, y)=\sum u_n(x)f_n(y). \tag{8.7}$$

If the sum is finite the above verification applies directly. If the sum in Eq. (8.7) is an infinite series an investigation of convergence is required. This has not been carried out in the general case. No difficulty is expected in this connection in view of the fact that in special cases Eq. (8.1) can be verified by other methods.

According to Eq. (8) two different expressions for K are used depending on whether $y>\eta$ or $y<\eta$. These approach the same value $\sum v_k(y)w_k(y)u_n(x)u_n(\xi)$ as the line $y=\eta$ is approached in the two regions and $K(x, y; \xi, \eta)$ is continuous on that line. The derivative normal to the line appears to be discontinuous being given by

$$[\partial K(x, y; \xi, \eta)/\partial y]_{y=\eta+0}-[\partial K(x, y; \xi, \eta)/\partial y]_{y=\eta-0}=\sum [v_k'(\eta)w_k(\eta)-v_k(\eta)w_k'(\eta)]u_n(x)u_n(\xi). \tag{8.8}$$

On account of Eq. (7.7) the right side of the above formula becomes

$$\sum u_n(x)u_n(\xi)=\delta(x-\xi).$$

The discontinuity in the derivative occurs, therefore, only at the point

$$(x, y)=(\xi, \eta).$$

If one wishes to work with complex eigenfunctions the product $u_n(x)u_n(\xi)$ in Eq. (8) can be replaced by

$$u_n(x)u_n^*(\xi)$$

and the above argument remains essentially unchanged. It should be noted that Eq. (8.1) has been verified only for such forms of ρ which can be expanded as in Eq. (8.7). This is a restriction which must be watched especially at the boundaries of x since the boundary conditions for ψ have no direct significance for ρ.

General plan for applications of Green's function

In proper units one can apply the wave equation (7) to the discussion of a quantum-mechanical system consisting of two particles with the following interpretation of quantities: κ^2=total energy, λ_n=energy of x particle in state n, k^2=energy of y particle, and $u_n(x)$=wave function of x particle in state n.

[15] R. Courant and D. Hilbert, *Methoden der mathematischen Physik* (Springer, Berlin, 2nd edition, 1931), Vol. I, p. 302.

In Fig. 3 a schematic picture of the two-dimensional condition is sketched. The wave function is confined to the strip of width $2a$ on the boundaries of which it is supposed to vanish. The wave equation (7) holds outside the shaded region A. Inside this region another and in general a nonseparable wave equation is supposed to hold. The potential energy function $V(y)$ is schematically represented as a barrier sticking out of the plane of the paper. In order not to complicate the figure $U(x)$ was taken as zero and $V(y)$ was made to vanish in the shaded region. Neither of these simplifications matters in the applicability of the method.

Outside the shaded region the wave function will be represented as

$$\psi(x, y)=\int\int K(x, y; \xi, \eta) \times \rho(\xi, \eta)d\xi d\eta+\psi_0(x, y) \quad (9)$$

and it will be supposed that

$$\rho(x, y)=0 \text{ (outside } A); \quad \mathfrak{L}\psi_0=0. \quad (9.1)$$

In consequence of Eq. (8.1) one has

$$\mathfrak{L}\psi=0, \quad \text{(outside } A). \quad (9.2)$$

The function ψ_0 will be used to represent the incident wave and $\psi-\psi_0$ will give its modification due to the interaction potential in the region A. The reflection of the waves is thus pictured as due to a source density ρ placed within the interaction region. In the analogous electrostatic problem the source density is replaced by a charge density. Since for $k^2>0$ the functions v_k, w_k are not uniquely determined by the boundary conditions and by Eq. (7.7) one can arrange for $\psi-\psi_0$ to have the desired asymptotic forms (outgoing, incoming, standing waves) at $y=\pm\infty$.

Some qualitative information can be obtained from the form of Eq. (9) without special assumptions concerning the location of $\rho(x, y)$. It should be pointed out, however, that in a number of cases it is possible to condense $\rho(x, y)$ to a very narrow strip on the boundary of A. This is a well-known procedure in electrostatics and it corresponds to representing the field due to a collection of charges by an equivalent surface charge density over a surface enclosing the charges. The possibility of doing so depends on the existence of solutions of elliptic differential equations in closed regions with prescribed boundary values and may be seen as follows. A will be bordered by a thin strip of uniform thickness just outside of it and shown shaded in Fig. 4. The original problem will be modified by requiring that the wave equation (7) holds everywhere except in the shaded area of the strip. The values of ψ on the boundary of A (inner boundary of strip) will be taken to be those given by Eq. (9). These values determine a new ψ inside A which will be called φ. φ is a solution of Eq. (7) and is continuous with ψ just outside the shaded border when the border is thin. The normal derivatives $\partial\psi/\partial n$, $\partial\varphi/\partial n$ are not continuous in going across the border as in electrostatics. Leaving the thickness of the strip finite but small one can join φ to ψ by smooth curves across the strip and define a function

$$\begin{aligned}&\Psi=\psi \text{ outside } A,\\ &\Psi=\varphi \text{ inside } A,\\ &\Psi=\text{joining function in strip.}\end{aligned} \quad (9.3)$$

Now form

$$\sigma(x, y)=\mathfrak{L}\Psi. \quad (9.4)$$

From the definition of Ψ it follows that $\sigma(x, y)$ has a value different from zero only in the shaded

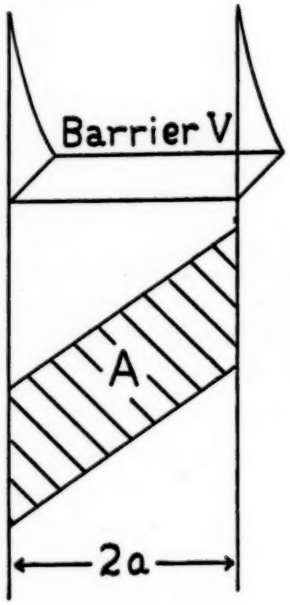

FIG. 3. Illustrating the two-dimensional strip model. The wave function vanishes within the vertical strip of width $2a$. The interaction between the particles takes place within area A.

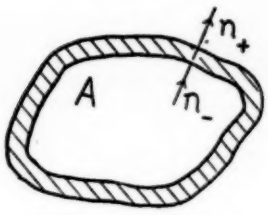

FIG. 4. Illustrating the concentration of source density to the periphery of region in which the interaction takes place.

strip. Consider

$$\chi(x, y)=\psi_0+\int\int K(x, y; \xi, \eta)\sigma(\xi, \eta)d\xi d\eta. \quad (9.5)$$

This function satisfies

$$\begin{aligned} &\mathfrak{L}\chi=0 \text{ outside strip,} \\ &\mathfrak{L}\chi=\sigma \text{ inside strip.} \end{aligned} \quad (9.6)$$

Comparing (9.6) with (9.4) one sees that χ and Ψ satisfy the same inhomogeneous equation. Also ψ_0 and K determine the asymptotic behavior of χ and ψ at $y=\pm\infty$ and one can see that this behavior is the same for ψ and χ. In fact the choice of $v_k(y)$ in (8.4) determines completely whether for $y=\pm\infty$ the nth state of the x particle is excited together with y particle moving towards $y=+\infty$ or $y=-\infty$. It is usually assumed that the specification of boundary conditions in the above sense determines the wave function. Adopting this view, it follows that

$$\begin{aligned} &\chi=\Psi, \\ &\chi=\psi \text{ outside strip.} \end{aligned} \quad (9.7)$$

According to the above one expects to be able to replace a surface distribution of sources by a distribution of sources on a contour in agreement with physical expectation. One has for an infinitely narrow strip

$$\begin{aligned} &\psi=\psi_0+\int K(x, y; \xi, \eta)\sigma(\xi, \eta)ds, \\ &ds^2=d\xi^2+d\eta^2. \end{aligned} \quad (9.8)$$

The integration is carried out along the outer boundary of A and σ in (9.8) is the previous σ integrated through the strip thickness.[16]

The value of ψ on the boundary of A and the differential equation inside A determine ψ inside A and hence also $\partial\psi/\partial n$ at the boundary. The connection between the values of ψ and those of $\partial\psi/\partial n$ on the boundary is linear, therefore, and the problem reduces itself to the solution of linear equations with the density function σ of Eq. (9.8) on the one-dimensional boundary of the region A.

This connection can be shown more explicitly by introducing Green's function for the interior of A for the differential equation obeyed by ψ inside this region. In terms of it one can write

$$\psi(x, y)=\int \bar{K}(x, y; \xi, \eta)\bar{\sigma}(\xi, \eta)ds. \quad (10)$$

The continuity of ψ and its normal derivative on the boundary gives

$$\psi_0(x, y)+\int K(x, y; \xi, \eta)\sigma(\xi, \eta)ds=\int \bar{K}(x, y; \xi, \eta)\bar{\sigma}(\xi, \eta)ds, \quad (10.1)$$

$$\frac{\partial\psi_0(x, y)}{\partial n_+}+\int \frac{\partial K(x, y; \xi, \eta)}{\partial n_+}\sigma(\xi, \eta)ds=\int \frac{\partial\bar{K}(x, y; \xi, \eta)}{\partial n_-}\bar{\sigma}(\xi, \eta)ds, \quad (10.2)$$

the outward drawn normal being denoted by n_+ just outside of the boundary and the inward drawn normal by n_- just inside, as in Fig. 4. The above equations involve values of σ and $\bar{\sigma}$ over the contour. To emphasize this write s for (x, y), s' for (ξ, η) and

$$\begin{aligned} &a(s, s')=K(x, y; \xi, \eta), && \bar{a}(s, s')=\bar{K}(x, y; \xi, \eta), \\ &b(s, s')=\partial K(x, y; \xi, \eta)/\partial n_+, && \bar{b}(s, s')=\partial\bar{K}(x, y; \xi, \eta)/\partial n_-, \\ &f_0(s)=\psi_0(x, y), && g_0(s)=\partial\psi_0(x, y)/\partial n_+. \end{aligned}$$

One has then

$$f_0(s)+\int a(s, s')\sigma(s')ds'=\int \bar{a}(s, s')\bar{\sigma}(s')ds', \quad (10.3)$$

$$g_0(s)+\int b(s, s')\sigma(s')ds'=\int \bar{b}(s, s')\bar{\sigma}(s')ds'. \quad (10.4)$$

[16] The possibility of singularities in σ is not excluded.

The construction of K and $\bar{K}$ thus reduces the problem to the solution of two simultaneous integral equations in a one-dimensional domain in two unknowns σ, $\bar{\sigma}$.

The linear connection between ψ and $\partial\psi/\partial n_-$ on the boundary is expressed in the above by

$$\psi=\int \bar{a}(s, s')\bar{\sigma}(s')ds', \quad \partial\psi/\partial n_-=\int \bar{b}(s, s')\bar{\sigma}(s')ds'.$$

It can also be expressed in other ways. Thus, for example, for the interior of a circle, inside of which the potential is axially symmetric, it is convenient to use polar coordinates and a Fourier expansion according to the azimuthal angle. The values of ψ on the boundary determine then the values of the radial functions by integrals involving $\psi(s)$ linearly and $\partial\psi/\partial n_-$ is a sum of such integrals. The formulas are

$$\psi(s)=\sum (e^{in\theta}/2\pi)\int_0^{2\pi}\psi(a\varphi)e^{-in\varphi}d\varphi; \quad ds=ad\theta$$

$$\partial\psi/\partial n_-=\sum [R_n'(a)/R_n(a)](e^{in\theta}/2\pi)\int_0^{2\pi}\psi(a\varphi)e^{-in\varphi}d\varphi.$$

Substituting into the last of these equations by means of $\psi(s)=f_0(s)+\int a(s, s')\sigma(s')ds'$ and $\partial\psi/\partial n_-=g_0(s)+\int b(s, s')\sigma(s')ds'$ one has a single integral equation in $\sigma(s)$. The radial function belonging to $e^{in\theta}$ is denoted here by R_n.

Degeneracy due to excitation

The spectrum of eigenvalues of Eq. (7.6) may be entirely a continuum. It is then always possible to find both v_k and w_k for every κ and n. If the spectrum of (7.6) has also a discrete part then it may happen that for certain values of κ and $n=\bar{n}$ it is not possible to find both v_{k^*} and w_{k^*}. This happens whenever $\bar{k}^2$ is an eigenvalue of Eq. (7.6) and in this case the energy of the two-particle system in the incident state ψ_0 is just equal to the sum of the energies of the x particle in the state $\bar{n}$ and the y particle in the state $\bar{k}$. The same function $v_{k^*}(y)$ is (to within a constant multiple) the only acceptable one both for $y=+\infty$ and $y=-\infty$, and it is impossible to construct a satisfactory $Y_{k^*}(y, \eta)$ by means of Eq. (8.4) on account of the failure of Eq. (7.7). This degeneracy of the kernel can be avoided by a slight shift of the total energy and no difficulty arises as long as the energy balance for simultaneous capture of the two particles is satisfied approximately rather than exactly. As this condition of resonance is approached the product of the normalizing factors in v_{k^*}, w_{k^*} must be increased in order to satisfy $v_{k^*}'w_{k^*}-v_{k^*}w_{k^*}'=1$ and $Y_{k^*}(y, \eta)\to\infty$. This does not mean, however, that one obtains an infinite probability of the formation of the state because $a(s, s')$ in Eq. (10.3) also becomes large.

For $k\approx\bar{k}$ both v_k and w_k are to within a constant factor $\approx v_{k^*}$ and it will be shown next that

$$Y_k(y, \eta)\sim v_{k^*}(y)v_{k^*}(\eta)/(k^2-\bar{k}^2).$$

This relation can be obtained as follows. From the differential equations satisfied by v_k, w_k, v_{k^*} one obtains

$$[v_{k^*}(y)v_k'(y)-v_k(y)v_{k^*}'(y)]_a^b+(k^2-\bar{k}^2)\int_a^b v_k(y)v_{k^*}(y)dy=0. \tag{11}$$

The asymptotic forms of the logarithmic derivatives of the functions are

$$v_k'(+\infty)/v_k(+\infty)=-(-k^2)^{\frac{1}{2}}; \quad w_k'(-\infty)/w_k(-\infty)=(-k^2)^{\frac{1}{2}},$$
$$v_{k^*}'(+\infty)/v_{k^*}(+\infty)=-(-\bar{k}^2)^{\frac{1}{2}}; \quad v_{k^*}'(-\infty)/v_{k^*}(-\infty)=(-\bar{k}^2)^{\frac{1}{2}},$$

and the functions vanish exponentially as follows

$$v_k(+\infty)=w_k(-\infty)=v_{k^*}(+\infty)=v_{k^*}(-\infty)=0.$$

From Eq. (11) one obtains on setting $a=y$, $b=+\infty$ a formula for $v_k'(y)/v_k(y)-v_{k^*}'(y)/v_{k^*}(y)$. Similarly forming an expression analogous to (11) with $w_k(y)$, $v_{k^*}(y)$ one obtains a formula for $w_k'(y)/w_k(y)-v_{k^*}'(y)/v_{k^*}(y)$. Subtracting the second formula from the first, one obtains

$$v_k'(y)w_k(y)-v_k(y)w_k'(y)=(k^2-\bar{k}^2)\left[\frac{w_k(y)}{v_{k^*}(y)}\int_y^\infty v_k(\eta)v_{k^*}(\eta)d\eta+\frac{v_k(y)}{v_{k^*}(y)}\int_{-\infty}^y w_k(\eta)v_{k^*}(\eta)d\eta\right].$$

In the limit of $k=\bar{k}$ the right side of this equation can be made equal to unity if one sets

$$v_k\approx w_k\approx v_{k^*}/(k^2-\bar{k}^2)^{\frac{1}{2}} \tag{11.1}$$

and normalizes

$$\int_{-\infty}^{+\infty} v_{k^*}^2(y)dy=1. \tag{11.2}$$

The two equations (11.1) can never be satisfied for all y. For fixed y, however, one can make $|k-\bar{k}|$ sufficiently small so that the shape of $v_k(\eta)$, $w_k(\eta)$ is practically the same as that of $v_{k^*}(\eta)$ for $|\eta|<|y|$. For fixed y and sufficiently small $|k-\bar{k}|$ one has then the limiting form

$$Y_k(y,\eta)\approx v_k(y)v_{k^*}(\eta)/(k^2-\bar{k}^2). \tag{11.3}$$

A special problem will now be considered. It will be required that the wave function be zero over the area of a small circle surrounding the point (ξ,η). The wave equation (7) will be supposed to hold outside the small circle. The interaction between the two particles is thus entirely inside the circle where it is infinitely great. This example will be considered in more detail later but at present, by means of Eq. (11.3) one can see the effect of resonance due to excitation. Close to resonance the values of $K(x,y;\xi,\eta)$ over the circle are[17]

$$K_C(x,y;\xi,\eta)\approx u_{n^*}^2(\xi)v_{k^*}^2(\eta)/(k^2-\bar{k}^2)+\sum c'. \tag{12}$$

Here $\sum c'$ represents the effect of other states in K and suffix C means: on circle. Denoting the incident wave by $\psi_0(x,y)$ one has the approximate solution

$$\psi(x,y)=\psi_0(x,y)-\psi_0(\xi,\eta)\frac{u_{n^*}(x)u_{n^*}(\xi)v_k(y)v_k(\eta)/(k^2-\bar{k}^2)+\sum' u_n(x)u_n(\xi)Y_k(y,\eta)}{u_{n^*}^2(\xi)v_{k^*}^2(\eta)/(k^2-\bar{k}^2)+\sum c'\,u_n(x)u_n(\xi)Y_k(y,\eta)}. \tag{12.1}$$

This formula is approximate only. Its main inaccuracy lies in the assumption that $\sum c'$ in the denominator has the same value for all points on the circle. This is the case to a first approximation, the logarithmic term in $(x-\xi)^2+(y-\eta)^2$ being predominant in $\sum c'$ for small circles. The effect of a single term in the summation in Eq. (12.1) may include in it a wave extending to $y=\infty$. The above formula shows that for $k\sim\bar{k}$ these waves become small. An individual term behaves as

$$-\frac{\psi_0(\xi,\eta)}{\sum c'}\left[1-\frac{u_{n^*}^2(\xi)v_{k^*}^2(\eta)/\sum c'}{k^2-\bar{k}^2+u_{n^*}^2(\xi)v_{k^*}^2(\eta)/\sum c'}\right]Y_k(y,\eta)u_n(x)u_n(\xi) \tag{12.2}$$

and shows a maximum for $k^2=\bar{k}^2-u_{n^*}^2(\xi)v_{k^*}^2(\eta)/\sum c'$. The latter equation cannot be satisfied accurately because $\sum c'$ is only approximately real. The resonance has, therefore, a finite width. At the maximum the above calculation breaks down because then the parts of $u_{n^*}(x)u_{n^*}(\xi)Y_k(y,\eta)$ which have been neglected become important. For $k=\bar{k}$, however, the above scattered wave is zero. This, of course, is also only an approximation. For $k=\bar{k}$ one has from (12.1)

$$\psi(x,y)=\psi_0(x,y)-\psi_0(\xi,\eta)u_{n^*}(x)v_{k^*}(y)/[u_{n^*}(\xi)v_{k^*}(\eta)]. \tag{12.3}$$

[17] It is natural that u_{n^*} and v_{k^*} occur symmetrically in this case.

This expression is an exact solution of the wave equation and it vanishes at (ξ, η). It is, therefore, also small on the little circle. It is understandable that the scattering due to the interaction within the circle is small at this energy.[18] The incident wave is in a sense "sucked in" to produce excitation.

Extension to several dimensions

An extension of Green's function given by Eq. (8) may be made by generalizing the variable x to a set of variables: $x_1, x_2, \cdots x_s$. The functions $u_n(x_1, x_2, \cdots, x_s)$ are supposed to satisfy

$$\left[\frac{\partial^2}{\partial x_1^2}+\cdots+\frac{\partial^2}{\partial x_s^2}+\lambda_n-U(x_1, \cdots, x_s)\right]u_n(x_1, \cdots, x_s)=0. \tag{13}$$

The λ_n and u_n are supposed to form a complete and discrete set of eigenvalues and of eigenfunctions for this equation. The wave equation outside the region of configuration space in which the particles interact is

$$\mathfrak{L}\psi(x, \cdots, x_s; y)=0 \tag{13.1}$$

and

$$\mathfrak{L}=\frac{\partial^2}{\partial x_1^2}+\cdots+\frac{\partial^2}{\partial x_s^2}+\frac{\partial^2}{\partial y^2}+\kappa^2-U(x_1, \cdots, x_s)-V(y). \tag{13.2}$$

Defining k^2 as before and subjecting $v_k(y)$, $w_k(y)$ to Eqs. (7.6), (7.7) one defines the kernel

$$\begin{aligned} K(x_1, \cdots, x_s, y; \xi_1, \cdots, \xi_s, \eta)&=\sum v_k(y)w_k(\eta)u_n(x_1, \cdots, x_s)u_n(\xi_1, \cdots, \xi_s) \quad (y>\eta)\\ &=\sum v_k(\eta)w_k(y)u_n(x_1, \cdots, x_s)u_n(\xi_1, \cdots, \xi_s) \quad (y<\eta). \end{aligned} \tag{13.3}$$

One verifies in the same way as before that

$$\mathfrak{L}\int K(x_1, \cdots, x_s, y; \xi_1, \cdots, \xi_s, \eta)\rho(\xi_1, \cdots, \xi_s, \eta)d\xi_1 \cdots d\xi_s d\eta=\rho(x_1, \cdots, x_s, y). \tag{13.4}$$

In applying the above generalization one may think of $x_1, x_2, \cdots x_s$ as describing the internal condition of the bombarded nucleus and of the coordinate y describing the incident particle. Green's function K is designed so as to represent coherently scattered waves and scattered waves with excitation of the bombarded nucleus by means of the source density $\rho(x_1, \cdots, x_s, y)$.

The restriction of the operator $\mathfrak{L}$ to the form of Eq. (13.2) is not essential. The method still works for

$$\mathfrak{L}=N+\kappa^2-V(y),$$

where N is the wave equation operator (multiple of Hamiltonian) for the bombarded nucleus. Equation (13) should then be replaced by

$$(N-\lambda_n)u_n(x_1, \cdots, x_s)=0.$$

The operator N may contain exchange forces. The separability of N into parts corresponding to $x_1, \cdots, x_s$ is not assumed and is not necessary for the working of the method. The degeneracy due to excitation works out very similarly in the many-dimensional and the two-dimensional models.

Modification for central fields

A schematic discussion of radial functions for particles colliding with a nucleus can be carried out along the above lines. The differential equation

$$\mathfrak{L}\psi(r_1, r)=\left[\frac{\partial^2}{\partial r_1^2}+\frac{\partial^2}{\partial r^2}+\kappa^2-V_1(r_1)-V(r)\right]\psi(r_1, r)=0 \tag{14}$$

[18] Minima in scattering can be produced also in other ways as has been brought out by M. R. MacPhail, Phys. Rev. 57, 669 (1940) from the general point of view of interference.

will be considered subject to boundary conditions

$$\psi(0, r)=\psi(r_1, 0)=0. \tag{14.1}$$

The distances of particles 1, 2 from the center of gravity of the system are here denoted by r_1, r. The potential energies V_1, V are supposed to include the centrifugal force terms $L(L+1)/r^2$ which enter if the angular momentum $L\neq 0$. Particle 1 will be supposed to be confined to the nucleus and, as in the preceding section, the scheme may be generalized to include the case of a composite system instead of the single particle 1.

Equation (14) corresponds to the two particles being in separate fields of force described by $V_1(r_1)$, $V(r)$. By an extension of the previous scheme one can discuss the interaction between the particles provided the potential energy is taken to be a function of r_1 and r only. Actually the potential energy is also a function of the polar angles of the two particles and the present discussion is incomplete in this respect. One may hope, however, that this idealization spoils only the quantitative side of the problem but does not affect radically the qualitative conclusions regarding effects of resonance.

The eigenvalues λ_n of

$$[\partial^2/\partial r_1^2+\lambda_n-V_1(r_1)]u_n(r_1)=0 \tag{14.2}$$

are supposed to form a discrete set and the eigenfunctions u_n are normalized by

$$\int_0^\infty |u_n(r_1)|^2 dr_1=1.$$

The number k is defined by

$$\kappa^2=\lambda_n+k^2 \tag{14.3}$$

and functions f_k, g_k are defined by

$$\begin{aligned}[d^2/d\rho^2+1-k^{-2}V(\rho/k)]f_k(\rho)&=0,\\ [d^2/d\rho^2+1-k^{-2}V(\rho/k)]g_k(\rho)&=0.\end{aligned} \tag{14.4}$$

The function f_k will be regular at $r=0$ and will be normalized so as to be asymptotic to a sine function of unit amplitude at large ρ. The function g_k will be asymptotic to a cosine function and g_k+if_k will contain ρ only as $e^{i\rho}$. One has the relation

$$f_k'g_k-f_kg_k'=1, \tag{14.5}$$

the differentiations being performed with respect to ρ. If the functions f_k, g_k are not oscillatory ($k^2<0$) then f_k will still be understood to be regular at $r=0$ and g_k will be made to vanish exponentially at $r=\infty$. In this case the normalizing constants in f_k, g_k will be adjusted so as to satisfy Eq. (14.5). The exceptional case analogous to that already discussed under "Degeneracy due to excitation" may also arise and can be treated analogously to Eqs. (11)$\cdots$(12.3).

The function $g_k(\rho)$ is analogous to $v_k(y)$ inasmuch as it is always admissible at $+\infty$. The smaller of the two arguments of the kernel cannot occur in g_k since g_k is not admissible at $r=0$. One is thus led to

$$\begin{aligned}-K_S(r_1, r; r_1', r')&=\sum u_n(r_1)u_n(r_1')f_k(kr')g_k(kr)/k \quad (r>r')\\ &=\sum u_n(r_1)u_n(r_1')f_k(kr)g_k(kr')/k \quad (r<r').\end{aligned} \tag{14.6}$$

The above kernel has the suffix S so as to indicate that its asymptotic behavior at $r=\infty$ is that of a standing wave. The $-$ sign present in Eq. (14.6) is due to the fact that substitutions $v\to g$, $w\to f$ made in (7.7) would give -1 on the right side of Eq. (14.5). Practically the same calculation as that carried out in Eqs. (8.5), (8.6) gives

$$\mathfrak{L}\int\int K_S(r_1, r; r_1', r')\rho(r_1', r')dr_1'dr'=\rho(r_1, r). \tag{14.7}$$

Another possible kernel is

$$-K_D(r_1, r; r_1', r') = \sum_{k^2>0} u_n(r_1)u_n(r_1')f_k(kr')[g_k(kr)+if_k(kr)]/k + \sum_{k^2<0} u_n(r_1)u_n(r_1')f_k(kr')g_k(kr)/k. \quad (14.8)$$

This kernel contains for large r only diverging waves and the index D refers to "diverging." By adding to the incident plane wave solutions of the type

$$\int\int K_D(r_1, r; r_1', r')\rho(r_1', r')dr_1'dr',$$

one is sure that at a large distance the asymptotic form of the wave function is the incident plane wave plus a diverging wave.

Qualitative Applications

Large repulsive interaction in small region

The interaction between the two particles will be supposed to be confined to a small circle as in Eqs. (12), $\cdots$(12.3). On the circumference of the circle the wave function is supposed to vanish so as to correspond to an infinite repulsion within the circle. The circle will be referred to as an "obstacle" because its interior is a region into which the wave cannot penetrate.[19]

In the absence of the obstacle the wave function will be taken to be of the form

$$\psi_0(r_1, r) = u_{n0}(r_1)f_{k0}(k_0r)\exp[i\delta(k_0)] \quad (15)$$

and for any real k the asymptotic form at $r=\infty$ will be

$$f_k(kr) \sim \sin[kr - L\pi/2 + \delta(k)].$$

The functions $f_k(kr)$, $g_k(kr)$ are analogous to f_L, g_L used in the discussion of the one-body problem in Eqs. (6), $\cdots$(6.43). The function $\psi_0(r_1, r)$ replaces the term

$$u_{n0}(r_1)F_L(k_0r) \rightarrow \psi_0(r_1, r) \quad (15.1)$$

in the expansion of the plane wave

$$u_{n0}(r_1)\exp(ik_0z) = u_{n0}(r_1)\sum i^L(2L+1)P_L(\cos\theta)F_L(k_0r)/(k_0r). \quad (15.2)$$

The substitution of (15) by means of (15.1) into (15.2) gives a modified plane wave consisting of the plane wave $u_{n0}(r_1)\exp(ik_0z)$ plus a scattered wave. The initial state of the particle 1 is n_0 and the particle 2 is in the state $\exp(ik_0z)$ and the substitution indicated by Eq. (15.1) gives, therefore, the solution of the scattering problem, taking into account the central field potential $V(r)$ but neglecting the interaction between particles 1, 2. To the function $\psi_0(r_1, r)$ one may add $\int\int K_D(r_1, r; r_1', r')\rho(r_1', r')dr_1'dr'$ with $\rho(r_1', r')=0$ outside the obstacle and the result may still be substituted in place of $u_{n0}(r_1)F_L(k_0r)$ in formula (15.2) without adding anything to the wave function except diverging and exponentially decaying waves. If the obstacle is sufficiently small to make $\psi_0(r_1, r)$ practically constant on the circumference, then one may use as an addition to ψ_0 a constant multiple times $K_D(r_1, r; r_{10}, r_0)$ where (r_{10}, r_0) is the center of the circle. In this approximation one has to replace

$$\psi_0(r_1, r) \rightarrow u_{n0}(r_1)f_{k0}(k_0r)\exp[i\delta(k_0)] - \frac{u_{n0}(r_{10})f_{k0}(k_0r_0)\exp[i\delta(k_0)]K_D(r_1, r; r_{10}, r_0)}{\langle K_D(r_{10}+a\cos\theta, r_0+a\sin\theta; r_{10}, r_0)\rangle_{Av\theta}}. \quad (15.3)$$

[19] In the present model the interaction is large whenever one of the particles is on the sphere $r_1=r_{10}$ and the other on the sphere $r=r_0$. It does not correspond to a simple law of force on a two-particle model. The requirement of a vanishing wave function in the triangular region $r_1<r$ would perhaps be more natural since it would correspond to the incident particle never penetrating closer to the center than particle 1. This type of interaction is of the type considered in Eqs. (16) $\cdots$ (16.4). No such model can represent the actual case perfectly and extreme cases are, therefore, worked out.

Here a is the radius of the circle. The value of K_D on the circumference is averaged over the angle θ between the radius and the r_1 axis. For a small circle the value of $\langle K_D\rangle_{Av}$ depends logarithmically on a as for the electrostatic potential and its dependence on the energy is not especially critical. The second term in Eq. (15.3) contains a part in $u_{n0}(r_1)[g_{k0}(k_0r)+if_{k0}(k_0r)]$ which combines itself with the divergent wave part of the first term to give the coherently scattered wave. The contribution due to this wave to the plane wave in Eq. (15.2) is

$$\psi_{s,\,\mathrm{coh}}=\frac{2L+1}{k_0r}\left\{\sin\,\delta(k_0)+\frac{\exp\,[i\delta(k_0)]}{k_0\langle K_D\rangle_{Av}}f_{k0}^{\,2}(k_0r_0)u_{n0}^{\,2}(r_{10})\right\}P_L(\cos\,\theta)u_{n0}(r_1)\,\exp\,\{i[k_0r+\delta(k_0)]\}. \quad (15.4)$$

Distinction of potential scattering.—Here the specific nuclear scattering adds itself to the potential scattering represented by $\sin\,\delta(k_0)$. It should be noted that in this problem a definite distinction between pure potential scattering and potential scattering + nuclear scattering can be made. For pure potential scattering one has

$$\psi_{s,\,\mathrm{coh,\,pot}}=\frac{2L+1}{k_0r}\sin\,\delta(k_0)P_L(\cos\,\theta)u_{n0}(r_1)\,\exp\,\{i[k_0r+\delta(k_0)]\}.$$

For a known $\psi_{s,\,\mathrm{coh}}$ one obtains a coefficient $\sin\,\delta(k_0)\,\exp\,[i\delta(k_0)]$ and the point is that an arbitrary number cannot be represented as $e^{i\delta}\sin\,\delta$ with a real δ. This complex number has the special property of having a square of its absolute value equal to its imaginary part.

For incoherent scattering with excitation n the above model gives

$$\psi_{s,\,\mathrm{incoh}}=+\frac{2L+1}{k_0r}u_n(r_1)\,\exp\,\{i[\rho+\delta(k_0)+\delta(k)]\}\frac{P_L(\cos\,\theta)}{k\langle K_D\rangle}u_{n0}(r_{10})u_n(r_{10})f_k(kr_0)f_{k0}(k_0r_0). \quad (15.5)$$

Equation (15.4) gives the scattered wave for which the nucleus is left in the original state n_0. Equation (15.5) gives the scattered wave for which the nucleus has been transferred into another (e.g. an excited) state.

The denominator $\langle K_D\rangle$ contains a number of the f_k and the barrier penetrabilities enter in compensating products f_kg_k since all quantities in $\langle K_D\rangle$ refer to the inside of the nucleus. The dependence of $\langle K_D\rangle$ on energy is, therefore, much less marked than that in the numerator. One sees that primarily it is

$$u_n(r_{10})f_k(kr_0)/k,$$

that matters for the amplitude of the scattered wave in the present example and in this case $|f_k|^2$ is a measure of the probability of escape to the state n.

Repulsive interaction in large region

Some of the qualitative features of the above example hold also in more general circumstances. Several small repulsive regions inside the nucleus give a dependence on energy of the scattered wave similar to that of Eqs. (15.4), (15.5). Sources of K_D put inside each obstacle have then strengths determined by $\langle K_D\rangle^{-1}$ for each obstacle and the intensity of the incident wave + wave scattered by other sources. If the obstacles are sufficiently small and there are not too many of them the wave scattered by other sources can be neglected and the energy dependence of scattering or excitation is the same as before.

If, however, the scattered wave inside the nucleus is comparable with $\psi_0(r_1, r)$ then the energy dependence of $\psi_{s,\,\mathrm{coh}}$, $\psi_{s,\,\mathrm{incoh}}$ outside the nucleus is also changed. Equation (15.3) may be used for a crude estimate of some of the effects. The repulsion will be supposed to take place in a circular region having dimensions comparable with the wave-length inside the nucleus and it will be supposed high in this region. As a crude approximation the wave $\psi_0(r_1, r)$ will be canceled approximately by a source

of K_D at the center so that Eq. (15.3) still will hold. Only in this case K_D does not depend primarily on the radius of the circle and the denominator may have a decided energy dependence.

If one of the terms in Eq. (14.8) for K_D is appreciably larger than the others inside the nucleus and if for it $g_{k'}(k'r_0) \gg f_{k'}(k'r_0)$ then one may set

$$-\langle K_D\rangle \sim u_{n'}(r_{10}) f_{k'}(k'r_0) g_{k'}(k'r_0)/k'. \tag{16}$$

Here $\kappa^2 = \lambda_{n'} + k'^2$ so that the state n' goes with the wave number k'. If, besides, $n' = n_0$, $k' = k_0$ i.e., if the incident state is the one that is important inside the nucleus then Eq. (15.4) becomes

$$\psi_{s,\,\mathrm{coh}} \sim \frac{2L+1}{k_0 r} u_{n0}(r_1) P_L(\cos\theta) \left\{ \sin\delta(k_0) - \frac{f_{k0}(k_0 r_0)}{g_{k0}(k_0 r_0)} \exp\left[i\delta(k_0)\right] \right\} \exp\left\{i(k_0 r + \delta(k_0)\right\} \tag{16.1}$$

and from Eq. (15.5) one obtains

$$\psi_{s,\,\mathrm{incoh}} \sim -\frac{2L+1}{kr} u_n(r_1) \frac{u_n(r_{10})}{u_{n0}(r_{10})} \frac{f_k(kr_0)}{g_{k0}(k_0 r_0)} P_L(\cos\theta) \exp\left\{i[\rho + \delta(k_0) + \delta(k)]\right\}. \tag{16.2}$$

Equation (16.1) corresponds to the scattering cross section

$$\sigma_{\mathrm{coh}} \sim (\Lambda_0^2/\pi)(2L+1) \left| \sin\delta(k_0) - [f_{k0}(k_0 r_{10})/g_{k0}(k_0 r_{10})] \exp\left[i\delta(k_0)\right] \right|^2 \tag{16.3}$$

and (16.2) to

$$\sigma_{\mathrm{incoh}} \sim (\Lambda\Lambda_0/\pi)(2L+1) \left| u_n(r_{10})/u_{n0}(r_{10}) \right|^2 \left| f_k(kr_0)/g_{k0}(k_0 r_0) \right|^2. \tag{16.4}$$

The last formula can be compared with the result of the considerations of Kapur and Peierls as used by Konopinski and Bethe[20] and those by Weisskopf and Ewing.[21] Konopinski and Bethe apply the theory to $Li^7 + H^1 \rightarrow He^4 + He^4$ and they use

$$\Gamma_l \propto E^{\frac{1}{2}}/G_l^2, \quad \sigma \sim \Lambda^2 \Gamma_l \propto E^{-\frac{1}{2}} G_L^{-1}, \tag{16.5}$$

where G_l according to their paper is the irregular function of the proton for the Coulomb field. Equation (16.4) contains the factor $\Lambda \left| g_{k0}(k_0 r_0) \right|^{-2}$ which shows a similar variation with energy. The following points may be noted in a comparison of the two results.

(a) Equation (16.4) does not give a solution of the $Li^7 + H^1 \rightarrow He^4 + He^4$ problem in a direct way. It is obtained only as an approximate solution of the excitation problem. One may nevertheless expect some similarity between the energy dependence of the excitation and disintegration processes. Since the factors $\Lambda \left| f_k(kr_0) \right|^2 \times \left| u_n(r_{10}) \right|^2$ and $\Lambda_0 \left| u_{n0}(r_{10}) \right|^{-2} \left| g_{k0}(k_0 r_0) \right|^{-2}$ are characteristic, respectively, of the final and initial states one has reasonable grounds for expecting the dependence $\Lambda_0 \left| u_{n0}(r_{10}) \right|^{-2} \left| g_{k0}(k_0 r_0) \right|^{-2}$ to hold also for disintegrations in the approximation in which Eq. (16.4) has been obtained.

(b) Since the formalism used is essentially the same for the case of several coordinates $r_1, \cdots, r_t$ replacing the single coordinate r_1 the above can be applied to the case of a nucleus excited by bombardment of the particle whose coordinate has been denoted by r_1. If the nucleus disintegrates into two products (with a small probability) from the state n a three-body disintegration is described.

(c) The approximation used to obtain Eq. (16.4) is very crude. Essentially it neglects the effect of all states except $u_{n0}(r_1) g_{k0}(k_0 r)/k_0$ which are produced by the sources of Green's function inside the nucleus. The complete expression according to Eq. (14.8) contains other terms besides and these contribute to $\langle K_D\rangle$. In addition the approximation of replacing the many sources of diverging waves inside the interaction region by one at the center neglects interference effects which contribute to an additional energy dependence.

(d) The function $g_{k0}(k_0 r)$ which enters into the present discussion is not the irregular function for the Coulomb field but the irregular function for the solution of the radial wave equation with

[20] E. J. Konopinski and H. A. Bethe, Phys. Rev. **54**, 130 (1938).
[21] V. F. Weisskopf and D. H. Ewing, Phys. Rev. **57**, 472 (1940).

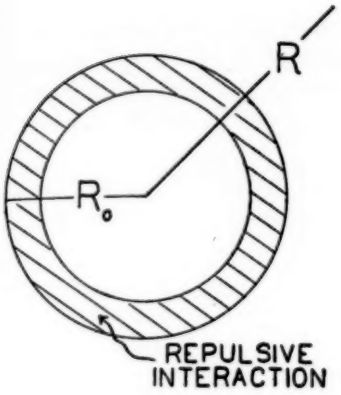

FIG. 5. The two-dimensional resonance model.

the Coulomb field modified by the average nuclear potential taken into account by the difference between $V(r)$ and the Coulomb potential. (The Coulomb field is here thought of as breaking off to zero at a reasonable distance outside the nucleus. If this is not done the above formulas must be changed to take into account the effects characteristic of the $1/r$ potential.)

Schematic representation of two-body resonance

The interaction potential will be supposed to be large and attractive in a small circular region surrounding the point (r_{10}, r_0). Outside this region there is a narrow ring [Fig. 5] within which the potential is repulsive and sufficiently high to serve as a barrier for waves emerging from (r_{10}, r_0). The two-dimensional region formed by the circle and the ring is somewhat analogous to the Gamow, Gurney-Condon model of radioactive decay. The depth of the potential well and the height of the barrier will be adjusted so that for a suitable energy the wave function is large inside the circle and small just outside the ring. For this energy the circular resonance region will be found to act as a strong source of two-dimensional waves which will give rise to strong scattering. The wave function within the circular region is in this model a schematic representation of the compound nucleus which is formed by the coupling of the two particles to each other. In this model the compound nucleus is screened against external disintegration by the repulsive region in the ring and in addition also by the barrier $V(r)$.

The resonating properties of the circle-ring system will be first defined by coupling it to an infinite plane with constant κ. In plane polar coordinates the axially symmetric solution satisfies

$$d^2\psi/dR^2+d\psi/RdR+[\kappa^2-V(R)]\psi=0, \quad (17)$$

which is the same as

$$d^2(R^{\frac{1}{2}}\psi)/dR^2+[\kappa^2-V(R)+1/4R^2] \times(R^{\frac{1}{2}}\psi)=0. \quad (17.1)$$

Here $V(R)$ is the potential within the circle-ring region and $V(R)=0$ for $R>R_0$. Outside the circle-ring system

$$\psi=J_0(\kappa R)\cos\varphi-N_0(\kappa R)\sin\varphi \quad (17.2)$$

is a solution of Eq. (17). One has

$$J_0(\kappa R)\sim(2/\pi\kappa R)^{\frac{1}{2}}\cos(\kappa R-\pi/4) \quad (\kappa R\gg 1) \quad (17.3)$$

$$N_0(\kappa R)\sim(2/\pi\kappa R)^{\frac{1}{2}}\sin(\kappa R-\pi/4),$$

so that by Eq. (17.2)

$$\psi\sim(2/\pi\kappa R)^{\frac{1}{2}}\cos(\kappa R-\pi/4+\varphi), \quad (\kappa R\gg 1). \quad (17.4)$$

Equations (17.4), (17.2) show that φ is caused by $V(R)$ in the same way as the phase shift K is produced in the single-body problem. It will be assumed, therefore, that close to the resonance

$$\tan\varphi\cong\Delta E/(E-E_0), \quad (17.5)$$

where ΔE is a positive constant. This assumption is reasonable in view of Eq. (17.1) which is like the radial equation for $\mathfrak{F}$ in the central field problem. Eq. (17.2) does not apply for $R<R_0$. At $R=R_0$ it joins smoothly to the internal solution. One has

$$\left(\frac{d\psi}{\psi dR}\right)_{R_0}=\kappa\frac{J_0'(\kappa R_0)\cos\varphi-N_0'(\kappa R_0)\sin\varphi}{J_0(\kappa R_0)\cos\varphi-N_0(\kappa R_0)\sin\varphi} \quad (17.6)$$

and this formula does not depend on whether the ring is coupled to an infinite plane or to the actual potential provided one may assume ψ to depend only on R for $R<R_0$. In fact this axially symmetric part of ψ is determined by Eq. (17) and the requirement of regularity at $R=0$. The requirement of axial symmetry is good only if

$$x=\kappa R_0\ll 1.$$

For small x

$$J_0(x)=1-x^2/4+\cdots;$$
$$\pi N_0(x)/2=J_0(x)\ln(\gamma x/2)+x^2/4+\cdots.$$

The formula

$$J_0(x)N_0'(x)-N_0(x)J_0'(x)=2/\pi x$$

when used to eliminate N_0' in Eq. (17.6) gives

$$\left(\frac{d\psi}{\psi dR}\right)_{R_0}\approx-\frac{\kappa x}{2}-\frac{2/\pi R_0}{\cot\varphi-(2/\pi)\ln(\gamma x/2)}.$$

Since $x\ll 1$ this expression will be approximated by

$$\left(\frac{d\psi}{\psi dR}\right)_{R_0}\approx\frac{-2\Delta E/\pi R_0}{E-E_0-(2\Delta E/\pi)\ln(\gamma x/2)}\approx\frac{-\kappa N_0',}{\cot\varphi-N_0}, \quad (17.7)$$

where the approximation (17.5) has been used.

In the presence of $V_1(r_1)$, $V(r)$ and with the boundary conditions $\psi(0,r)=\psi(r_1,0)=0$ the approximation

$$\psi(r_1,r)=\psi_0(r_1,r)+\alpha\psi_0(r_{10},r_0)K_D(r_1,r;r_{10},r_0) \quad (18)$$

will be used. Here ψ_0 is given by Eq. (15) and it is assumed as in Eqs. (15), $\cdots$ (15.5) that the density ρ in $R<R_0$ can be replaced by a point source. This assumption is a poor one close to $R=R_0$ but the axially symmetric part of ψ can be represented by a point source. One has

$$d\psi/dR\approx\alpha\psi_0(r_{10},r_0)(dK_D/dR)_{R_0}$$

and

$$\left(\frac{d\psi}{\psi dR}\right)_{R_0}\approx\frac{(dK_D/dR)_{R_0}}{1/\alpha+(K_D)_{R_0}}. \quad (18.1)$$

The variation of ψ_0 over the circle-ring system is neglected and in (18.1) the average values of ψ, $d\psi/dR$ over $R=R_0$ are used. These values will be denoted as $\langle\psi\rangle$, $\langle d\psi/\psi dR\rangle$ and one obtains

$$\alpha=\frac{\langle d\psi/\psi dR\rangle}{-\langle K_D\rangle\langle d\psi/\psi dR\rangle+\langle dK_D/dR\rangle}\approx\left[-\langle K_D\rangle-\frac{\cot\varphi-N_0}{\kappa N_0'}\langle dK_D/dR\rangle\right]^{-1}.$$

One has approximately

$$4iK_D\sim J_0+iN_0 \quad (18.2)$$

and hence $4\langle dK_D/dR\rangle\sim\kappa N_0'$ so that

$$\alpha\approx\frac{4}{\langle N_0\rangle-\cot\varphi-4\langle K_D\rangle}\approx-\frac{4\Delta E}{E-E_0-\Delta E\langle N_0\rangle+4\Delta E\langle K_D\rangle}. \quad (18.3)$$

On account of the potential field $V(r)$ the quantity $u_{n0}(r_1)F_L(k_0r)$ in (15.2) should be replaced by $\psi_0(r_1,r)$ as in Eq. (15.1). On account of the resonance interaction in $R<R_0$ one must make the substitution

$$\psi_0\rightarrow\psi$$

with ψ given by (18), (18.3). These substitutions are made in the right side of (15.3) and $u_{n0}(r_1)\exp[ik_0z]$ is subtracted from the result. The difference is the scattered wave. Its value for large r is obtained by means of the asymptotic expressions

$$f_{k0}(k_0r)\exp[i\delta(k_0)]\sim i^{-L}\sin\delta(k_0)\exp\{i[k_0r+\delta(k_0)]\}+F_{k0}(k_0r)$$
$$g_k(kr)+if_k(kr)\sim i^{-L}\exp\{i[kr+\delta(k)]\}.$$

The scattered wave at a large distance is

$$\psi_s\sim\frac{2L+1}{k_0r}P_L\Big\{u_{n0}(r_1)\sin\delta(k_0)\exp[ik_0r+i\delta(k_0)]-\alpha u_{n0}(r_{10})f_{k0}(k_0r_0)\sum(k^2>0)u_n(r_1)u_n(r_{10})\frac{1}{k}f_k(kr_0)\exp[ikr+i\delta(k)+i\delta(k_0)]\Big\}. \quad (18.4)$$

The first term in the braces represents scattering due to $V(r)$. The remainder is due to the resonance interaction. Neglecting the former one obtains the scattering cross section due to resonance scattering

$$\sigma_{res}=\sum(k^2>0)\int d\Omega\cdot r^2\int_0^\infty dr_1\cdot\frac{k}{k_0}|\psi_{sk}|^2, \quad (18.5)$$

where ψ_{nk} is the part of ψ_n due to excitation into the state n and emission of the wave g_k+if_k. The factor k/k_0 is introduced into (18.5) because the number of emitted particles is proportional to their velocity. Substituting into (18.5) one finds

$$\sigma_{res}=(2L+1)\frac{\Lambda_0^2}{\pi}|\alpha|^2 u_{n0}^2(r_{10})\frac{1}{k_0}f_{k0}^2(k_0r_{10})\sum(k^2>0)u_n^2(r_{10})\frac{1}{k}f_k^2(kr_0). \tag{18.6}$$

Introducing α by means of Eq. (18.3) one has

$$\sigma_{res}=\frac{(2L+1)\Lambda_0^2\Gamma_{n0}\sum\Gamma_n}{\pi|E-E_0-\Delta E\langle N_0\rangle+4\Delta E\langle K_D\rangle|^2}, \tag{18.7}$$

where

$$\Gamma_n=4\Delta E u_n^2(r_{10})\frac{1}{k}f_k^2(kr_0). \tag{18.8}$$

The expression (14.8) for K_D is now used to obtain $\langle K_D\rangle$. The imaginary part comes only from $\sum(k^2>0)$ and consists of a finite number of terms. The real part is an infinite series and has a logarithmic singularity like that of $N_0/4$. Denoting the real part by *Re* and the coefficient of the imaginary part by *Im* one has from Eq. (14.8)

$$4\Delta E Im\langle K_D\rangle \cong -\sum\Gamma_n, \tag{18.9}$$

which when introduced into (18.7) gives

$$\sigma_{res}=\frac{(2L+1)\Lambda_0^2\Gamma_{n0}\sum\Gamma_n}{\pi|E-E_0-\langle N_0\rangle\Delta E+4\Delta E Re\langle K_D\rangle-i\sum\Gamma_n|^2}. \tag{19}$$

This is the ordinary formula for resonance competition. It has been obtained with the following restricting assumptions.

(a) The two-dimensional region within which the interaction takes place is small. This assumption does not mean that within this region the interaction is small. The result of this assumption is to simplify the result by making Γ_n depend only on u_n^2, f_k^2 at $r_1=r_{10}$, $r=r_0$. (b) Resonance was assumed to be sharp.

According to Eq. (18.9) the damping constants Γ_n depend on the constant $4\Delta E$ which is characteristic of the resonance region. Besides, there is present also the dimensionless factor $u_n^2(r_{10})f_k^2(kr_0)/k$ which is characteristic of the binding of particle 1 in the residual nucleus, the energy of the escaping particle and the potential barrier through which this particle must escape. The barrier enters implicitly through $f_k^2(kr_0)$. The presence of this factor could be expected by analogy with the result of Wigner and the writer by a method analogous to the Weisskopf-Wigner theory of the absorption and emission of light. The damping constant is then proportional to the square of the matrix element of the interaction energy divided by the average energy interval, $|M_s|^2/\Delta\nu_s$ in the notation of the above reference. This quantity varies with the energy as f_k^2/k in exact agreement with the result obtained on the present model. It is claimed, on the other hand, from the considerations of Kapur and Peierls that $\Gamma\propto E^{\frac{1}{2}}/G_k^2$. The difference between the results is in a sense quantitative rather than qualitative and it is perhaps unnecessary to emphasize it. For slow neutrons both results give $\Gamma\propto E^{\frac{1}{2}}$ and for small r one has $F_kG_k\propto\rho\propto E^{\frac{1}{2}}$ so that F_k^2/k and $E^{\frac{1}{2}}/G_k^2$ vary with energy in the same way. For low energies f_k^2 and F_k^2 also vary similarly. On the other hand f_k^2/k, $E^{\frac{1}{2}}/G_k^2$ do not vary with energy in exactly the same way and it should be noted that $f_k^2(r_0)$ is here taken at $r=r_0$ i.e., at the mean r of the compound state rather than at the arbitrary nuclear radius of Kapur-Peierls.

Special Two-Dimensional Green's Functions

(A) Infinite plane

The differential equation

$$(\partial^2/\partial x^2+\partial^2/\partial y^2+1)\psi=0$$

is supposed to hold through an infinite plane. Green's function is

$$K_D=(1/4i)H_0^{(1)}([(x-\xi)^2+(y-\eta)^2]^{\frac{1}{2}}), \tag{20}$$

where $H_0^{(1)}$ is the Hankel cylindrical function of the first kind. The method of Eqs. (7) will now be applied to the computation of K_D and the result will be shown to agree with Eq. (20). The point of doing so is to make sure that the method works also for a continuous spectrum of λ_n.

Quantizing in the interval $-L/2<x<L/2$ by means of the periodic boundary condition one has

$$u_n(x)=L^{-\frac{1}{2}}e^{i\tau x}$$
$$\tau=2\pi n/L; \quad n=0, \pm1, \pm2, \cdots$$

and

$$u_n(x)u_n^*(\xi)=L^{-1}\exp[i\tau(x-\xi)]. \tag{20.1}$$

Equation (7.6) gives

$$v_k(y)=N_ke^{iky}, \quad w_k(y)=N_ke^{-iky}$$

with

$$\begin{aligned} k&=(1-\tau^2)^{\frac{1}{2}} \quad \text{for} \quad 1>\tau^2 \\ k&=i|(1-\tau^2)^{\frac{1}{2}}| \quad \text{for} \quad 1<\tau^2 \end{aligned} \tag{20.2}$$

and according to the normalizing condition (7.7) one has

$$2ikN_k^2=1. \tag{20.3}$$

Substituting (20.1), (20.2), (20.3) into Eq. (8) and remembering that the interval between successive τ is $2\pi/L$ one has for large L

$$K_D(x, y; \xi, \eta)=\frac{1}{4\pi i}\int_{-\infty}^{+\infty}\frac{1}{(1-\tau^2)^{\frac{1}{2}}}\exp[i\tau(x-\xi)+i(1-\tau^2)^{\frac{1}{2}}(y-\eta)]d\tau; \quad (y>\eta). \tag{20.4}$$

According to Eq. (20) one has then

$$H_0^{(1)}((x^2+y^2)^{\frac{1}{2}})=\frac{2}{\pi}\int_0^{\infty}\frac{\cos\tau x}{(1-\tau^2)^{\frac{1}{2}}}\exp[i|y|(1-\tau^2)^{\frac{1}{2}}]d\tau$$

$$=\frac{2}{\pi}\int_0^1\frac{\cos(\tau x)}{(1-\tau^2)^{\frac{1}{2}}}\exp[i|y|(1-\tau^2)^{\frac{1}{2}}]d\tau+\frac{2}{\pi i}\int_1^{\infty}\frac{\cos\tau x}{(\tau^2-1)^{\frac{1}{2}}}\exp[-(\tau^2-1)^{\frac{1}{2}}|y|]d\tau. \tag{20.5}$$

This expression for $H_0^{(1)}$ is not obviously symmetric in x, y. It shows the importance of states with negative kinetic energy for motion in the y direction. The $\int_1^{\infty}$ part of the formula consists of such states. It should be noted that these states of negative kinetic energy may contribute to the asymptotic value of $H_0^{(1)}$ for $x\to\infty$. Setting $x=0$ in Eq. (20.5) one obtains

$$H_0^{(1)}(y)=\frac{2}{\pi i}\int_0^{\infty}e^{-y\sinh t}dt+\frac{1}{\pi}\int_0^{\pi}e^{iy\sin\theta}d\theta, \quad (y>0), \tag{20.6}$$

which is obtainable from Eq. (2) in Watson's *Theory of Bessel Functions*, p. 178.[22] Setting $y=0$ one has

$$H_0^{(1)}(x)=\frac{2}{\pi}\int_0^1\frac{\cos\tau x}{(1-\tau^2)^{\frac{1}{2}}}d\tau+\frac{2}{\pi i}\int_1^{\infty}\frac{\cos\tau x}{(\tau^2-1)^{\frac{1}{2}}}d\tau, \tag{20.7}$$

[22] G. N. Watson, *Theory of Bessel Functions* (Cambridge University Press, 1922).

which is verified by means of

$$J_0(x)=\frac{1}{\pi}\int_0^{\pi}\cos(x\sin\theta)d\theta,\quad N_0(x)=-\frac{2}{\pi}\int_0^{\infty}\cos(x\cosh t)dt,\quad H_0^{(1)}=J_0+iN_0.$$

For large x, $J_0(x)$, $N_0(x)$ have comparable values and Eq. (20.7) shows that N_0 arises in this case from waves with a negative kinetic energy of the y motion. The most important values of τ are those slightly >1 which correspond to only slightly negative kinetic energies of the y motion. In Eq. (20.6), on the other hand, the negative kinetic energies contribute the first integral and one has

$$\int_0^{\infty}e^{-|y|\sinh t}dt<\int_0^{\infty}e^{-|y|t}dt=\frac{1}{|y|}.$$

This is negligible in comparison with $H_0^{(1)}(y)$ for large $|y|$. Along the y axis, therefore, the negative kinetic energies of the y motion do not contribute to the dominating term of the outgoing wave.

(B) Quadrant $x>0$, $y>0$

The same differential equation as in case (a) is being solved subject to boundary conditions $\psi(0, y)=\psi(x, 0)=0$. Green's function can be obtained again by the general method and this time by the modification for central fields, as in Eq. (14.8). The substitution $r_1\to x$, $r\to y$ is made, the functions u_n are quantized in the finite interval $0<x<L$ and are $(2/L)^{\frac{1}{2}}\sin\tau x$ while the interval between successive τ is $\Delta\tau=\pi/L$. One obtains

$$K_D=-\frac{2}{\pi}\int_0^{\infty}\frac{\sin\tau x\sin\tau\xi}{(1-\tau^2)^{\frac{1}{2}}}\sin[(1-\tau^2)^{\frac{1}{2}}\eta]\exp[i(1-\tau^2)^{\frac{1}{2}}y]d\tau \tag{21}$$

with the understanding that for

$$\tau^2>1,\quad (1-\tau^2)^{\frac{1}{2}}=i(\tau^2-1)^{\frac{1}{2}}. \tag{21.1}$$

Rearranging expression (21) one expresses it in terms of integrals of the form (20.5) and obtains

$$K_D=\frac{1}{4i}\{H_0^{(1)}([(x-\xi)^2+(y-\eta)^2]^{\frac{1}{2}})-H_0^{(1)}([(x+\xi)^2+(y-\eta)^2]^{\frac{1}{2}})$$
$$-H_0^{(1)}([(x-\xi)^2+(y+\eta)^2]^{\frac{1}{2}})+H_0^{(1)}([(x+\xi)^2+(y+\xi)^2]^{\frac{1}{2}})\}, \tag{21.2}$$

which can be also obtained from (20) by placing negative images of the source at $(-\xi, \eta)$, $(\xi, -\eta)$ and a positive image at $(-\xi, -\eta)$.

It will be noted that in both of the above examples K_D is asymptotically an outgoing wave at a large distance even though this is not obvious in the forms (20.6), (21).

(C) Straight channel

The region considered is $-a<x<a$, $0<y<\infty$ and $\psi(x, y)$ is subject to the boundary conditions

$$\psi(a, y)=\psi(-a, y)=0$$

and for $y=\infty$ it is required that K_D be an outgoing wave. These are the boundary conditions required for Eq. (14.8) for use with central fields. The substitution

$$(r_1, r)=(x+a, y)$$

is made. The wave equation in the strip is taken to be

$$(\partial^2/\partial x^2+\partial^2/\partial y^2+\kappa^2)\psi=0.$$

One has

$$u_n(x)=a^{-\frac{1}{2}}\sin\left[\pi n(x+a)/2a\right];\quad k^2=\kappa^2-\pi^2n^2/4a^2;\quad n=1,2,3,\cdots \tag{22}$$

$$-K_D=\sum(k^2>0)\frac{1}{2ak}\left[\cos\frac{\pi n}{2a}(x-\xi)-(-)^n\cos\frac{\pi n}{2a}(x+\xi)\right]\sin\kappa\eta\cdot e^{ik_y}$$

$$+\sum(k^2<0)\frac{1}{2a|k|}\left[\cos\frac{\pi n}{2a}(x-\xi)-(-)^n\cos\frac{\pi n}{2a}(x+\xi)\right]\sinh|k|\eta e^{-|k|y}. \qquad (y>\eta)$$

For $\kappa\to0$ this expression becomes

$$-K_D=\frac{1}{2\pi}\text{R.P. ln}\left\{\frac{1+\exp\{(\pi/2a)[-(y-\eta)+i(x+\xi)]\}}{1-\exp\{(\pi/2a)[-(y-\eta)+i(x-\xi)]\}}\cdot\frac{1-\exp\{(\pi/2a)[-(y+\eta)+i(x-\xi)]\}}{1+\exp\{(\pi/2a)[-(y+\eta)+i(x+\xi)]\}}\right\}$$

$$(y>\eta). \tag{22.1}$$

The expression under the logarithm is a function of $x+iy$ and, therefore, the right side is a solution of Laplace's equation as it should be. The boundary conditions are verified directly in Eq. (22.1). Also one sees that K_D and its derivatives are continuous except at $x+iy=\xi+i\eta$. At the latter point K_D behaves as

$$K_D\approx\frac{1}{2\pi}\ln\left\{\frac{\pi}{2a}[(x-\xi)^2+(y-\eta)^2]^{\frac{1}{2}}\right\}. \tag{22.2}$$

Constant terms have been dropped. Except for constant terms K_D is seen to be the electrostatic potential due to an electric charge of linear density $(-1/4\pi)$ on an infinitely long filament perpendicular to the plane (x, y) and crossing it at the point (ξ, η). This is in agreement with Poisson's equation in electrostatics which is in two dimensions

$$\left(\frac{\partial^2}{\partial x^2}+\frac{\partial^2}{\partial y^2}\right)\int\int\frac{1}{2\pi}\rho(\xi,\eta)\ln\left[(x-\xi)^2+(y-\eta)^2\right]^{\frac{1}{2}}d\xi d\eta=\rho(x,y),$$

which is the same as Eq. (14.7) for K_D in the limiting case of Eq. (22.2).

If $\kappa^2>0$ but $\ll\pi^2/4a^2$ one may still apply Eq. (22.1) in the rectangle $0<y<2a$ as an approximation. Since in the form of Eq. (22) the series converges slowly one sees here the importance of taking into account many states of excitation of the residual nucleus.

For any κ the series (22) for K_D behaves for high n like the series (22.1) and as long as $|y-\eta|\neq0$ this series remains convergent when differentiated with respect to y. The convergence is due to the presence of the factor $\exp\left[-\pi n|y-\eta|/2a\right]$. It will now be verified that $\partial K_D/\partial y$ is continuous on the line $y=\eta$. For a small $\epsilon>0$ one has for $\kappa^2<\pi^2/4a^2$

$$(\partial K_D/\partial y)_{y-\eta+\epsilon}-(\partial K_D/\partial y)_{y-\eta-\epsilon}=\sum\frac{1}{2a}\left[\cos\frac{\pi n}{2a}(x-\xi)-(-)^n\cos\frac{\pi n}{2a}(x+\xi)\right]\left[e^{-|k|\epsilon}+e^{-2|k|\eta}\sinh|k|\epsilon\right].$$

The second term in square brackets gives an absolutely converging series which vanishes with ϵ and may, therefore, be disregarded. The first term also gives an absolutely converging series if $\epsilon>0$. For $\epsilon=0$ the series does not converge. As $\epsilon\to0$ the sum can be seen to $\to0$. In fact ϵ can be made so small that $\epsilon\pi N/2a\ll1$ for $N\gg2a\kappa/\pi$. The $\sum_{n=1}^{\infty}$ is split into $\sum_1^N+\sum_N^\infty$ and the series is compared with its value for the same ϵ and $\kappa=0$. The difference of the $\sum_1^N$ is negligible on account of the assumption about ϵ and the difference of $\sum_N^\infty$ is negligible on account of the assumption about N. On the other

hand for $\kappa=0$ the series can be summed and gives 0. It is thus seen that $\partial K_D/\partial y$ is continuous on the line $y=\eta$. The point $(x, y)=(\xi, \eta)$ is, of course, an exception.

The main object of the above example is to illustrate the importance of excited states in the vicinity of the region in which interaction takes place. This is seen in the limiting form of Eq. (22.1) in which the outgoing waves combine to give the electrostatic solution. If there are two obstacles, instead of one, and if their distance apart is smaller than the wave-length the wave scattered by (ξ_1, η_1) gives a contribution to ψ at (ξ_2, η_2) which contains many states of excitation.

(D) Transformation of Hankel function

The relations of Eq. (20) suggest formula (20.6) for the Hankel function $H_0^{(1)}$. This will now be verified by means of contour integration. According to Courant-Hilbert.[23]

$$H_0^{(1)}(r)=-\frac{1}{\pi}\int_{L_1} e^{-ir\sin\zeta}d\zeta, \tag{23}$$

where the path of integration is from $-i\infty$ to 0, then to $-\pi$ and finally to $-\pi+i\infty$ as indicated in Fig. 6. The differential equation for $H_0^{(1)}$ is satisfied also for other paths of integration provided

$$[\cos\zeta\, e^{-ir\sin\zeta}]_a^b=0, \tag{23.1}$$

where $\zeta=a$ and $\zeta=b$ are the limits of integration. The path will be deformed into L_1' which starts at $\xi_0-i\infty$ and goes over ξ_0, $-\pi+\xi_0$ to $-\pi+\xi_0+i\infty$ with $\pi/2>\xi_0>\infty$. [This path is not the path denoted by L_1' on p. 408 of Courant-Hilbert I.] The condition (23.1) is satisfied by L_1' because $\cos\xi_0>1$. The integrand of (23) vanishes at the ends of the path for both L_1 and L_1' and no poles of the integrand have been crossed in the deformation. One has, therefore,

$$H_0^{(1)}(r)=-\frac{1}{\pi}\int_{L_1'} e^{-ir\sin\zeta}d\zeta. \tag{23.2}$$

Setting $\zeta=\xi+i\eta$ and introducing the abbreviations

$$y=r\cos\xi_0, \quad x=r\sin\xi_0, \tag{23.3}$$

one obtains

$$H_0^{(1)}(r)=\frac{2}{\pi i}\int_0^\infty \cos(x\cosh\eta)e^{-y\sinh\eta}d\eta+\frac{1}{\pi}\int_{-\xi_0}^{\pi-\xi_0} e^{ir\sin\theta}d\theta. \tag{23.4}$$

Substitution of $\tau=\cosh\eta$ in the first integral changes it into the second integral of Eq. (20.5). The second integral in (23.4) is transformed as follows

$$\frac{1}{\pi}\int_{-\xi_0}^{\pi-\xi_0}\exp(ir\sin\theta)d\theta=\frac{1}{\pi}\int_0^\pi \exp(iy\sin\theta-ix\cos\theta)d\theta=\frac{2}{\pi}\int_0^{\pi/2} e^{iy\cos\theta}\cos(x\sin\theta)d\theta.$$

The second integral in (23.4) is thus the first integral in (20.5) so that the latter representation is equal to (23). It will be noted that the restrictions

$$0<\xi_0<\pi/2, \quad x>0, \quad y>0$$

are essential for the deformation of L_1 into L_1' and that these conditions are also essential for the applicability of the construction of $H_0^{(1)}$ as $4iK_D$.

The somewhat unexpected features of (20.5) are its dissymmetry between x and y and the fact that it is not obvious from its form that it represents outgoing waves in any direction but that of

[23] Reference 15, Vol. I, p. 407.

increasing y. The way in which (20.5) gives an outgoing wave for $y=0$ has been discussed in connection with Eq. (20.7). It may be pointed out that

$$\frac{2}{\pi}\int_0^\infty \frac{\sin \tau x}{(1-\tau^2)^{\frac{1}{2}}}d\tau=\frac{2}{\pi}\int_0^1 \frac{\sin \tau x}{(1-\tau^2)^{\frac{1}{2}}}d\tau+\frac{2}{\pi i}\int_1^\infty \frac{\sin \tau x}{(\tau^2-1)^{\frac{1}{2}}}d\tau$$

is also an outgoing wave for $x>0$. One has in fact

$$\frac{2}{\pi i}\int_1^\infty \frac{\sin \tau x}{(\tau^2-1)^{\frac{1}{2}}}d\tau=-iJ_0(x)\sim -i\left(\frac{2}{\pi x}\right)^{\frac{1}{2}}\cos\left(x-\frac{\pi}{4}\right)$$

and

$$\frac{2}{\pi}\int_0^1 \frac{\sin \tau x}{(1-\tau^2)^{\frac{1}{2}}}d\tau=\frac{4}{\pi}[J_1(x)+\tfrac{1}{3}J_3(x)+\tfrac{1}{5}J_5(x)+\cdots]\sim\left(\frac{2}{\pi x}\right)^{\frac{1}{2}}\sin\left(x-\frac{\pi}{4}\right).$$

Combining these relations one has

$$\frac{2}{\pi}\int_0^\infty \frac{\sin \tau x}{(1-\tau^2)^{\frac{1}{2}}}d\tau\sim -i\left(\frac{2}{\pi x}\right)^{\frac{1}{2}}e^{i(x-\pi/4)}. \tag{23.5}$$

This formula is another example of an outgoing wave which is compounded of stationary waves. It and Eq. (21) show that the general method of Eq. (14.8) when applied to a continuum can give in special cases outgoing waves in all directions within the quadrant $x>0$, $y>0$. This does not mean, however, that the same is true in the general case.

Final Remarks

The calculations of the last section show that the behavior of K_D close to the singular point is in fact such as has been used in the calculation of scattering by a small obstacle in the (r_1, r) plane and the related calculations on the interaction in a large region as well as with resonance. The example of the straight channel shows how at the singularity the logarithmic dependence on $(x-\xi)^2+(y-\eta)^2$ is obtained. In fact for small values of this quantity the contributions of high terms in the series of Eq. (22) approach the limit for $\kappa=0$ and give the electrostatic term. It is clear, therefore, that close to (ξ, η) one needs a larger number of excitation states to represent the wave function.

In the two-dimensional model the singularity is logarithmic. In m dimensions the dependence of K close to the singularity is of type const. $[\sum(x_i-\xi_i)^2]^{(-m+2)/2}$. The effect of a source of a diverging wave is the more localized in the m space the higher the number of dimensions and the region in which the higher states are especially important becomes more confined as m increases. The scattered wave function outside the nucleus may be expected to be small in comparison with the difference between the actual and incident wave functions inside the nucleus in a many-dimensional diagram. The importance of the intermediate state is in this sense increased by increasing the number of interacting particles.

The two-dimensional resonance model treated above gives the expected answer. It does not

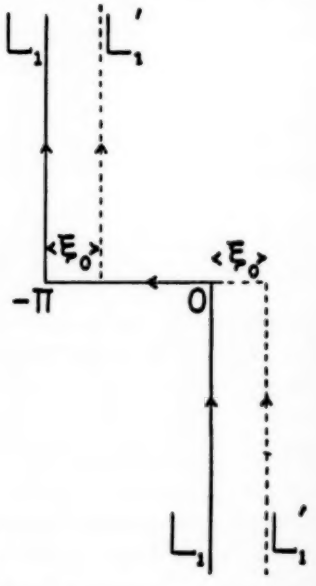

Fig. 6. Contours of integration for $H_0^{(1)}$.

include the effect of competitive emission of several particles but only the effect of competition between various types of emission of the same particle. For the discussion of more general competitive processes it is obviously more suitable to bring in the intermediate state in a more pronounced way. It is possible to do so by a generalization of the method of complex eigenvalues to many-dimensional problems. This will be treated in another publication.

The occurrence of the regular and irregular solutions of the radial equation (f_k and g_k) in the formulas for the scattered waves is not special to the two-dimensional model as is clear from the many-dimensional extension in Eqs. (13.1) ··· (13.4). The examples show that in special cases the factor f_k^2 occurs in the formulas. If the interaction is distributed within the nucleus, however, then the general form of Green's function shows that the g_k occur in the denominators. In the general case the g_k for all excited states will occur and very special assumptions about the relative importance of excited states are necessary to leave the simple factor $[g_{k0}(k_0r_0)]^{-2}$ in Eq. (16.4). Quantitative agreement with experiment obtained by application of formulas with one or another simple choice of such factors does not appear therefore to be very significant.

SEPTEMBER 15, 1940 PHYSICAL REVIEW VOLUME 58

The Principal *M*-Series Emission Lines of Tungsten and the *K* Absorption of Magnesium and Aluminum

J. H. MUNIER, J. A. BEARDEN AND C. H. SHAW
The Johns Hopkins University, Baltimore, Maryland

(Received June 22, 1940)

A study of the *M*-series lines of tungsten and of the *K*-absorption edges of magnesium and aluminum has been made by means of a double crystal x-ray spectrometer. The extension of the double crystal technique to these long x-ray wave-lengths has been made possible by thorough evacuation of the spectrograph and a windowless x-ray tube. The crystals were the aquamarine form of beryl in which the 1010 planes have a grating constant of 8.06A. The detector was a Geiger-Müller counter with an aluminum window of 2.5×10^{-4} cm thickness. The width and relative intensities of the prominent *M*-series tungsten lines were measured. Accompanying the diagram lines are some 33 satellite lines. In the study of the *K*-absorption edges of magnesium and aluminum, structure not heretofore resolved photographically has been recorded. A qualitative comparison of the intensity of the continuous radiation from tungsten to that from aluminum at 10A indicates that the ratio is less than one, whereas theory predicts about six.

INTRODUCTION

PRECISION measurements with the double crystal x-ray spectrometer have shown the effectiveness of the x-ray method in checking experimentally the theoretical calculations on the electronic conduction bands of solids.[1] Ruled grating methods for the longer wave-lengths have given valuable information on the conduction bands of the light elements.[2] Photographic measurements in the intermediate range have not yielded results of definitive accuracy because of low resolving power and inaccuracies of intensity measurements. This region, however, is one of considerable theoretical interest, because here the present theory of metals makes sufficiently accurate predictions that their comparison with experiment may be expected to be significant.[3]

[1] W. W. Beeman and H. Friedman, Phys. Rev. **56**, 392 (1939); H. Friedman and J. A. Bearden, Phys. Rev. **57**, 1085A (1940); T. M. Snyder and J. A. Bearden, Phys. Rev. **57**, 1085A (1940); W. W. Beeman and J. A. Bearden, Phys. Rev. **57**, 1085A (1940).

[2] See, for example, *Reports on Progress in Physics*, Vol. 5 (Physical Society, London, 1939).

[3] M. F. Manning and H. M. Krutter, Phys. Rev. **51**, 761 (1937); J. C. Slater, Phys. Rev. **45**, 794 (1934).

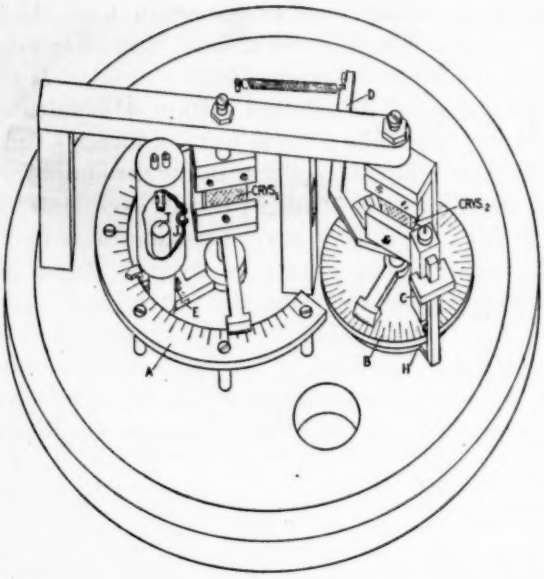

FIG. 1. Detailed construction of the spectrometer. The locations of the first and second crystals are shown. The walls J of the x-ray tube and the target T are of solid copper, kept cool by water. The target, which rotates about the first crystal, may be removed from the instrument through the connection E. A baffle connected electrically to the high voltage prevents electrons reflected from the target from passing into the vacuum chamber. A tangent arm indicates the angular setting of the first crystal on the circle A graduated in degrees. The position of the second crystal is read by a pointer on the circle B which also serves to locate the counter C. The counter rotates about the second crystal by the slip-ring pivot H. The arm D leads to the lever and micrometer head for slow motion of the second crystal.

A vacuum double crystal spectrometer capable of making accurate measurements in a part of this intermediate region from 5A to 15A has been constructed and used to measure the width and relative intensities of the M-series lines of tungsten and the K-absorption edges of magnesium and aluminum.

EXPERIMENTAL

The double crystal spectrometer was assembled on a circular steel bed-plate as shown in Fig. 1. A steel bell jar permitted a vacuum of 10^{-4} mm to be obtained. The x-ray tube was placed inside the vacuum chamber, eliminating the window which would otherwise be necessary.

The crystal mountings were set in fixed positions on the bed-plate and rotated on pivot bearings.[4] The second crystal could be rotated from outside the chamber by a micrometer head, the motion being introduced through the bed-plate with the aid of a Sylphon bellows and lever. A large dial containing 200 divisions was attached to the micrometer head, making it possible to read the position of the second crystal within two seconds of arc, or 0.07 x.u. at 7A.

The detector was a Geiger-Müller counter containing air at a pressure of 7 cm of mercury. Due to the extremely thin window (aluminum foil 2.5×10^{-4} cm thick), a means was provided for lowering and raising the pressure in the counter simultaneously with that in the chamber. The Neher-Harper circuit[5] with a scale-of-eight thyratron circuit[6] and a Cenco counter were used for recording the counter pulses.

The crystals used were the aquamarine form of beryl ($Be_3Al_2Si_6O_{18}$), cut from a single specimen along the direction of the 1010 planes which have an x-ray grating constant of 8.06A.[7] The parallel rocking curves were recorded for three different wave-lengths and the full widths at half-maximum in seconds and x.u. are given in Table I.

The percent reflection[8] was measured at 8559 x.u. with the result $P(0)=3$ percent. This low percent reflection is due to the low atomic population of the 1010 planes.[9]

The physical resolving power of the crystals[10] from the measured $(1,-1)$ widths is 1900 at 7000 x.u. and 1700 at 8559 x.u.

RESULTS

M-emission lines of tungsten

In recording the M-series lines, the target used was a thin disk of tungsten, spot-welded to

TABLE I. $(1,-1)$ *widths of crystals.*

x.u.	w (sec.)	w (x.u.)
6969	135	4.8
8559	159	5.15
8900	199	6.5

[4] J. A. Bearden, Phys. Rev. **56**, 1023 (1939).

[5] H. V. Neher and W. H. Pickering, Phys. Rev. **53**, 316 (1938).

[6] J. Giarratana, Rev. Sci. Inst. **8**, 390 (1937).

[7] A. Stenstrom, Ann. d. Physik **57**, 347 (1918).

[8] A. H. Compton and S. K. Allison, *X-rays in Theory and Experiment* (D. Van Nostrand, 1935), p. 722.

[9] W. L. Bragg and J. West, Proc. Roy. Soc. **A111**, 691 (1926).

[10] S. K. Allison, Phys. Rev. **38**, 203 (1931).

nickel, which was in turn soldered to the base of the x-ray tube. The curves were all recorded with a current of 10 ma and at a potential of 4800 volts; each curve was repeated a sufficient number of times to reduce the probable error to a satisfactory value. A sample of the data is given in Fig. 2 which shows the tungsten $M\delta$ line and the accompanying satellites. The other lines were recorded with comparable accuracy. The widths of the observed curves could be read to about 2 percent. In the absence of the data necessary for the development of a correction formula[11] for these crystals, the true width values have been obtained by decreasing the observed width by an amount equal to the full width at half-maximum of the (1, −1) curve for the corresponding wave-length. Table II gives a complete list of all the lines and satellites studied in the present work.

The width of a diagram line varies from 0.31 volt for the α_2 line to 12.5 volts for the ζ_1 line.[12] This tremendous variation in width probably arises mostly from unresolved lines. For example, the line $M\eta$ which arises from the transition $M_{IV}O_{II,III}$ in which the $O_{II,III}$ levels are so close as to be indistinguishable, is doubtless an unresolved doublet.

Certainly the abnormal width of the $M\zeta_1$ cannot be explained on the basis of the sum of the widths of the levels from which it comes, since both these levels are involved in the transitions of $M\delta$ and $M\alpha_1$, which have the widths 0.84v and 1.68v, respectively.

A check on the relative intensities of $M\alpha_1$ and $M\beta$ can be made on the assumption that they fit the equation[13]

$$I=a/(1-(x/b)^2),$$

in which a is the maximum intensity, b is the half-width at half-maximum, and x is the abscissa coordinate in appropriate units. The area under this curve is πab, from which it is a simple matter to calculate the relative intensities, defined for an instrument of high resolving power as the ratio of the areas under the curves.

[11] L. G. Parratt, Rev. Sci. Inst. **6**, 387 (1935).
[12] M. Siegbahn and T. Magnusson, Zeits. f. Physik **88**, 559 (1934).
[13] A. Hoyt, Phys. Rev. **40**, 477 (1932).

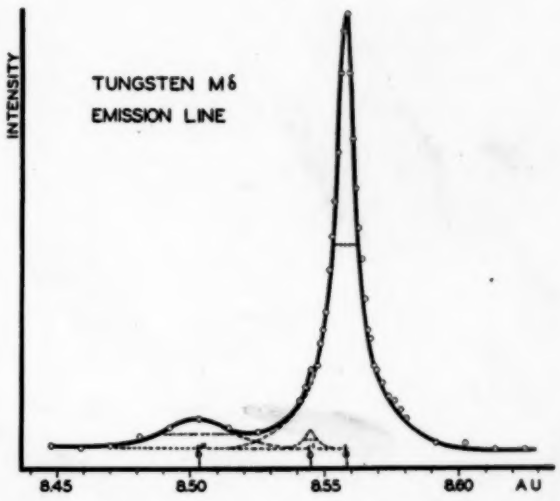

FIG. 2. Intensity curve of $M\delta$, showing two satellites. It is possible that δ'' is more complex than is apparent, as suggested by the large width. The accuracy of the data in this curve is typical of all those reported in this paper.

Experimentally this gives

$$M\alpha_1/M\beta=20.8/14;$$

whereas the theoretical ratio is 20 : 14.

The satellites were obtained by drawing in arbitrarily the background due to the parent line. Special methods were used in some cases, for example $M\zeta_1$ was drawn in as logical a way as possible, taking into account the fact that theory predicts the relative intensities of the three lines $M\zeta_1$, $M\delta$ and $M\zeta_2$ to be in the ratio 9 : 5 : 1.

The satellite contours were resolved into satellite lines as shown by the dashed lines in Figs. 3, 4, 5 and 6. The individual satellites are of approximately classical shape and so chosen that they add to give the recorded curve. While the error may in some cases be very large, this is nevertheless the most satisfactory and accurate method available. The number of satellites appearing on some of the curves is surprisingly large. Three of the $M\alpha_1$ and three of the $M\beta$ satellites have been photographed by Hirsch;[14] all others appear here for the first time.

The *K*-absorption edges of Mg and Al

In view of the necessity of a good source of continuous radiation when studying absorption phenomena, a test was made to compare the

[14] F. R. Hirsch, Phys. Rev. **38**, 914 (1931).

TABLE II. *Wave-lengths of peaks and full width at half-maximum of emission lines of the M series of* W(74)

LINE	TRANSITION	WAVE-LENGTH X.U.	SEPARATION X.U.	SEC.	WIDTH, X.U.	CORRECTED VOLTS	PREVIOUS MEAS.	OBS.
α_2	$M_V N_{VI}$	6978		33.8	1.2	0.31	6976	L-H
α_1	$M_V N_{VII}$	(6969)	0	186.0	6.6	1.68	6967	H
α_1^1	Sat.	6962	7					
α_1^2	Sat.	6960	9	50.7	1.8	0.46		
α_1^3	Sat.	6956	13	50.7	1.8	0.46	6956	H
α_1^4	Sat.	6947	22	152.0	5.4	1.37	6947	H
α_1^5	Sat.	6939	30	101.0	3.6	0.92		
α_1^6	Sat.	6931	38	169.0	6.0	1.53	6933	H
β	$M_{IV} N_{VI}$	(6743)	0	220.0	7.85	2.14	6941	H
β^1	Sat.	6735	6	67.6	2.42	0.62	6734	H
β^2	Sat.	6729	12	101.0	3.64	1.00		
β^3	Sat.	6723	18	67.6	2.42	0.62		
β^4	Sat.	6717	24	50.7	1.83	0.49	6719	H
β^5	Sat.	6712	29	60.8	2.18	0.59		
β^6	Sat.	6705	36	152.0	5.42	1.42	6707	H
δ	$M_{IV} N_{III}$	(8559)	0		4.97	0.84		
δ^1	Sat.	8544	15					
δ^2	Sat.	8503	56	840	28.1	2.75		
ζ_1	$M_V N_{III}$	(8943)	0	2470	80.5	12.5		
ζ_1^1	Sat.	8867	76	335	10.9	1.69		
ζ_1^2	Sat.	8865	78					
ζ_1^3	Sat.	8858	85					
ζ_1^4	Sat.	8851	92	44	2.32	0.36		
ζ_1^5	Sat.	8842	101					
ζ_1^6	Sat.	8837	106					
ζ_1^7	Sat.	8828	115	173	5.6	0.87		
ζ_1^8	Sat.	8812	131	258	8.4	1.3		
ζ_1^9	Sat.	8802	141	105	3.42	0.53		
ζ_1^{10}	Sat.	8795	148	54	1.76	0.27		
ζ_1^{11}	Sat.	8783	160					
ζ_1^{12}	Sat.	8775	168	460	15.0	2.32		
ζ_2	$M_{IV} N_{II}$	8972	0	410	13.3	2.3	8977	L
ζ_2^1	Sat.	8953	24	274	8.8	1.37		
ζ_2^2	Sat.	8934	43	54	1.76	1.27		
ζ_2^3	Sat.	8928	49					
ζ_2^4	Sat.	8920	57	105	3.42	0.53		
ζ_2^5	Sat.	8913	64					
ζ_2^6	Sat.	8909	68					
ζ_2^7	Sat.	8905	72					
η	$M_{IV} O_{II,III}$	6794		304	10.9	3.01	6794	L

L: Lindberg; H: Hirsch; ( ) in col. 3 from Lindberg, used as reference points.

intensity of the general radiation from a heavy element with that from a light one. The elements tested were W (74) and Al (13), and radiation of 10A was used, since it was far removed from the characteristic radiation of either element. Under identical operating conditions (4500 volts, 8 ma) the counting rate with the Al target, over a twenty-minute period, showed a 30 percent increase over that for the tungsten target, the recorded intensity being due to both scattered and reflected radiation. About 50 percent of the measured intensity was due to scattering, which should be proportional to the intensity of the radiation incident on the first crystal. Since a 30 percent increase is not likely to be due to the reflected 10A radiation alone, there must be an increase in x-ray production for Al over that for W in this wave-length region. The efficiency relation predicts, at this potential, $\epsilon = 0.029$ percent for W, and 0.005 percent for Al. Further investigation in this wave-length region is needed.

The present study of the *K*-absorption edges of Mg (12) and Al (13) was made using the continuous radiation from a tungsten target, the intensity of which was constant over the ranges used, which is not the case for an aluminum target. Although the aluminum in the beryl crystals might be expected to affect the reflectivity of the crystals in the region of the absorption edge, the percentage of the aluminum is low and probably affects the reflectivity inappreciably. For the aluminum, the counter window served as the absorber with a thickness of 2.54×10^{-4} cm. In the case of magnesium, an

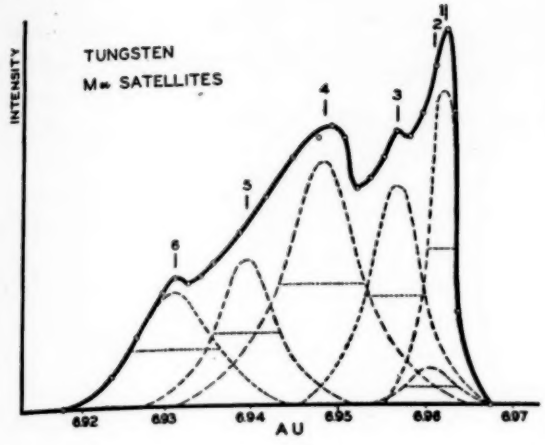

FIG. 3.

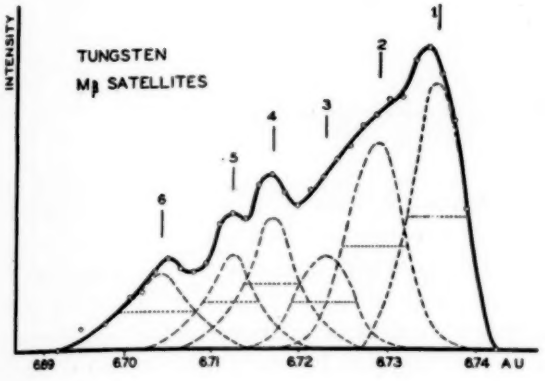

FIG. 4.

absorbing foil 3×10^{-4} cm thick was hung before the counter window. The transmission curve for aluminum was repeated eight times, giving a total of 2500 counts per point on the high absorption side and 5000 on the low side. The probable error is indicated on some of the points on the curve (Fig. 8). The magnesium curve was repeated twelve times, giving a probable error slightly less than that for aluminum. The curves have been plotted with mass absorption coefficient against wave-length to eliminate the effect of foil thickness.[15]

By application of the quantum-mechanical radiation theory of Weisskopf and Wigner to absorption phenomena, Richtmyer, Barnes and Ramberg[16] arrived at an expression for the shape of an x-ray absorption limit in the case where the absorption is due to the ejection of electrons from inner orbits to the continuum of unoccupied Fermi-Sommerfeld levels. The expression is in the form of a simple arctangent curve in which the horizontal separation of the two points, where the curve reaches $\frac{1}{4}$ and $\frac{3}{4}$ of its asymptotic ordinate for high frequencies, is the width of the limit. Applying this relation to the observed contours of the Mg (Fig. 7) and Al (Fig. 8) curves yields the results shown in Table III for the width of the K states of the two atoms.

The Kronig theory applies strictly to the structure 100 volts or more from the edge, where the energy of the electron is great enough that it may be considered practically free in the lattice. The present curves for Mg and Al indicate that the effect of the crystal structure is appreciable to within a short distance of the edge. Because of the similarity between cubic

[15] F. K. Richtmyer and S. W. Barnes, Phys. Rev. **45**, 754A (1934).
[16] F. K. Richtmyer, S. W. Barnes and E. G. Ramberg, Phys. Rev. **46**, 843 (1934).

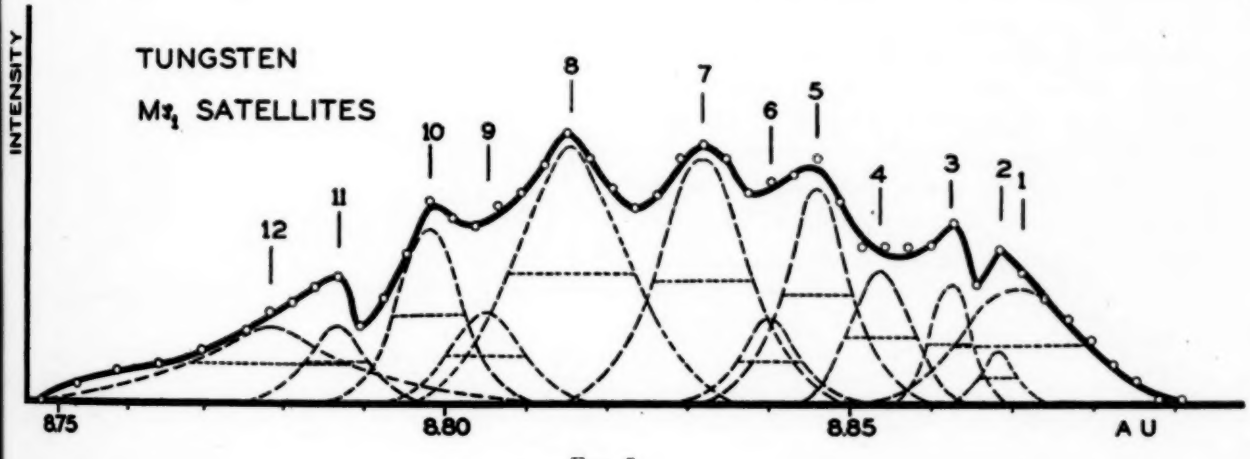

FIG. 5.

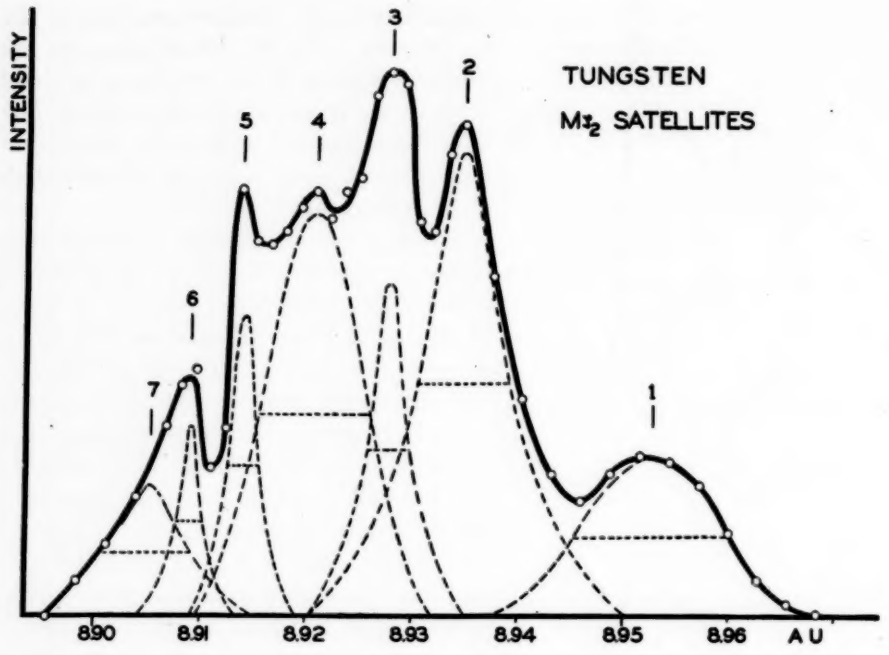

FIG. 6.

close-packed lattices and close-packed hexagonal lattices as regards the shells of nearest and next nearest neighbors, there should be a correspondence between the maxima and minima of the absorption edges in the two types of lattices. This has been pointed out by Coster,[17] and the present curves bear out this fact. The distance to nearest neighbors in the Al lattice is 2.87A. On reducing the Mg lattice to an ideal close-packed hexagonal lattice, the distance to nearest neighbors is 3.18A. The distances of the maxima and minima of the Mg curve from the edge, multiplied by $(3.18/2.87)$,[2] may be compared with those of the Al curve, the results being given in Table IV. The agreement is seen to be within experimental error. The first few maxima and minima do not check as well as might be expected, since within about 15 volts of the edge the atomic fields predominate over the crystal potentials. The Mg curve matches each of the fluctuations in the Al curve and in addition contains three maximum-minimum pairs, inserted in the spaces corresponding to the $B-\beta$, $\beta-C$, and $\gamma-D$ intervals of the Al curve. The appearance of these may be explained as due to the additional reflection planes (zones of discontinuity) made possible by the increase in complexity of the hexagonal crystal over the cubic crystal.

These same two contours were recorded photographically by Sandstrom[18] and it is interesting to note that the first maxima observed there were

TABLE III. *Width of the K states of* Mg(*12*) *and* Al(*13*).

EDGE	w NOT CORRECTED	w CORRECTED FOR RESOLVING POWER
Mg	1.5 volts	0.5 volt
Al	1.25 volts	0.35 volt

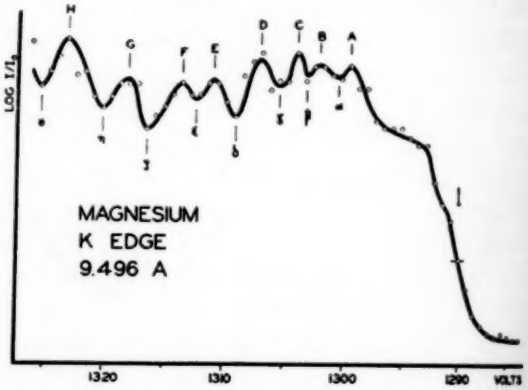

FIG. 7. The absorption coefficient of Mg (12) in the neighborhood of the *K*-absorption limit. The width of the *K* state is indicated by the line directly below the arrow.

[17] D. Coster, Physica 2, 606 (1935).

[18] A. Sandstrom, Dissertation, Uppsala, Sweden, 1935.

for Al, $\alpha=27$v and Mg, $\alpha=26$v from the edge. These correspond to γ and ζ, respectively, in the present cases.

A comparison between the K and L edges in crystals of the same type is also possible,[19] for while the selection rules involved in the two cases differ, the electron removed by absorption may be considered free. The crystal structure is the determining factor and the positions should agree quite close to the edge; the shape of the maxima and minima, depending on the transition probabilities, is mostly determined by the lower state.

TABLE IV. *Positions of secondary structures of* Mg (*12*) *(reduced),* Al(*13*) *and* Ag(*47*) *measured in volts from the main edge of each curve, respectively.*

Distances in Volts of the Maxima and Minima, of the Recorded Curves, from the Main Edge		Mg, Reduced (Compare with Al)	Ag (to be Compared with Al)
Mg	Al		
α 10.3	α 11.5	12.6	α 12.0
B 11.8	B 13.5	14.5	B 17.0
β 12.8			
C 13.9			
γ 15.4	β 18.0	18.5	β 20.0
D 17.2			
δ 19.2			
E 20.15	C 24.5	25.0	C 24.0
ϵ 22.3	γ 28.0	27.5	γ 28.0
F 23.3			
ζ 26.0			
G 27.86	D 34.0	34.3	D 33.0
η 30.0	δ 38.0	37.0	δ 37.0
H 33.0	E 42.0	40.6	E 44.0
θ 35.3	ϵ 45.0	43.5	ϵ 51.0

[19] J. Veldkamp, Physica **2**, 32 (1935).

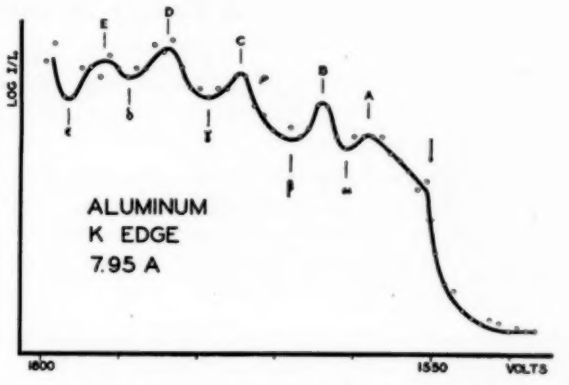

FIG. 8. The absorption coefficient of Al (13) in the neighborhood of the K-absorption limit. The width of the K state is indicated by the dash below the arrow.

Silver has a grating constant of 4.08A, or a distance to nearest neighbors of 2.89A, almost identical with Al, both having the same crystal structure. The L_{III} edge of Ag was recently recorded on a double crystal spectrometer[20] and in the final column of Table IV are given the distances of the maxima and minima from the edge for the Ag curve for all points corresponding to ϵ on the Al curve. In spite of the nearness to the edge, the agreement is quite remarkable.

The effect of nuclear (ionic) charge is also noticeable. Al has three conduction electrons, Mg two. The variation in potential through the lattice should be greater for Al, the effects of which show up in the curves in the sharpness of the fluctuations.

[20] L. G. Parratt, Phys. Rev. **54**, 99 (1938).

A Theory on Cathode Luminescence

UGO FANO
Washington Biophysical Institute, Bethesda, Maryland
(Received May 31, 1940)

A tentative explanation is given of experiments concerning the dependence of the brightness of a luminescent material on the voltage of electron bombardment. A model is assumed in which surface effects prevail over luminescence in using radiation energy. The possibility of a quantitative theoretical treatment is largely due to symmetry properties in the diffusion of scattered electrons in a solid body.

1. INTRODUCTION

T. B. BROWN[1] performed accurate measurements of the amount of light emitted by a luminescent material known as "artificial willemite" (Zn_2SiO_4+about $\frac{1}{2}$ percent MnO_2 activator) when bombarded by cathode rays of 200 to 1300 volts.[2] Measurements were made varying both voltage and current density. Luminescent energy was emitted within a band at about 5500A. The important feature of the experimental result is expressed by the formula:

$$W=5.10^{-6}V^2+0.17. \quad (1)$$

W is the luminescent energy per impinging electron measured in electron volts, V is the voltage of the impinging electrons. This formula is valid for small currents and represents a very good approximation of the experimental results between 200 and 800 volts; above 800 volts W becomes slightly larger than indicated in (1). We shall call *efficiency* the fraction of the electronic energy converted into light, that is W/V. The efficiency is small: at 200 volts its value is 0.002; that is, one obtains an average of 2/10 of a light quantum per electron. If the slight correction arising from the term 0.17 is neglected, *the efficiency increases proportionally with the energy*. The term 0.17 will be neglected in the general lines of the explanation; its meaning will appear only in the final discussion. It is very striking to find a steady variation of efficiency following a simple formula, since the phenomenon itself is quite complex and since the elementary processes involving slow electrons are not known to follow any simple quantitative law.

Further information may be obtained from experimental results quoted by N. Riehl.[3] This information concerns production of luminescence by α-particles in ZnS+activator Cu which takes place with very high efficiency (order of magnitude 80 percent). The mechanism of the phenomenon is not supposed to be very different in the two cases studied by Brown and Riehl. Assuming that each atom of Cu can only emit one or two quanta under the influence of the same α-particle, Riehl calculates the number of Cu atoms which are needed to convert into light the energy of a single α-particle. From this number he calculates, then, that an α-particle is able to excite Cu atoms at a distance of 4×10^{-5} cm from its path.

It is striking to find a large difference in the order of magnitude of the efficiency of α-rays and cathode rays whose velocities are nearly the same. (Because of general arguments of the theory of the stopping power, the density of production of excited atoms cannot be very different if the velocities are nearly equal.)

2. GENERAL LINES OF EXPLANATION

We shall call Δ the effective range of diffusion of the energy transferred by charged particles to

[1] T. B. Brown, J. Opt. Soc. Am. **27**, 186 (1937).
[2] An independent research by W. H. Nottingham (J. App. Phys. **8**, 762 (1937)) confirmed Brown's results and was extended to a wider interval of voltage, in which, however, the quantitative relations are not so impressive as in Brown's interval.
[3] N. Riehl, Ann. d. Physik **29**, 636 (1937).
[4] The information given by α-particle experiments precludes any explanation of Brown's small efficiency which would rely on the crowding of excitations along the path and on the fact that crowding decreases with increasing energy. Ultraviolet rays also produce luminescence with very high efficiency (about 50 percent); however, no strong argument may be derived from this since the mechanism of luminescence may conceivably be quite different in the case of ultraviolet rays.

a luminescent crystal. Thus Δ is the maximum distance at which charged particles are able to excite luminescent atoms. It is reasonable to assume that Δ is of the same order of magnitude for α-particles and slow electrons and not very far from the value 4×10^{-5} cm calculated by Riehl.

The energies of α-particles and slow electrons having the same velocities are quite different. Alpha-particles are not strongly scattered and penetrate very deeply ($\sim3\times10^{-3}$ cm) into a crystal before being stopped; slow electrons are strongly scattered and readily stopped before penetrating deeply: One may guess that the penetration of 200-volt electrons is about 10^{-7} cm. Hence the penetration of cathode rays into the crystal is much smaller than Δ, whereas it is much larger in the case of α-particles. Therefore the diffusion of energy takes place in the case of α-particles far away from the surface, whereas its very origin lies near the surface in the case of electrons.

Parasitic processes, as production of heat or emission of secondary electrons, may prevent the diffusing energy from reaching luminescent atoms. *We shall assume that parasitic processes are much stronger on the surface* than in the interior of the crystal. This explains that the efficiency of slow electrons is very small and that it increases with increasing energy and penetration of the electrons. Our assumption cannot be proved, since sufficient knowledge of the excited states of crystals is not available, but it may be easily made plausible. As a general rule, the coupling between electronic and nuclear motion in solid matter is very effective in transforming excitation energy into heat; special symmetry and periodicity relations may reduce the intensity of this process strongly, but irregularities of symmetry or periodicity will conversely destroy any metastability. The surface of a crystal constitutes a very important irregularity, not only as a discontinuity, but also because the surface itself may not be smooth.

We shall first make the particular assumption that energy reaching the surface by diffusion is very likely to be lost for the luminescence process. The actual probability of loss on the surface will be deduced as an experimental result.

In §3 we shall consider the diffusion of energy. Excitation energy may be transferred from an atom to the neighboring ones in the lattice; wandering excitations may be treated as diffusing particles, called *excitons*.[5] Excitons are scattered (elastically or inelastically) by any irregularity in the lattice: thermal motion, foreign atoms and so on. The energy of the excitons is absorbed in one or several steps. We shall assume that the efficiency of an exciton is proportional to its probability of diffusing to a distance Δ without having previously reached the surface. Elementary considerations of diffusion theory show then, that *the efficiency is proportional to the distance of the origin of the excitons from the surface* and that the proportionality coefficient is about $1/\Delta$. Hence one obtains *agreement with the experimental efficiency* 10^{-3} for 200 volts, taking as reasonable figures $\Delta\sim10^{-4}$ cm and the distance of the origin of the excitons from the surface $\sim10^{-7}$ cm.

One will then investigate (§4) how the "average depth" of production of excitons depends upon the initial energy of the electrons. It is helpful to apply symmetry considerations to the process of multiple scattering and diffusion of the electrons. The "average depth" may be expressed in terms of simpler physical quantities: free path of scattering and stopping power of electrons, and "effective albedo"[6] of the material for impinging electrons.

Free path of scattering and stopping power will require some particular discussion, since the approximations generally used are rather inaccurate within our range of energies. Knowledge of the "effective albedo" would require a detailed solution of the diffusion problem, but one may show that its influence on the results is very small. One will finally show that the average depth of production of excitons is nearly proportional to the electronic energy (§5). The final formula may be fitted quite well to Brown's experimental results (§6).

---

[5] The properties of excitons may vary within a wide range, since they are very sensitive to quantitative relations of the particular crystal lattice (reference may be made to a paper by J. Frank and E. Teller, J. Chem. Phys. **6**, 861 (1938)).

[6] Following the analogy with neutron diffusion, we indicate as "effective albedo" a physical quantity concerning that fraction of the impinging electrons, which emerges again from the surface after diffusion.

3. Exciton Diffusion and Surface Absorption

To determine the efficiency η of an exciton of energy ϵ produced at a small distance x from the surface, we assume first that the exciton is lost if it reaches the surface. We conclude from α-particle experiments that the efficiency is practically unity if the surface losses are avoided. The efficiency η is then equal to the probability $p(x)$, that the exciton does not reach the surface and we want to calculate this function under the assumption: $p(x)\ll 1$. A second exciton produced at a depth $2x$ has the probability $p(x)$ of never coming within a distance x from the surface; if, however, it does come within such a distance—the probability for this is $(1-p(x))$—it still has the same probability $p(x)$ of escaping as the exciton considered first. Hence we find a total probability: $p(2x)=p(x)+(1-p(x))p(x)\sim 2p(x)$, neglecting $p(x)^2$, and we deduce, that $\eta=p(x)$ is proportional to the depth:

$$\eta\sim kx \quad \text{if} \quad kx\ll 1. \tag{2}$$

Moreover, since $\eta\sim 1$ for $x\sim\Delta$, we have:

$$k\sim 1/\Delta, \quad \eta\sim x/\Delta, \quad \text{if} \quad x\ll\Delta. \tag{3}$$[7]

Calling w the average amount of energy radiated as luminescent light, one has:

$$w=\eta\epsilon\sim x\epsilon/\Delta. \tag{4}$$

We shall now take into account two factors neglected heretofore. First the probability of an exciton's reaching the surface and being reflected by it without absorption is the product of the probability of its reaching the surface, and the reflection coefficient r (which is still supposed to be small). This product is nearly equal to r, since the first factor is $(1-x/\Delta)\sim 1$ within the limits of our approximation. Second, we have so far considered the free path of diffusion l as infinitely small as compared with x (according to the usual assumption of diffusion theory). If $l\neq 0$, but still $l\ll x$, one has to add to (3) a constant of the order of l/Δ. Then, putting C as:

$$C=l/\Delta+r \tag{5'}$$

one has:

$$\eta\sim x/\Delta+C; \quad w\sim x\epsilon/\Delta+C\epsilon. \tag{5}$$

The generalization to the actual production of many excitons by the electrons is carried out by introducing the amount of energy $\epsilon(x)dx$ lost by the electrons between the depths x and $x+dx$. Hence (5) goes over to:

$$W=\frac{\int_0^\infty x\epsilon(x)dx}{\Delta}+C\int_0^\infty \epsilon(x)dx, \tag{6}$$

which is the theoretical expression to be compared with (1). The physical meaning of $\int_0^\infty x\epsilon(x)dx$ is evidently: the *excitation energy times the average depth* at which the excitation takes place.

4. Symmetry Properties of Electron Diffusion

Electrons entering a solid body undergo multiple scattering, which goes over into diffusion and may eventually lead to the re-emission of the electrons. This phenomenon is rather complicated by the parallel action of diffusion and energy losses; slowing down changes the probability of scattering, as the diffusion goes on. The following qualitative considerations of simple diffusion phenomena will be helpful for the calculation of $\int_0^\infty x\epsilon(x)dx$.

We shall consider the diffusion of particles with unit mean lifetime produced at a rate of N per second (their total number is then N). The particles diffuse in a three-dimensional space without boundaries and are produced along the plane $x=a$. Call $n(x)dx$ the number of such particles between the planes x and $x+dx$; we want to discuss the average value of the x coordinate of the particles, that is, $(1/N)\int_{-\infty}^{\infty} xn(x)dx$. The symmetry of the system requires $n(a+\delta)=n(a-\delta)$, and hence:

$$\int_{-\infty}^{\infty} xn(x)dx=aN. \tag{7}$$

We shall now distinguish as particles of "class 1" those particles which have already crossed the plane $x=b$ $(b<a)$ at least once; all

[7] The formula without the condition $x/\Delta\ll 1$ is of the type:

$$\eta\sim 1-e^{-x/\Delta}.$$

the remaining particles shall be called of "class 2," so that: $n(x)=n_1(x)+n_2(x)$. The particles of class 1 (N_1 in number) are distributed as particles produced along the plane $x=b$; hence:

$$\int_{-\infty}^{\infty} x n_1(x)dx = bN_1. \tag{7'}$$

Since no particle of class 2 is found to the left of $x=b$, we have:

$$aN=\int_{-\infty}^{\infty} x n(x)dx=\int_{-\infty}^{\infty} x n_1(x)dx$$

$$+\int_{-\infty}^{\infty} x n_2(x)dx = bN_1+\int_{b}^{\infty} x n_2(x)dx. \tag{8}$$

We consider now particles which are produced at $x=a$ and which are lost if they reach the surface $x=0$. Their distribution is represented by $n(x)=n_2(x)$, if one takes $b=0$; then (8) becomes:

$$\int_{0}^{\infty} x n(x)dx = aN. \tag{9}$$

The integral on the left side of (9) is *independent of the number of surviving particles* $\int_0^\infty n(x)dx$: the more particles flow out through the surface $x=0$, the farther the survivals diffuse in the interior towards $x=\infty$.[8]

If one takes into account that the value of the free path λ of the particles is not negligible one cannot consider the particles of class 1 as if they were produced at $x=b$ because they are all directed towards $x=-\infty$ when they cross this plane. The coherence of their directions is lost at the end of their free path; we have then to substitute in (7'):

$$b \rightarrow b-\lambda\langle|\cos\theta|\rangle_{Av}, \tag{10}$$

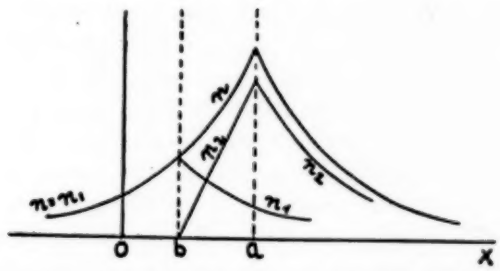

FIG. 1. $n(x)$: Plot of the approximate distribution of particles originating along the plane $x=a$. $n_1(x)$: Plot of the approximate distribution of particles having already crossed the plane $x=b$. $n_2(x)$: Plot of the approximate distribution of particles which have not yet crossed the plane $x=b$.

where θ is the angle between the directions of the particles at $x=b$ and the x axis, and where $\langle|\cos\theta|\rangle_{Av}$ is the average of the absolute value of $\cos\theta$. The same method may be applied to the case of a nonisotropic source of particles, for instance directed towards $x=\infty$, substituting:

$$a \rightarrow a+\lambda\langle|\cos\theta|\rangle_{Av}. \tag{10'}$$

We consider now the diffusion within a body extending from $x=0$ to $x=\infty$; particles enter the boundary surface $x=0$ and are lost, if they flow out again through it. In this case we have to introduce the substitutions (10) and (10') into (8) and then to put $a=b=0$. Calling J the current of particles, we have then:

$$\int_0^\infty x n(x)dx = J_{in}\lambda_{in}\langle|\cos\theta_{in}|\rangle_{Av}$$

$$+J_{out}\lambda_{out}\langle|\cos\theta_{out}|\rangle_{Av}. \tag{11}$$

The *average depth* of the particles is thus determined by the flow of particles through the boundary and by their free path, independently of the actual details of the diffusion problem.

The problem of finding $\int_0^\infty x\epsilon(x)dx$ for electrons scattered in a solid body is still more complex. One may consider electrons having been slowed down as classified according to their energy; slowing down shifts electrons from one class to the next one. One finds that symmetry considerations still apply to each class so that a final result analogous to (11) may be found. Anisotropy of scattering has also to be taken into account; this must be done here—as in many other problems—by dividing the actual mean free path by $1-\langle\cos\vartheta\rangle_{Av}$ (ϑ = deflection).

[8] The mathematical treatment of the same problem is this: Call $q(x)$ the distribution of production of the particles, τ their mean lifetime, D the diffusion coefficient of the particles. $n(\infty)=0$ with its derivatives is the general boundary condition; $n(0)=0$ is the effect of the absorption at $x=0$. Then:

$$D\frac{d^2n}{dx^2}-\frac{1}{\tau}n(x)+q(x)=0$$

$$\int_0^\infty x n(x)dx=\int_0^\infty x\tau\left[D\frac{d^2n}{dx^2}+q(x)\right]dx$$

$$=D\tau\left[x\frac{dn}{dx}-n\right]_0^\infty+\tau\int_0^\infty xq(x)dx=\tau\int_0^\infty xq(x)dx.$$

We shall now go over to quantitative calculations. We introduce a system of polar coordinates θ, ϕ, having x as polar axis, and call $F(x, s, \theta)$ the current of electrons of residual "true" range s [9] at a depth x with direction θ, per unit residual range, per unit solid angle. We call ϑ the angle between the directions (θ, ϕ) and (θ', ϕ'), $\sigma(\vartheta)d\Omega'$ the differential cross section for elastic scattering from (θ, ϕ) into (θ', ϕ') within the solid angle $d\Omega'$ and N the number of scattering atoms per cc. $F(x, s, \theta)$ is a solution of the equation:

$$\cos\theta\frac{\partial F}{\partial x}=\frac{\partial F}{\partial s}-NF(x, s, \theta)\int_{4\pi}\sigma(\vartheta)d\Omega'$$
$$+N\int_{4\pi}F(x, s, \theta')\,\sigma(\vartheta)d\Omega'. \quad (12)^{10}$$

Putting:

$$\int_{4\pi}\cos^n\theta\ F(x, s, \theta)d\Omega=F_n(x, s)$$

and taking into account the properties of the spherical harmonics, one has:

$$\frac{\partial F_2}{\partial x}=\frac{\partial F_1}{\partial s}-F_1N\int_{4\pi}\sigma(\vartheta)(1-\cos\vartheta)d\Omega'$$
$$=\frac{\partial F_1}{\partial s}-F_1\frac{1}{\lambda}, \quad (13)^{11}$$

where:

$$1/\lambda=N\int_{4\pi}\sigma(\vartheta)(1-\cos\vartheta)d\Omega',$$

and hence:

$$F_1(x, s)=\int_{\infty}^{s}ds'\frac{\partial F_2(x, s')}{\partial x}\exp\left[-\int_{s}^{s'}\frac{ds''}{\lambda}\right]. \quad (14)$$

$F_1(x, s)$ represents the positive current of particles with residual range s across the plane x. $\int_0^\infty E(s)F_1(x, s)ds$ is the total stream of kinetic energy across it towards $x=\infty$ where $E(s)$ is the energy corresponding to the residual range s. Hence the negative gradient of $\int_0^\infty E(s)F_1(x, s)ds$ represents the density of energy loss of the electrons;

$$\epsilon(x)=-\int_0^\infty E(s)\frac{\partial F_1}{\partial x}ds.$$

Integrating by parts, using (13), changing the order of integrations and using the condition $F=0$ for $x=\infty$, we obtain the final formula:

$$\int_0^\infty x\epsilon(x)dx=\int_0^\infty ds\,F_2(0, s)\mathcal{E}(s),$$
$$\mathcal{E}(s)=\int_0^s ds'E(s')\exp\left[-\int_{s'}^{s}\frac{ds''}{\lambda}\right]. \quad (15)$$

This formula closely corresponds to (11), since $F_2(0, s)$ may be represented as:

$$J_{\text{in}}\langle|\cos\theta_{\text{in}}|\rangle_{\text{Av}}+J_{\text{out}}\langle|\cos\theta_{\text{out}}|\rangle_{\text{Av}}.$$

$\mathcal{E}(s)$ replaces λ; its dimensions are: energy loss of electrons times depth of their penetration. The dependence of $\mathcal{E}(s)$ on the elements determining the penetration, scattering cross section and stopping power dE/ds, appears more clearly in the asymptotic formulae:

$$\mathcal{E}(s)\sim E(s)\lambda(s), \quad \text{if} \quad \lambda(s)\ll s, \quad (16)$$
$$\mathcal{E}(s)\sim E(s_{\text{av}})s, \quad \text{if} \quad \lambda(s)\gg s. \quad (17)$$

A better approximation than (16) is:

$$\mathcal{E}(s)=E(s)\lambda(s)\left(1-\frac{d\lambda}{ds}-\frac{1}{E}\cdot\frac{dE}{ds}+\cdots\right). \quad (16')$$

For the second integral in (6) one has, obviously:

$$\int_0^\infty\epsilon(x)dx=\int_0^\infty ds E(s)F_1(0, s). \quad (18)$$

5. Discussion

We have now to collect the evidence available at present concerning the dependence of the quantity (15) on the initial energy of the

[9] "True" range is the range measured along the actual path. We consider s as a suitable measurement of the energy of the electrons.

[10] See for an analogous equation: W. Bothe, Zeits. f. Physik **54**, 161 (1929).

[11] Expansion in spherical harmonics may be considered as a general method of attack to the integral-differential equation (12) and transforms it into a chain of differential equations;

$$\frac{l}{2l+1}\frac{\partial F^{(l-1)}}{\partial x}+\frac{l+1}{2l+1}\frac{\partial F^{(l+1)}}{\partial x}=\frac{\partial F^{(l)}}{\partial s}-\frac{1}{\lambda_l}F^{(l)};$$
$$F^{(l)}=\int_{4\pi}F(x, s, \theta)P_l(\cos\theta)d\Omega,$$
$$\frac{1}{\lambda_l}=N(\sigma_0-\sigma_l)=N\int_{4\pi}\sigma(\vartheta)[1-P_l(\cos\vartheta)]d\Omega'.$$

electrons. Equation (15) is given as a function of the free path $\lambda(E)=\lambda(s)$, of the stopping power dE/ds (appearing as $E(s)$) and of $F_2(0, s)$. The quantity $F_2(0, s)$ is an integral over θ and consists of the contributions of the impinging electrons ($\theta \leqslant \pi/2$), which is known, and of the outgoing ones ($\theta \geqslant \pi/2$). The unknown features of the diffusion[12] affect only the integration for $\theta \geqslant \pi/2$.

The contribution to (15) arising from the incoming electrons is proportional to the square of their voltage V^2 if any one of the following conditions is fulfilled:

(a) if $\lambda(s) \ll s$ and $\lambda(E) \sim$ const. E, on account of (16);

(b) if $\lambda(s) \gg s$ and $dE/ds \sim$ const., on account of (17);

(c) if both $\lambda(E) \sim$ const. E and $dE/ds \sim$ const., whatever the average of λ and s may be, since then, putting $\lambda=\alpha E$, $s=\beta E$:

$$\mathcal{S}(s)=\frac{\alpha\beta}{2\alpha+\beta}E^2=\frac{\beta}{2\alpha+\beta}E\lambda=\frac{\alpha}{2\alpha+\beta}Es. \quad (19)$$

The contribution of incoming electrons is sufficient to determine the dependence of (15) on V completely;

(A) if the contribution of the outgoing electrons is negligible;

(B) if the contribution of the outgoing electrons is proportional to the contribution of the incoming ones and the proportionality factor is independent of the energy.

Fulfillment of one among the conditions (a), (b), (c) and of (A) or (B) is sufficient to show that (15) is proportional to V^2. Proportionality of the second term of (6), that is of (18), to V is also a consequence of fulfillment of (A) or (B).

We shall next discuss how (A) and (B) are connected with (a), (b) and (c). Condition (b) leads automatically to (A), since then practically no electron is scattered back. Condition (a) involves an approximation opposite to that of (b); however, (a) is consistent with (A), if the relative energy loss along a free path is not negligible. In this case every free path is shorter than the former one; thus an electron is prevented in most cases from reaching the surface of the crystal soon after its first penetration with a large residual energy. (A) is then fulfilled, since the contribution of outgoing electrons to (15) depends strongly upon their energy (possibly upon its square, according to (a)).[13] Condition (B) is fulfilled if:

(B′) $\sigma(\vartheta)$, as a function of energy, is inversely proportional to s[14] and the relation between energy and range has the form $E=as^b$ where a and b are constants. The proof of this is obtained through a similarity transformation of (11) showing that, if (B′) is fulfilled, a change of initial energy affects the solution F of the diffusion equation only as a change of units of x and s. Condition (c) together with the additional assumption that the dependence of the angular distribution of scattering on the energy may be neglected, is sufficient to fulfill (B′), so that (B) follows then as a consequence. The additional condition is required, since proportionality of λ to s is less stringent than the condition $\sigma(\vartheta)=$ const./s.

Going over to discussion of the quantitative relations involved in (a), (b), (c), we have first to evaluate by a wave-mechanical calculation the effect of shielding on scattering of slow electrons. The scattering cross section in a central field is:

$$\sigma(\vartheta)=\frac{h^2}{32\pi^2mE}\left|\sum_{l=0}^{\infty}(2l+1)P_l(\cos\vartheta)(e^{2i\delta_l}-1)\right|^2. \quad (20)$$

($m=$ electron mass, $E=$ electron energy, $\delta_l=$ phase shifts of the wave functions determined by field and energy).

$$\frac{1}{\lambda}=N\int_{4\pi}\sigma(\vartheta)(1-\cos\vartheta)d\Omega' =\frac{Nh^2}{2\pi mE}\sum_l l\sin^2(\delta_l-\delta_{l-1}). \quad (21)$$

[12] The determination of the outgoing part of $F(0, s, \theta)$ is analogous, but more complex, to that of the "albedo" of neutrons impinging on a paraffin block.

[13] This picture is also supported by the experimental evidence, that all but a small fraction of the electronic energy is absorbed in a solid body. See the results discussed by W. Bothe (*Handbuch der Physik*, Vol. XXII/2, 1 (1933)), particularly those of B. F. J. Schonland (*ibid.*, p. 44); very soft re-emitted electrons are not taken into account in these experiments. Secondary electrons emitted by the surface are considered in our theory as "lost excitons."

[14] This condition is fulfilled for instance (neglecting logarithmic factors) in the case of high energy electrons, for which Rutherford scattering is inversely proportional to E^2, while the range is directly proportional to it.

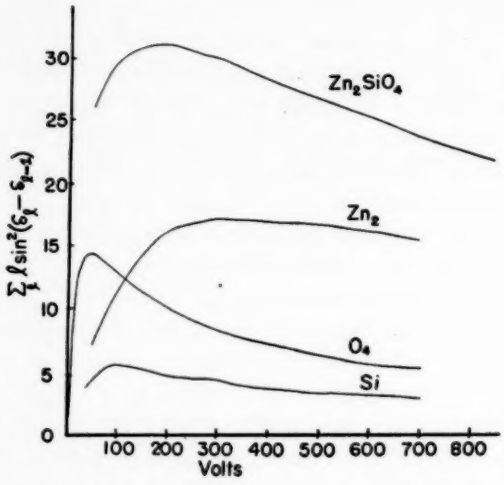

FIG. 2. The effective average cross section for elastic scattering of electrons: $\bar{\sigma} = \int_{4\pi} \sigma(\vartheta)(1-\cos\vartheta)d\Omega$ is given by the square of the wave-length of electrons times $\sum_l l \sin^2(\delta_l - \delta_{l-1})$ divided by π. (From calculations based on Thomas-Fermi model.)

Constant δ_l's (and therefore constant λ/E) are the consequence of a potential field $1/r^2$ for all distances from the nucleus. The δ_l for a Thomas-Fermi field have been calculated by Henneberg.[15] For high energy electrons all δ_l's are very small and decrease with increasing energy; therefore the terms $\sin^2(\delta_l - \delta_{l-1})$ also decrease with increasing energy. One finds λ to be proportional to E^2. At $E=0$ all δ_l's are multiples of π and λ tends to a finite value. In the intermediate region (which is the interesting one)

$$\sum_l l \sin^2(\delta_l - \delta_{l-1})$$

—that is E/λ—goes through a *flat maximum*. Inasmuch as this function may be considered as a constant in the neighborhood of its maximum, one finds the relation $\lambda \sim$ const. E.[16] Because of the characteristic features of a Thomas-Fermi field, only the waves corresponding to the low values of l [17] are strongly distorted, giving rise to large values of their δ_l; hence the first terms $\sin^2(\delta_l - \delta_{l-1})$ are of the order of 1 and the sum converges rapidly after a certain value of l, which is characteristic for the atomic number, but does not depend upon the energy of the scattered electron.

Figure 2 represents the values of:

$$2[\sum_l l \sin^2(\delta_l - \delta_{l-1})]_{Zn} + [\sum_l l \sin^2(\delta_l - \delta_{l-1})]_{Si} + 4[\sum_l l \sin^2(\delta_l - \delta_{l-1})]_{O}$$

and of its single terms as functions of the energy, deduced from Henneberg's results by graphical methods. Some approximations in these or analogous calculations could hardly be avoided. The result is fairly constant, since it varies only by 28 percent within the range of $E=200$ to 800 volts; as a consequence, λ increases in this interval by a factor ~ 5.6 as compared to 4 in the case of a $1/r^2$ field and 16 in the case of a $1/r$ field. Variations of E/λ are chiefly due to the large amount of oxygen contained in the material, since the typical $1/r^2$ region corresponds for oxygen to energies lower than 200 volts. Henneberg's calculation neglects the effects of electronic exchange and of polarization of the internal electronic shells. Polarization is not expected to influence our result; electronic exchange might be effective in improving the constancy of λ/E appreciably. Both effects are difficult to take into account quantitatively.

Through discussion of the stopping power as a function of energy, we wish to justify two fundamental qualitative assumptions and two subsidiary ones: (1) the range s is definitely larger than λ (this is also known from experiments) and hence (a) is nearly fulfilled; (2) the relative energy loss along a free path $[\sim(\lambda/E) \times (dE/ds)]$ is of the order of $\frac{1}{6}$, hence (A) may be fulfilled together with (a); (3) the stopping power is fairly constant over our range of energies, therefore (c) as well as (a) is nearly fulfilled; (4) the ratio of the free path to the "true" range and the relative energy loss along a free path are fairly constant over a wide range of energies, thus also (B) is not very far from being fulfilled and one feels—though indirectly—encouraged to use formula (19).

[15] W. Henneberg, Zeits. f. Physik **83**, 553 (1933).

[16] The Thomas-Fermi potential field is: $Ze^2/r \cdot \varphi(r/\mu) = Ze^2/r^2 \cdot r\varphi(r/\mu)$; the function $x\varphi(x)$ has a very flat maximum and varies slightly if one changes the distance from the nucleus within a factor 10. Further evidence on the inverse linear dependence of scattering from the energy is obtained by plotting Lenard's experimental data of apparent absorption coefficients, as given by W. Bothe (*Handbuch der Physik*, Vol. XXII/2 (1933), p. 41).

[17] These values correspond essentially to the possible values of l for atomic electrons (see for instance: E. Fermi, Zeits. f. Physik **48**, 73 (1928)).

One can hardly evaluate the stopping power in our range of energies, since every theory assumes that the particle to be stopped is much faster than atomic electrons, while this condition is not fulfilled in our case. Considering, however, that we need only qualitative results, we shall tentatively use Bloch's formula[18] in the form:

$$\frac{dE}{ds}=0.385N\frac{h^2}{m}\frac{E_0}{E}\log\frac{E}{E_0};$$
$$E_0=\frac{6.04}{2\pi}\left(\frac{2}{e}\right)^{\frac{1}{2}}Z\cdot 13.54\sim 11.2Z \text{ volts}. \tag{22}$$

This formula relies on Thomas-Fermi model and might be not too inaccurate for slow electrons, since it has been applied successfully to α-particles having a velocity equal to that of 900-volt electrons. Comparison with experiments is difficult in this region; experiments on ionizing action in gases are available[19] and show a more irregular dependence on energy than (22) does.

The zero point of (22) at $E=E_0$ is obviously incorrect but a rapid improvement in accuracy may be expected for increasing energy. For $E/E_0\gg 1$ the variation of the log factor is negligible and one has the well-known result $s\sim$const. E^2. A maximum occurs at $E=E_0e\sim 30Z$ volts, which is very flat. Hence dE/ds is nearly constant over a wide region (point (3) above). This last fact is also due to the different position of the maxima for different elements. Figure 3 represents the stopping power of Zn_2SiO_4 and of its single components. The result is certainly very inaccurate below 600 volts since E_0 is $\sim$336 volts for Zn; the stopping power should probably be larger in this region than is indicated in the figure.

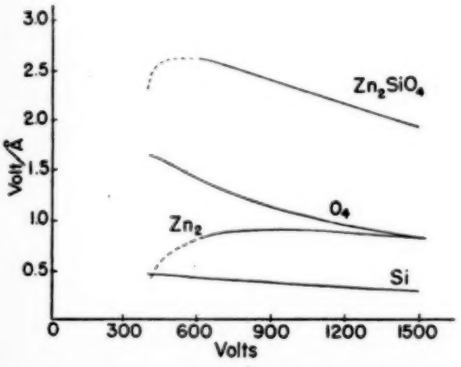

FIG. 3. Stopping power of willemite, calculated from Bloch's formula, assuming density 4. The contributions of the single elements are also indicated.

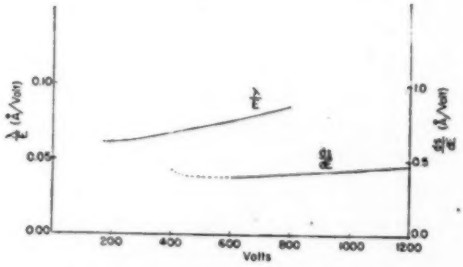

FIG. 4. Correspondence between the "true" residual range of electrons and their energy and between "effective" free path and energy. The ratio $(\lambda/E)/(ds/dE)$ roughly represents the fraction of electronic energy lost along a free path.

The quantities λ/E and ds/dE, which are directly comparable, and, if constant, should be equal to the parameters α and β of (19), are plotted in absolute units in Fig. 4. Points (1), (2), and (4) are verified by inspection of this figure. The asymptotic behavior of both λ/E and ds/dE for large energies ($1/r$ field) is proportional to the energy and their ratio is then $4Z_N/(Z^2)_N=1/5.3$; this result gives further evidence for (4).

Figure 4 shows that λ/E may be fairly well represented by a straight line between 200 and 800 volts; then:

$$\lambda\sim 5.5\times 10^{-10}(1+7.3\times 10^{-4}E)E \text{ cm}, \tag{23}$$

where E is expressed in volts.

The results (1), (2), (3), (4), indicated above allow us to use any one of the formulae:

$$\mathcal{E}(s)\sim E(s)\lambda(s)\left(1-\frac{d\lambda}{ds}-\frac{1}{E}\frac{dE}{ds}+\cdots\right), \tag{16'}$$

$$\mathcal{E}(s)\sim\frac{\beta}{2\alpha+\beta}E(s)\lambda(s). \tag{19}$$

[18] F. Bloch, Zeits. f. Physik **81**, 363 (1933). It might be questionable, which way one should take into account the effects arising from the largest energy transfers to atomic electrons. Formula (22) contains elements from Bloch's formula and from a formula by H. A. Bethe (*Handbuch der Physik*, Vol. XXIV/1 (1933), p. 521 (56.10)). This is because the characteristic of Bloch's formula concerns large values of the impact parameter, while the factor $(e/2)^{\frac{1}{2}}$ concerns close impacts. Anyway, a change of this factor would probably not affect the results too much.

[19] See for instance: R. B. Brode, Rev. Mod. Phys. **5**, 257 (1933).

Remembering our former results it is easily seen that the factors multiplying $E\lambda$ in both formulae are equivalent and that their value is approximately 0.75. Putting then (16′) or (19) into (15), we have:

$$\int_0^\infty x\epsilon(x)dx \sim 5.5\times10^{-10}\gamma_1 \times(1+7.3\times10^{-4}V)\,V^2 \text{ volts cm.} \quad (24)$$

γ_1 includes: the correction 0.75, as mentioned above, a factor <1, if the incidence is not normal, and the possible contribution (factor >1) of outgoing electrons to (15); γ_1 is expected to be of the order of $\frac{2}{3}$. We call γ_2 the fraction of incoming energy absorbed within the crystal, i.e., not taken away by re-emitted electrons; γ_2 is constant if (A) or (B) is fulfilled and has to be very near to 1. Then (6) becomes:

$$W\sim\gamma_1/\Delta\cdot5.5\times10^{-10}(1+7.3\times10^{-4}V)\,V^2 +\gamma_2 CV. \quad (25)$$

6. Conclusion

The results of the quantitative discussion seem to justify the following picture of the luminescent phenomenon. The average penetration of slow electrons in a crystal is essentially given by their effective free path of scattering λ (defined in formula (13)). Because of characteristics of the atomic field as represented by the Thomas-Fermi model, λ is nearly proportional to the energy of slow electrons. A better approximation is given in Fig. 4 and formula (23).

Slow electrons undergo multiple scattering and diffusion within the crystal, but it is not necessary to calculate this process in detail. One may calculate directly $\int_0^\infty x\epsilon(x)dx$, which is the product of the energy lost by the electrons within the crystal and the average depth of energy loss. A careful discussion is necessary to show, that $\int_0^\infty x\epsilon(x)dx$ may be considered as proportional to the voltage of the electrons and to their penetration λ. The efficiency of production of luminescence is proportional to the average depth of production of excitons (i.e., of energy loss by electrons) as stated in §2. Thus one finds finally, that the efficiency may be considered as a linear function of the penetration λ of the electrons. Formula (25) is then obtained,

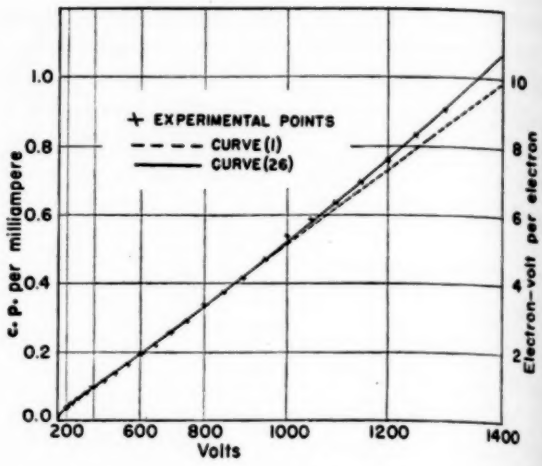

FIG. 5. Luminescent energy emitted by willemite when bombarded by cathode rays, as a function of electron energy, expressed both as brightness and as energy output. The theoretical curve (26) agrees with the experimental points still better than the empirical interpolation (1). Two parameters have been adjusted to fit the points at 200 volts and 800 volts.

which gives the amount of luminescent energy, that is, the efficiency times the incident energy.

γ_1 and γ_2 may be considered constant and slightly smaller than 1. Δ is the range of diffusion of excitation energy within the crystal. C is a physical constant defined by formula (5′) and still to be determined. The third term of (25) corresponds to the constant term in the linear representation of the efficiency as a function of the penetration of the electrons (see formula (5)).

Comparison of (25) with (1), neglect of the second and third term of (25) and the second term of (1), gives:

$$\gamma_1/\Delta\cdot5.5\times10^{-10}V^2\sim5\times10^{-6}V^2;$$

$$\Delta\sim1.1\gamma_1 10^{-4}\sim0.7\times10^{-4}\text{ cm.}$$

This comparison corresponds to a rough theory aiming to show that the efficiency is *proportional* to the energy of impinging electrons. The agreement is improved, if one tries to compare the complete expressions (25) and (1) by suitable determination of the unknown constants Δ and C:

$$aV^2+7.3\times10^{-4}aV^3+bV\to5\times10^{-6}V^2+0.17.$$

Numerical evaluation shows that these two analytical expressions may be made nearly coincident over a wide range of values of V by

suitable choice of a and b. If we take, for instance:

$$a=\gamma_1/\Delta\cdot 5.5\times 10^{-10}=2.28\times 10^{-6},$$
$$b=C\gamma_2=0.133, \tag{26}$$

in order to fit the points at 200 and 800 volts exactly, that is:

$$\Delta\sim 1.6\times 10^{-4}\text{ cm},\quad C\sim 0.14, \tag{26'}$$

then the discrepancy between (25) and (1) never becomes larger than 0.03 volt in absolute value, or 5 percent in relative value, between 200 and 800 volts (Fig. 5). This agreement is as good as one could expect. Above 800 volts (25) correctly represents the faster increase of W (see §1). Equation (25) is certainly not very reliable below 200 volts, but it is important that the theory indicates $W=0$ for $V=0$ since the extrapolation of (1) to $V=0$ is obviously incorrect.

The interpretation of the experimental results now becomes slightly different from the simple one outlined in §2. The theory does not consider that the experimental points of the plot $W(V^2)$ lie on a straight line as represented by (1). Instead it yields an S-shaped curve which fits the experimental points as well as a straight line between 200 and 800 volts and still better than a straight line above this interval.[20] The result is essentially due to the approximate constancy of λ/E, but the apparent linear dependence of W on V^2 is due to the opposite action of two different factors. The slight increasing trend of λ/E tends to bend the curve $W(V^2)$ upwards, whereas the constant term C in the efficiency tends to bend it downwards. The accuracy of the agreement with the experimental results appears not to be due to accidental relations among the numerical constants, since it is only slightly affected by rather large changes of the numerical values (26').

From the formulae (5'), (26'):

$$C=l/\Delta+r\sim 0.14$$

we may obtain further information. The free path of diffusion of excitons l should not be larger than λ, according to the assumptions of our theory; now, since $\lambda/\Delta\ll 0.14$, one concludes, that:

$$l/\Delta\ll C\sim 0.14.$$

Hence we obtain an evaluation of the probability that an exciton impinging on the surface is *not* absorbed by it:

$$r\sim C\sim 0.14.$$

I am very much indebted to Dr. E. Teller, who suggested this work to me and supported me with encouragement and advice in many discussions. Dr. T. B. Brown kindly furnished me with additional information and data on his experiments.

[20] No important deviation of λ from (23) is likely to take place above 800 volts, since the slope of λ/E already corresponds to its asymptotic value given by the theory of Rutherford scattering.

Capture Cross Sections for Thermal Energy Neutrons

CHRISTIAN LAPOINTE AND FRANCO RASETTI
Laval University, Quebec, Canada

(Received June 10, 1940)

Cross sections for capture of thermal energy neutrons were measured for several elements. The method consisted in comparing, by a BF_3 ionization chamber, the density of thermal neutrons in water and in a solution of the element investigated. In order to avoid corrections for geometry, the effect of the substance was compared with that of boron solutions of different concentrations, and consequently the measurements directly give the ratio of the cross sections of the elements investigated to the cross section of boron. Data are given for N, F, Na, P, Cl, K, V, Mn, Co, As, Se, Br, Cd, I, Ba.

MOST of the experiments on scattering and absorption of slow neutrons give values of the total (scattering+capture) cross section. When the cross section is of the order of 10^{-22} cm^2 or more, it is well known to be almost wholly due to capture. Our present knowledge about the character of the cross sections lying between 10^{-24} and 10^{-23} cm^2 is much less definite. Measurements of the scattering cross section have been performed,[1] but in most cases they are not accurate enough to give a significant value of the capture cross section by subtraction from the total cross section measured by neutron beam experiments.

EXPERIMENTAL PROCEDURE

To perform a direct measurement of the capture cross section, the simplest method which suggests itself is the one already employed by Frisch, von Halban and Koch.[2] It consists in measuring, by a BF_3 ionization chamber, the decrease in density of the thermal neutrons inside a certain volume of water when a given percentage of an absorbing element is added. Since Frisch, von Halban and Koch intended to compare the cross sections of boron and hydrogen, the volume of the solution had to be taken large enough so that practically all neutrons emitted by the source were slowed down to thermal velocities, and eventually captured, either by hydrogen or by boron nuclei. The same method would be unpractical, when applied to most other substances, since it would require exceedingly large volumes of concentrated solutions. This can, however, be avoided if the cross section of the element to be investigated is measured in terms of the capture cross section of boron. An amount of solution of any volume and shape may be taken, provided one measures the concentration c_B of boron which produces the same density decrease of the thermal neutrons as the element investigated under the concentration c. Then the relation holds:

$$\sigma_B c_B = \sigma c,$$

where σ and σ_B, respectively, represent the capture cross sections of the element in question and of boron.

The neutron source consisted of 250 mg Ra and Be powder. The BF_3 ionization chamber had a diameter of 2.5 cm and a length of 8 cm. The boron disintegrations were recorded by means of a linear amplifier and a thyratron scale of four. The solution was contained in a cylindrical glass beaker, 14 cm in diameter and filled to a height of about 20 cm, the ionization chamber being immersed in the center of the solution. The neutron source, shielded by 2 cm of lead, was placed outside of the solution, on the axis of the cylinder. The number of counts, under such conditions, was already over one thousand per minute. The effect of neutrons of energies higher than thermal in the present experiment is negligible and was not corrected for. The ionization chamber and the glass cylinder were rigidly

[1] M. Goldhaber and G. H. Briggs, Proc. Roy. Soc. **A162**, 127 (1937); A. C. G. Mitchell and E. J. Murphy, Phys. Rev. **48**, 653 (1935); A. C. G. Mitchell, E. J. Murphy and M. D. Whitaker, Phys. Rev. **49**, 870 (1936); **50**, 133 (1936).

[2] O. R. Frisch, H. v. Halban and J. Koch, Proc. Danske Vidensk. Selskab **15**, 10 (1938).

connected together, and the investigated solutions could be quickly drained through a stopcock at the bottom of the container and replaced with water. Many alternate measurements with water and with the solution were taken for each element. Each reading comprised about 20,000 counts and the discrepancies observed were no larger than the statistical fluctuations.

Results and Discussion

Since large cross sections have already been determined by beam absorption measurements, and cross sections smaller than 10^{-24} cm^2 are unpractical to measure by the present method, we confined our attention to elements which, either from the values of the total and the scattering cross sections given in the literature,[1] or from the intensity of activation under slow neutron bombardment, were expected to possess capture cross sections lying between 10^{-24} and 10^{-22} cm^2.

The compounds employed had to answer the conditions of being sufficiently soluble in water and of not containing other strongly absorbing elements besides the one to be investigated. The concentration was chosen such as to reduce the density of the neutrons by at least ten percent, when allowed by the solubility of the compound.

Most of the elements investigated (probably all except Cd) do not possess neutron resonance levels for thermal energies, and therefore the cross section in this region will follow the 1/v law. The ratio of the cross sections to the cross section of boron therefore possesses a definite meaning, being independent of the velocity of the neutrons.

No corrections were required for geometrical factors, since the effect of the solution was compared with the effect of a boron solution of known concentration under the same conditions. It was first determined how the neutron density depended on the concentration of boric acid solutions. Within the limits of experimental error (about one percent) it was found that the ratio of the intensity I_0 with water to the intensity I with a boron solution of concentration c_B was a linear function of c_B, the empirical relation being

$$I_0/I=1+kc_B/c_H=1+1.02\times10^3c_B/c_H,$$

where with c_H we have indicated the hydrogen concentration. In a solution of infinite volume, the coefficient k should be equal to the ratio of the capture cross sections of boron and hydrogen. The smaller measured value evidently depends on the fact that about half of the thermal neutrons diffuse out of the solution before being captured, either by hydrogen or by boron nuclei.

In most cases, the amount of substance which had to be dissolved in water in order to absorb a measurable fraction of the neutrons was large enough to alter to an appreciable extent the hydrogen concentration. Since a change in hydrogen concentration will, in general, affect the density of the thermal neutrons, measurements were undertaken to determine the magnitude of the effect. It would not be correct to compare water with hydrocarbons or other hydrogenous substances, since a difference in the chemical bond of hydrogen might produce effects of the same order of magnitude. The procedure employed was to dissolve in water a substance which would decrease the hydrogen concentration without appreciably absorbing the neutrons. The experiment was performed by using either a 30 percent solution of H_2O_2 (hydrogen density, 5.5 percent lower than in water) or a saturated solution of oxalic acid (hydrogen concentration, 3.7 percent lower than in water). The density of neutrons was found to be lower than in water by 4.3 percent in the first case and by 3.1 percent in the second case. As an average, we assumed that a decrease of one percent in hydrogen concentration produced a decrease of 0.8 percent in neutron density. The correction has been applied to the values reported in Table I.

Part of the decrease in the number of thermal neutrons when an absorbing substance is dissolved in water will be due to capture of the neutrons through resonance levels before they have been slowed down to thermal energies, and a correction may be required therefor. In order to estimate the importance of the effect, the following experiment was performed. A rhodium plate 5 by 5 cm, shielded by Cd, was substituted for the BF_3 chamber, and irradiated. Under such conditions, it is well known that rhodium is practically activated only by neutrons of about one volt energy. The activity of rhodium was

measured (by means of a pressure ionization chamber connected to an Edelmann electrometer) when the container was filled either with water or with the solutions that had been investigated. For most elements, the characteristic resonance energies lie higher than the resonance energy of rhodium, this applying in particular to As, Br, and I. Then, the observed decrease in the number of characteristic rhodium neutrons will determine the effect of resonance absorption by the dissolved element in decreasing the number of neutrons which are slowed down to thermal velocities. Measurements performed with Cl, Co, As, Br, I, indicated that the decrease in activity of the rhodium was certainly smaller than 2 percent, and probably within one percent. Some of the above-mentioned elements (As, Br, and I) would be likely to produce a more considerable effect than others, since it is known[3] that their activation is due, for an unusually high percentage, to resonance neutrons. The effect being hardly measurable, even in these cases, we decided not to correct our results for resonance capture.

A certain disagreement exists in the literature[2-4] about the cross section of boron for thermal neutrons, the values given lying between 500×10^{-24} and 700×10^{-24}. The value will also, of course, depend on the average effective energy assumed for the thermal neutrons. We assumed $\sigma_B=600\times10^{-24}$. Any change in the cross section of boron would evidently affect all our data by the same factor. A measurement of the cross section of Cd performed as a check on the method gave the correct value.

Table I includes all of our results. Column 3 indicates the number of hydrogen atoms per atom of the element in the solution. Column 4 gives the ratio I_0/I of the number of neutrons with water and with the solution, and the statistical error. Column 5 gives the same ratio, corrected for the change in hydrogen density as above explained. The last column gives the capture cross sections in 10^{-24} cm^2. The value of σ was calculated by means of the formula

$$\sigma=\sigma_B\frac{c_H}{c}\cdot0.98\times10^{-3}\left(\frac{I_0}{I}-1\right).$$

TABLE I. *Capture cross sections for thermal neutrons.*

ELEMENT	COMPOUND USED	c_H/c	I_0/I UNCORR.	I_0/I CORR.	$\sigma\times10^{24}$ cm^2
5 B	H_3BO_3	1,000	2.02 ±0.02	2.02	600
7 N	NH_4NO_3	24.3	1.124±0.006	1.086	1.2
9 F	NaF	105	0.998±0.006	0.990	<0.5
11 Na	NaF	105	0.998±0.006	0.990	<0.5
15 P	H_3PO_4	43.5	1.088±0.007	1.040	1.0
17 Cl	HCl	145	1.32 ±0.01	1.32	27
19 K	KF	82	1.067±0.005	1.067	3.2
23 V	$VOSO_4$	190	1.094±0.006	1.061	6.8
25 Mn	$MnSO_4$	161	1.117±0.005	1.099	9.4
27 Co	$CoSO_4$	470	1.12 ±0.01	1.12	33
33 As	As_2O_5	75	1.187±0.006	1.147	6.5
34 Se	H_2SeO_3	75	1.283±0.007	1.261	11.5
35 Br	NaBr	104	1.14 ±0.01	1.116	7
48 Cd	$Cd(NO_3)_2$	10,000	1.49 ±0.01	1.49	2900
53 I	NaI	115	1.133±0.006	1.101	6.8
56 Ba	$Ba(C_2H_3O_2)_2$	200	1.001±0.007	0.985	<1

When the element investigated possesses only one isotope, no doubt exists about the process responsible for the absorption. Some other cases may warrant a few remarks.

Cl—The weakness of the 37-minute activity of Cl^{38} indicates that the high absorption is mainly due to capture by Cl^{35}, with formation of long-lived Cl^{36}.

K—By a similar argument, most of the absorption appears to be due to capture by K^{39} with formation of K^{40}.

Se—No strong activation corresponds to the large capture cross section, which must therefore correspond to formation of stable isotopes.

Br—Both capture by Br^{79} and Br^{81} will be important, since all activities are strong.

As it can be seen from the statistical errors reported in column 4 of the Table I, the values of the cross sections may be considered as accurate within 10 percent or better for the higher values, and within about 25 percent for the smallest.

[3] H. H. Goldsmith and F. Rasetti, Phys. Rev. **50**, 328 (1936).

[4] J. R. Dunning, G. B. Pegram, G. A. Fink and D. P. Mitchell, Phys. Rev. **48**, 265 (1935); E. Amaldi and E. Fermi, Phys. Rev. **50**, 899 (1936); G. A. Fink, Phys. Rev. **50**, 738 (1936); J. G. Hoffman and M. S. Livingston, Phys. Rev. **52**, 1228 (1937).

Self-Consistent Fields and Diamagnetic Susceptibility for Magnesium III*

W. JACQUE YOST†
Brown University, Providence, Rhode Island
(Received June 24, 1940)

Self-consistent fields, both with and without exchange, have been calculated for doubly ionized magnesium in the normal state. All of the equations have been solved numerically with the aid of an electrical calculating machine. The Z_0 functions have been tabulated along with the corresponding P functions in each case. The former functions do not differ by more than ± 0.003, at any point, in the two last stages of the work. The diamagnetic susceptibility has been calculated, yielding the value: -3.74×10^{-6}.

INTRODUCTION

IN the theoretical investigation of the metallic state of a particular metal, it is desirable to have the radial wave functions for the free ion. The self-consistent field calculations yield the best set of such functions available by present methods. In order to make available a suitable set of radial functions for the double ion of magnesium, the self-consistent fields for the $1s^2 2s^2 2p^6$ configuration have been calculated, both with and without the inclusion of the exchange terms. Since this configuration is a relatively simple one, it offers the opportunity of investigating the question raised by Hartree[1] concerning the relative merits of two methods suggested for solving the so-called Fock equations. The present paper represents the results of the calculation for Mg III in which both methods have been employed, together with a comparative analysis of the two methods.

METHOD OF SOLUTION

Both Hartree[1] and Fock[2] have discussed the details of the derivation of the self-consistent field equations with the use of the variation principle. We shall refer to the equations in which the exchange terms occur as the Fock equations, those in which they are neglected as the Hartree equations. Basically, the difference lies in the inclusion of the symmetry demands of the Pauli exclusion principle in the Fock equations. In addition, the Hartree equations result from the assumption of spherical charge distribution, whereas higher order Coulombic terms are included in the Fock equations. With these points in mind, the resulting equations for the radial functions for any nl shell can be written, in the Hartree case, as:

$$P''(nl|r)+[V(nl|r)-\epsilon(nl)]P(nl|r)=0; \tag{1}$$

while the corresponding Fock equation is:

$$P''(nl|r)+[V_E(nl|r)-\epsilon(nl)]P(nl|r)+T(nl|r)=0. \tag{2}$$

In these equations, and throughout the remainder of this work, atomic units are used. In the case of Mg III, there are three equations of each type to be solved. If two sets of functions, defined by:

$$\begin{aligned} Z_k(nl, n'l'|r) &\equiv \int_0^r P(nl|\rho)P(n'l'|\rho)\rho^k d\rho, \\ W_k(nl, n'l'|r) &\equiv 2\int_r^\infty Z_k(nl, n'l'|\rho)\rho^{-2(k+1)}d\rho \end{aligned} \tag{3}$$

* Part of a dissertation presented to the faculty of the Graduate School of Brown University in candidacy for the degree of Doctor of Philosophy.
† Now at Syracuse University, Syracuse, New York.
[1] D. R. Hartree and W. Hartree, Proc. Roy. Soc. **A150**, 9 (1935).
[2] V. Fock, Zeits. f. Physik **62**, 795 (1930).

are introduced, the various $V(r)$ and $T(r)$ functions can be written:

$$\begin{aligned}
V(1s) &= V_E(1s) = 24/r - W_0(1s\ 1s) - 2W_0(2s\ 2s) - 6W_0(2p\ 2p),\\
V(2s) &= V_E(2s) = 24/r - 2W_0(1s\ 1s) - W_0(2s\ 2s) - 6W_0(2p\ 2p),\\
V(2p) &= 24/r - 2W_0(1s\ 1s) - 2W_0(2s\ 2s) - 5W_0(2p\ 2p),\\
V_E(2p) &= V(2p) + 2r^2W_2(2p\ 2p),\\
T(1s) &= [W_0(1s\ 2s) - \epsilon(1s\ 2s)]P(2s) + 3rW_1(1s\ 2p)P(2p),\\
T(2s) &= [W_0(1s\ 2s) - \epsilon(1s\ 2s)]P(1s) + 3rW_1(2s\ 2p)P(2p),\\
T(2p) &= rW_1(1s\ 2p)P(1s) + rW_1(2s\ 2p)P(2s).
\end{aligned} \tag{4}$$

The W_k functions are related to the Y_k functions, used by Hartree, by the relation:

$$W_k(nl, n'l'|r) = \left(\frac{2}{2k+1}\right)\frac{Y_k(nl, n'l'|r)}{r^{k+1}}, \tag{5}$$

as can be verified by a partial integration of the defining Eq. (3).

The method usually adopted for solving these equations is one of successive approximations, in which the solutions of the Hartree equations are used to form the first approximation of the Fock solutions. In this method, it is customary to continue the work until the maximum change in each Z_0 function in going from one approximation to the next becomes smaller than some arbitrarily prescribed amount.

An alternate method has been used by Torrance[3] in the case of the Hartree equations for carbon. The principle of this method is to solve the equations as a simultaneous set of integro-differential equations, subject to a group of boundary conditions. This method will be referred to as the method of direct solution. Hartree[1] has suggested the use of such a method for the Fock equations and has discussed the advantages and disadvantages, in principle, of such a method. In the present work, both methods have been used in an attempt to determine their relative merits as judged by the actual computational work involved. The numerical methods used were the same as those discussed by Mooney.[4] These are the most valuable whenever the computational work is all carried out with the aid of an electric calculating machine. On the basis of the present investigation, the method of successive approximations (s.a.) is definitely superior to that of direct solution (d.s.) for both the Hartree and the Fock equations. The reasons for this opinion are: (1) The d.s. prohibits the inward integration of the η-equation, which is of great help in the Hartree equations; (2) in d.s., it is necessary to estimate each W_k function at the origin. This introduces several additional parameters which are difficult to estimate; (3) the total number of trials necessary to obtain the correct ϵ-parameters is less in the s.a. than in the d.s. method; (4) in the d.s., each W_k function must be calculated for all of the solutions attempted, whether they satisfy the boundary conditions or not. This last objection is probably the most serious since there are seven W_k functions in the case of Mg III and these had to be calculated for sixty-two solutions which were of no further value because they did not satisfy the boundary conditions.

It should be emphasized that the boundary conditions present a far greater problem in the Fock equations than in the Hartree equations.

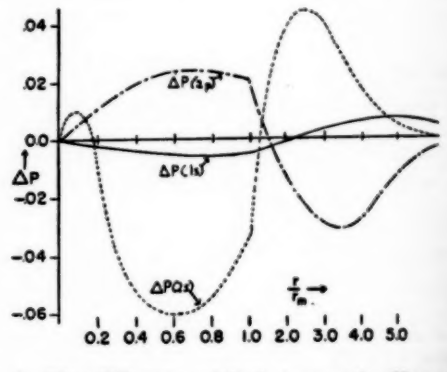

FIG. 1. The difference, ΔP, between the Hartree and Fock solutions. r_m represents the position of the maximum of the respective function.

[3] C. C. Torrance, Phys. Rev. **46**, 388 (1934).
[4] R. L. Mooney, Phys. Rev. **55**, 557 (1939).

TABLE I. *Radial wave functions.*

r	Without Exchange P(1s)	P(2s)	P(2p)	With Exchange P(1s)	P(2s)	P(2p)
0.0050	0.379	0.093	0.001	0.378	0.095	0.001
0.0100	.713	.175	.005	.712	.179	.005
0.0150	1.008	.246	.010	1.006	.253	.011
0.0200	1.266	.309	.018	1.264	.317	.019
0.0250	1.491	.362	.027	1.488	.372	.028
0.0300	1.686	.408	.038	1.683	.419	.039
0.0350	1.853	.446	.050	1.850	.458	.052
0.0400	1.996	.478	.063	1.993	.489	.066
0.0450	2.116	.503	.078	2.113	.515	.081
0.0500	2.216	.523	.093	2.213	.534	.097
0.06	2.363	.546	.127	2.360	.557	.132
0.07	2.451	.552	.163	2.447	.560	.170
0.08	2.491	.542	.202	2.487	.548	.211
0.09	2.493	.520	.243	2.489	.523	.252
0.10	2.465	.488	.284	2.461	.487	.295
0.11	2.413	.447	.326	2.410	.442	.339
0.12	2.343	.399	.369	2.340	.391	.382
0.13	2.261	.346	.411	2.258	.333	.426
0.14	2.168	.288	.453	2.166	.271	.469
0.15	2.069	.227	.495	2.068	.206	.511
0.16	1.967	.164	.535	1.966	.139	.552
0.18	1.758	.033	.614	1.758	.001	.632
0.20	1.552	−0.098	.687	1.553	−0.138	.707
0.22	1.358	−0.228	.755	1.360	−0.273	.776
0.24	1.179	−0.351	.817	1.183	−0.402	.839
0.26	1.017	−0.468	.873	1.022	−0.522	.895
0.28	.873	−0.576	.923	.878	−0.633	.945
0.30	.746	−0.676	.967	.751	−0.735	.990
0.32	.634	−0.766	1.005	.641	−0.826	1.028
0.36	.455	−0.917	1.064	.462	−0.977	1.088
0.40	.322	−1.033	1.104	.330	−1.090	1.127
0.44	.227	−1.116	1.126	.234	−1.169	1.149
0.48	.158	−1.171	1.135	.166	−1.217	1.157
0.52	.110	−1.201	1.131	.117	−1.241	1.152
0.56	.076	−1.212	1.119	.083	−1.245	1.138
0.60	.053	−1.206	1.099	.058	−1.231	1.116
0.64	.036	−1.188	1.072	.040	−1.205	1.087
0.68	.025	−1.160	1.042	.028	−1.169	1.054
0.72	.017	−1.124	1.008	.019	−1.126	1.017
0.76	.012	−1.083	.972	.012	−1.078	.978
0.80	.008	−1.037	.934	.007	−1.026	.937
0.84	.005	−0.989	.896	.005	−0.972	.895
0.88	.004	−0.940	.857	.003	−0.917	.853
0.92	.003	−0.890	.818	.002	−0.863	.811
0.96	.002	−0.840	.779	.001	−0.809	.769

This is due to the fact that the latter are homogeneous, whereas the Fock equations are nonhomogeneous. Consequently, two aids generally used in the Hartree solutions are not possible with the Fock solutions. These are the use of inward integration of the so-called η-equation, and the normalization of solutions by multiplication of unnormalized solutions with the appropriate constants.

RESULTS OF THE SOLUTION

In Table I, the three normalized P functions are tabulated for both the Hartree and the Fock

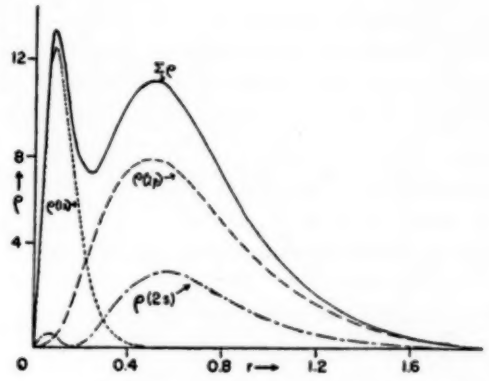

FIG. 2. Total radial charge density and the contribution from the various nl shells.

equations. Three digits to the right of the decimal are given, although six were retained throughout the computational work. Also, only half of the actual tabulations are given.* At the end of this table, the various ϵ-parameters are listed. The curves in Fig. 1 show a marked resemblance to similar graphs given by Hartree[5] for argon-like configurations. This suggests the use of such graphs in order to obtain approximate

TABLE I. (*Continued*)

r	Without Exchange P(1s)	P(2s)	P(2p)	With Exchange P(1s)	P(2s)	P(2p)
1.00	.001	−0.791	.741	.001	−0.756	.728
1.04	.001	−0.743	.704	.001	−0.705	.688
1.08	.001	−0.697	.668		−0.656	.649
1.12		−0.652	.633		−0.609	.612
1.20		−0.567	.566		−0.522	.541
1.28		−0.491	.505		−0.445	.477
1.36		−0.423	.448		−0.377	.418
1.44		−0.363	.397		−0.318	.365
1.52		−0.310	.350		−0.267	.318
1.60		−0.264	.309		−0.224	.276
1.68		−0.224	.261		−0.187	.240
1.84		−0.161	.208		−0.129	.179
2.00		−0.114	.159		−0.089	.132
2.16		−0.080	.120		−0.060	.097
2.32		−0.056	.091		−0.041	.071
2.6		−0.030	.054		−0.023	.041
3.0		−0.012	.026		−0.010	.018
3.4		−0.005	.012		−0.003	.008
3.8		−0.002	.006		−0.001	.003
4.2		−0.001	.003		−0.000	.001
4.6			.001			.001
ϵ	99.692	7.426	5.210	99.469	8.944	5.990

* More complete tables, which are essential for certain applications, can be obtained upon application to the author.

[5] D. R. Hartree and W. Hartree, Proc. Roy. Soc. A166, 450 (1938).

Fock solutions whenever the corresponding Hartree solutions are available. The various Z_0 functions can be calculated from the proper P functions. These functions represent the total charge within a sphere of radius r, due to a single electron. The Z_0 functions do not vary by more than ± 0.003 at any point in the two last stages of the work for either the Hartree or the Fock solutions.

The radial charge distribution due to a particular nl shell is given by

$$\rho(nl|r)=2(2l+1)P^2(nl|r), \qquad (6)$$

in electrons per unit r interval. These functions for the various shells in Mg III are plotted in Fig. 2. In order to illustrate more clearly the effect of the exchange terms, the change in the total radial charge distribution has been plotted in Fig. 3. The general result is a shrinking of the ion when the exchange terms are introduced. This gives an increase in the charge density near its principal maximum, with a corresponding decrease at large r values.

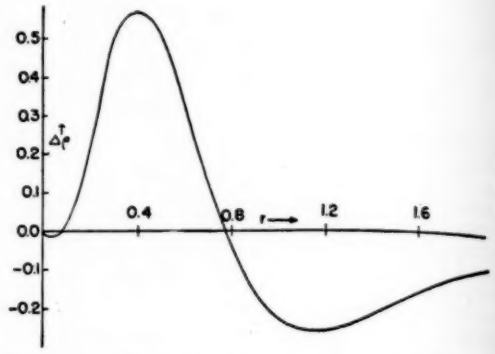

FIG. 3. The difference, $\Delta\rho$, in the total radial charge density as calculated from the Hartree and the Fock solutions plotted as a function of electron-nuclear distance, r.

DIAMAGNETIC SUSCEPTIBILITY

The molar diamagnetic susceptibility of any atomic or ionic species in the free state is given by:[6]

$$-\chi=\frac{Ne^2a_0^2}{6mc^2}\sum_{nl}2(2l+1)\overline{r^2(nl)}=10^{-6}\times 0.790\sum_{nl}2(2l+1)\int_0^\infty P^2(nl|r)r^2dr, \qquad (7)$$

where r is expressed in multiples of a_0, the atomic unit of length. Table II gives the result of the calculations for Mg III based on the solutions of the Fock equations. The table also includes results based upon experimental work. The earlier result quoted by Joos is believed to be in error because it cannot be correlated with other data. However, both of the last two values are estimates based on experimental data for various salts. Pauling gives several reasons for believing the value he quotes is more reliable. The present calculation seems to substantiate Pauling's value.

TABLE II. *Calculated susceptibilities.*

	$-\chi\times 10^6$
Contribution from 1*s* shell	0.04
Contribution from 2*s* shell	0.90
Contribution from 2*p* shell	2.80
Total calculated value	3.74
Result given by Joos[1]	8.5
Result given by Pauling[2]	3.3

[1] G. Joos, Zeits. f. Physik **19**, 347 (1923).
[2] L. Pauling, Proc. Roy. Soc. **A114**, 204 (1927).

ACKNOWLEDGMENTS

The author wishes to express his appreciation to Professor R. B. Lindsay for valuable assistance during the course of this work. He also wishes to thank Dr. Torrance for helpful discussions concerning the method of solution. All of this work was carried out while the author was a University Junior Fellow at Brown University.

[6] Stoner, *Magnetism and Matter* (London, 1934), Chap. I.

Thermal Conductivity of Metals

C. C. BIDWELL
Lehigh University, Bethlehem, Pennsylvania
(Received March 6, 1940)

As indicated in a previous paper, elementary classical considerations suggested a relation between thermal conductivity k, atomic heat C, density ρ, and absolute temperature T of the form $k/C\rho=K/T+K'$. This is now shown to be in agreement with recent theories on the metallic state. The first term on the right relates to conduction by the crystal lattice, the second term, K', refers to conduction by electrons. It is found experimentally that K' is the conductivity in the molten condition. The present paper shows these relations for lead, tin, and zinc. The data reported for lead are new. A modification of the experimental method previously used for zinc was required for the work on lead (a much poorer conductor) and is here explained.

INTRODUCTION

IN a previous paper[1] an attempt was made to explain the thermal conductivity of metals and its change with temperature on the basis of a transfer of heat partly by elastic waves in the crystal lattice and their rapid absorption and partly by atomic collisions as in a gas. The former introduced a temperature coefficient, the latter did not, the temperature coefficient being associated with the velocity of the elastic waves. Elementary classical considerations led to an equation of the type

$$k/\rho C=K/T+K' \tag{1}$$

where k is the thermal conductivity; C, the atomic heat; ρ, the density; T, the absolute temperature, and K and K' constants. The theory suggested that the intercept should be the value of $k/\rho C$ for the liquid state. The present paper offers data on lead, tin and zinc confirming this suggestion and interprets the equation in the light of recent theory.

THEORY

A. H. Wilson[2] from the standpoint of modern theory shows that thermal conductivity should require two terms, one due to the lattice, which as given by classical physics is $k_g=\frac{1}{3}\rho Clu$, and one due to electrons, which on the basis of modern theory is

$$k_e=\frac{\pi^2}{3}\cdot\frac{n\tau k^2T}{m}.$$

l is the mean free path in the lattice; u, the velocity of sound in the lattice; n, the number of free electrons per unit volume; k, the molecular gas constant; T, the temperature; m, the mass of the electron; and τ, the "relaxation time," the average time between collisions.

We may write $k=k_g+k_e$ (although these are not independent, since the electrons afford a mechanism for scattering the lattice waves). Hence

$$k=\tfrac{1}{3}\rho Clu+\frac{\pi^2}{3}\cdot\frac{n\tau k^2T}{m}. \tag{2}$$

According to Wilson, k_e becomes constant at high temperatures, while k_g reaches a maximum and then decreases as T^{-1}. The experimental data on lead, tin and zinc here reported do not yield straight lines when k is plotted against $1/T$; but straight lines are obtained if $k/\rho C$ is plotted against $1/T$. The theoretical equation in the form

$$\frac{k}{\rho C}=\tfrac{1}{3}lu+\frac{\pi^2}{3}\cdot\frac{n\tau k^2T}{m\rho C} \tag{3}$$

must then be equivalent to

$$\frac{k}{\rho C}=K\frac{1}{T}+K'. \tag{1}$$

According to this $\tau\propto T^{-1}$ and $lu\propto T^{-1}$. The *International Critical Tables* give data on the velocity of sound for platinum and copper at 20° C, 100° C and 200° C. For these data $u\propto T^{-1}$. According to Wilson, l depends on the grain size and is therefore only slightly affected by the temperature. Thus with ρ and C approximately compensating

[1] C. C. Bidwell, Phys. Rev. **32**, 311–314 (1928).
[2] A. H. Wilson, *Semi-Conductors and Metals* (Macmillan, New York, 1939).

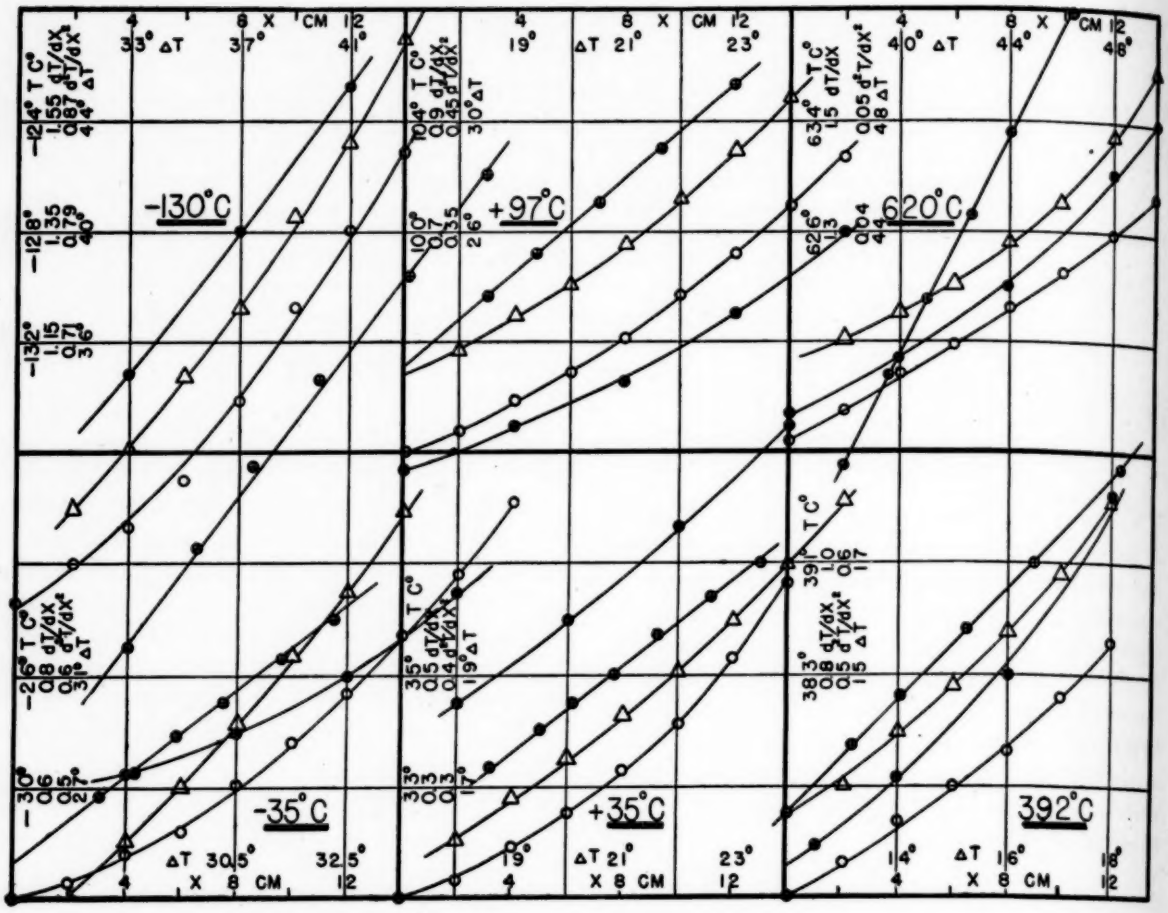

FIG. 1. Experimental data for lead at various temperatures.

in their temperature effects, Eqs. (3) and (1) are in agreement.

The intercept term must include the atomic as well as electronic conductivity for the liquid metal. If the atomic conductivity is that of an insulating liquid, it will be only one or two percent of the electron conductivity. Such conductivity increases with temperature and may thus account for the slight positive slope experimentally observed.

The experimental evidence

The data on zinc previously reported[3] were obtained by a new experimental method and agree closely with values found by Konno,[4] the only other data published for molten zinc. The data here presented on tin are Konno's, no work on tin having been done by the author. For lead, however, Konno's values for the molten state are far too low to give value of $k/C\rho$ in agreement with the intercept of the equation for the solid metal. Hence new observations were made on lead with the newly developed experimental method. These observations are shown graphically in Fig. 1. Figure 2 shows the author's values for the thermal conductivity of lead together with values obtained by Konno[4] and Van Dusen and Shelton.[5] Konno's values for the molten state are about 30 percent lower than the newer values here reported. Figures 3 and 4 show the course of the thermal conductivity curves for zinc and tin. For all these plots specific heats and densities were obtained from the published tables and are averages of what

[3] C. C. Bidwell, Phys. Rev. **56**, 594 (1939).
[4] S. Konno, Phil. Mag. **40**, 542 (1920).
[5] M. S. Van Dusen and S. M. Shelton, J. Research Nat. Bur. Stand. **12**, 429 (1934).

appear to be the best values. With the author's values for molten lead, the plots for tin, lead and zinc are seen to be in agreement with the suggested law, *the intercepts giving the value of $k/C\rho$ for the molten state.*

Modification of the Experimental Method in its Application to Lead

The experimental procedure as reported in a previous paper on zinc (reference 3) consisted, in brief, in establishing a flow of heat vertically down a specimen packed in Silocel, measuring the temperature at various levels (from which can be computed the gradient dT/dx and the change in gradient d^2T/dx^2) and measuring the lateral radial drop ΔT across the Silocel at the various levels.

The procedure as reported in the work on zinc was improved by centering the graphite cylinder containing the test metal in an iron cylinder of about 12 cm inside diameter on which was wound a Nichrome heater ribbon. The space between the graphite cylinder (5 cm diameter) and the iron cylinder was filled with Silocel as was also a space between the iron cylinder and an outer asbestos cylinder of about 20 cm diameter. The Nichrome windings on the iron cylinder were in parallel with similar winding on the graphite. By adjustment of currents in these two windings, the radial temperature drop across the Silocel could be reduced to small values or zero. The addition of the intermediate iron cylinder with its heater coil is found to be a great improvement.

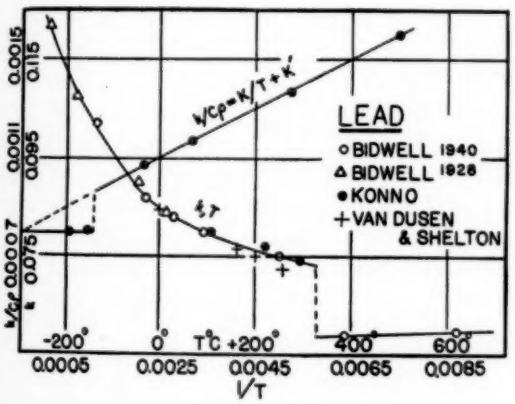

Fig. 2. Thermal conductivity of lead. k in cal. per sec. per cm per degree C.

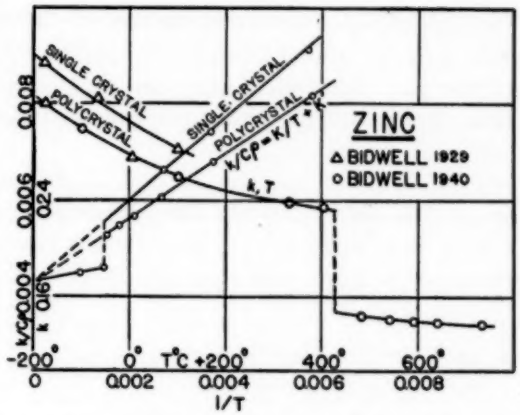

Fig. 3. Thermal conductivity of zinc. k in cal. per sec. per cm per degree C.

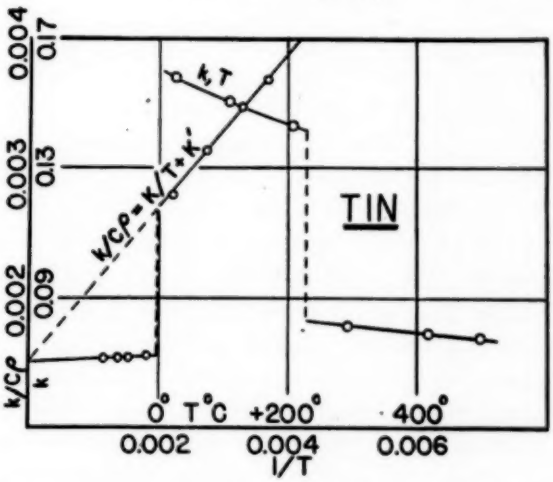

Fig. 4. Thermal conductivity of tin. k in cal. per sec. per cm per degree C.

A further modification of the method of handling the data in the case of such a relatively poor conductor as lead was found necessary. In the method used, the lateral, radial heat loss between two levels is equated to the difference between the heat entering at the upper level and leaving at the lower level. The equation is

$$k_z A_m (dT/dx)_1 - k_z A_m (dT/dx)_2 = \int_{r_1}^{r_2} k_s 2\pi r l dT/dr. \quad (5)$$

This becomes

$$k_z A_m d^2T/dx^2 = \frac{2\pi k_s \Delta T}{2.3 \log (r_2/r_1)}, \quad (6)$$

since $(dT/dx_1 - dT/dx_2)/l = d^2T/dx^2$. k_z is the thermal conductivity of the test metal; k_s, that

of the Silocel; A_m, the cross section of the test metal; ΔT, the radial temperature drop across the Silocel at the level in question; r_2, the outer radius of the Silocel (inside the iron cylinder); r_1, its inner radius.[6]

In the case of molten metals it becomes necessary to add to the left side a term to cover the heat flow down the walls of the graphite-containing cylinder. The equation then becomes

$$k_x A_m (d^2T/dx^2)_m = \frac{2\pi k_s \Delta T}{2.3 \log (r_2/r_1)} - k_{gr} A_{gr} (d^2T/dx^2)_{gr}. \quad (7)$$

This may be written

$$(d^2T/dx^2)_m = \frac{2\pi k_s}{k_x A_m 2.3 \log (r_2/r_1)} \Delta T - \frac{k_{gr} A_{gr} (d^2T/dx^2)_{gr}}{k_x A_m}. \quad (8)$$

It is found for lead that values of d^2T/dx^2 plotted against corresponding values of ΔT give straight lines in all cases. The intercept term is small and the variation of $(d^2T/dx^2)_{gr}$ from top to bottom of the cylinder appears to be negligible. This is reasonable, at least when the contained metal is a comparatively poor conductor like lead, where the graphite has about five times the conductivity of the solid lead and about ten times that of molten lead. The comparatively high conductivity of the graphite means a correspondingly small temperature gradient in the graphite, changing at an approximately constant rate. In the case of zinc (see reference 3), the conductivity of the metal was about the same as that of the graphite and, for zinc, d^2T/dx^2 was found to be constant over a considerable range. This is in agreement with the above explanation of the constancy of $(d^2T/dx^2)_{gr}$.

[6] For temperatures −130°, −35°, +35°, +97°, +250°, $r_1 = 2.6$ cm; r_2, 4.5 cm; $A_m = 13.83$. For 392°, 620°, $r_1 = 2.5$ cm; r_2, 5.65 cm; $A_m = 13.83$. Values of k_s for various temperatures are shown in the previous paper. The lead specimen was prepared by slow freezing from the bottom. This was effected by lowering the molten lot slowly through a furnace at the rate of about two cm per hour.

In the case of zinc it was necessary merely to add the cross section of the graphite to that of the zinc and use Eq. (7), ΔT and the slope of the dT/dx line both being constant. For lead however, d^2T/dx^2 and ΔT are not constant but, when d^2T/dx^2 is plotted against ΔT, a straight line results as indicated by Eq. (8). From the slope of this line the thermal conductivity k_x is obtained. No correction for the graphite walls is required since the quantities having to do with the heat flow down the walls all appear in the intercept.

Precautions

In the use of this method it is of the utmost importance that stable unchanging temperature conditions be attained before starting the heat flow down the specimen. Four $\frac{1}{8}''$ quartz tubes were inserted at the outer radius of the Silocel (just inside the iron cylinder) and two such tubes in the molten specimen (or frozen in the solid specimen). Only three junctions were used, the Chromel wires welded at a common point and the copper leads connected to binding posts. One of the junctions was kept at the bottom of one of the quartz tubes in the metal, the second raised or lowered to the various levels in the other quartz tubes and temperature differentials between these junctions read on a galvanometer. The third junction was kept in ice and differentials between it and either of the others read on a potentiometer indicator gave actual temperatures.

It is usually necessary to wait two or more hours before unchanging conditions are attained. Readings up and down the specimen and across the Silocel at all levels are taken and then the downward heat flow started by applying heat in the d.c. heater at the top of the specimen. Final readings may be taken after another hour and corrections made for the initial readings. The fact that one gets smooth curves and straight lines as required by the equations is no guarantee of the correctness of the result. Only from absolutely stable conditions can satisfactory results be obtained.

Properties of Rochelle Salt. III[1]

HANS MUELLER
Massachusetts Institute of Technology, Cambridge, Massachusetts
(Received June 28, 1940)

The interaction theory of Rochelle salt is extended by supplementing the expression for the free energy of the deformed and polarized crystal by a term proportional to the fourth power of the polarization in the a direction. This second approximation explains the dielectric and elastic saturation phenomena above the upper Curie point and the dielectric, elastic, piezoelectric and pyroelectric properties in the ferroelectric temperature range. All experimental results are compatible with the hypothesis that the clamped crystal has only one transition point at about 5° C, where its dielectric constant has a very high maximum. The two Curie points of the free crystal are due to the interaction between the elastic deformation and the electric polarization. Instead of sudden changes of the heat capacity the new theory predicts slight changes of the slope of the specific heat curve at the Curie points. The dispersion of the dielectric constant is explained without assuming a relaxation time.

THE results of paper II suggest the following explanation of the anomalous properties of Rochelle salt: If the crystal could be clamped in such a way that all elastic deformations are suppressed it would show only a single transition at about 5°C. At this temperature the dielectric constant in the a direction of the clamped crystal has a sharp and very high maximum, i.e., the reciprocal susceptibility χ_1 vanishes (see Fig. 3, II). This transition is not a Curie point, because below this temperature the clamped crystal is not spontaneously polarized, its dielectric behavior remains normal and χ_1 increases again to reach a normal value at low temperatures. The transition appears to be similar to those observed in other crystals, e.g. HBr, HI.[2] Most probably it is due to a modification of proton bonds or to hindered rotation of polar groups. The transition of the clamped Rochelle salt crystal does not involve changes of the crystal symmetry and it leaves the crystal structure essentially unaltered. It produces a change of the optical properties as is indicated by the fact that the temperature gradient of the birefringence $n_a - n_c$ is almost three times smaller below −20°C than it is above 25°C (see Figs. 18 and 19, I).

In the experiments on freely deformable crystals the existence of this transition is masqued by a series of other effects. As was shown in paper II these effects result from the interaction between the elastic deformation and the electric polarization. They can be accounted for by the laws of classical crystal physics. Because of this interaction the free crystal has two Curie points, one above and one below the transition temperature. Between the Curie points the free crystal is spontaneously polarized and deformed. The spontaneous deformation changes the symmetry of the crystal from rhombic hemiedric to monoclinic hemimorphic with the a axis as polar axis.[3] Although the interaction theory makes no use of the concept of an inner field $F=E+fP$, it furnishes an equation, $1/\kappa_1=\chi_1(1-f_{14}^2/\chi_1 c_{44})$ (from Eqs. (4), II), for the susceptibility κ_1 of the free crystal above the Curie point, which is analogous to that, $1/\kappa_1=(1-\Theta/T)fT/\Theta$ (Eq. (9), I), given by the inner field theory. A comparison of these relations shows, that the interaction gives rise to an "apparent Lorentz factor" $f=f_{14}^2/c_{44}=0.045$, while the Curie temperature is $\Theta=f_{14}^2T/\chi_1 c_{44}$. The Curie points of the free crystal are the temperatures $T=\Theta$ at which the determinant $D_{14}=\chi_1 c_{44}-f_{14}^2=(T-\Theta)\chi_1 c_{44}/T$ vanishes. $c_{44}=11.6\times10^{10}$ and $f_{14}=7.2\times10^4$ are the true elastic and piezoelectric constants[4] for shearing strains y_z.

[1] This is the third publication on this subject by the writer. The previous articles, Phys. Rev. **47**, 175 (1935) and Phys. Rev. **57**, 829 (1940), will be referred to as paper I and II, respectively. The numerals I and II are used also in the references to figures and equations given in these previous papers.

[2] C. P. Smyth and C. S. Hitchcock, J. Am. Chem. Soc. **55**, 1830 (1933); G. Damköhler, Ann. d. Physik **31**, 76 (1938).

[3] H. von R. Jaffe, Phys. Rev. **51**, 43 (1937).

[4] The present investigation shows that the values of f_{14} as derived in paper II from Norgorden's or Mikhailov's measurements are too small.

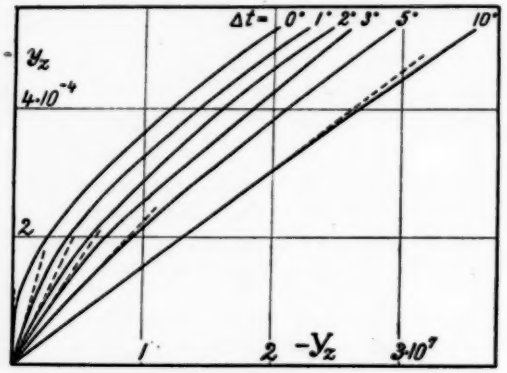

FIG. 1. Theoretical stress-strain relation for shear in the (b, c) plane of Rochelle salt above the Curie point.

The interaction theory has served to explain the relations between the dielectric, piezoelectric and elastic properties of Rochelle salt above the upper Curie point. We will show here that it can account also for the ferroelectric anomalies at temperatures between the Curie points. To this purpose it is necessary to supplement the expression (1, II) for the free energy Φ of the polarized and deformed crystal by terms of higher order. The origin of the new terms can be explained as follows: At temperatures near the transition point, where χ_1 is very small, the $P_x(E_x)$ relation for the clamped crystal must show saturation. Since the clamped crystal is orthorhombic this saturation effect introduces only terms in even powers of P_x and we shall therefore use as a second approximation

$$\Phi=\Phi^{(1)}+\tfrac{1}{4}BP_x^4, \tag{1}$$

where $\Phi^{(1)}$ is the quadratic form (1, II). Terms involving higher powers of the strains or of P_y and P_z or mixed terms, e.g. $P_x^2y_z^2$, are not likely to be of importance, because it was shown that the true elastic and piezoelectric properties of Rochelle salt are not unusual. A second set of correction terms arises from the change of the crystal symmetry at the Curie points. This fact would require the introduction of ten new terms involving four new elastic constants c_{14}, c_{24}, c_{34}, c_{56}, five new piezoelectric constants $f_{11}, f_{12}, f_{13}, f_{26}$, f_{35} and a new susceptibility χ_{23}. New experimental evidence, which will be presented in an other paper, shows that these correction terms of the second kind play an important role in the theory of the electro-optical and photoelastic effects, the anomalous thermal expansion and the electrostriction in Rochelle salt. However, these terms are small in comparison with $\frac{1}{4}BP_x^4$, and while they are not entirely negligible they play a secondary role in the following discussion of the dielectric, elastic and piezoelectric effects. The second approximation, Eq. (1), furnishes the fundamental relations

$$-Y_x=\partial\Phi/\partial y_x=c_{44}y_x+f_{14}P_x, \tag{2a}$$

$$E_x=\partial\Phi/\partial P_x=f_{14}y_x+\chi_1P_x+BP_x^3. \tag{2b}$$

To test their validity we shall follow the procedure adopted in paper I by discussing first the saturation effects which occur above the Curie point, where $D_{14}=\chi_1c_{44}-f_{14}^2>0$, and where the experiments furnish more reliable data because no hysteresis effects occur. These data will furnish the value of B and it will then be possible to test the theory for the ferroelectric range.

Dielectric and Piezoelectric Saturation Above the Curie Point

The laws for the dielectric properties and the inverse piezoelectric effect of the free crystal are found from Eqs. (2) by setting $Y_x=0$. The direct piezoelectric effect is obtained by elimination of y_x and by assuming $E_x=0$. If one takes into account Eqs. ((4), II) these procedures furnish

$$E_x=P_x/\kappa_1+BP_x^3. \tag{3a}$$

$$-E_x=y_x/d_{14}+B(c_{44}/f_{14})^3y_x^3, \tag{3b}$$

$$Y_x=P_x/d_{14}+B(c_{44}/f_{14})P_x^3. \tag{3c}$$

The $P_x(E_x)$, $y_x(E_x)$ and $P_x(Y_x)$ relations must therefore show saturation effects when $1/\kappa_1$ or $1/d_{14}$ are small, i.e., at temperatures slightly above the Curie point. At higher temperatures the cubic terms are negligible in comparison with the linear terms. This remark explains why it would be futile to search for saturation effects in the elastic or piezoelectric properties of the isolated crystal. In an isolated crystal the polarization creates a depolarization field $E_x=-4\pi P_x$ and hence the coefficient of P_x in Eq. (2b) is $(4\pi+\chi_1)$ and is about 100 times larger than $1/\kappa_1$.

The existence of saturation in the piezoelectric

effects has been reported by Schulwas-Sorokin[5] and Hinz,[6] but sufficient data for the determination of B are available only from the dielectric measurements. The validity of Eq. (3a) was demonstrated by Kurtschatow[7] for static, and by the writer for dynamic measurements by the method of Sawyer and Towers (Fig. 10, I). This equation is equivalent with the relation $E=(1-\Theta/T)F+\beta fF^3$ (Eq. (7), I) of the inner field theory when the approximation $F=fP$ is valid. It leads directly, without resorting to approximations as was necessary in paper I, to the experimentally verified relation (see Fig. 8, I and Eq. (19), I)

$$E_x/X^{\frac{1}{2}}=M(t-t_c)+NX, \qquad (4)$$

where $X=(\kappa_1-\kappa_E)/\kappa_1\kappa_E$, and where $\kappa_E=\partial P_x/\partial E_x$ is the reversible susceptibility. $M=1/C(3B)^{\frac{1}{2}}$, $N=1/3(3B)^{\frac{1}{2}}$ and C is the Curie constant. For small fields Eq. (4) reduces to

$$\kappa_E=\kappa_1(1-GE_x^2), \quad G^{-\frac{1}{2}}=g(t-t_c), \qquad (4')$$

where $g=1/C(3B)^{\frac{1}{2}}$. It was shown in paper I that the observations verify the relations $g^3=M^2/C$, $N=CM/3$, as demanded by the theory. The experimental values $g=1.05$, $N=800$, $M=13.5$, $C=178$ (near the upper Curie point) furnish $B=5.8\pm0.7\times10^{-8}$. B takes the place of βf^4 of the inner field theory. Its value may vary somewhat with temperature, but more accurate data would be required to establish this dependence.

Elastic Saturation in the Foiled Crystal

Although the true elastic properties of Rochelle salt follow Hooke's law, this law is not satisfied for shearing stresses Y_s when the crystal is covered with a grounded foil. From Eqs. (2) and the Curie-Weiss law (10, II) for the elastic compliance s_{44} one finds for the foiled crystal ($E_x=0$)

$$Y_s=(Y_s+c_{44}y_s)[1+(Y_s+c_{44}y_s)^2 \times(1+c_{44}\sigma/(t-t_c))B/\chi_1 f_{14}^2](t-t_c)/\sigma c_{44}. \qquad (5)$$

At the Curie point, $t=t_c$, the relation is

$$Y_s=(Y_s+c_{44}y_s)^3B/\chi_1 f_{14}^2. \qquad (5')$$

Figure 1 presents the resulting strain-stress curves for various temperatures $t=t_c+\Delta t$. The values $B=5.8\times10^{-8}$, $c_{44}=11.6\times10^{10}$,

$$f_{14}=7.2\times10^4, \quad \chi_1=0.05+(t-t_c)/178,$$

$\sigma=66.7\times10^{-12}$ were used in the calculation. We note that large deviations from Hooke's law must be expected if the temperature of the foiled crystal is between 24° and 27°C. The elastic saturation should become apparent for shearing stresses of only a few kg/cm² and it should therefore not be difficult to verify this effect by ordinary elastic measurements. At higher temperatures the deviations from Hooke's law vanish.

A simpler and more accurate method for studying the elastic saturation in Rochelle salt is based on the fact that the resonance and

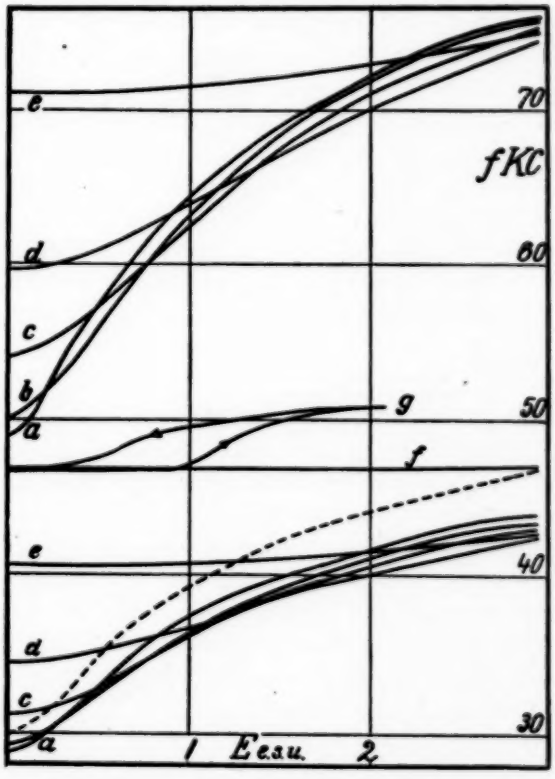

FIG. 2. Influence of a steady electric field on the resonance frequencies of a plate of Rochelle salt at various temperatures above the Curie point: (a) 24.1°, (b) 24.2°, (c) 24.5°, (d) 25.0°, (e) 26.8°, (f) 30°, (g) 18°. (f) and (g) refer to the lower resonance frequency. The dotted curve gives the change of an antiresonance frequency at 24.1°C.

[5] R. D. Schulwas-Sorokin, Zeits. f. Physik **77**, 541 (1932).
[6] H. Hinz, Zeits. f. Physik **111**, 617 (1938).
[7] I. V. Kurtschatow, *Seignette electricity* (Moscow, 1933), Fig. 15. The isothermal static values may differ from the adiabatic dynamic values. To be exact, one should differentiate between the free energy and the enthalpy. The existence of an electrocaloric effect indicates that the difference is not negligible.

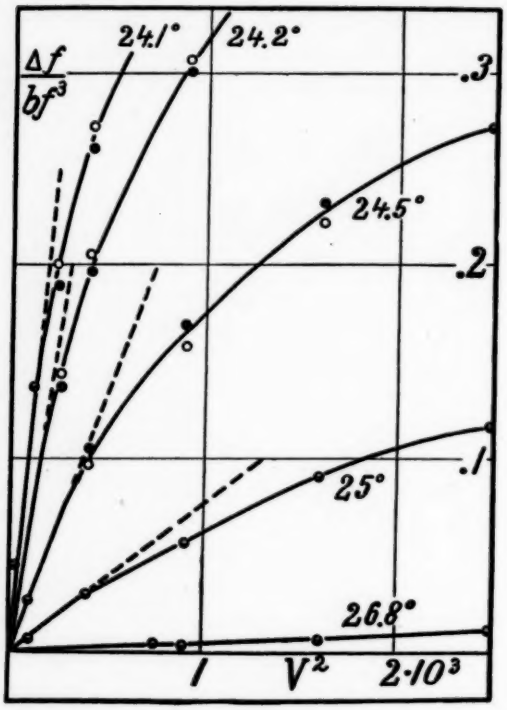

FIG. 3. Verification of the limiting law for the change of the resonance frequencies in small steady fields.

antiresonance frequencies of all those vibrations of a crystal plate, which can be excited by an alternating field in the a direction, must depend on the compliance coefficient s_{44}. For any resonance frequency f this dependence generally will be of the form $f=(\alpha+\beta s_{44})^{-\frac{1}{2}}$, or since $s_{44}-1/c_{44}=\sigma/(t-t_c)$,

$$f=[a+b/(t-t_c)]^{-\frac{1}{2}}, \tag{6}$$

where the constants a and b depend on the mode of vibration and therefore on the size and shape of the plate and on the other elastic compliance coefficients s_{ik}, which are to be considered as temperature independent. If the plate is deformed by a constant strain y_z^0 the values of α and β remain practically unchanged, but if the electrodes are in close electrical contact with the crystal the compliance s_{44} must be replaced by the "reversible compliance" $s_{44}^0=-\partial y_z/\partial Y_z$, which is given by the slope of the $y_z(Y_z)$ curves in Fig. 1 and depends on y_z^0. Since a constant strain cannot be produced by mechanical means without altering the boundary conditions for the vibrations, it is more convenient to produce it by the application of a steady electric field E_0 in the a direction. A simple calculation shows that a field E_0 changes the compliance from s_{44} to s_{44}^E, where

$$1/s_{44}^E=c_{44}-f_{14}^2/(\chi_1+3BP_0^2),$$

and where P_0 is the polarization due to E_0 in a free crystal. Therefore, according to Eq. (3a), $3BP_0^2=1/\kappa_E-1/\kappa_1$, where κ_E is the reversible susceptibility in the field E_0. By combining these relations it is found that the steady field E_0 changes the resonance frequency from f to $f_E=f+\Delta f=(\alpha+\beta s_{44}^E)^{-\frac{1}{2}}$, and the calculation gives

$$\Delta(1/f^2)/b=(1/f^2-1/f_E^2)/b$$
$$=(1-\kappa_E/\kappa_1)/(t-t_c). \tag{7}$$

For small fields E_0 the approximation (4[1]) furnishes

$$\Delta f/bf^3=E_0^2/2g(t-t_c)^4. \tag{7'}$$

The change of the resonance frequencies of a foiled Rochelle salt plate by a steady field has been reported in a previous note.[8] Figure 2 gives the measurements on two resonance frequencies of a second crystal of approximately the same dimensions as the first, 3×5 cm in area and 0.096 cm thick in the a direction.[9] Table I gives

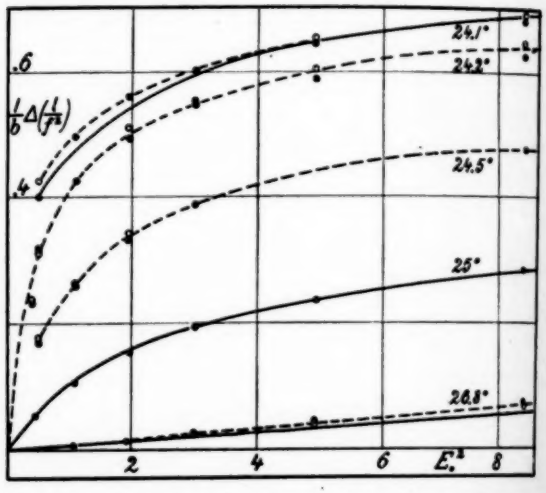

FIG. 4. Verification of the law relating the change of the resonance frequency to the change of the susceptibility of Rochelle salt in a steady electric field. The dotted curves result from the elastic measurements, the full curves for 24.1°, 25° and 26.8° are calculated from the dielectric data.

[8] H. Mueller, Phys. Rev. **57**, 842 (1940).

[9] The crystal plates were supplied by the Brush Development Company, Cleveland, Ohio, with "graphoil" electrodes attached. The orientation of the edges could not be ascertained without damaging the electrodes.

TABLE I. *Temperature dependence of two resonance frequencies of a Rochelle salt plate.*

t°C	24.1	24.2	24.5	25.0	26.8	$a\times10^{10}$	$b\times10^{10}$
f KC	28.9	29.1	31.2	34.5	40.6$_5$	3.38	10.1
f KC	49.0	50.0	54.0	59.7	71.2$_5$	1.03	3.57

the temperature dependence of these frequencies when no steady field is acting. These data satisfy the law (6), with $t_c=23.0$°C. Thus the constants a and b can be determined in spite of the fact that the modes of vibration are not known.

Figure 3 is a plot of $2\Delta f/bf^3$ *versus* the square of the steady voltage. In accordance with Eq. (7[1]) both frequencies lead to identical curves with initial slopes which vary with the temperatures in the ratios $(1/1.1)^4:(1/1.2)^4:(1/1.5)^4:2^4:(3.8)^4$ as indicated by the dotted lines. In Fig. 4 the variation of $\Delta(1/f^2)/b$ is compared with the variation of $(1-\kappa_E/\kappa_1)/(t-t_c)$ as deduced from the dielectric data given in Fig. 7, I. This verification of Eq. (7) involves no adjustable parameter. The agreement signifies that the fundamental equations are valid and that the elastic data lead to the same value of B as the one derived from the dielectric measurements.

THE FERROELECTRIC PROPERTIES OF ROCHELLE SALT

At temperatures near the transition point χ_1 is small, and the determinant $D_{14}=\chi_1 c_{44}-f_{14}^2$ is therefore negative between the two Curie points. From Eqs. (2) it follows that in this temperature range the state of minimum free energy of a free and foiled crystal ($E_x=0$; $Y_x=0$) has a spontaneous polarization P_x^0 and a spontaneous deformation y_x^0

$$P_x^0=(-D_{14}/c_{44}B)^{\frac{1}{2}};\quad y_x^0=-f_{14}P_x^0/c_{44}. \tag{8}$$

The spontaneous polarization can be directed along the $+a$ or $-a$ axis. Since it is associated with a spontaneous shearing deformation, all parts of a crystal will usually become polarized in the same direction, because, for purely geometrical reasons, different parts cannot be sheared in opposite directions without creating internal stresses. A small crystal, when cooled slowly, acts therefore as a single Weiss region and is pyroelectric, but in a large crystal it is difficult to prevent twinning, and frequently the crystals crack when they are cooled too rapidly.

The influence of the spontaneous polarization and deformation on the dielectric, elastic and piezoelectric properties of the crystal is analogous to that resulting from the application of a steady field above the Curie point. The dielectric and piezoelectric constants are decreased, and the resonance frequency of a foiled plate increases. To arrive at a theory of these effects one takes into account that a small stress δY_x and a small field δE_x change the polarization from P_x^0 to $P_x^0+\delta P_x$, and the strain from y_x^0 to $y_x^0+\delta y_x$. If one neglects all terms containing higher powers of δP_x and δy_x one finds from Eqs. (2) and (8)

$$-\delta Y_x=c_{44}\delta y_x+f_{14}\delta P_x, \tag{9a}$$

$$\delta E_x=f_{14}\delta y_x+\chi_1^0\delta P_x, \tag{9b}$$

$$\chi_1^0=\chi_1-3D_{14}/c_{44}. \tag{9c}$$

χ_1^0 is the reciprocal of the susceptibility κ_{cl}^0 of the spontaneously deformed clamped crystal, i.e., of a crystal which has been cooled without stresses to below the upper Curie point but which is prevented to deform any further if the field δE_x is applied. The solution of the linear equations (9a, b) gives

$$-\delta y_x=s_{44}^0\delta Y_x+d_{14}^0\delta E_x, \tag{10a}$$

$$\delta P_x=d_{14}^0\delta Y_x+\kappa_1^0\delta E_x, \tag{10b}$$

TABLE II. *Elastic, dielectric and piezoelectric data for Rochelle salt between the Curie points.*

t°C	$f\times10^{-5}$	k^2	κ_1^0	P_x^0	$(s_{44}^0-1/c_{44})\times10^{12}$	$d_{14}^0\times10^8$	$f_{14}\times10^{-4}$	$B\times10^8$
20	1.49	0.51	38	420	12.9	22.2	6.8	7.4
15	1.62	0.42	20	620	9.1	13.4	8.0	6.5
10	1.68	0.38	15	720	7.6	10.7	8.5	6.4
5	1.69$_5$	0.37	15	740	7.4	10.4	8.4	6.1
0	1.70	0.37	17.5	740	7.4	11.3	7.9	5.2
−5	1.66$_5$	0.40	23	700	8.3	13.7	7.4	4.4
−10	1.57	0.47	32	600	10.9	18.6	7.2	4.3
−15	—	—	80	380	—	—	—	4.3

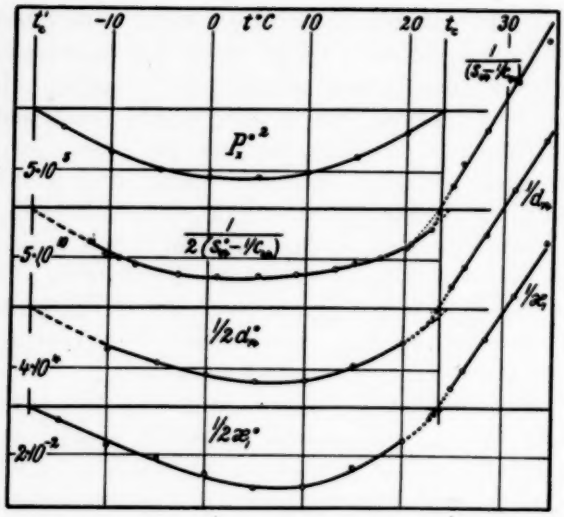

FIG. 5. Verification of the relations between the spontaneous polarization, the elastic, piezoelectric and dielectric properties of Rochelle salt between the Curie points and of their relations to the corresponding properties above the upper Curie point.

where

$$s_{44}^0 = -\chi_1/2D_{14} + 3/2c_{44}, \qquad (11a)$$

$$d_{14}^0 = -f_{14}/2D_{14}. \qquad (11b)$$

$$\kappa_1^0 = -c_{44}/2D_{14}. \qquad (11c)$$

s_{44}^0 is the compliance coefficient of the foiled crystal, d_{14}^0 is the piezoelectric constant and κ_1^0 is the susceptibility of the free crystal in the ferroelectric state. Equations (10) hold only for small stresses and weak electric fields.

If one assumes that in a small temperature range the variation of D_{14} can be approximated by a linear law $D_{14}=(t-t_c)c_{44}/C$ Eqs. (11) can be cast into the form of Curie-Weiss laws:

$$2(s_{44}^0 - 1/c_{44}) = \sigma/(t_c - t); \quad \sigma = C(f_{14}/c_{44})^2,$$

$$2d_{14}^0 = \Delta/(t_c - t); \quad \Delta = Cf_{14}/c_{44},$$

$$2\kappa_1^0 = C/(t_c - t);$$

$$(P_x^0)^2 = h(t_c - t); \quad h = 1/CB.$$

Since the "Curie constants" vary with the temperature, we shall not use these relations, though they give a satisfactory representation of the observations near the Curie points.[10] Instead we follow the procedure adopted in paper II, i.e., we calculate the fundamental quantities c_{44}, f_{14}, χ_1 and B from the available data.

Equations (9) and (10) have the same form as the corresponding Eqs. ((2), II) and ((3), II) for temperatures above the Curie point. Hence we can use all the relations of paper II if we substitute s_{44}, d_{14}, κ_1 and χ_1 by s_{44}^0, d_{14}^0, κ_1^0 and χ_1^0, respectively. Thus it follows from Eq. ((8), II) that the compliance of the isolated crystal is[11]

$$s_{44}^i = s_{44}^0 - 4\pi d_{14}^{0^2}/\epsilon_P^0 = 1/c_{44}$$

and the resonance frequency f^i for longitudinal vibrations at 45° to the b and c axes is

$$f^i = [\rho(s_{22}+s_{33}+2s_{23}+1/c_{44})]^{-\frac{1}{2}}$$

and has no anomaly at the Curie points. The resonance frequency of the foiled crystal is $f=[\rho(s_{22}+s_{33}+2s_{23}+s_{44}^0)]^{-\frac{1}{2}}$, and it is easy to prove that Mason's[12] relation is still valid. The electromechanical coupling coefficient is

$$k^2 = 1-(f/f^i)^2 = \rho d_{14}^{0^2} f^2/\kappa_1^0 \qquad (13)$$

and from the equations for f, f^i and (11a) it follows that

$$s_{44}^0 - 1/c_{44} = (1/f^2 - 1/f^{i^2})/\rho = f_{14}^2/2c_{44}D_{14}. \qquad (14)$$

According to (11b) and (11c)

$$d_{14}^0/\kappa_1^0 = f_{14}/c_{44}. \qquad (15)$$

This ratio must have the same value as d_{14}/κ_1, because Eq. ((16'), II) is valid also below the Curie point and Mikhailov[13] has found that $\delta f/\delta D$ is very nearly constant at all temperatures. Eqs. (11) furnish also

$$\chi_1 + 1/2\kappa_1^0 = f_{14}^2/c_{44} = c_{44}(d_{14}/\kappa_1)^2. \qquad (16)$$

This relation justifies the procedure used in Fig. 3, II for the construction of the $\chi_1(t)$ curve. It should be noted that the susceptibility κ_{el}^0 of the spontaneously deformed clamped crystal differs from the susceptibility $\kappa_{el}=1/\chi_1$ of the crystal in which all deformations are suppressed. While κ_{el} has a single and very high maximum at the transition point near 5°C, κ_{el}^0 has at this

[10] Paper I, Fig. 5 and O. Norgorden, Phys. Rev. **49**, 820 (1936); **50**, 782 (1936).

[11] The approximation $\epsilon_P^0 = 4\pi\kappa_1^0$ is justified also in the ferroelectric range, because the dielectric constant is nowhere smaller than 150.

[12] W. P. Mason, Phys. Rev. **55**, 775 (1939).

[13] G. Mikhailov, Tech. Physik USSR **4**, 461 (1937).

temperature a minimum $\kappa_{cl}^0=(\frac{2}{3})\kappa_1^0$. κ_{cl}^0 has two maxima at the Curie points, where $\kappa_{cl}^0=\kappa_{cl}$.

Table II gives the experimental data on Rochelle salt at temperatures between the Curie points. f and k are from Mason's[12] work. The values for κ_1^0 and P_x^0 are Bradford's[14] measurements. From these data (s_{44}^0-1/c_{44}), d_{14}^0 and f_{14} were calculated by using Eqs. (14), (13) and (15), respectively. The value of B is obtained from Eqs. (8) and (11c), which give

$$B=1/2\kappa_1^0 P_x^{0^2}. \tag{17}$$

Within the rather large experimental errors f_{14} and B have the same values as were found from the data above the Curie point. Both constants seem to decrease somewhat with temperature.

The crucial test of the theory is carried out in Fig. 5. According to Eqs. (8), (11b), (11c) and (14) the quantities $(P_x^0)^2$, $\frac{1}{2}(s_{44}^0-1/c_{44})$, $\frac{1}{2}d_{14}^0$ and $1/\kappa_1^0$ are all proportional to D_{14} and should therefore have the same temperature variation, provided that c_{44}, f_{14} and B are constant. Furthermore, the last three curves should be continuations of the curves for $1/(s_{44}-1/c_{44})$, $1/d_{14}$ and $1/\kappa_1$, as given in paper II for temperatures above the Curie point. To illustrate the agreement the scales for the last three curves were adjusted so that the straight lines above the Curie point have the same slope. This procedure leads indeed to the result that the three curves become very nearly identical in the temperature range between the Curie points. They also coincide with the $P_x^{0^2}$ curve, for which the scale was chosen so as to give the same minimum at 5°C. It would not be difficult to interpolate the results on both sides of the upper Curie point by smooth curves, and to ascribe the small deviations to experimental errors, which, due to the gap effects, are particularly large near the Curie points. However, the elastic data[15] show quite clearly that the curves have a small discontinuity at the Curie point. In a later paper we can show that such anomalies are to be expected. They are the result of the neglected correction terms of the second kind and they can be explained as due to small changes of the values of the constants c_{44}, f_{14} and B at the Curie points. It is therefore not possible, on the basis of the present theory, to predict the ferroelectric properties near the Curie point from the measurements above this temperature, as was attempted with moderate success in paper I. However, since the changes of c_{44}, f_{14} and B are small, our theory is adequate in predicting the minimum or maximum values of the various quantities at the transition point. At this temperature χ_1 is very small, and the assumption $\chi_1=0$ gives $(D_{14})_{\min}=-f_{14}^2$. By using Eqs. (8) and (11) and the values of f_{14}, c_{44} and B as derived from the measurements above the Curie point, one finds the following approximate values:

	calculated	observed
$(P_x^0)_{\max}=f_{14}(c_{44}B)^{-\frac{1}{2}}$	$=860$	740 e.s.u.
$(y_x^0)_{\max}=f_{14}^2(c_{44}B)^{-\frac{1}{2}}/c_{44}$	$=5\times10^{-4}=2'$	$3.7'$
$f_{\max}=[(4\times10^{-12}+3/2c_{44})\rho]^{-\frac{1}{2}}$	$=1.85\times10^5$	1.71×10^5
$(\kappa_1^0)_{\min}=c_{44}/2f_{14}^2$	$=11.4$	12.5[16]
$(d_{14}^0)_{\min}=1/2f_{14}$	$=7\times10^{-6}$	10.4×10^{-6}

With the exception of $(y_x^0)_{\max}$, which has been measured for only one crystal, the deviations from the observed values indicate that at the transition point $\chi_1>0$. The experimental evidence, resulting from the three independent investigations of Bradford, Hablützel and Mason, supports therefore the conclusion that the

[14] E. B. Bradford, B.S. Thesis, Massachusetts Institute of Technology, 1934. P_x^0 is obtained from the height of the hysteresis loops. Bradford's values of P_x^0 agree with those given by J. Hablützel, Helv. Phys. Acta **12**, 489 (1939), but they are larger than those resulting from the pyroelectric measurements in paper I. Bradford's values for the susceptibilities, at 1000 cycles/sec., are slightly higher than Hablützel's, but they are lower than Mason's values. The data in Table II are in e.s.u.

[15] The elastic data are more accurate than the dielectric measurements. Figure 5 is based on the original data of Dr. Mason.

[16] J. Hablützel, Helv. Phys. Acta **12**, 489 (1939).

clamped crystal has no Curie point. It possesses a transition point where the dielectric constant reaches an extremely high maximum.

The spontaneous polarization and deformation lower the free energy of the crystal by

$$\Phi=\tfrac{1}{2}c_{44}(y_z^0)^2+f_{14}y_z^0P_x^0+\tfrac{1}{2}\chi_1(P_x^0)^2 +\tfrac{1}{4}B(P_x^0)^4=-\tfrac{1}{4}B(P_x^0)^4. \quad (18)$$

The maximum energy change is about 4500 erg/cm^3=0.017 cal./mol. Since, near the Curie point, $(P_x^0)^2=h(t_c-t)$, where h is about 5×10^4, the theory does not demand a sudden change of the specific heat at the Curie points, but only a change of the slope of the specific heat curve. This change of slope is only about 3×10^{-4} cal./mol/°C [2] and is much too small to be detected by the usual methods. For the crystals of H_2KPO_4 and H_2KAsO_4, for which our theory should also be applicable, a large and sudden change of the specific heat has been observed,[17] but this is not necessarily in contradiction with the theory, because one might expect such a change to occur at the transition temperature, i.e., at a temperature somewhat lower than the Curie point. The experiments leave some doubt whether the temperature, where the specific heat changes, is identical with that of the Curie point. In Rochelle salt no anomaly has been found, either at the Curie points or at the transition temperature.

For large electric fields and large shearing stresses Y_z Eqs. (2) predict hysteresis curves for the electric polarization of the free crystal, for the deformation y_z of a foiled plate and for the direct and inverse piezoelectric effect. The dielectric hysteresis has been studied by numerous investigators. Bloomenthal[18] and Hinz[6] have reported hysteresis of the inverse piezoelectric effect and the existence of elastic hysteresis follows from the recent work of the writer.[8] Contrary to the theory, the hysteresis loops have not a single Barkhausen jump and the coercive field is smaller than the theoretical values. These discrepancies are not surprising if one realizes that the theoretical Barkhausen jump corresponds to a transition from an instable to a stable equilibrium state. Structural inhomogeneities, internal stresses or inhomogeneities of the electric field may be responsible for the transition's occurring at smaller field intensities.

[17] W. Bantle and P. Scherrer, Nature **143**, 980 (1939); J. G. Hooley and C. C. Stevenson, Phys. Rev. **56**, 121 (1939); J. Mendelsohn and K. Mendelsohn, Nature **144**, 595 (1939).

[18] S. Bloomenthal, Physics **4**, 172 (1933).

Dielectric Dispersion in Rochelle Salt

Schulwas-Sorokin and Posnov[19] and Goedecke,[20] among others, have reported results which are assumed to arise from relaxation phenomena in Rochelle salt. The first two authors ascribe the relaxation to viscous resistance against mechanical deformations, the latter to the retardation time of the dipole orientation. It should, however, be noted that the measurements were carried out in the ferroelectric temperature range and that the interpretations are based on the erroneous assumption that the dielectric and elastic properties of Rochelle salt follow the laws which hold for ordinary solids. A closer inspection reveals that the observed phenomena are due to the interaction, saturation and hysteresis effects, and that the existence of a relaxation time longer than 10^{-4} sec. is not justified by any experiment. It seems rather obvious that power factor data and voltage decay curves cannot be interpreted in terms of a relaxation time when most of the power loss is due to hysteresis and when the polarization is not proportional to the electric field. The fact that at the resonance frequency of a foiled plate the impedance minimum is unusually broad in Rochelle salt, can be explained without assuming strong viscous damping. Since an electric field changes the elastic compliance s_{44} the resonance frequency is modulated by the exciting a.c. field and the resonance peak is broadened. It is sharp only when a large steady field is applied across the electrodes. In this case, it follows from the data in Fig. 2 that a small variation of the field has little effect, and our experiments show indeed a considerably sharper resonance point when a strong steady field is acting.

The strongest point in favor of the dipolar relaxation theory seems to be the fact that at high frequencies the dielectric constant in the

[19] R. D. Schulwas-Sorokin and M. V. Posnov, Phys. Rev. **47**, 166 (1935).

[20] H. Goedecke, Zeits. f. Physik **94**, 574 (1935).

direction has considerably smaller values than at audiofrequencies. But also this effect can be explained by the interaction theory by using the discussion in the appendix of paper II. There it was shown, for the special case of a plate, 1 cm long, in the state of longitudinal vibration in the direction at 45° to the b and c axes, that the polarization of a volume element at the distance y' from the center of the plate is

$$P_x=E_x[\kappa_1-\{1-\cos(y'\omega/v)/\times\cos\{\omega/2v)\}d_{12}'^2/s_{22}'].$$

The dielectric measurements record the average polarization

$$P_h=\int_{-\frac{1}{2}}^{+\frac{1}{2}}P_x dy'$$

and give therefore a susceptibility

$$\kappa_h=\kappa_1-\left(1-\frac{2v}{\omega}\tan\omega/2v\right)d_{12}'^2/s_{22}'.$$

For low frequencies $\tan\omega/2v=\omega/2v$, and hence $\kappa_h=\kappa_1$, but for a high frequency, which is not near a resonance point of the plate, $2v/\omega\tan\omega/2v=0$, whence

$$\kappa_H=\kappa_1-d_{12}'^2/s_{22}'.$$

Since $d_{12}'^2/s_{22}'=\epsilon_F k^2/4\pi$, (Eq. (13), II), where k is Mason's electromechanical coupling coefficient, we obtain for the dielectric constant of a free crystal at high frequencies

$$\epsilon_H=\epsilon_F(1-k^2). \tag{19}$$

This relation was given by Mason, but his statement, that ϵ_H is the dielectric constant of the clamped crystal, is not correct. A high frequency field creates a strain distribution in the crystal. The average value of these strains is zero, but this fact does not imply that ϵ_H is identical with ϵ_{cl}. Above the Curie point ϵ_H is larger than ϵ_{cl}, but is much smaller than ϵ_F, the dielectric constant at low frequencies. Between the Curie points Eq. (19) is also valid, but here ϵ_H is much smaller than ϵ_{cl} or $\epsilon_F{}^0$, however, it is slightly larger than $\epsilon_{cl}{}^0$, the dielectric constant of the spontaneously deformed clamped crystal. A simple calculation leads, for temperatures above the Curie point, to the relation

$$(\chi_1-1/\kappa_1)/(1/\kappa_H-1/\kappa_1)=c_{44}(s_{22}+s_{33}+2s_{23})+1=1.46. \tag{20}$$

For the ferroelectric temperature range an analogous relation holds

$$(\chi_1{}^0-1/\kappa_1{}^0)/(1/\kappa_H-1/\kappa_1{}^0)=1.46. \tag{20'}$$

From Eqs. (20') and (16) it follows that the susceptibility of Rochelle salt at high frequencies reaches at the Curie points its largest value $(\kappa_H)_{max}=1.46\ c_{44}/f_{14}{}^2$. This corresponds to a maximum dielectric constant of about 400. At the transition temperature near 5°C κ_H has a minimum. Eqs. (20') and (9c) furnish $(\kappa_H)_{min}=(\kappa_1{}^0)_{min}/(1+\frac{1}{2}\cdot 1.46)$ which gives, approximately, $(\epsilon_H)_{min}=0.6(\epsilon_F{}^0)_{min}\leqq 100$. According to Eq. (19) this relation implies that k has a minimum value of 0.65. Mason measured a minimum $k=0.60$, but since his values of $\epsilon_1{}^0$ are rather large, he finds also a large value of $(\epsilon_H)_{min}=160$. Direct measurements of the dielectric constant at high frequencies have been carried out by Mikhailov.[13] He checks the theoretical value $(\epsilon_H)_{min}=95$, and finds at the upper Curie point a maximum of about 250. Also the measurements of Busch[21] and Doborzynski[22] are in fair agreement with the theory. The above calculations hold, of course, only if the crystal vibrates in the assumed manner. For other modes of vibration the dielectric constant at high frequencies is different, but in general κ_H will differ only slightly from the dielectric susceptibility of the clamped crystal (above the Curie point) or of the spontaneously deformed clamped crystal (between the Curie points). The existence of relaxation effects can be accepted only if future measurements should lead to still smaller values.

---

[21] G. Busch, Helv. Phys. Acta **6**, 315 (1933).
[22] D. Doborzynski, Acad. Polonaise Sci. et lettres, Bull. (1938) p. 37.

The Decay Constant of H^3

R. D. O'NEAL AND M. GOLDHABER
Department of Physics, University of Illinois, Urbana, Illinois
(Received August 2, 1940)

THE decay constant λ of H^3 is too small to be determined conveniently in the usual way from the decay curve.[1] If, however, we can produce a known number N of H^3 nuclei, and observe which number N' of these nuclei decay per unit time, we can obtain λ from the relation $\lambda=N'/N$. We have carried out a determination of λ in this manner. H^3 was produced by exposing lithium to slow neutrons, which leads to the reaction[2] $Li^6+n^1\rightarrow He^4+H^3$.

(1) In a first experiment lithium metal, sealed in a soft glass tube, was exposed inside a large paraffin block in a fixed position A to neutrons from a 100-mg Ra$-\alpha-$Be source. The total time of irradiation was four months. When the irradiation was completed, water was added to the Li metal until it was all transformed into LiOH whereby hydrogen gas was developed. In this way H^3 can be extracted from the Li metal with an efficiency of about 94 percent (see below). A known fraction of the hydrogen gas, together with some alcohol vapor, was introduced into a large Geiger counter, and an activity of 56 counts/min. in excess of a background of 108 counts/min. was established. This activity varied with the pressure in the Geiger counter in the expected manner. By "scanning" the counter with a well-collimated beam of γ-rays we found that it was sensitive over about 90 percent of its length. If we assume, as is plausible, that every H^3 nucleus decaying in the sensitive portion of the counter is detected, we can calculate from the above measurements N' for the whole piece of Li metal used.

N can be put equal to the total number of C neutrons absorbed in the Li metal, if we neglect two corrections of opposite sign which in this experiment should be of the order of a few percent each: The contribution of neutrons with an energy above the Cd absorption limit, and the loss of some of the H^3 nuclei produced near the surface. (Their range in lithium is about 1/10 mm.) To obtain the total number of C neutrons absorbed in the Li the following experiments were carried out.

(a) The ratio of the number of C neutrons absorbed in the Li to that absorbed in Mn in position A per unit time was measured with an In foil as neutron detector. This foil could be wrapped round the samples.

(b) Mn metal powder was exposed in position A, until the 2.6-hr. period produced by slow neutron capture was saturated. A similar experiment was carried out with the Mn surrounded by Cd. The initial activity of the Mn was measured in each case under identical geometrical conditions by means of a thin-walled Geiger counter.

(c) By mixing a small, known amount of U_3O_8 with Mn powder and measuring its activity in the same way as was used for the activated Mn, the counting arrangement was calibrated. Assuming similar β-ray spectra for Mn^{56} and UX_2, which we found by absorption experiments to be a reasonably good approximation, we obtained the total number of β-rays emitted per minute from the saturated Mn sample. This number is equal to the number of neutrons absorbed by the Mn per minute.

From these measurements we deduce

$$\lambda=7\times10^{-10}\ \text{sec.}^{-1}\pm25\ \text{percent},$$

or the half-lifetime of H^3, $T=31\pm8$ years.

(2) Through the courtesy of Professor Cork, we were able to use for a second set of experiments Li bombarded, intermittently, during three weeks with slow neutrons from the Michigan cyclotron. As a "neutron integrator" which allowed us to estimate the total number of slow neutrons absorbed by the Li we used Sb, which is activated by slow neutrons with a period of 60 days, and which was bombarded close together with the Li. The hydrogen extracted from this Li sample by the procedure described in (1) showed an activity, N', about 100 times larger

[1] L. Alvarez and R. Cornog, Phys. Rev. **58**, 197A (1940).
[2] J. Chadwick and M. Goldhaber, Proc. Camb. Phil. Soc. **31**, 612 (1935).

than in the first experiment. By electrolyzing some of the remaining LiOH solution we found a small activity in the hydrogen developed. From this it followed that the efficiency with which H^3 was extracted from Li by the procedure described in (1) was 94 ± 3 percent.[3]

The activity of Sb^{124} (60-day) was measured 5 weeks after the last irradiation when Sb^{122} (2.6-day) had already decayed. It was compared with the activity of an Sb sample bombarded here (position A). If we assume the percentage contribution of C neutrons to the 60-day activity to be the same under the different conditions of bombardment employed in Michigan and here, we can estimate the number of H^3 nuclei formed in the Li sample. (This assumption, however, may introduce a serious error, as we found by a separate experiment (position A) that the contribution of neutrons above the Cd absorption limit to the 60-day activity of Sb is considerable.) In this way we obtained a value of about 50 years for the half-lifetime of H^3. Though this experiment is less accurate than the first it yielded a valuable check on our method.

We had observed previously[4] that the electrons emitted from H^3 have a range of about 0.5 mg Al/cm^2. This corresponds to an upper limit of the β-ray spectrum $E_0=15\pm3$ kev. As the β-transition may be considered as allowed, we can now check the relation between E_0 and λ, as given by Fermi's theory of β-decay, for this rather extreme case. Using the value for the constant of proportionality as deduced by Grönblom[5] from an analysis of the β-ray data on light elements, we find good agreement between theory and experiment within the present accuracy.

This research was aided by a grant from the Graduate School Research Fund of the University of Illinois.

[3] This high efficiency is not unexpected as a similarly high efficiency has been found for the production of HD in the reaction $LiH+D_2O\rightarrow HD+LiOD$ (Beutler, Brauer and Juenger, Naturwiss. **24**, 347 (1936)).

[4] R. D. O'Neal and M. Goldhaber, Phys. Rev. **57**, 1086A (1940).

[5] B. O. Grönblom, Phys. Rev. **56**, 508 (1939).

LETTERS TO THE EDITOR

Prompt publication of brief reports of important discoveries in physics may be secured by addressing them to this department. Closing dates for this department are, for the first issue of the month, the eighteenth of the preceding month, for the second issue, the third of the month. Because of the late closing dates for the section no proof can be shown to authors. The Board of Editors does not hold itself responsible for the opinions expressed by the correspondents.

Communications should not in general exceed 600 words in length.

Connection Between the Meson Decay and the Beta-Decay

According to Yukawa's theory of the meson,[1] the beta-disintegration process can be described as the transformation of a neutron (N) in the nucleus into a proton (P) with the emission of a meson (Y^-) and the disappearance of the meson with the simultaneous emission of an electron (e^-) and an antineutrino (n'). Thus the two basic hypotheses of his theory introduce the following interactions between elementary particles:

$$N \rightleftarrows P + Y^-, \qquad P \rightleftarrows N + Y^+, \tag{1}$$

$$Y^- \rightleftarrows e^- + n', \qquad Y^+ \rightleftarrows e^+ + n. \tag{2}$$

From the interaction of the latter type, connecting a meson with light particles, it follows immediately that the mesons are unstable and disintegrate spontaneously each into an electron and a neutrino. The proper lifetime, i.e., the mean lifetime at rest, of the meson calculated from the above theory was given by[2]

$$\tau_0 \sim (g^2/\hbar c) \cdot (m/m_u)^5 \cdot T, \tag{3}$$

where $g^2/\hbar c$ is a dimensionless constant which characterizes the strength of the interaction (1) and which can be determined by the magnitude of the nuclear forces. In Eq. (3) m_u and m denote masses of the meson and the electron, respectively; T is a time constant which appears in the theoretical formula for the beta-decay and which can be estimated by comparing the formula with lifetimes of light nuclei.[3] Since the most probable values for these constants are

$$g^2/\hbar c \sim 0.1, \quad m_u \sim 170m, \quad T \sim 10^3 \text{ sec.}, \tag{4}$$

we find from (3)

$$\tau_0 \sim 10^{-6} \text{ sec.} \tag{5}$$

On the other hand, a striking confirmation of the meson decay has been received from observations on the mass absorption anomaly for cosmic rays[4] and more direct evidence has also been reported by Williams and his collaborators.[5] These observations all indicate that the proper lifetime of the meson is about

$$\tau_0 \sim 1 \text{ to } 5 \times 10^{-6} \text{ sec.} \tag{6}$$

Thus the theoretical estimate (5) is too short by a factor 10^{-2} in comparison with the experimental value.

We shall point out here that there are at least two ways of removing this discrepancy:

(I) As was recently suggested by Møller, Rosenfeld and Rozenthal,[6] we assume that there exist two kinds of mesons and that while one of them has a lifetime of the order of 10^{-6} second, in accord with experiments, the lifetime of the other is so short that it can explain the sufficiently rapid nuclear beta-decay.

(II) We reverse the connection between the meson decay and the beta-decay. Namely, instead of (2) we shall introduce the original Fermi interaction

$$N \rightleftarrows P + e^- + n', \qquad P \rightleftarrows N + e^+ + n, \tag{7}$$

as a new basic hypothesis. If this is done, the meson decay takes place as a compound process of (1) and (7) in the following way. First a negative meson, for example, is absorbed by a proton, which is in the negative energy state, and a pair of a neutron and an antiproton (P') is created. Then this pair disappears with the simultaneous emission of an electron and an antineutrino:

$$Y^- \rightarrow P' + N \rightarrow e^- + n'. \tag{8}$$

From this theory, we obtain for the proper lifetime of the meson

$$\tau_0 \sim (\hbar c/g^2) \cdot (m/m_u)^5 \cdot T, \tag{9}$$

which is about $(\hbar c/g^2)^2$ times as long as (3) and which is in good accord with the experimental value (6).

It is to be noted that in this calculation there appears a diverging integral with respect to the momentum of the heavy particle which is virtually created in the intermediate state. This difficulty is quite similar to those which arise in calculations for the self-energy and the magnetic moment of the heavy particle.[7] Hence we have cut off this integral at such a value of the momentum that it gives the right order of magnitude for the self-energy and the magnetic moment.

A more detailed account will be published later in the *Proceedings of the Physico-Mathematical Society of Japan*.

In conclusion, I wish to express my cordial thanks to Professor H. Yukawa for his kind interest in this work.

SHOICHI SAKATA

Institute of Theoretical Physics,
Kyoto Imperial University,
Kyoto, Japan,
July 30, 1940.

[1] H. Yukawa, Proc. Phys.-Math. Soc. Japan **17**, 46 (1935); Yukawa, Sakata, Kobayasi and Taketani, *ibid.* **20**, 993 (1938).
[2] H. Yukawa and S. Sakata, Nature **143**, 761 (1939); H. A. Bethe and L. W. Nordheim, Phys. Rev. **57**, 998 (1940).
[3] B. O. Grönblom, Phys. Rev. **56**, 508 (1939).
[4] H. Euler and W. Heisenberg, Ergeb. d. exakt. Naturwiss. **17**, 1 (1938); B. Rossi, Rev. Mod. Phys. **11**, 296 (1939).
[5] E. J. Williams and G. E. Roberts, Nature **145**, 102 (1940); E. J. Williams and G. R. Evans, *ibid.* **145**, 818 (1940).
[6] Møller, Rosenfeld and Rozenthal, Nature **144**, 629 (1939).
[7] N. Kemmer, Proc. Roy. Soc. **166**, 127 (1938). A diverging integral of the same kind appears also in the calculation for the lifetime of the neutral meson (S. Sakata and Y. Tanikawa, Phys. Rev. **57**, 548 (1940).

The Nuclear Spin of C^{13}

Using Rabi's magnetic-resonance molecular-beam method, Hay has observed both the sign and the magnitude of the gyromagnetic ratio of the C^{13} nucleus.[1] By making the rather safe but still slightly theoretical assumptions that he is dealing with a ^2P state and that the spin part S of the "nuclear spin" I consists of neutron spin with no large admixture of proton spin, he is able to conclude from the sign of the gyromagnetic ratio that the nuclear spin is 1/2. This disagrees with the nuclear spin 3/2 inferred earlier from analysis of a band spectrum which could not be completely resolved.[2] It is unfortunate, especially in view of such a disagreement, that an experimental determination should have to lean so heavily on theoretical hypotheses.

It is possible to reach Hay's conclusion from a well-established empirical rule, instead of theoretical hypothesis, if we make use of the observed magnitude of the gyromagnetic ratio as well as its sign. The rule is that all hitherto known magnetic moments of odd nuclei (there are more than fifty of them) lie between the limits given by the simple single-particle model.[3] The corresponding limits for the gyromagnetic ratio g in the odd-neutron case are

$$\mu_n/I < g < -\mu_n/(I+1),$$

where $\mu_n = -1.96$, the lower limit of the observed magnetic moment of the neutron,[4] in nuclear magnetons. The measured gyromagnetic ratio, $g = +1.401 \pm 0.004$, does not lie strictly within these limits for any value of I. However, it exceeds the upper limit 1.30 for $I = 1/2$ by only a few percent. For higher values of I, it exceeds the limit by about a factor two or more.

In Fig. 1, nuclear magnetic moments are plotted against

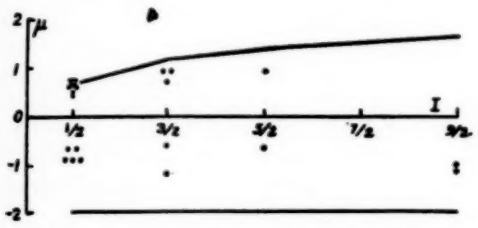

FIG. 1. The magnetic moments and nuclear spins of the odd-neutron nuclei. The triangles are possibilities for C^{13}.

nuclear spins, for odd-neutron nuclei only.[3] The upper line is the limit given by the single-particle model with $I = L - 1/2$, and the lower line with $I = L + 1/2$. The dots represent the previously known data for the odd-neutron nuclei. (The data for the odd-proton nuclei, not shown, are about twice as numerous.) The triangles show two possibilities for C^{13}. The previous data for small values of I tend to crowd close to the limit given by $I = L - 1/2$, *both in Fig. 1 and in the odd-proton case*,[3] and the triangle for $I = 1/2$, just above the limit, does not deviate appreciably from the regularity of the other data. The triangle for $I = 3/2$ would be seriously discordant with the other data, and may therefore be rejected.

One notes that the nuclear spin 1/2 for C^{13}, thus determined in another way from Hay's data with a minimum of theoretical description, is the value predicted both by the Hartree model[5] and by the alpha-model[6] on the basis of the Larmor-Thomas type of spin-orbit coupling. The magnetic moment is smaller than these models would suggest.

D. R. INGLIS

Johns Hopkins University,
Baltimore, Maryland,
August 16, 1940.

[1] R. H. Hay, Phys. Rev. **58**, 180 (1940).
[2] C. H. Townes and W. R. Smythe, Phys. Rev. **56**, 1210 (1939).
[3] Th. Schmidt, Zeits. f. Physik **106**, 358 (1937).
[4] L. W. Alvarez and F. Bloch, Phys. Rev. **57**, 111 (1940).
[5] M. E. Rose and H. A. Bethe, Phys. Rev. **51**, 205 (1937).
[6] D. R. Inglis, Phys. Rev. **56**, 1125 (1939).

Concentration of Radioactive Bromine Produced by Gamma-Radiation

One of the difficulties encountered in the study of nuclear reactions of the (γ, n) type is the small beta-ray activity ordinarily obtained, even with the strongest gamma-ray sources. The high energy gamma-rays used for such work (*viz.* those from the reaction $Li^7(p, \gamma)Be^8$) are but weakly absorbed in matter, and this suggests that a concentration of the radioactive atoms produced in a large bulk of material should increase the activity obtained. Moreover, the (γ, n) reaction, which is the only one thus far observed under gamma-ray bombardment, leads to an isotope of the irradiated element. Accordingly, we have made some experiments with a view to adapting the Szilard-Chalmers[1] technique to this problem.

Bromine was irradiated in the form of ethyl bromide, 500 cc of which were contained in a spherical vessel constructed so as to surround almost completely the source of gamma-rays. The active bromine was separated as silver bromide in the usual way. A composite decay curve was obtained which was resolvable into periods of 6.4 minutes, 18 minutes and 4.5 hours with relative intensities at saturation of 1 : 3 : 2, respectively. The 6.4-minute period is that of Br^{78} and the others belong to the isomeric Br^{80}. These isotopes are formed from the two stable ones Br^{79} and Br^{81}, in each case by the loss of a neutron. It is noteworthy that the method of concentrating the activity also establishes the chemical nature of the isotope.

The radioactive sources prepared in this way were at least ten times as strong as those obtainable without concentrating the activity. Beta-ray sources with initial activity of several thousand counts per minute were made. Contaminating activity produced by fast neutrons from the normal deuterium content of the ion beam striking the lithium target was shown to be negligible.

WALTER H. BARKAS*
PHILLIP R. CARLSON
J. E. HENDERSON
WILLIAM H. MOORE

Department of Physics,
University of Washington,
Seattle, Washington,
August 28, 1940.

* Member, The Institute for Advanced Study, Princeton, New Jersey.
[1] L. Szilard and T. A. Chalmers, Nature 134, 494 (1934).

Luminescence Excited by Exposure to Neutrons*

Since many elements, during exposure to neutrons, release energy in the form of gamma-rays, beta-rays and alpha-particles, it is reasonable to expect that these radiations may be used to excite luminescence. We have made observations which show that certain luminescent materials, which are known to be excited by x-rays, cathode rays, and radiations from radium, emit light as a result of exposure to neutrons. We have used photographic methods to detect this emission during exposure, and have made visual observations, after exposure, of thermoluminescence excited in many substances and of phosphorescence in luminescent ZnS.

Exposures were made for varying lengths of time up to several hours at distances up to 50 cm from a neutron source with radium equivalent 100 kg and at a distance of a few cm from a source with radium equivalent about 1 kg. Specimens were simultaneously exposed in black paper, inside a solid box of paraffin 12 cm thick, and in a lead box 1 cm thick placed inside this same paraffin box. The effect was observed to be least in the specimens wrapped in black paper and exposed to fast neutrons. The two sets of specimens inside the paraffin box were observed to emit luminescence of practically the same intensity although one set was enclosed in a lead box and the other was not.

Photographic observations.—Two identical specimens of luminescent $CaWO_4$, one wrapped in black paper and the other in Cellophane, were placed in contact with the sensitive side of a panchromatic film and exposed to neutrons as described. The part of the film under the Cellophane was strongly blackened while the part under the black paper showed little or no blackening. A similar difference was observed when the $CaWO_4$ was painted on black cardboard with a binder and part of it covered with black paper during exposure. Other materials were observed to show this same effect especially $CdWO_4$ activated by 1 percent Mn and phosphorescent ZnS. It is of interest to note that the three substances which we have found to be most strongly luminescent under neutron exposure are all known to show scintillations under alpha-particles from radium.

Thermoluminescence.—After exposure to neutrons, about thirty substances were found to emit light when they were heated on a small electric stove to a temperature considerably below that of red heat. The strongest effect was shown in fluorites from certain localities, kunzite, ThO_2 activated by Tb, and in $CaSO_4$, CaF_2, and $CdSO_4$ activated by Mn. The thermoluminescence is, in most cases, very dim and not comparable in intensity with that excited by x-rays. The intensity may be increased by mixing with the luminescent material some substance which reacts strongly with neutrons such as $GdSO_4$. The effect is diminished by screening the luminescent substance during exposure with boron carbide. The effect of surrounding some specimens such as fluorite and $CaSO_4$ excited by Mn, with cadmium metal during exposure is to increase the intensity of thermoluminescence excited because, although cadmium absorbs slow neutrons, it emits,[1] as a result of this absorption, radiations which are effective in excitation.

Summary of results.—(1) Luminescence is excited in some materials as a result of exposure to neutrons. In a material for neutron excitation it is desirable that the luminescent material contain some element which is highly reactive to neutrons and that it contain some heavy element capable of absorbing radiations such as gamma-rays. Materials excited by neutrons are excited also by x-rays, cathode rays or the radiations from radium. (2) Slow neutrons are more effective as a source of excitation than fast neutrons. (3) The intensity of luminescence may be increased by mixing with the luminescent material a small quantity of some material containing an element which is highly reactive to neutrons. (4) Excitation of luminescence by exposure to neutrons may be explained as follows: Neutrons react with the nuclei of certain atoms which form a component part of the luminescent substance or with the nuclei of atoms of some other substance highly reactive to neutrons which may be mixed with the luminescent substance or placed near it. As a result of this reaction, radiations are emitted which excite luminescence. Gamma-rays appear to be a factor in the excitation and secondary radiations and internal conversions may also play a part.

The exposures to neutrons were made by the use of the cyclotrons at Columbia and Cornell Universities through the kindness of Dr. J. R. Dunning and Dr. R. F. Bacher whose assistance we greatly appreciate.

FRANCES G. WICK
MABEL S. VINCENT

Department of Physics,
Vassar College,
Poughkeepsie, New York,
August 15, 1940.

* This research was made possible by a grant from the American Philosophical Society.

[1] J. G. Hoffman and R. F. Bacher, Phys. Rev. **34**, 644 (1938).

On the Isotopic Weights of Chlorine, Argon and Iron by the Doublet Method

With a mass spectrograph of Bainbridge-Jordan type whose resolving power is about 17,000, the isotopic weights of Cl^{35}, Cl^{37}, A^{40} and Fe^{56} were measured by the doublet method.

The cylindrical discharge tube employed in this work was provided with an aluminum bar anode and an iron concave cathode. All photographic plates used were of the Schumann type prepared in our laboratory.

The plate was calibrated with the bromine isotopes Br^{79} and Br^{81}, for the mass difference of which we accepted 250.0 packing fraction units as determined by Aston.

(1) *Chlorine.*—Three doublets $C^{12}{}_3-HCl^{35}$, $C^{12}{}_2H-Cl^{35}$ and $C^{12}{}_3H_2-HCl^{37}$ were obtained by electric discharge through the vapor mixture of normal hexane and carbon tetrachloride.

These mass differences were as follows:

$$\left.\begin{aligned} C^{12}{}_3-HCl^{35} &= 246.7\pm1.7, \quad (\Delta M.10^{-4}) \\ C^{12}{}_2H-Cl^{37} &= 421.7\pm0.9, \\ C^{12}{}_3H_2-HCl^{37} &= 419.8\pm1.1, \end{aligned}\right\} 420.8\pm0.7.$$

From these results and from the values $H^1=1.00812\pm0.00004$ [1] and $C^{12}=12.00394\pm0.00018$,[2] the following isotopic weights of Cl^{35} and Cl^{37} were obtained:

$$Cl^{35}=34.97903\pm0.00038,$$
$$Cl^{37}=36.97786\pm0.00036.$$

(2) *Argon.*—By introducing the mixture of normal hexane vapor and argon into the discharge tube, the two doublets $C^{13}_2H_4-A^{40}$ and $C^{12}_2H_8-HA^{40}$ were photographed. The following mass differences of these doublets are obtained,

$$C^{13}_2H_4-A^{40}=679.3\pm0.7, \quad (1)$$

$$C^{12}_2H_8-HA^{40}=693.0\pm2.3. \quad (2)$$

From the results (1) and (2), the isotopic weight of A^{40} is as follows:

(1) $A^{40}=39.97637\pm0.00057$,
(2) $A^{40}=39.97500\pm0.00062$.

At present, we have no interpretation of the discrepancy between the mass differences of the above two doublets.

(3) *Iron.*—The wide and faint doublet $C^{12}_4H_8-Fe^{56}$ was photographed, from which we obtained 1235 ± 17 as its mass difference. The ion of Fe^{56} was considered to originate from the iron cathode. We obtain a provisional value 55.9572 ± 0.0012 as the isotopic weight of Fe^{56}. Its packing fraction -7.7 is smaller than Dempster's value -7.0 ± 0.4.[3]

T. Okuda
K. Ogata
K. Aoki
Y. Sugawara

Physical Laboratory,
Osaka Imperial University,
Osaka, Japan,
July 22, 1940.

[1] F. W. Aston, Proc. Roy. Soc. **A163**, 391 (1937).
[2] Asada, Okuda, Ogata and Yoshimoto, Nature **143**, 797 (1939).
[3] A. J. Dempster, Phys. Rev. **53**, 64 (1938).

Electrostatic Generator with Concentric Electrodes

Our 2.6-million-volt generator has been described in previous issues of this journal.[1, 2] It was housed in a tank 20 ft. long and 5½ ft. in diameter, with a working pressure of 100 lb. per sq. in. With only high pressure air in the tank this generator was limited to approximately 2.2 Mv by sparking directly across the air gap. As Freon was added to the high pressure air the direct spark-over voltage rose, but at 2.6 Mv sparking set in along the charging belt and additional Freon then gave no improvement.

This apparatus was dismantled, the tank was provided with a large, removable end plate, and new apparatus was installed as shown in Fig. 1. In the new installation the apparatus is supported from one end only by three Textolite tubes, *T*, of 3¾ inches outside diameter and ⅜ inch wall thickness. This arrangement gives a charging belt length and a minimum insulator length (except for insulator *t*) almost twice as great as in the previous installation. The new tube consists of 62 sections, each 2½ inches long, compared to 53, 2½-inch sections for the old tube.

Electrodes *B* and *C* were expected to give improvement in the spark-over voltage for two reasons: First, they provide a more uniform gradient between electrode *A* and the tank wall; and second, test work indicated that high pressure air withstands higher gradients in a short gap than in a long gap.

Adjustable corona gaps provide potential distribution along the supporting structure and determine the potentials of electrodes *B* and *C* relative to the potential of *A*. Insulator *K* supports the hemispherical end of electrode *C*. Flexing of the structure by electrostatic forces would probably cause trouble if this electrode were supported only from its open end.

The potential of electrode *C* is measured by means of a generating voltmeter. This measurement also gives a rough indication of the total voltage. In a recent test run the ion beam was brought out into the air through an aluminum foil with an air equivalent of approximately 12 mm and the range of the proton beam, measured visually, was used to determine the generator voltage.

With an air pressure of 100 lb./in². in the tank, the maximum range of the proton beam was 18 cm (room temperature 27.2°C, barometric pressure 742 mm of Hg). After adding the air equivalent of the aluminum foil this gave a voltage of 3.5 Mv from the 1937 range curve of Bethe and Livingston. When 10 lb. (weight) of Freon was added, the maximum range of the proton beam was 27 cm, giving a voltage of 4.3 Mv. The voltage was limited by direct spark-over, although insulator *K* gave some trouble. With 15 lb. of Freon the maximum range was 29 cm (4.5 Mv). The voltage was then limited by sparking along insulator *K*. In previous tests it withstood higher voltage, but in recent

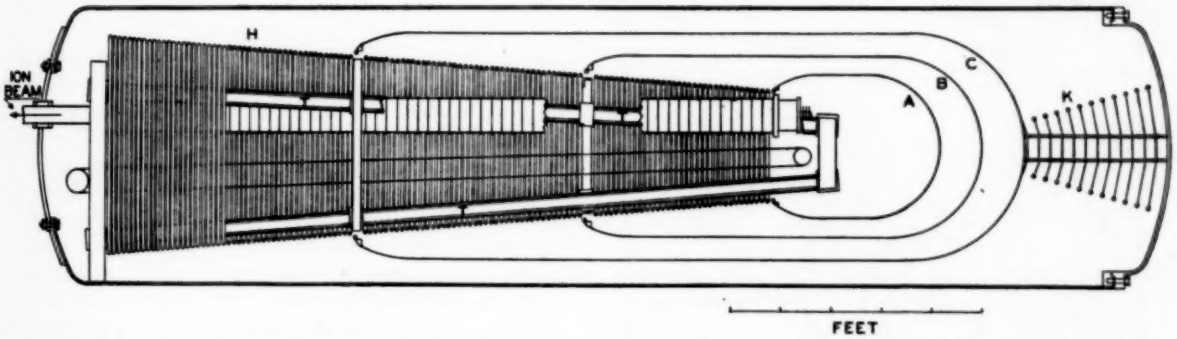

FIG. 1. *A*, *B*, *C*; aluminum shells ¼ inch thick. *T*; Textolite tubes 3¾ inch outside diameter and ¼ inch wall thickness. Each Textolite tube is equipped with aluminum rings, made up from ⅛-inch diameter rod, clamped tightly to the Textolite and spaced 1½ inches apart (not shown in the drawing). *H*; aluminum hoops supported by studs with saddle-shaped ends. One stud projects from each ring. *K*; Textolite tube equipped with metal diaphragms and a corona gap system for potential distribution. Porcelain rings for the accelerating tube are 2½ inches long, corrugated inside and outside. The separating electrodes are steel spinnings. Gaskets of rubber dam 0.01 inch thick make the seals. Springs apply a compressional force of 5000 lb. on the tube. Belt; cotton fabric, woven endless, 16 inches wide.

exposure to the atmosphere during hot, humid weather it soaked up too much moisture and drying treatments attempted so far have not been entirely successful.

The performance of the tube and charging belt indicate that they will be satisfactory for still higher voltage.

We are indebted to Dr. J. L. McKibben for many valuable suggestions and for much help in the design work. Results of his test work were utilized and contributed greatly toward the success of the generator. N. D. Crane and A. O. Hanson gave valuable help with construction work and the Wisconsin Alumni Research Foundation provided financial support.

R. G. HERB
C. M. TURNER
C. M. HUDSON
R. E. WARREN

Department of Physics,
University of Wisconsin,
Madison, Wisconsin,
August 15, 1940.

[1] R. G. Herb, D. B. Parkinson and D. W. Kerst, Phys. Rev. **51**, 75 (1937).
[2] D. B. Parkinson, R. G. Herb, E. J. Bernet and J. L. McKibben, Phys. Rev. **53**, 642 (1938).

Internally Converted Gamma-Rays from Radioactive Gold

The electron spectrum of radioactive gold chemically separated from platinum bombarded with 9.5-Mev deuterons has been obtained with the magnetic spectrometer. A typical result with various peaks due to internally converted gamma-rays is shown in Fig. 1. It is evident that the spectrum of this element is very complex. The lower curve in this figure was taken 18 days after the upper one, and was obtained in order to evaluate the half-life of each electron group.

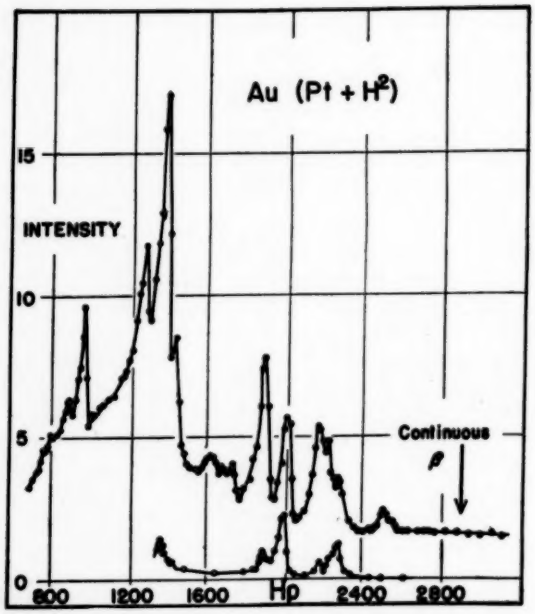

FIG. 1. Electron spectra of radioactive gold taken 18 days apart. The ordinates of the lower curve have been multiplied by 4 before plotting.

The results so far obtained may be summarized as follows: The activity of 164 days half-life shown[1] by absorption measurements to emit beta-particles of energy 0.45 Mev and gamma-radiation of energy 0.11 Mev is too weak for analysis in the spectrometer. The activity of half-life 5.6 days, which from absorption measurements was reported to emit beta-particles of energy 0.36 Mev and gamma-radiation of energy 0.41 Mev, is now shown to be due to a partially converted gamma-ray of energy 356±4 kev. The responsible isotope may be either Au^{196} or Au^{197g}. The other 4 peaks of $H\rho$ greater than 1800 oersted cm can be resolved into K- and L-conversion electron groups corresponding to gamma-ray energies of 331±3 and 410±4 kev, respectively. The half-life of these gamma-rays appears to be about 3 days which is somewhat longer than the value reported from an analysis of the decay curves taken with an ionization chamber. Early observations in the spectrometer confirm the existence of a positron emitter of short half-life. Further work with stronger samples must be carried out to analyze satisfactorily the electron groups of lower energy.

This investigation was made possible by a grant from the Horace H. Rackham Fund.

J. L. LAWSON
J. M. CORK

Department of Physics,
University of Michigan,
Ann Arbor, Michigan,
August 16, 1940.

[1] J. M. Cork and J. Halpern, Phys. Rev. **58**, 201 (1940).

The Photographic Registration of Heavy Particles Emitted During Bombardment

In order to observe the particles emitted from a target during its actual bombardment in the cyclotron, independent of the disturbing effects of the scattered primary particles and the neutron background, a magnetic spectrograph has been devised. The arrangement employed is shown in Fig. 1.

The primary beam of deuterons is incident upon a narrow strip of very thin foil of the element being studied, suspended at the center of a cavity in a cast lead block. Particles leaving the target at an angle of ninety degrees are collimated by a slit in the wall of the lead block. The strong field of the cyclotron together with an auxiliary field produced by a magnetic shunt on the gap of the large magnet, suffices to resolve the emergent particles. Their deflections are approximately proportional to $ne/(mE)^{\frac{1}{2}}$ where ne is the charge, m the mass and E the energy of the particle. The photographic plate is held in a light-tight carriage that can be set at any desired position on an accurately milled track. By placing immediately in contact with the plate during bombardment, a stepped aluminum foil it is possible to also observe the range of each group of particles. This gives sufficient information to determine the nature of the particle and its energy.

Preliminary observations have been made on aluminum, copper, palladium, gold and platinum, using foils about 0.00004 in. thick. Considering the geometry of the sample

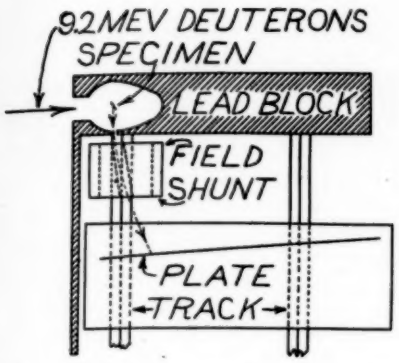

FIG. 1. Schematic diagram of magnetic spectrograph.

and slit the lines are of satisfactory width. Platinum and gold show mainly only the scattered deuteron beam. In aluminum only protons are observed. The maximum range of the protons is 126 cm air equivalent or about 11.0 Mev which is in agreement with the early observations of McMillan and Lawrence,[1] considering their bombarding energy was 2.2 Mev. Palladium shows in addition to scattered deuterons, protons of low energy with something like a continuous distribution. With copper a proton group of energy about 8.5 Mev is observed together with the scattered deuterons. An additional line in the case of copper as yet not satisfactorily explained has a range of about 47 cm air equivalent but shows a deflection even smaller than would be expected for alpha-particles of this energy (25 Mev).

The apparatus with certain improvements should prove to be a valuable aid in the study of nuclear reactions.

This investigation was made possible by a grant from the Horace H. Rackham Fund.

J. M. CORK
P. F. BARTUNEK

Department of Physics,
University of Michigan,
Ann Arbor, Michigan,
August 15, 1940.

[1] E. McMillan and E. O. Lawrence, Phys. Rev. **47**, 343 (1935).